



This is to certify that the

dissertation entitled

METAL LOCALIZED PHOTOCHEMISTRY OF QUADRUPLY BIMETALLIC COMPLEXES

presented by

SARA ANNE HELVOIGT

has been accepted towards fulfillment of the requirements for

Ph.D. degree in Chemistry

Janiel G. Naces Major professor

Date 17 June 1997

MSU is an Affirmative Action/Equal Opportunity Institution

0-12771

LIBRARY Michigan State University

PLACE IN RETURN BOX to remove this checkout from your record. TO AVOID FINES return on or before date due.

DATE DUE	DATE DUE	DATE DUE

MSU is An Affirmative Action/Equal Opportunity Institution ct/circ/detectue.pm3-p.1

METAL LOCALIZED PHOTOCHEMISTRY OF QUADRUPLY BONDED BIMETALLIC COMPLEXES

By

Sara Anne Helvoigt

A DISSERTATION

Submitted to
Michigan State University
in partial fulfillment of the requirements
for the degree of

DOCTOR OF PHILOSOPHY

Department of Chemistry

1997

ABSTRACT

METAL LOCALIZED PHOTOCHEMISTRY OF QUADRUPLY BONDED BIMETALLIC COMPLEXES

By

Sara Anne Helvoigt

Multielectron reactions are fundamental to energy conversion, which is illustrated in the biological systems, photosynthesis and nitrogenase. Many synthetic systems developed use metal complexes capable of one electron reactions. This requires the coupling of successive reactions to effect the net multielectron reaction. The goal of our research is to perform important discrete multielectron photochemistry.

Our general approach has been to use quadruply bonded bimetallic complexes, M-4-M. These complexes possess the zwitterionic excited state, $^1\delta\delta^*$, accessible with low energy excitation. Calculation of the electronic coupling between the metal centers by Hush theory supports the tenet that the metals are weakly coupled indicating that the valence electrons are contained in essentially atomic orbitals as opposed to molecular orbitals. Therefore, the ground state, $^2\delta$, corresponds to one electron localized on each metal center and the $^1\delta\delta^*$ excited state is a metal-to-metal charge transfer transition, which due to localization of two electrons on one metal center is ionic. For symmetric M-4-M complexes, the electrons have an equal probability of being localized on either metal center due to

the symmetry that exists for the molecule. This creates an excited state that is, overall, nonpolar and inaccessable for photochemistry. Intramolecular distortions are efficient at removing this symmetry and trapping the zwitterion. Studies of the temperature dependence of the emission lifetimes of $M_2Cl_4(PR_3)_4$ ($M_2 = Mo_2$, MoW, W_2 ; $PR_3 = PMe_3$, PMe_2Ph , $PMePh_2$) show that the $^1\delta\delta^*$ excited state is in thermal equilibruin with a higher energy state, providing an additional nonradiative decay pathway.

This excited state is predisposed to two electron reactions, such as oxidative addition, as shown by the photoreaction of W₂Cl₄(dppm)₂ and PhSSPh and EtSSEt. However, the homonuclear complexes are limited to oxidative addition, typically exhibited by substrates with low activation barriers, due to the loss of energy in the excited state upon formation of the intermediate. This is illustrated in the reaction of W₂Cl₄(dppm)₂ with N₂O, which has a high activation barrier (59 kcal/mol) and typically displays atom transfer chemisty. The inherent assymetry of MoWCl₄(PMe₂Ph)₄ avoids the need for distortions and atom transfer photochemistry is observed with the substrate Ph₃PS.

To Mom, Dad, Heidi and Joe

ACKNOWLEDGMENTS

I would like to thank Dan Nocera his encouragement and guidance over the years. I am also grateful to everyone in the Nocera group, both present: J.P., Al, Wanda, Dan, Eric, Jim, Jude, Deng and past members: Ann, Carolyn, Janice, Claudia, Jeff, Janice, Doug, Mark, Zoe for all the stimulating conversations and making the work fun. I would especially like to thank Carolyn Hsu for teaching me so much and being so patient with me. The other members of the "quadruple bond club" Dan Engebretson, Ann Macintosh, and Claudia Turró, were always willing to discuss chemistry and help with experiments. J.P. Kirby and Al Barney were always ready to goof-off with me whenever I got tired of writing or just being in the building.

Kerry and Rob Cedergren, Susan Baker, Greg Noonan, Mike Thelen, Charles Ngowe, Carl Iverson made graduate that much more bearable and even fun. I will miss the trips to Dag's with Michelle Mac, Chris Powell, Per Askeland and Matt Gardner and Friday happy hours. Michelle is always so goofy ("I didn't say she was crazy...") that she can make anything fun. Chris has been, among other things, my bestest buddy and drinking partner at MSU. These are the people that I will miss the most when I am gone. Luckily, I am moving to the greater Chicago area, where half of MSU already resides, so it won't really be like leaving.

Of course, I never would have made it this far without the glass shop or the electronic shop. They were very understanding when *everything* had to be done *right away*. Linda Krause, Lisa Dillingham, Beth Townsend and Long Le have always been especially helpful and always with a smile. I don't know how they do it. I also appreciate all the help the Mass Spec facility has given to me over the years, particularly Bev Chamberlin and Dr. Huang.

TABLE OF CONTENTS

Pa

LIST OF TABLES
LIST OF FIGURES
LIST OF ABBREVIATIONS
CHAPTER 1
INTRODUCTION
A. Photosynthesis ⁶ B. Nitrogenase ⁸ C. Multielectron Transfer D. Bimetallic Systems E. Quadruply Bonded Bimetallic Complexes
F. Photochemistry G. Thesis Outline H. References
CHAPTER 2
EXPERIMENTAL
A. General Procedures B. Synthesis 1. Homonuclear Molydenum and Tungsten Complexes a. Mo ₂ Cl ₄ (PR ₃) ₄ (PR ₃ = PMe ₃ , PMe ₂ Ph, PMePh ₂) ³
b. $W_2Cl_4(PR_3)_4$ (PR ₃ = PR ₃ = PMe ₃ , PMe ₂ Ph, PMePh ₂ , PBu ₃) ⁴
e. W ₂ Cl ₄ (dppm) ₂ (SPh) ₂
a. $Mo(^6\eta-PhPMePh)(PMePh_2)_3^7$ b. $Mo(^6\eta-PhPMe_2)(PMe_2Ph)_3^8$
c. WCl ₄ (PPh ₃) ₂ ⁹

f. MoWCl ₄ (PMe ₃) ₄ ¹⁰
3. W(S)Cl ₄ (PMe ₂ Ph)
4. Reactions of W ₂ Cl ₄ (dppm) ₂
a. Photoreaction of W ₂ Cl ₄ (dppm) ₂ with PhSSPh, EtSSEt
b. Thermal reactions of W ₂ Cl ₄ (dppm) ₂ with PhSSPh, EtSSEt
c. Photoreaction of W ₂ Cl ₄ (dppm) ₂ with N ₂ O
5. Reactions of MoWCl ₄ (PMe ₂ Ph) ₄
a. Photoreaction of MoWCl ₄ (PMe ₂ Ph) ₄ with Ph ₃ PS
b. Thermal reaction MoWCl ₄ (PMe ₂ Ph) ₄ with Ph ₃ PS
6. Reactions of $M_2Cl_4(PMe_2Ph)_4$ with Ph_3PS (M = Mo, W)
C. Instrumentation and Methods
1. Photolysis
2. Absorption Spectroscopy
3. Solution Infrared Spectroscopy
4. Nuclear Magnetic Resonance Spectroscopy (NMR)
5. Electron Paramagnetic Resonance Spectroscopy (EPR)
6. Electron Spin Echo Envelope Modulation (ESEEM)
7. Steady-State Luminescence Spectroscopy
8. Time-Resolved Laser Spectroscopy
a. Nanosecond Lifetimes and Transient Absorption
b. Picosecond Transient Absorption
9. Variable-Temperature Emission, Absorption and Nanosecond Lifetimes
10. Electrochemistry
1 1. Mass Spectrometry
a. FAB/MS
b. GC/MS
D. References
CHAPTER 3
PHOTOREDUCTION OF DIARYL/DIALKYL DISULFIDES BY
QUADRUPLY BONDED DITUNGSTEN COMPLEXES
A. Background
B. Photochemistry of W ₂ Cl ₄ (dppm) ₂ and PhSSPh
1. Quantum Yields
C. Transient Absorption
Photochemistry of W ₂ Cl ₄ (dppm) ₂ and EtSSEt
E. Conclusions
F. References
CHAPTER 4
TOM TRANSFER PHOTOCHEMISTRY OF W ₂ Cl ₄ (dppm) ₂ AND
WCl ₄ (PMe ₂ Ph) ₄
A. Background

1. Atom Transfer
B. Photoreaction of W ₂ Cl ₄ (dppm) ₂ and N ₂ O
1. Characterization of Inorganic Products
2. Characterization of Organic Products
3. Reaction Pathway
C. Photoinitiated Sulfur Atom Transfer to MoWCl ₄ (PMe ₂ Ph) ₄
1. Photophysics
4. Quantum Yields
5. Electron Paramagnetic Resonance Spectroscopy
6. Electron Spin Echo Envelope Modulation ⁷²
a. Nuclear Modulation Effect ⁷²
D. Summary
E. Future Directions
F. References
CH APTER 5
▲ STUDY OF THE NONRADIATIVE DECAY OF M ₂ Cl ₄ (PR ₃) ₄
A. Background B. Temperature Dependence of Emissive Lifetimes
C. Nonradiative Decay Theory 11
1 Coloulation of the Huang Phys Factor
 Calculation of the Huang-Rhys Factor Weak Coupling Limit¹¹
1 0
a. Low-Temperature Limit of Weak Coupling
b. Temperature-Dependent Limit of Weak Coupling
3. Intervalence Charge Transfer.
D. Results and Discussion
E. References

LIST OF TABLES

Page
Table 1.1 $\delta \rightarrow \delta^*$ Electronic Transition Energies For Selected Quadruply Bonded Bimetallic Complexes
Table 3.1 Wavelength Dependent Quantum Yields for the Photoreaction of M ₂ Cl ₄ (dppm) ₂ and PhSSPh
Table 4.1 Bond Dissociation Energies for Atom Transfer and Oxidative Addition Substrates
Table 4.2 Physical Properties of M ₂ Cl ₄ (PMe ₂ Ph) ₄
Table 4.3 Wavelength Dependence of Quantum Yields for Photoreaction of MoWCl ₄ (PMe ₂ Ph) ₄ with Ph ₃ PS
Table 4.4 Representative g-values of Mo ^V Octahedral Complexes
Table5.1 Vibrational Frequencies of the Excited and Ground State for Several M— M Complexes and Their Corresponding Change in the M–M Bond Length in the Excited State
Table 5.2 Temperature Dependence of ΔE , k_1 and k_2 of $M_2Cl_4(PR_3)_4$
Table 5.3 Temperature Dependence of ϕ_e , τ , k_r and k_{nr} of $Mo_2Cl_4(PMe_3)_4155$
Table 5.4 Temperature Dependence of ϕ_e , τ , k_r and k_{nr} of Mo ₂ Cl ₄ (PMe ₂ Ph) ₄ 156
Table 5.5 Temperature Dependence of ϕ_e , τ , k_r and k_{nr} of Mo ₂ Cl ₄ (PMePh ₂) ₄ 157
Table 5.6 Fractional of Decay Through the Upper Excited State at 290K and 40K
Table 5.7 k_r and k_{nr} for a Series of $Mo_2X_4(PR_3)_4$ Complexes
Table 5.8 Calculated Excited and Ground state M-M Bond Lengths, Experimental M-M Bond Lengths and the Calculated Huang-Rhys Factor
Table 5.9 Temperature Dependence of ϕ_e , τ , k_r and k_{nr} of $W_2Cl_4(PMe_3)_4168$
Table 5.10 Temperature Dependence of ϕ_e , τ , k_r and k_{nr} of $W_2Cl_4(PMe_2Ph)_4$ 169
Table 5.11 Temperature dependence of ϕ_e , τ , k_r and k_{nr} of $W_2Cl_4(PMePh_2)_4$ 170

Table 5.12 Temperature Dependence of ϕ_e , τ , k_r and k_{nr} of MoWCl ₄ (PMe ₃) ₄	1
Table 5.13 Temperature Dependence of ϕ_e , τ , k_r and k_{nr} of MoWCl ₄ (PMe ₂ Ph)	4 1
Table 5.14 Temperature Dependence of ϕ_e , τ , k_r and k_{nr} of MoWCl ₄ (PMePh ₂)	4 1
Table 5.15 ε_{max} , ν_{max} , $\Delta \overline{\nu}_{1/2}$ and Calculated H_{AB} for $M_2Cl_4(PR_3)_4$	1

LIST OF FIGURES

rembrane. Zigzag (Z) scheme of the electrons and protons in the thylako
Figure 1.2 The schematic representation of N ₂ fixation by Nitrogenase
Figure 1.3 Strategy for the development of multielectron photochemistry
Figure 1.4 Mechanism of photoinduced charge separation in layered zirconiu viologen phosphonate compounds
Figure 1.5 Assembly of thin film chromophores. The first step involve attachment of the Ru chromophore (1%). The second step is the partial hydologist of the remaining SO ₂ groups (<5%)
Figure 1.6 Schematic representation of the events occurring within the polymer film following excitation (reference 20)
Figure 1.7 Mechanism for the formation of associative biradicals (a) and dissociative biradicals (b)
Figure 1.8 Upon irradiation of Cp' ₂ Mo ₂ (CO) ₅ L the mixed valence carbon bridged intermediate forms. This complex disproportionates upon coordination of a second phosphine ligand
Figure 1.9 Qualitative molecular orbital diagram for M ₂ L ₈ quadruply bondobimetallic complexes
Figure 1.10 State diagram for the $\delta\delta^*$ manifold of Mo ₂ Cl ₄ (PMe ₃) ₄
Eigure 1.11 Proposed mechanism for photochemical reduction of 1, dihalocarbons by Mo ₂ [O ₂ P(OPh) ₂] ₄
thermal chemistry of Vaska's complex for the oxidative addition of alk

Figure 3.1 The two electron oxidation of $[Ph_4P]_2[Mo_2(O_2CPh)_4Cl_2]$ by CCl_4 . Two benzoate ligands rearrange from μ - η^2 to μ - η^1 bonding modes
Figure 3.2 The formation of an edge-sharing bioctahedron (ESBO) upon two electron oxidation of a quadruply bonded bimetallic complex
Figure 3.3 Electronic absorption spectral changes during photolysis of toluene solutions of W ₂ Cl ₄ (dppm) ₂ with excess PhSSPh at -10 °C
Figure 3.4 FAB/MS spectrum of the photoproducts isolated from the irradiation of toluene solutions of W ₂ Cl ₄ (dppm) ₂ and excess PhSSPh
Figure 3.5 Quantum yields for the photolysis of M ₂ Cl ₄ (dppm) ₂ and excess PhSSPh. Panel (a) is W ₂ Cl ₄ (dppm) ₂ in toluene at 0 °C; (b) is Mo ₂ Cl ₄ (dppm) ₂ in CH ₂ Cl ₂ at 20 °C.
Figure 3.6 Qualitative correlation diagram for D _{2h} and D _{2d} symmetry quadruply bonded bimetallic complexes. (reference 17)
Figure 3.7 Picosecond transient absorption of Mo ₂ Cl ₄ (dmpm) ₂ in CH ₂ Cl ₄ following a 3 ps excitation pulse at 600 nm. Spectra were recorded at 2, 20 and 50 ps following excitation. The inset shows the ln plot of the recovery of the bleach at 630 nm.
Figure 3.8 Comparison of the transient absorption, following a 532 nm excitation pulse , of W ₂ Cl ₄ (dppm) ₂ (o) to the ground state absorption of W ₂ Cl ₆ (dppm) ₂ (—), both are in benzene
Figure 3.9 Formation of the chemically distorted ESBO upon excitation of the πδ* absorption band of M ₂ Cl ₄ (LL) ₂ complexes
Figure 3.10 Electronic absorption spectral changes during photolysis of toluene solutions of W ₂ Cl ₄ (dppm) ₂ with excess EtSSEt at -20 °C
W ₂ Cl ₄ (dppm) ₂ and EtSSEt in toluene at -20 °C. The irradiation was stopped after 1 hour and 45 minutes. (b) FAB/MS spectrum of the photoproducts isolated from the final spectrum above
Figure 4.1 General reaction mechanism for atom transfer reactions
Dissociation of a phosphine ligand is the first step in the reactions of MCl ₂ P ₄ and M ₂ Cl ₄ P ₄ Complexes. As a result, atom transfer occurs at a square pyramidal coordination sphere in both complexes.

Figure 4.3 The photoreactivity of Cp ₂ Ta(C ₂ H ₄)CH ₃ . The coordinative unsaturated "Cp ₂ TaCH ₃ " is generated upon photolysis Cp ₂ Ta(C ₂ H ₄)CH ₃ .
Figure 4.4 (a) Spectral changes observed upon irradiation of W ₂ Cl ₄ (dppm) ₂ at N ₂ O in THF. (b) Absorption spectrum of independently synthesiz W ₂ Cl ₆ (dppm) ₂ .
Figure 4.5 ¹ H NMR of photoreaction of W ₂ Cl ₄ (dppm) ₂ and N ₂ O. The * indicate resonances due to W ₂ Cl ₆ (dppm) ₂
Figure 4.6 Products from the photolysis of THF ($\lambda_{exc} > 185$ nm). Quantum yiel are shown in parenthesis9
Figure 4.7 FTIR spectrum of organic side products from the photolysis W ₂ Cl ₄ (dppm) ₂ and N ₂ O in a THF solution9
Figure 4.8 The formation of the Ni(II) alkoxide by reaction of bpyNi(C ₄ H ₈) win N ₂ O. A variety of functionalized hydrocarbons can be generated und different reaction conditions
Figure 4.9 Proposed mechanism for the formation of the mixed valence excite state of heteronuclear and homonuclear quadruply bonded bimetall complexes
Figure 4.10 Formation of the mixed-metal dimers from MCl ₂ P ₄ at M(S)Cl ₂ P ₃
Figure 4.11 Absorbance spectra of Mo ₂ Cl ₄ (PMe ₂ Ph) ₄ (— -), MoWCl ₄ (PMe ₂ Ph) ₄ (—), and W ₂ Cl ₄ (PMe ₂ Ph) ₄ () in benzene
Figure 4.12 Electronic absorption and emission spectra of the δδ* transition MoWCl ₄ (PMe ₂ Ph) ₄ in benzene
Figure 4.13 Spectral changes associated with the photolysis (λ > 375 nm) MoWCl ₄ (PMe ₂ Ph) ₄ and Ph ₃ PS in benzene
Figure 4.14 ¹ H NMR of the photoreaction upon photolysis of MoWCl ₄ (PMe ₂ Ph and Ph ₃ PS. * denotes resonances due to MoW starting material
Figure 4.15 ³¹ P{1H} NMR of the photoreaction of MoWCl ₄ (PMe ₂ Ph) ₄ and Ph ₂ P

......11

W(S)Cl ₄ (PMe ₂ Ph). The absorbances between 550 and 400 cm ⁻¹ in (a) are to Ph ₃ PS and Ph ₃ P.	d
Figure 4.17 The X-band EPR spectrum of the photoreaction in a 2-MeT glass.	
Figure 4.18 (a) The inhomogeneously broadened EPR line of a paramagn center. (b) Each spin packet can be considered independently from each ot each having its own Larmor frequency.	h
Figure 4.19 Magnetization of spin packets i and j during a two pulse experim (a) during a $\pi/2$ pulse; (b) after time t; (c) after the π pulse; (d) time t after π pulse.	t
Figure 4.20 (a) Energy level diagram for a $S = 1/2$ and $I = 1/2$ system. The behavior for the magnetization of "forbidden" spin packet A and "allow spin packet B. (b) at time that after the $\pi/2$ pulse; (c) after the π pulse; (d) at time of the echo.	e t
Figure 4.21 Fourier transforms of the photoproduct spin-echo envelope. (a) measured at 3260 G and $\tau = 300$ ns and (b) was measured at 4375 G and 250 ns.	τ
Figure 5.1 Electronic absorption spectra of Mo ₂ Cl ₄ (PMe ₂ Ph) ₄ (— –) W ₂ Cl ₄ (PMe ₂ Ph) ₄ () in benzene	
Figure 5.2 Potential energy diagram for nonradiative excited state decay	1
Figure 5.3 Potential energy wells in the weak coupling limit (a) and the str coupling limit (b) of nonradiative decay	
Figure 5.4 Fit of the variation of the observed emission decay constant Mo ₂ Cl ₄ (PMe ₃) ₄ to equation 5.4 in the 40-290 K temperature range	
Figure 5.5 Fit of the variation of the observed emission decay constant Mo ₂ Cl ₄ (PMe ₂ Ph) ₄ to equation 5.4 in the 40-290 K temperature range	
Figure 5.6 Fit of the variation of the observed emission decay constant Mo ₂ Cl ₄ (PMePh ₂) ₄ to equation 5.4 in the 40-290 K temperature range	
Figure 5.7 Energy gap plots for Mo ₂ Cl ₄ (PR ₃) ₄ at 290 K (•) and 40 K (o)1	1
Figure 5.8 Fit of the variation of the observed emission decay constant W ₂ Cl ₄ (PMe ₃) ₄ to equation 5.4 in the 40-290 K temperature range	

W ₂ Cl ₄ (PMe ₂ Ph) ₄ to equation 5.4 in the 130-290 K temperature range16
Figure 5.10 Fit of the variation of the observed emission decay constant $W_2Cl_4(PMePh_2)_4$ to equation 5.4 in the 40-300 K temperature range16
Figure 5.11 Energy gap plots for MoWCl ₄ (PR ₃) ₄ (o) and W ₂ Cl ₄ (PR ₃) ₄ (•) at 6 and 40 K, respectively
Figure 5.12 Fit of the variation of the observed emission decay constant MoWCl ₄ (PMe ₃) ₄ to equation 5.4 in the 60-280 K temperature range
Figure 5.13 Fit of the variation of the observed emission decay constant MoWCl ₄ (PMe ₂ Ph) ₄ to equation 5.4 in the 60-290 K temperature range17
Figure 5.14 Fit of the variation of the observed emission decay constant MoWCl ₄ (PMePh ₂) ₄ to equation 5.4 in the 60-290 K temperature range17
Figure 5.15 Proposed energy diagram for Mo ₂ Cl ₄ (PMe ₂ Ph) ₄

LIST OF ABBREVIATIONS

ADP adenosine diphosphate

ATP adenosine triphosphate

bpy bipyridine

^tBu-LNS bis(p-tert-butylphenyl)-2-pyridylmethanethiolate¹⁻

3-Clpyr 3-chloropyridine

Cp' methlycyclopentane

DMA p-cyano-N,N-dimethylaniline

dmpm bis(dimethylphosphino)methane

dppm bis(diphenylphosphino)methane

edta ethylenediaminetetracetate

ESBO edge-sharing bioctahedron

IT intervalence charge transfer

LL bidentate ligand

LMCT ligand-to-metal charge transfer

4-Mepyr 4-methylpyridine

MLCT metal-to-ligand charge transfer

MMCT metal-to-metal charge transfer

M-3.5-M one electron oxidized quadruple bond

M-4-M quadruple bond

NADP⁺ nicotinamide adenine dinucleotide phosphate (oxidized form)

NADPH nicotinamide adenine dinucleotide phosphate (reduced form)

NO p-cyano-N,N-dimethylaniline N-oxide

OEC oxygen evolving complex

OEP octaethylporphyrinato²

PED 1-phenyl-1,2-ethanediol

phen 1,10-phenanthroline

pop $P_2O_5H_2^-$

PQ⁺ paraquat

pr-salen N,N'-ethylenebis(2,2'-dipropylsalicylideneiminato)²⁻

PR₃ monodentate phosphine

pyr pyridine

pyz pyrazine

 $tetraphos \quad Ph_2PCH_2CH_2P(Ph)CH_2CH_2P(Ph)CH_2CH_2PPh_2$

TPP *meso*-tetraphenylporphyrinato²-

TTP meso-tetrakis(p-tolyl)porphyrinato²

CHAPTER 1

INTRODUCTION

The importance of electron transfer reactions is reflected in the sheer volume of literature that has been generated on the subject. Multiple electron oxidation-reduction reactions are typical of many biological and chemical transformations; these reactions, such as small molecule activation, include H₂O \rightarrow H₂ + ½ O₂ (photosynthesis), 1 N₂ + 3H₂ \rightarrow 2NH₃ (nitrogenase), 2 SO₃ $^{2-}$ \rightarrow HS⁻ (sulfite reductase),³ and $NO_3^- \rightarrow NO_2^-$ (nitrate reductase).⁴ The success of these chemical transformations relies on the ability to overcome large kinetic and/or thermodynamic barriers. Electronically excited transition metal complexes are useful in this endeavor since the increased chemical potential provides the driving force necessary to surmount the barriers that exist for the ground state partner. Excitation of a molecule promotes an electron to a high energy orbital generating an electron hole. In this new excited state configuration, the molecule is both easier to oxidize and reduce with the availability of the low energy hole and the high energy electron, respectively. Most attempts at multielectron photochemistry have relied on the one electron hole/charge separation/storage strategy that is Inspired by biological systems, such as photosynthesis and nitrogenase.

Although the driving force of photosynthesis and nitrogen fixation differs, fundamentally both involve systems that utilize a series of 1 or 2 electron transfer

reactions designed to prevent back electron transfer and store electrons in order achieve the net reaction. Enzymes and membranes are basically la supramolecular arrays where the main purpose of the protein and lipids is impose long range order for the specialized donor and acceptor molecules.⁵ The efficiency of energy and electron transfer is a function of the donor-accept distances, their orientation and environment, thus requiring long range organization.

The photosynthetic process in green plants takes place in the thylak

A. Photosynthesis⁶

membrane of chloroplasts and consists of 2 reaction centers, Photosystem I and (PSI and PSII), where the reduction of NADP⁺ and the oxidation of water occ respectively. P₆₈₀, a specialized chlorophyll, is central to NADP⁺ reduction. The subscript, 680, refers to the λ_{max} of the excitation wavelength for this chlorophydimer. Excitation of P₆₈₀ generates the excited state, P₆₈₀*, which is a both a strong reductant and oxidant. P₆₈₀* reduces pheophytin generating P₆₈₀⁺; the pheophydim turn reduces plastoquinone Q_A and the electron is finally transferred plastoquinone Q_B. Upon reduction by 2 electrons, Q_B is protonated by 2 protonand leaves the binding site as Q_BH₂. This is then replaced by another plastoquinon from the quinone pool. This process is shown schematically in Figure 1.1. Q_BH₂ reoxidized by the cytochrome b₆/f complex to result in transmembrane protonanter and the electrons are transferred to plastocyanin and finally to PSI. He absorption of a photon by the P₇₀₀ reaction center of PSI initiates electrons fer through a series of acceptors, iron sulfur proteins, ferrodoxin and series of acceptors, irong sulfur proteins, ferrodoxin and series of acceptors, irong sulfur proteins, ferrodoxin and series of acceptors, irong sulfur proteins, ferrodoxin and series of acceptors.

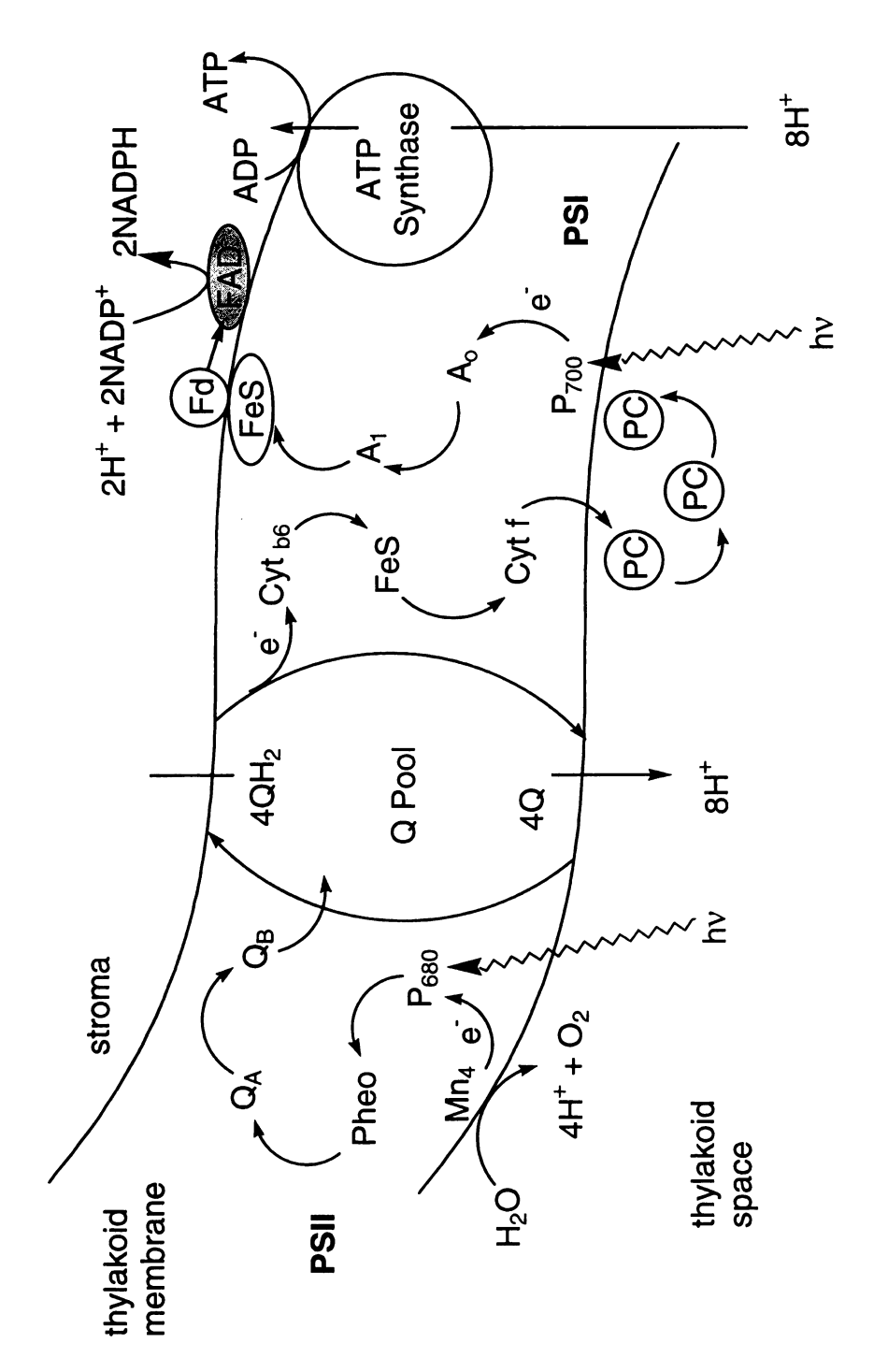


Figure 1.1 Zigzag (Z) scheme of the electrons and protons in the thylakoid membrane.

ferrodoxin NADP⁺ reductase, where NADP⁺ is reduced to NADPH. To complete the cycle, P_{680}^{+} , a strong oxidant, is reduced by a tyrosine residue, Y_z , which is in turn reduced by the Mn₄ oxygen evolving complex (OEC). The OEC goes through 5 oxidation states, $S_0 \rightarrow S_4$, and in the S_4 oxidation water is oxidized to release H⁺, which is used in the production of NADPH, and O_2 .

B. Nitrogenase⁸

The enzyme nitrogenase and the Haber-Bosch process each account for the conversion of approximately 10⁸ tons of N₂ to NH₃ per year. The Haber-Bosch process uses an Fe catalyst and temperature and pressure as high as 450 °C and 250 atm to overcome a large kinetic barrier. Biology's counterpart, nitrogenase, is able to perform this reaction at ambient temperature and 1 atm. This is possible due to the sophisticated mechanism of the enzyme, shown schematically in Figure 1.2. Nitrogenase consists of two proteins, an Fe protein and MoFe protein.

The Fe protein has two subunits and contains one redox active $[Fe_4S_4]^{1+/2+}$ cluster. It is the site of MgATP hydrolysis and has two binding sites for MgATP, one on each subunit. The protein is reduced in a series of 2-electron steps by a low potential ferredoxin or flavodoxin, probably via the $[Fe_4S_4]^{1+/2+}$ cluster.⁸ Upon hydrolysis of 2 MgATP molecules two electrons are transferred by this cluster to the MoFe protein using dithionite as an electron donor. To complete the Fe protein cycle, the protein is reduced by $SO_2^{\bullet-}$, two MgADP molecules are released and replaced by two MgATP to be hydrolyzed again.

The MoFe protein is made up of four subunits in an $\alpha_2\beta_2$ arrangement and it contains two P clusters ([Fe₄S₄]₂(S)₂) and two FeMo cofactors (MoFe₇S₈₋₉), the

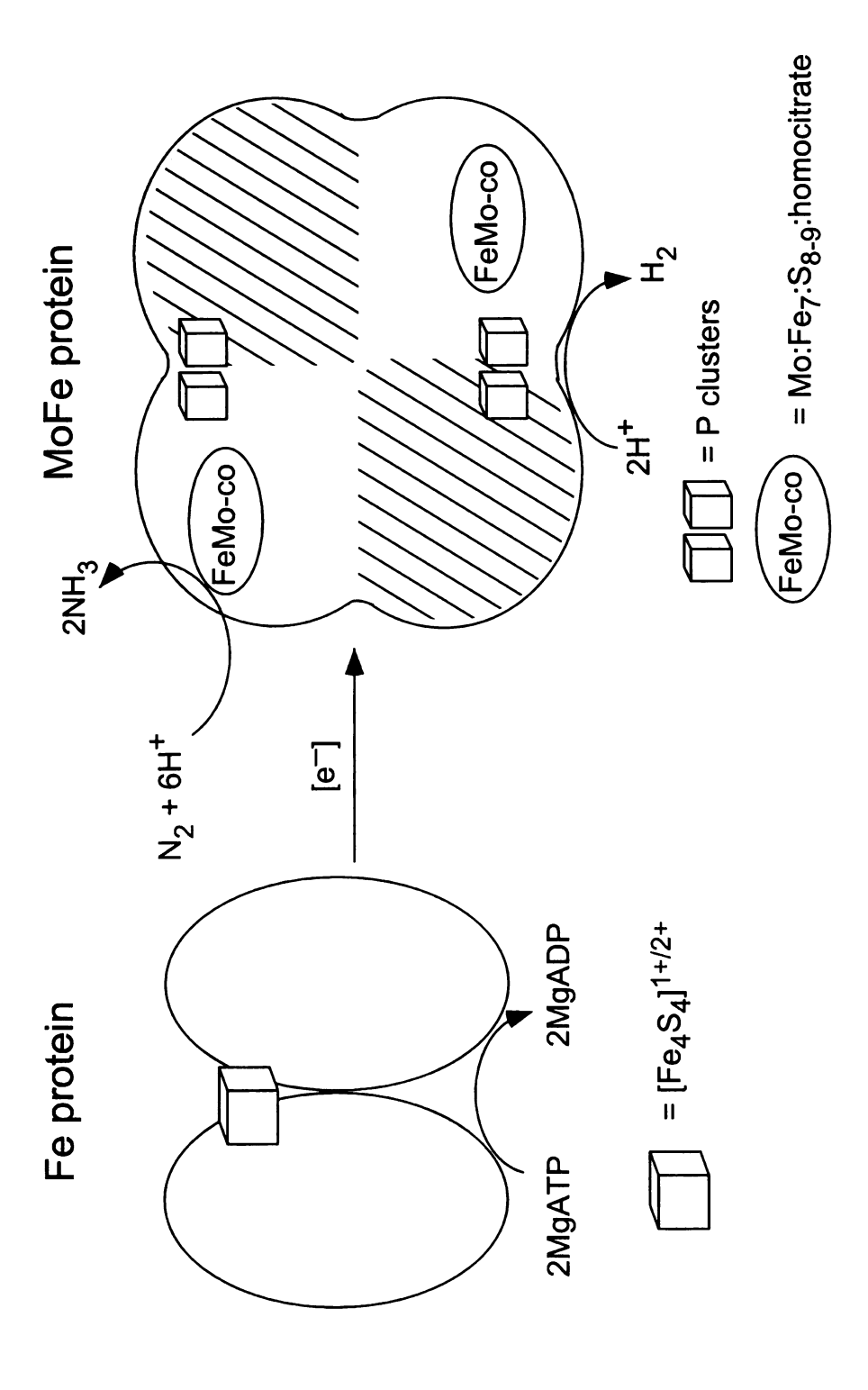


Figure 1.2 A schematic representation of N_2 fixation by Nitrogenase.

structures of which were recently solved.¹⁰ The proposed function of the P clusters is to transfer electrons from the Fe protein to the FeMo cofactor. N₂ is most likely reduced at the FeMo cofactor, although the mode of binding has not been established. While a total of 8 electrons are transferred between the proteins, N₂ is released before the full complement of electrons has been transferred. It is believed that the coupling of MgATP hydrolysis to the electron transfer step is necessary either to overcome the unfavorable activation energy or to prevent back electron transfer.²

C. Multielectron Transfer

This thesis is concerned with effecting multielectron reactions with a photon. The strategy for multielectron processes is derived from biological systems, such as the ones above. Figure 1.3 summarizes the strategy from a photochemical perspective. A receptor molecule acts as a light harvester to initiate charge separation. An electron is promoted to the excited state, generating a hole, and is moved spatially away through a series of electron transfer steps. The design goal of molecular systems is to ensure forward electron transfer that is more efficient than the recombination of the electron with the hole. This is difficult in photochemically driven charge separation schemes because inevitably back recombination is a thermodynamically favorable process. However, the recombination becomes less favorable as the electron and the hole become more spatially separated due to the inverse exponential distance dependence of the electron transfer rate.¹¹

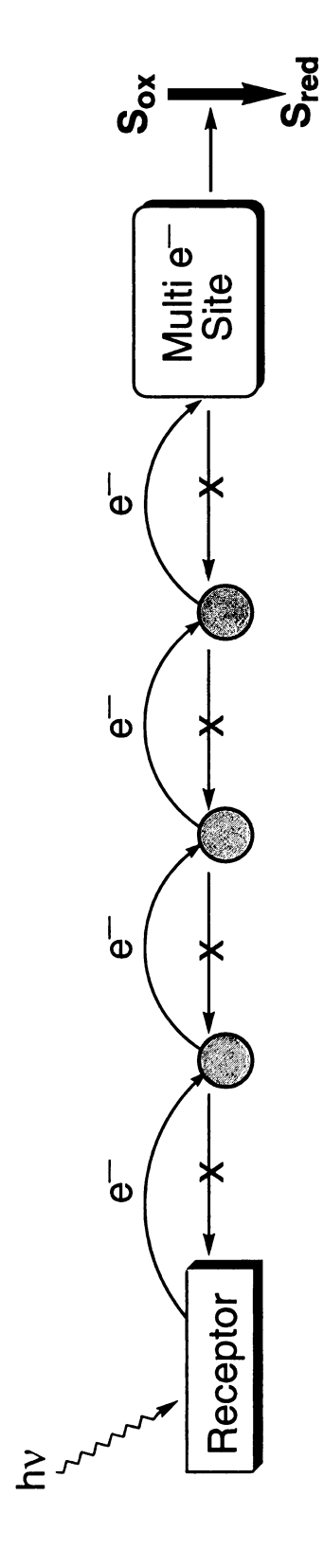


Figure 1.3 Strategy for the development of multielectron photochemistry.

Successful schemes, therefore, are ones that can achieve charge separation and impose some sort of long range order on the system. Some strategies have utilized sol-gel glasses, 12 clays, 13 colloids, 14 polymer films 15 , hydrogen bonding 16 and zeolites 17 to achieve organization of the photosensitizers and electron donors and acceptors. The importance of spatial organization can be observed in the photoinduced charge separation in layered zirconium viologen phosphonate compounds. The irradiation ($\lambda = 300$ nm) of thin films of $Zr(O_3PCH_2CH_2(bipyridinium)CH_2CH_2PO_3)X_2$ (X = Cl, Br), produces the characteristic blue color of a viologen radical with a photochemical quantum yield greater than 0.03. When the UV light is removed the blue color of the reduced viologen gradually fades. The photochemistry involves a viologen centered transition, probably a $\pi \rightarrow \pi^*$ transition, creating a strong oxidant which oxidizes the X^- contained between the viologen appendages, equations 1.1 and 1.2.

$$\sim VIOL^{2+} \sim VIOL^{2+}$$
 (1.1)

$$VIOL^{2+}$$
 $+ X^ \longrightarrow$ $VIOL^{\bullet+}$ $+ X^{\bullet}$ (1.2)

The halide radical then abstracts a hydrogen from the α -methylene on an adjacent viologen group. The incipient methylene-based radical can be stabilized by delocalization onto the pyridine, Figure 1.4, resulting in charge separation that is stable for several hours under vacuum or under Ar.

Charge separation, while a major research area on its own, is only the first step to multielectron photochemistry. The charge separation step needs to be

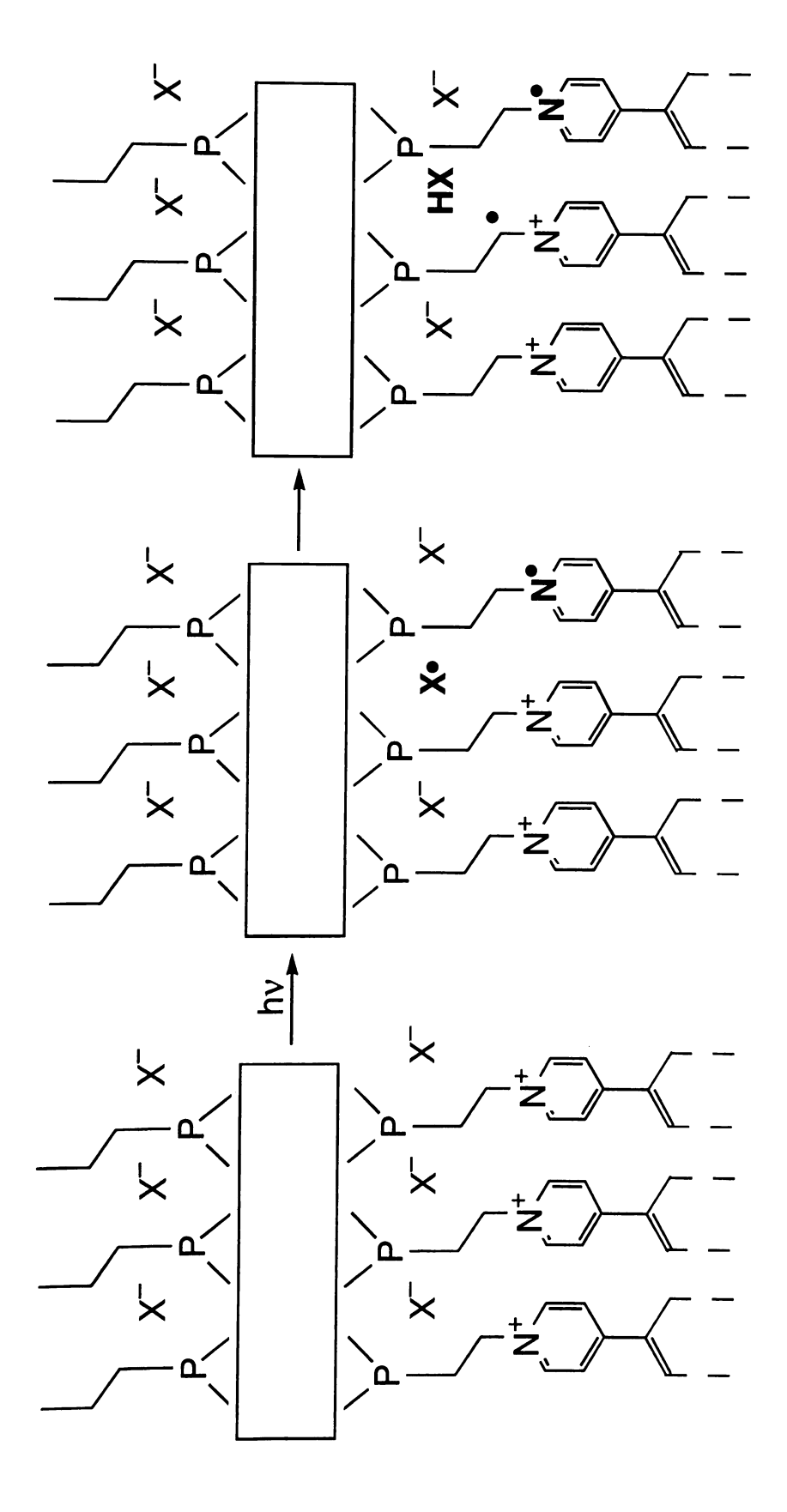


Figure 1.4 Mechanism of photoinduced charge separation in layered zirconium viologen phosphonate compounds.

coupled to a catalyst, such as $M(bpy)_3^{n+}$, which can either oxidize or reduce a substrate. The metal-to-ligand charge transfer (MLCT) excited state of polypyridyl complexes of Ru(II), Os(II), and Re(I) typically undergo efficient oxidative or reductive electron transfer quenching in solution generating separate redox products, ¹⁹ equations 1.3 and 1.4.

$$Ru(bpy)_3^{2+} \xrightarrow{hv} Ru(bpy)_3^{2+*}$$
 (1.3)

$$Ru(bpy)_3^{2+*} + PQ^{2+} \longrightarrow Ru(bpy)_3^{3+} + PQ^{+}$$
 (1.4)

$$Ru(bpy)_3^{3+} + PQ^+ \longrightarrow Ru(bpy)_3^{2+} + PQ^{2+}$$
 (1.5)

bpy = 2,2'-bipyridine;
$$PQ^{2+} = Me - N N - Me$$

The ability to harvest the stored redox equivalents is hindered by the fast recombination of $Ru(bpy)_3^{3+}$ and PQ^+ , equation 1.5. This quenching can be controlled by mounting the Ru^{2+} on a polymer film.²⁰ For instance, $(bpy)_2Ru(5-NH_2phen)^{2+}$ can be attached to a chlorosulfonated polystyrene ([-CH₂CH(p-C₆H₄SO₂Cl)-]_n = PS-SO₂Cl) on a Pt electrode at a 1% loading. The chromophore is added to the polymer by soaking the PS-SO₂Cl film in a Ru^{2+} solution; the concentration of Ru^{2+} is therefore greatest at the top of the film and lowest near the electrode. Subsequent partial (< 5%) hydrolysis of the remaining sites creates ion channels in the film (Figure 1.5). The hydrolysis of PS-SO₂Cl also provides an ion-exchange environment for incorporating PQ^{2+} .

$$+ y (bpy)_2 Ru(5-NH_2 phen)(PF_6)_2$$

$$+ y (bpy)_2 Ru(5-NH_2 phen)(PF_6)_2$$

$$+ y NH_2$$

$$+ CH_2 - CH_{x-y} + CH_2 - CH_{y}$$

$$+ y CH_2 - CH_{y} + y CI^- + y H_2O$$

$$+ CH_2 - CH_{x-y} + CH_2 - CH_{y} + y CI^- + y H_2O$$

$$+ CH_2 - CH_{x-y} + CH_2 - CH_{y} + y CI^- + y H_2O$$

$$+ CH_2 - CH_{x-y} + CH_2 - CH_{y} + y CI^- + y H_2O$$

$$+ CH_2 - CH_{x-y} + CH_2 - CH_{y} + y CI^- + y H_2O$$

$$+ CH_2 - CH_{x-y} + CH_2 - CH_{y} + y CI^- + y H_2O$$

$$+ CH_2 - CH_{x-y} + CH_2 - CH_{y} + y CI^- + y H_2O$$

$$+ CH_2 - CH_{x-y} + CH_2 - CH_{y} + y CI^- + y H_2O$$

$$+ CH_2 - CH_{x-y} + CH_2 - CH_{y} + y CI^- + y H_2O$$

$$+ CH_2 - CH_{x-y} + CH_2 - CH_{y} + y CI^- + y H_2O$$

$$+ CH_2 - CH_{x-y} + CH_2 - CH_{y} + y CI^- + y H_2O$$

$$+ CH_2 - CH_{x-y} + CH_2 - CH_{y} + y CI^- + y H_2O$$

$$+ CH_2 - CH_{x-y} + CH_2 - CH_{y} + y CI^- + y H_2O$$

$$+ CH_2 - CH_{x-y} + CH_2 - CH_{y} + y CI^- + y H_2O$$

$$+ CH_2 - CH_{x-y} + CH_2 - CH_{y} + y CI^- + y H_2O$$

$$+ CH_2 - CH_{x-y} + CH_2 - CH_{y} + y CI^- + y H_2O$$

$$+ CH_2 - CH_{x-y} + CH_2 - CH_{y} + y CI^- + y H_2O$$

Figure 1.5 Assembly of thin film chromophores. The first step involves attachment of the Ru chromophore (1%). The second step is the partial hydrologis of the remaining SO_2 groups (<5%).

The partially hydrolyzed films with the chromophore and PQ²⁺ generate a current when irradiated in the presence of an acetonitrile solution of tetraethanolamine (TEOA) as an oxidative scavenger, Figure 1.6. The absorption of light by Ru²⁺ generates Ru^{2+*}, which is oxidatively quenched by PQ²⁺ to give PQ⁺. The reduction equivalent (an electron) is transferred through PQ⁺ migration and electron transfer to the Pt electrode. Ru³⁺ is reduced by TEOA that has diffused through the surface of the film and upon one electron oxidation TEOA decomposes. A photocurrent is generated with a quantum yield of about 0.14. The photocurrent comes from the diffusional quenching of Ru²⁺ sites that are near SO₃⁻ ion channels created in the hydrolysis step. This system has combined spatial organization and the mobilization of electron transport species to create a current.

As demonstrated above, whereas systems developed for multielectron photochemistry¹⁰ are diverse and sophisticated, they all have a common feature of single metal centers capable of only single electron reactions.²¹ An approach pursued in the Nocera group is to tie two metal centers together, such as a bimetallic complex, in order to couple the reactivity of the redox centers to achieve multielectron reactions.

D. Bimetallic Systems

Most bimetallic complexes are of the three basic structure types shown below.²¹ Type I dimers have bridging atoms, ions or groups holding the metals together. There is no direct metal interaction in this structure type. Dimers of type II are held in close contact by bridging ligands. While there is intermetal interaction, there is no M–M bond. In dimers of type III, there is a direct M–M

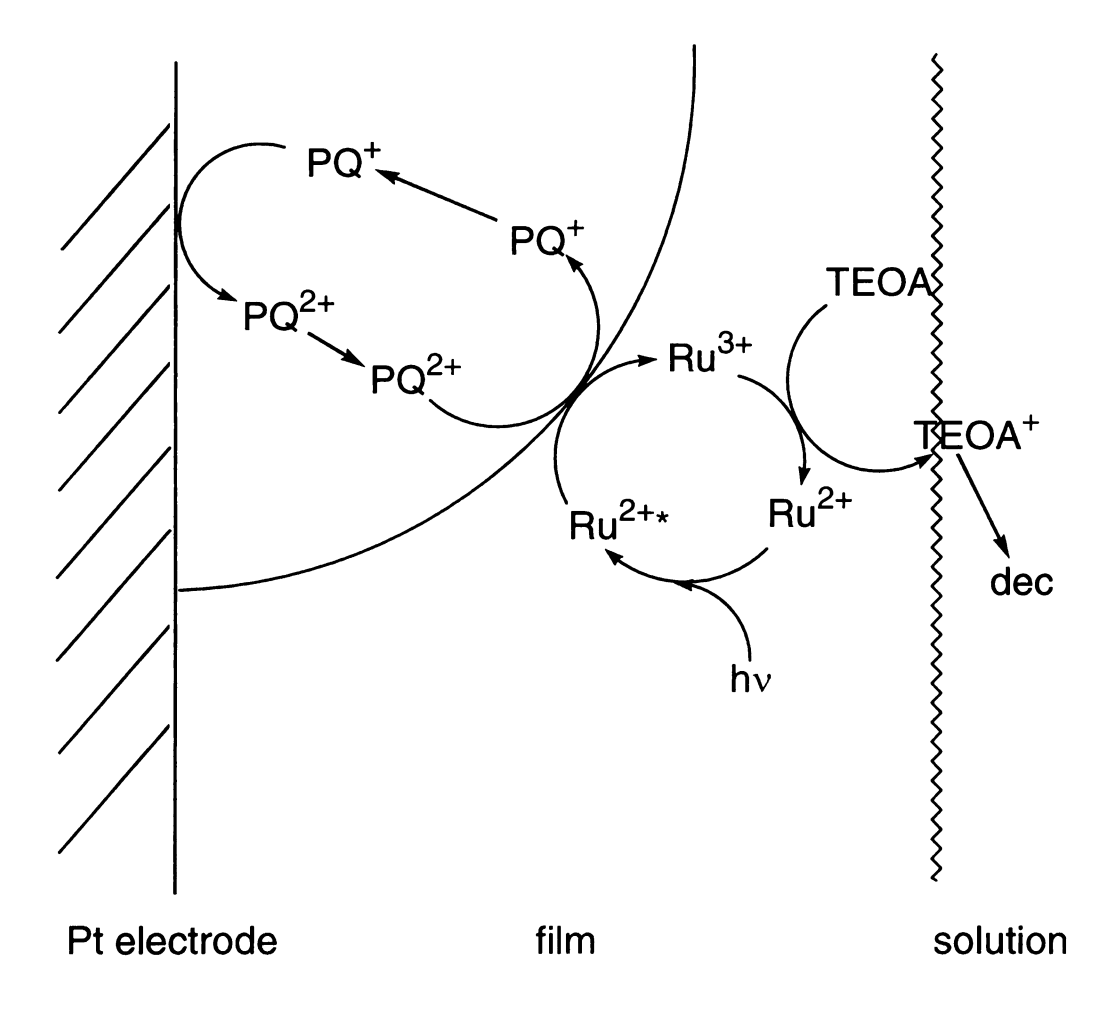
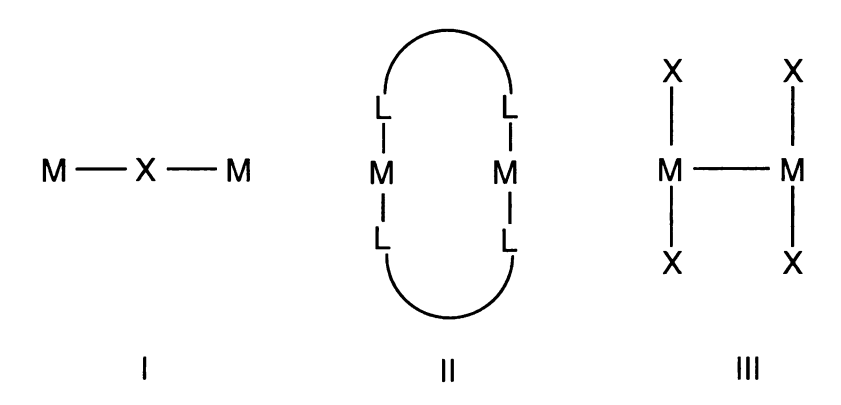


Figure 1.6 Schematic representation of the events occurring within the polymeric film following excitation (reference 20).

bond that, for this discussion, is a single bond. X, in this case, may be either a monodentate or bidentate ligand.



In linearly bridged dimers, structure I, the two metals are typically in different oxidation states and are bridged by either an atom or a bridging ligand, such as Cl⁻ and CN⁻, respectively.²¹ These complexes exhibit low energy metal-to-metal charge transfer (MMCT) transitions from the reducing metal to the oxidizing metal via the bridging group. The photochemistry of these complexes is dominated by rapid back electron transfer. For example, upon excitation, the binuclear complex (NH₃)₅Os^{III}–NC–M^{II}(CN)₅⁻ (M = Fe, Ru, Os) undergoes MMCT to form the redox isomer, (NH₃)₅Os^{II}–NC–M^{III}(CN)₅⁻.²¹ This isomer is substitutionally inert and through thermal back electron transfer forms the original complex. For complexes that are substitutionally labile, decomposition can result before back electron transfer occurs. This is observed for (PPh₃)₃Cu^I(μ-Cl)Fe^{III}Cl₃, which undergoes photolysis in low polarity solvents.²² Upon excitation of low energy MMCT transitions, the complex decomposes to Cu²⁺ and Fe²⁺.

In structure II, there is no formal M-M bond in the ground state. Upon excitation, a M-M bond is formed, giving rise to an associative diradical excited

state, 21 Figure 1.7. This excited state is characteristic of d^8-d^8 systems, such as $Pt_2(P_2O_5H_2)_4^{4-}$ (= $Pt_2(pop)_4^{4-})^{23}$ and $Rh_2(1,3\text{-diisocyanopropane})_4^{2+},^{24}$ $d^{10}-d^{10}$ systems, such as $Au_2(dppm)_2^{2+}$ (dppm = bis(diphenylphospino)methane) 25 and $d^{10}-d^8$ systems, $AuPt(dppm)_2(CN)_2^{+},^{26}$ The excited states of the above molecules are quenched by halogen atom transfer agents, such as alkyl and aryl halides, and hydrogen atom donors, such as $(CH_3)_2CHOH$, $PhCH(OH)CH_3$, Bu_3SnH , Et_3SiH and H_3PO_3 . In the two electron reaction of the triplet excited state of $Pt_2(pop)_4^{-4}$, halogen atom abstraction is the first step (equation 1.6) followed by comproportionation of two $Pt_2(II,III)(pop)_4X^4$ complexes to give $Pt_2(III,III)(pop)_4X_2^{4-}$ and $Pt_2(II,III)(pop)_4X^4$ (equation 1.7). This net two electron reaction is observed through consecutive one electron reactions.

$$Pt_2(pop)_4^{4-*} + RX \longrightarrow Pt_2(pop)_4X^{4-} + R \cdot$$
 (1.6)

$$2 \text{ Pt}_2(\text{pop})_4 X^{4-} \longrightarrow \text{Pt}_2(\text{pop})_4 X_2^{4-} + \text{Pt}_2(\text{pop})_4^{4-}$$
 (1.7)

The lowest energy excited states of singly bonded bimetallic d^7-d^7 and d^9-d^9 systems, structure III, correspond to $\sigma{\to}\sigma^*$ and $\pi_d{\to}\sigma^*$ transitions.²⁷ Excitation of these dimers results in dissociative diradicals formed from the homolytic cleavage of the M–M bond to yield 17 electron radicals as shown in equation 1.8.

$$M_2(CO)_{10} \xrightarrow{hv} 2 \cdot M(CO)_5$$
 (1.8)

The formation of a dissociative diradical can only give rise to one electron products (Figure 1.7). The radical produced can be trapped by halogen donors,

Associative Biradical Dissociative Biradical

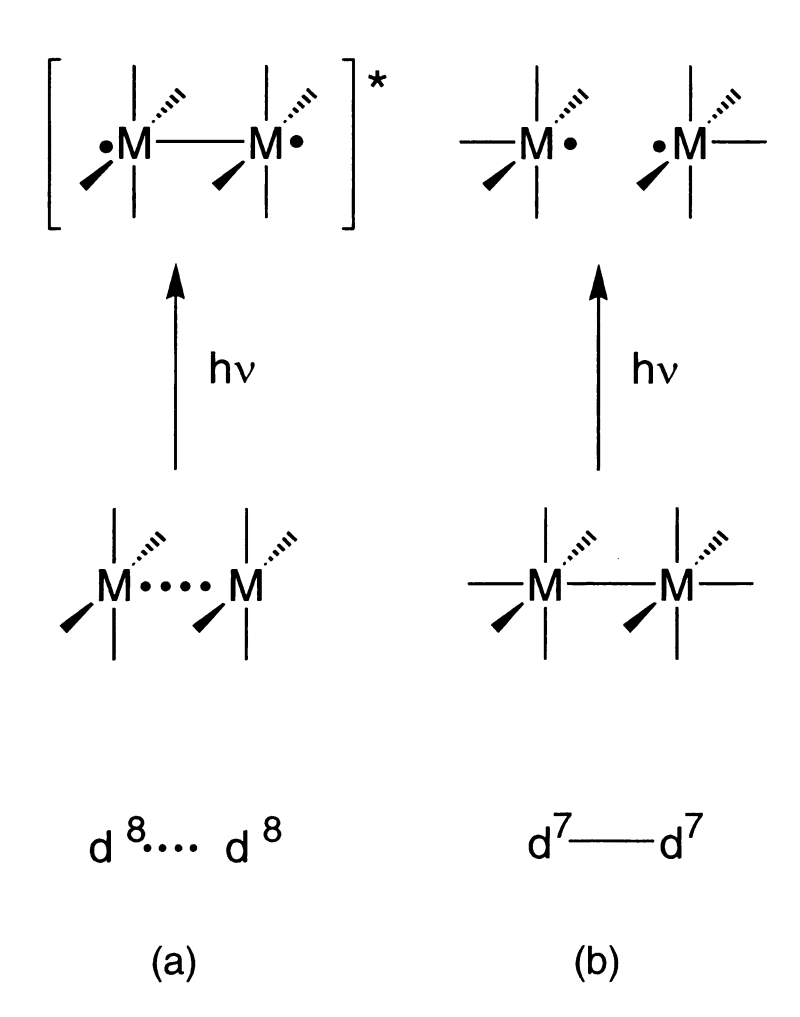


Figure 1.7 Mechanism for the formation of associative biradicals (a) and dissociative biradicals (b).

polar solvents or other metal radicals. $Re(CO)_5Cl$ is formed with a quantum efficiency of 0.6 from the irradiation of CCl_4 solutions of $Re_2(CO)_{10}$, demonstrating that this is a highly efficient process.²⁸ The rate of photolytic M–M cleavage is $>10^{10}$ s⁻¹ and competes effectively with the cleavage of M–CO bonds; however, irradiation of $M_2(CO)_{10}$ in the presence of good ligating substrates, such as PPh₃, results in products that are due to CO substitution.²⁹

While the typical reaction of M-M bonded carbonyl dimers, $M_2(CO)_{10}$, is M-M homolytic cleavage or M-CO bond dissociation, 21,27,29 this structure exhibits another reaction type 30 that is important to the work described in this thesis. In addition to homolytic cleavage, internal charge transfer can result in heterolytic cleavage to afford ionic products. The lowest energy bands of metal carbonyl dimers are generally assumed to be $\pi_d \rightarrow \sigma^*$ and $\sigma \rightarrow \sigma^*$ transitions 31 and accordingly, they have been assigned as such in the dimer $Cp'_2Mo_2(CO)_6$. Irradiation of $Cp'_2Mo_2(CO)_6$ with L (= PR_3) proceeds as shown below. 32

$$Cp'_2Mo_2(CO)_6 + L \xrightarrow{290nm} Cp'Mo(CO)_2L_2^+ + Cp'Mo(CO)_3^- (1.9)$$

The primary photoproduct is $Cp'_2Mo_2(CO)_5L$. Excitation of the $^1\sigma\sigma^*$ transition of $Cp'_2Mo_2(CO)_5L$ causes the formation of a carbonyl bridged intermediate. Coordination of a second ligand forms a mixed valence intermediate and polarizes the M-CO-M unit. This induces inner sphere electron transfer, which leads to disproportionation to form $Cp'Mo(CO)_3^-$ and $Cp'Mo(CO)_2L_2^+$. This reaction mechanism is summarized in Figure 1.8. Disproportionation of $Cp'_2Mo_2(CO)_5L$ is only observed upon irradiation with $\lambda > 290$ nm. This wavelength dependence implies

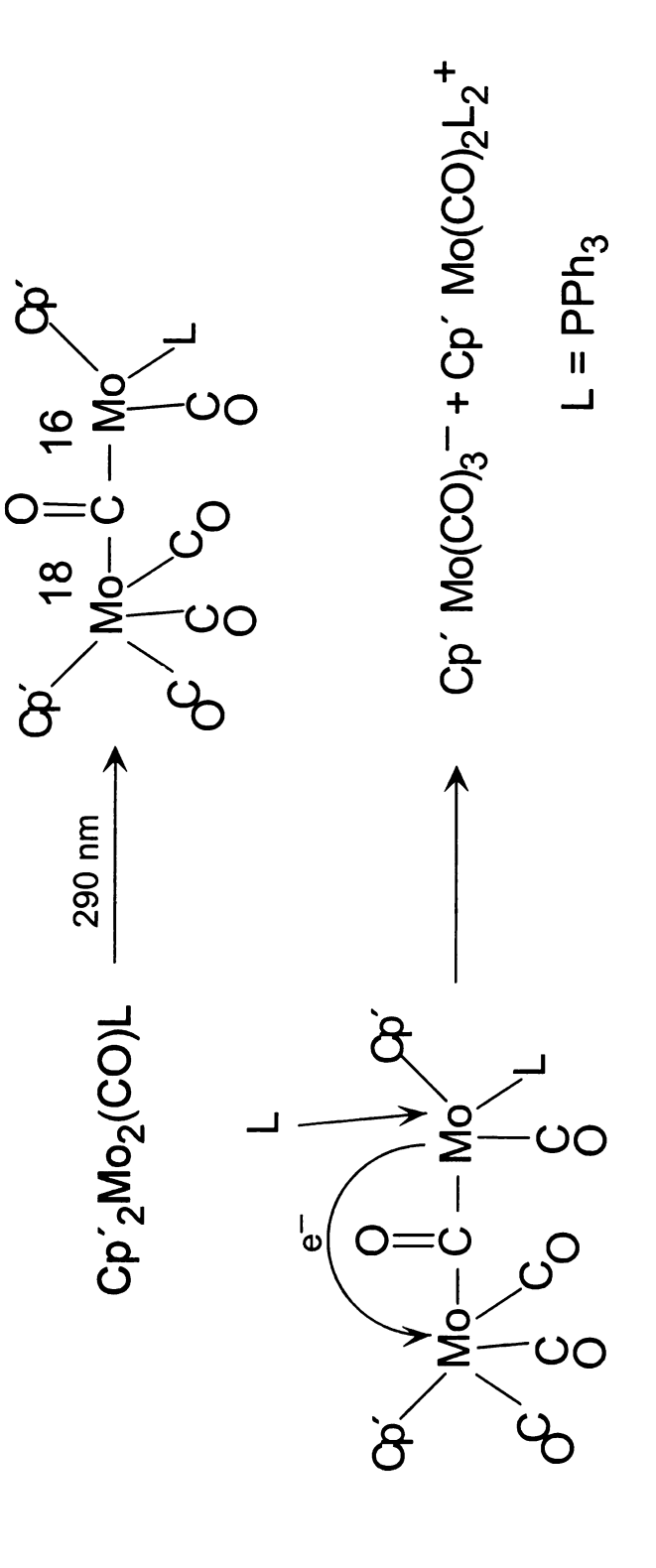


Figure 1.8 Upon irradiation of Cp²Mo₂(CO)₅L the mixed valence carbonyl bridged intermediate forms. This complex disproportionates upon coordination of a second phosphine ligand.

that the M-M bond homolysis, through the ${}^3\sigma\sigma^*$ state, is not sufficient to induce the disproportionation.

In the system above, two electrons are paired on one metal center which leads to the formation of ionic products. Is it possible to perform similar chemistry in an excited state where two electrons could be localized on one metal center of a bimetallic dimer? This type of excited state, known as a zwitterion, was proposed to exist in systems where two electrons reside in weakly coupled orbitals³³ and has been the subject of theoretical studies for over 50 years. It has roots in organic chemistry with twisted ethylene,³⁴ and in physical chemistry with stretched hydrogen.³⁵ For the latter, there is significant overlap between the atomic orbitals of hydrogen in its equilibrium state; when the bond is stretched from its equilibrium position, however, the overlap decreases. The situation is also similar in twisted ethylene. As one half of the molecule twists relative to the other, the overlap of the π orbitals decreases and at 90° the overlap is zero. As the σ orbitals in hydrogen and π orbitals in ethylene become more weakly coupled, a molecular orbital description of the atomic orbitals is no longer appropriate and the electronic structure is better described by a valence bond description.

Four states arise from two electrons in two weakly coupled orbitals. Using H_2 as the example, these states are ${}^1\sigma^2$, ${}^3\sigma\sigma^*$, ${}^1\sigma\sigma^*$. The two lower energy states, ${}^1\sigma^2$ and ${}^3\sigma\sigma^*$, are diradical, while the two higher energy states, ${}^1\sigma\sigma^*$ and ${}^1\sigma^{*2}$, are zwitterionic in nature. In the diradical states each orbital is half filled, while in the zwitterionic state the electrons are spin paired. The lower energy diradical, ${}^1\sigma^2$, corresponds to two electrons spin paired in bonding orbitals and ${}^3\sigma\sigma^*$ has one electron each in a bonding and antibonding orbital with parallel

spins. The lower energy zwitterion, ${}^{1}\sigma\sigma^{*}$, has paired electrons in a bonding and antibonding orbital, while ${}^{1}\sigma^{*2}$ has a doubly occupied antibonding orbital. Zwitterions are by definition singlet excited states and are localized on one center. The problem with identifying zwitterionic excited states in σ and π manifolds, is that the states are not stable. It is difficult to stretch a σ bond to a stable configuration for spectroscopic investigation. Inevitably the excitation places the system on a dissociative surface and the molecule dissociates. Similarly, it is difficult to twist an olefin and trap it in its 90° configuration. This has led the Nocera group to consider δ bonds as the place to find the zwitterionic excited states. Ironically, the weakly coupled orbitals necessary for the formation of this excited state are found in complexes with some of the shortest M–M bond distances, quadruple bond complexes.³⁷

E. Quadruply Bonded Bimetallic Complexes

The qualitative molecular orbital diagram for the D_{4h} symmetry M_2L_8 complexes is shown in Figure 1.9. Two ML_4 fragments are brought together to form a σ (d_{z^2}), two π (d_{xz} , d_{yz}), and a δ (d_{xy}) bond. Each metal is d^4 leading to four M-M bonds. The lowest energy transition is between the highest occupied molecular orbital, δ , and the lowest unoccupied molecular orbital, δ^* , and corresponds to $delta \to delta$. The next highest energy transitions are $delta \to delta$ and $delta \to delta$.

While the molecular orbital scheme is conceptually appealing, several observations imply that it may not be an accurate description. The spectroscopy of M-4-M and M-3.5-M, the one electron oxidized quadruple bond, is not consistent with the MO scheme. Consider the energy of the δ to δ^* transitions of the

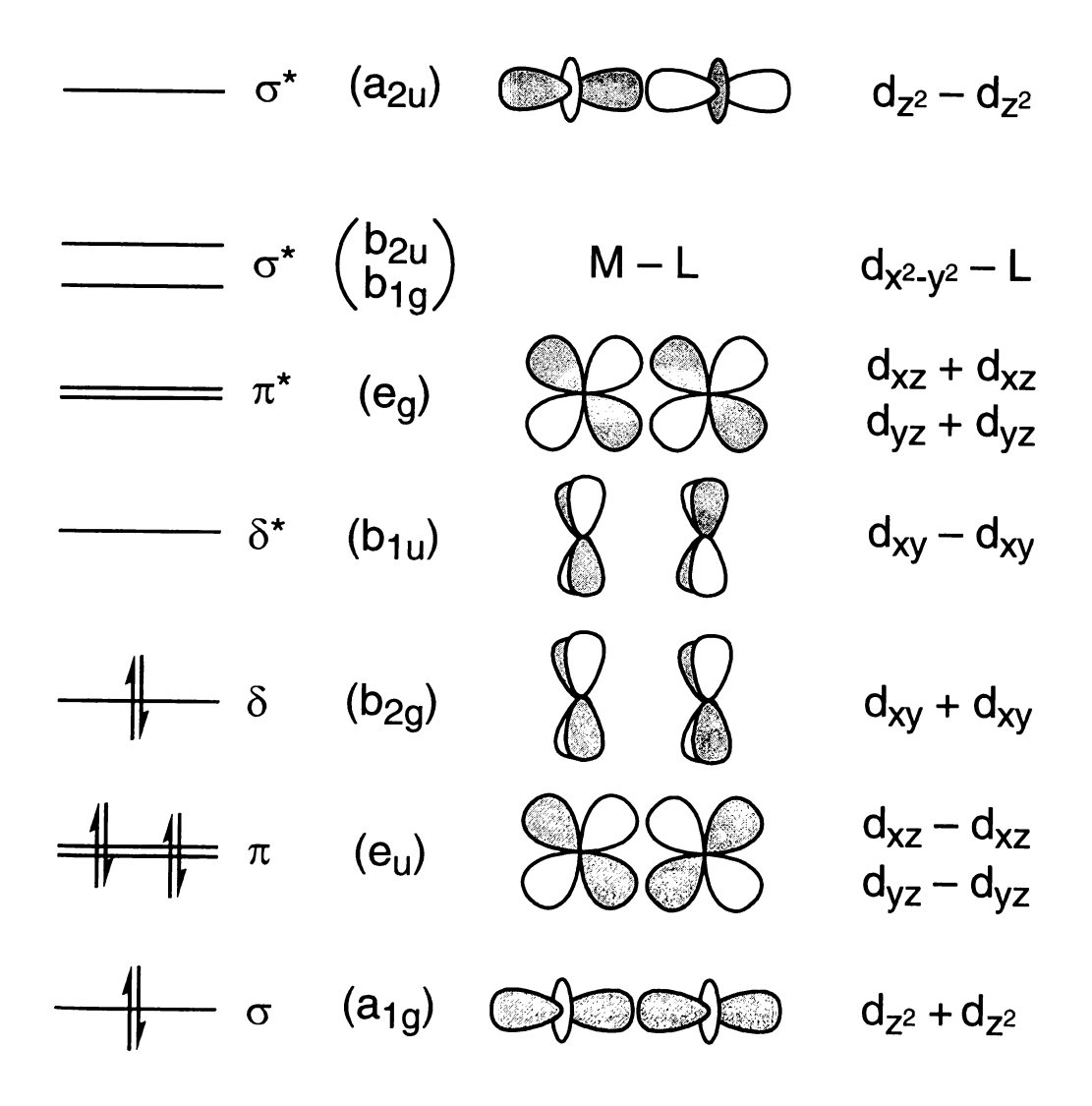


Figure 1.9 Qualitative molecular orbital diagram for M_2L_8 quadruply bonded bimetallic complexes.

compounds in Table 1.1.³⁸ $^{1}(\delta \rightarrow \delta^{*})$ and $^{2}(\delta \rightarrow \delta^{*})$ denote transitions for M-4-N and M-3.5-M, respectively. The latter transition is consistently red shifted, by a much as 12,280 cm⁻¹ for the Mo₂(SO₄)₄^{4-/3-} couple. To a first approximation, by an MO description, these transitions should be equivalent. Additionally, SCF-X α -SW calculations of the δ/δ^{*} splitting (Δ W(calc) in Table 1.1) are approximately equal to the experimental $^{2}(\delta \rightarrow \delta^{*})$ values.³⁸ These results indicate that the one electron energy, Δ W (δ - δ^{*} splitting), contributes less significantly than the two electron energy (Coulomb and exchange) in the δ manifold.

Table 1.1 $\delta \rightarrow \delta^*$ Electronic Transition Energies For Selected Quadruply Bonded Bimetallic Complexes

	·		
compound	$^{1}(\delta \rightarrow \delta^{*}) / \text{cm}^{-1}$	$^{2}(\delta \rightarrow \delta^{*}) / \text{cm}^{-1}$	Δ W(calc) / cm ⁻¹
$Mo_2(O_2CPr^n)^{0/+}$	22,700	13,300	12,200
$Mo_2(SO_4)_4^{4-/3}$	19,420	7140	_
$Mo_2Cl_4(PMe_3)_4$	17,090		8390
$W_2Cl_4(PMe_3)_4^{0/+}$	15,150	7350	7340

Moreover, the d(W–W) is, on average, only 0.12 Å longer than that for the Mo_2 complexes.³⁷ The larger radial extension of the W d_{xy} orbitals should compensate for the marginal increase in the distance and a blue shift in the ${}^1(\delta\delta^*)$ transition might be expected. However, a significant red shift is observed in going from Mo to W. Additionally, the absorption intensity of the ${}^1(\delta\delta^*)$ transition is low, with an extinction coefficient (ϵ) of about 1 x 10³ M⁻¹cm⁻¹, while other meta

localized transitions are an order of magnitude higher $(Mn_2(CO)_{10} \ \epsilon_{max} \sim 10^4 \ M^{-1} \ cm^{-1})$. The oscillator strength, which is proportional to the extinction coefficient for that transition, can be related to the square of the overlap of the orbitals. Finally, the stabilization due to the δ bond has been calculated to be worth about $10 \ kcal/mol$. The red shift of the $W_2 \ \delta \delta^*$ as compared to the $Mo_2 \ \delta \delta^*$ transition, the low intensity of the absorbance of the $\delta \delta^*$ transition, and the small amount of stabilization due to the δ bond all point to poor overlap of the d_{xy} orbitals.

Owing to this weak overlap of the d_{xy} orbitals and the failure of MO theory to predict the energy of ${}^{1}(\delta \rightarrow \delta^{*})$, valence bond theory gives a better description of the transitions involving the δ and δ^* orbitals. Figure 1.10 shows the experimentally determined state diagram for Mo₂Cl₄(PMe₃)₄. In the ground state, one electron is localized on each metal, giving an ¹A_{1g} state. This correlates with the δ^2 state of the molecular orbital model. ³¹P NMR spectroscopy ⁴¹ and magnetic susceptibility measurements⁴² show that the ${}^{3}A_{2u}$ state lies 4840 cm ${}^{-1}$ above the ¹A_{1g} state. In a valence bond model these states can be considered diradicals. Thus their splitting is small when the electrons are in orbitals that are weakly coupled, as is the case for the situation here. At higher energy are the ${}^{1}A_{2u}$ and ${}^{1}A_{1g}$ states corresponding to the ${}^{1}(\delta\delta^{*})$ and ${}^{1}(\delta^{*}\delta^{*})$ states, respectively. The ${}^{1}A_{2u}$ and ${}^{1}A_{1g}$ states lie high in energy because two electrons are paired in the confined volume of an "atomic-like" orbital. Thus the population of the ${}^{1}(\delta\delta^*)$ excited state corresponds to charge transfer from one metal center to another. The energy separation of the ¹A_{2u} and ¹A_{1g} excited states has recently been measured by twophoton spectroscopy⁴³ to be 4800 cm⁻¹ apart thereby confirming the zwitterionic

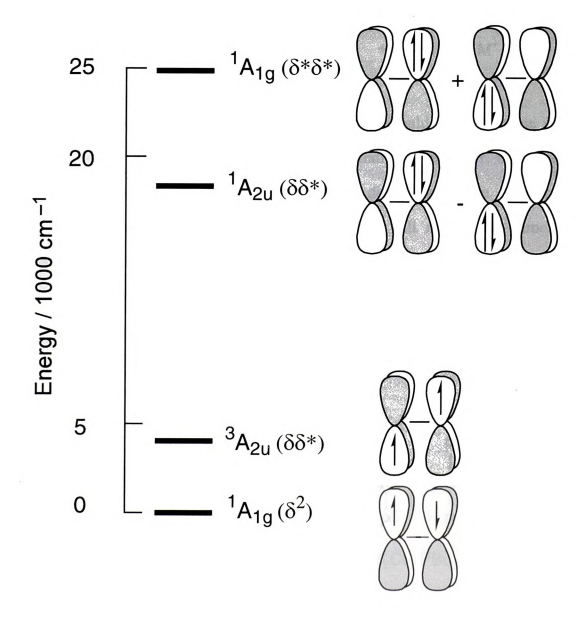


Figure 1.10 State diagram for the $\delta\delta^*$ manifold of $Mo_2Cl_4(PMe_3)_4$.

nature. The transition can be formally written as the linear combination shown below:

$$M \stackrel{hv}{=} M \stackrel{hv}{\longrightarrow} ^+M \stackrel{}{\longrightarrow} M^- M^- + ^-:M \stackrel{}{\longrightarrow} M^+$$

As a result of the linear combination, there should be no electric dipole moment because each ion pair will contribute equally. If, however, the molecule loses its inversion center by a low symmetry distortion in the coordination environment, then the contribution from each pair will not be the same. The transient absorption spectrum of $W_2Cl_4(PBu_3)_4$ in CH_2Cl_2 suggests that intramolecular distortion may trap the zwitterionic state.⁴⁴ The excited state absorption ($\lambda_{exc} = 355$ nm) of $W_2Cl_4(PBu_3)_4$ is remarkably similar to the ground state absorbance of $W_2Cl_6(PBu_3)_4$. A high energy intermediate based on this is proposed below:⁴⁵

Upon MMCT excitation, there is an increase in charge at one metal center and a decrease at the other. The Cl⁻ ligands shift towards the decreased electron density in order to balance the charge shift. This chemical distortion opens up a coordination site on the metal center where a pair of electrons are proposed to reside. The low symmetry distortion, which traps the zwitterion, is attractive

because it offers a site for multielectron activation of substrate via the $^1\delta\delta^*$ excited state for multielectron photochemistry. Aside from the zwitterionic nature of the excited state, the M-4-M complexes are coordinatively unsaturated allowing substrate activation without dissociation of a ligand, the metal centers are electron rich to reduce substrates, and metal-metal cleavage is less likely due to the quadruple bond. All of these features suggest that the M-4-M complexes are attractive multielectron reagents. This is the basic tenet that will be investigated in this thesis.

F. Photochemistry

Photochemical studies of quadruply bonded bimetallic complexes began in our group with a M-4-M core strapped by four bridging ligands. Visible irradiation ($\lambda > 546$ nm) of Mo₂[O₂P(OPh)₂]₄ leads to the two electron reduction of saturated dihalocarbons to olefins.⁴⁶ This reaction has also been generalized to unsaturated dihalocarbons.⁴⁷ As summarized in Figure 1.11, the reaction proceeds through one electron, chlorine abstraction intermediates, producing the mixed-valence photoproduct, Mo₂(II,III)[O₂P(OPh)₂]₄Cl. The two electron oxidized species, Mo₂(III,III)[O₂P(OPh)₂]₄Cl₂, is not observed because the rigid coordination sphere can not accommodate the increased charge at the metal center. Thus, the zwitterionic excited state can not be trapped due to the bulky bidentate ligand.

By utilizing a more flexible coordination sphere, the first example of photoinduced concerted two electron oxidation of a quadruply bonded bimetallic complex was observed.⁴⁸ Irradiation ($\lambda > 435$ nm) of MeI solutions of

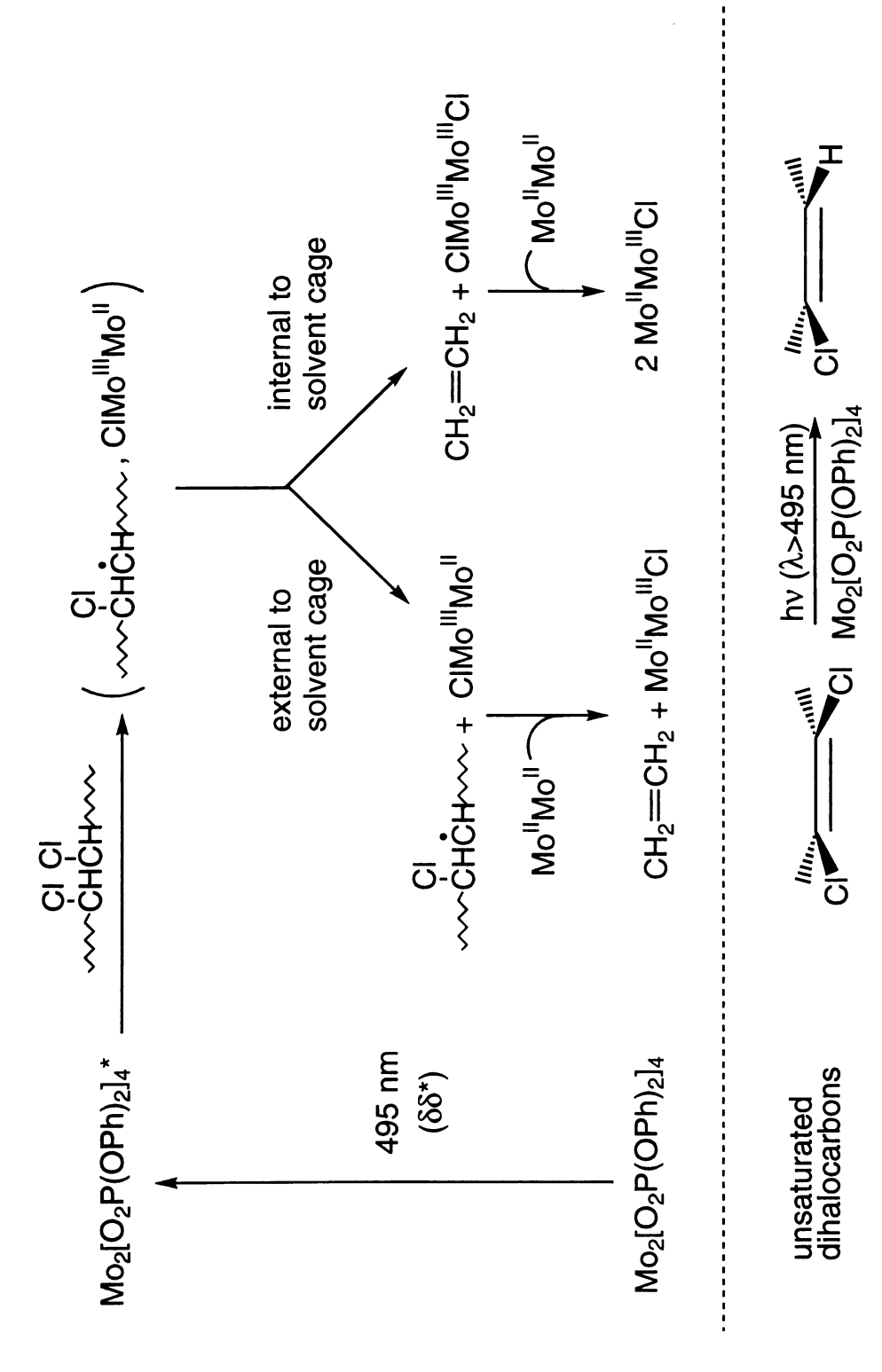


Figure 1.11 Proposed mechanism for photochemical reduction of 1,2-dihalocarbons by Mo₂[O₂P(OPh)₂]₄.

oxidative addition $W_2Cl_4(dppm)_2$ reacts cleanly the product, to W₂Cl₄(dppm)₂(Me)(I). This reaction progresses with wavelengths coincident with the $\pi\delta^*$ state, ⁴⁹ which lies just to lower energy of $\delta\delta^*$. In order to reach the distorted intermediate, excess energy must be used to weaken the M-M π bonds so they are available for bonding with the bridging Cl⁻ ligands. Figure 1.12 summarizes the similarities between the W₂Cl₄(dppm)₂ photochemistry and the thermal chemistry of Vaska's complex, Ir(CO)(PR₃)₂Cl.⁵⁰ Both are d⁴ metals in a square planar coordination sphere with open coordination sites, which form complexes with octahedral geometries upon reaction. Both react with MeI to form the two electron oxidative addition products. Vaska's complex reacts with longer chain alkyl groups, such as EtI, to form the one electron product, $Ir(CO)(PR3)_2(CI)(I)_2$. Likewise, $W_2CI_4(dppm)_2(I)_2$ and $W_2CI_5(dppm)_2(I)$ are observed with EtI, which are indicative of a radical mechanism.

G. Thesis Outline

The discovery of the two electron mixed valence excited state in the d^4-d^4 quadruply bonded bimetallic systems presents the possibility of discrete multielectron transformations. The $^1(\delta\delta^*)$ excited state of M-4-M complexes is, in general, sufficiently long lived (τ ~100 ns) for bimolecular photochemistry. Chapter 2 gives the experimental details of all the reactions and Chapter 3 generalizes the photochemistry of $W_2Cl_4(dppm)_2$ to dialkyl/diaryl disulfides. Photoreaction with dialkyl/diaryl disulfides proceeds upon excitation with visible light to two electron products.

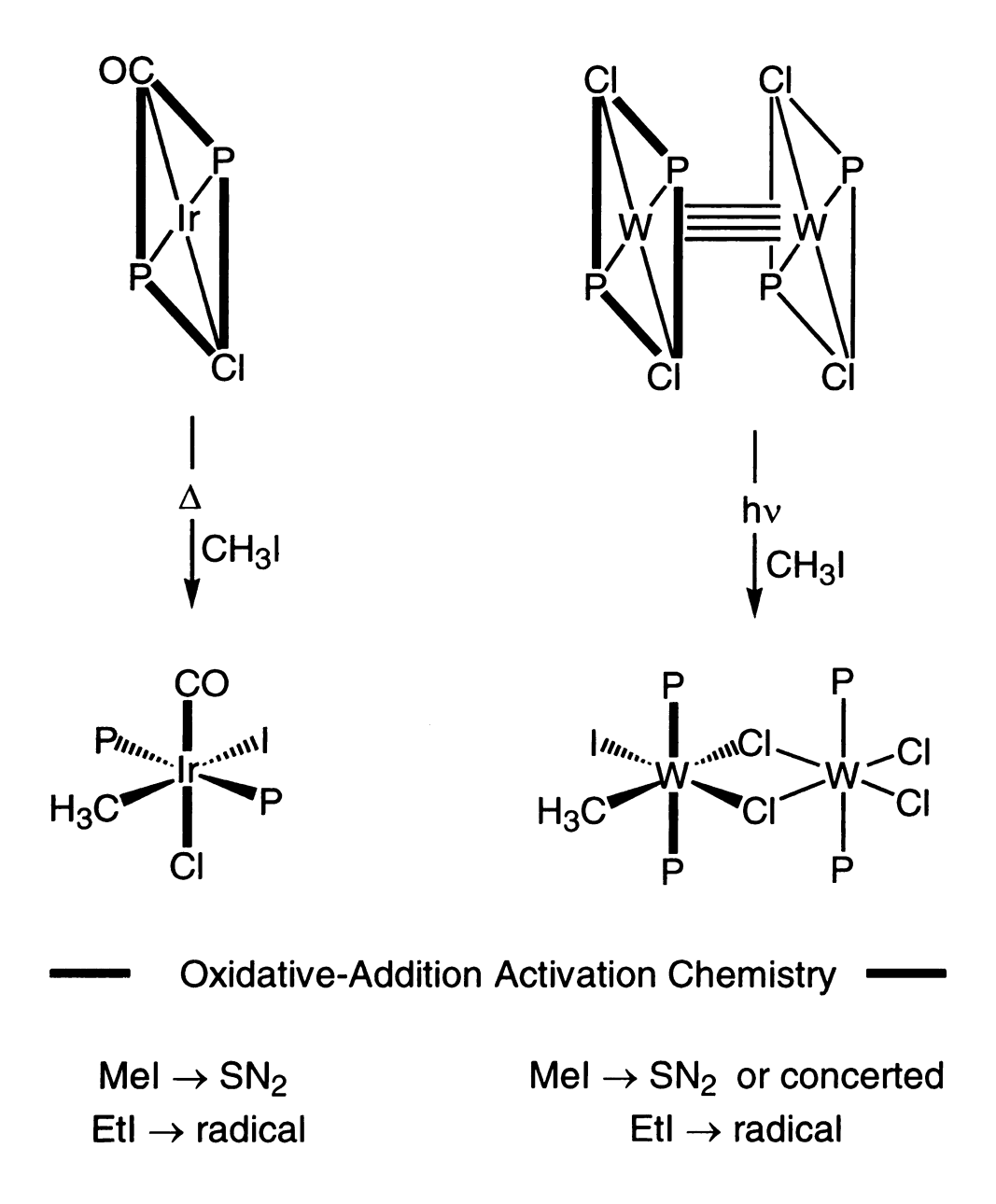


Figure 1.12 A comparison of the photochemistry of $W_2Cl_4(dppm)_2$ and the thermal chemistry of Vaska's complex for the oxidative addition of alkyl iodides.

Chapter 4 presents work on atom transfer photochemistry of the M-4-M complexes, W2Cl4(dppm)2 and MoWCl4(PMe2Ph)4. The first half of the Chapter focuses on the photochemistry of W₂Cl₄(dppm)₂ and N₂O. As shown in Chapter 3, upon excitation, this complex forms a high energy intermediate with two electrons localized on one W metal center. In order to access this excited state of W₂Cl₄(dppm)₂, the complex must undergo intramolecular distortion to form the structure proposed previously. Energy is wasted through the process of rearranging the chloride ligands and therefore the excited state is not as energetic as might be expected. As a result, the excited state of this complex is limited to the oxidative addition chemistry that is typical of MeI and RSSR.⁵¹ Furthermore, atom transfer photochemistry with N₂O is not observed. A more efficient way to trap the excited state is to build asymmetry into the ground state by using mixed metal quadruply bonded complexes. The second half of Chapter 4 presents the sulfur atom transfer photochemistry of MoWCl₄(PMe₂Ph)₄. This system uses lower excitation energy to create MoWCl₄(PMe₂Ph)₄*, which is used to cleave the Ph₃P-S bond. This bond is substantially stronger than previous substrates (Ph₃P-S: 92 kcal/mol; ⁵² Me-I: 56 kcal/mol;⁵³ PhS-SPh: 55 kcal/mol;⁵⁴ EtS-SEt: 74 kcal/mol;⁵⁴ N₂O: 34 kcal/mol⁵⁵).

In Chapter 5, a systematic study of the photophysics of $M_2Cl_4P_4$ (M = Mo, W, MoW; P = PMe₂Ph, PMe₃) will be discussed. Temperature dependent absorption, emission and lifetime measurements have been undertaken. With this, the nonradiative decay processes can be studied to gain a better understanding of the deactivation of the excited state. It may be possible to predict the reactivity of these complexes and better design a system capable of a catalytic energy cycle with enough understanding of the excited states.

H. References

- 1. Stryer, L. Biochemistry; W. H. Freeman: New York, 1988; Ch 22.
- 2. Orme-Johnson, W. H. Science 1992, 257, 1639.
- 3. (a) Lui, S. M.; Soriano, A.; Cowan, J. A. J. Am. Chem. Soc. 1993, 115, 10483.
- (b) Lui, S. M.; Liang, W; Soriano, A.; Cowan, J. A. J. Am. Chem. Soc. 1994, 116, 4531.
- 4. Adams, M. W.; Mortenson, L. E. In Molybdenum Enzymes; Spiro, T. G.,
- Ed.; Wiley-Interscience: New York, 1985; pp 519-593.
- 5. Balzani, V.; Moggi, L.; Scandola, F. In Supramolecular Photochemistry; Balzani, V., Ed.; D. Reidel: Boston, 1987; pp 1-28.
- 6. Hoganson, C. W.; Babcock, G. T. In Metal Ions in Biological Systems; Sigel,
- H.; Sigel, A., Eds.; Dekker: New York, 1994; Vol. 30, pp 77-107.
- 7. Graige, M. S.; Paddock, M. L.; Bruce, J. M.; Feher, G.; Okamura, M. Y. J. Am. Chem. Soc. 1996, 118, 9005.
- 8. Burgess, B. K.; Lowe, D. J. Chem. Rev. 1996, 96, 2983.
- 9. Jolly, J. L. The Inorganic Chemistry of Nitrogen; Benjamin: New York, 1964.
- 10. (a) Georgiadis, M. M.; Komiya, H.; Chakrabarti, P.; Woo, D.; Kornuc, J. J.;
- Rees, D. C. Science 1992, 257, 1653. (b) Bolin, J. T.; Ronco, A. E.; Morgan, T. V.;
- Mortenson, L. E.; Xuong, N.-H. Proc. Natl. Acad. Sci. U. S. A. 1993, 90, 1078.
- 11. (a) Marcus, R. A.; Sutin, N. Biochem. Biophys. Acta. 1985, 811, 265. (b)
- Connelly, J. S.; Bolton, J. R. In *Photoinduced Electron Transfer*; Fox, M. A., Chanon, M. Eds.; Elsevier: Amsterdam, **1988**; Part D, pp 303-393.
- 12. Slama-Schwok, A.; Ottolenghi, M.; Avnir, D. Nature 1992, 335, 240.
- 13. Villemure, G.; Detellier, C.; Szabo, A. G. J. Am. Chem. Soc. 1986, 108, 4658.

- 14. Dürr, H.; Trierweiler, H.-P.; Willner, I.; Maidan, R. New. J. Chem 1990, 14, 317.
- 15. Ohtani, B.; Ye, M.; Miyadzu, H.; Nishimoto, S.; Kagiya, T. J. Photochem. Photobiol. A: Chem. 1991, 56, 359.
- 16. Cusack, L.; Rao, S. N.; Fitzmaurice, D. Chem. Eur. J. 1997, 3, 202.
- 17. Krueger, J. S.; Mayer, J. E.; Mallouk, T. E. J. Am. Chem. Soc. 1988, 110, 8232.
- 18. Vermeulin, L. A. In *Progress in Inorganic Chemistry*; Meyer, G. J. Ed.; John Wiley and Sons: New York, 1997; Vol 44, pp 143-166.
- 19. (a) Meyer, T. J. Acc. Chem. Res. 1978, 11, 94. (b) Adamson, A. W.; Gafney, H.D. J. Am. Chem. Soc. 1972, 94, 8238.
- 20. (a) Meyer, T. J. Acc. Chem. Res. 1989, 22, 163. (b) Surridge, N. A.; McClanahan, S. F.; Hupp, J. T.; Danielson, E.; Gould, S.; Meyer, T. J. J. Phys. Chem. 1989, 93, 294. (c) Surridge, N. A.; Hupp, J. T.; McClanahan, S. F.; Gould, S.; Meyer, T. J. J. Phys. Chem. 1989, 93, 304.
- 21. Roundhill, D. M. *Photochemistry and Photophysics of Metal Complexes*; Plenum: New York, 1994.
- 22. Kunkely, H.; Vogler, A. Inorg. Chem. 1995, 34, 2468.
- 23. Roundhill, D. M.; Gray, H. B.; Che, C.-M. Acc. Chem. Res. 1989, 22, 55.
- 24. (a) Sigal, I. S.; Mann, K. R.; Gray, H. B.; J. Am. Chem. Soc. 1980, 102, 7252.
- (b) Miskowski, V. M.; Sigal, I. S.; Mann, K. R.; Gray, H. B.; Midler, S. J.; Hammond, G. S.; Ryanson, P. R. J. Am. Chem. Soc. 1979, 101, 4383.
- 25. (a) Che, C.-M.; Kwong, H.-L.; Yam, V. W.-W.; Cho, K.-C J. Chem. Soc. Chem. Comm. 1989, 885. (b) Che, C.-M.; Kwong, H.-L.; Poon, C.-K.; Yam, V. W.-W. J. Chem. Soc. Dalton Trans. 1989, 3215.

- 26. Yip, H.-K; Lin, H.-M. Cheung, K.-K., Che, C.-M.; Wang, Y. *Inorg. Chem.* **1994**, *33*, 1644.
- 27. Wrighton, M. S.; Graff, J. L.; Luong, J. C.; Rechel, C. L.; Robbins, J. L. In *Reactivity of Metal-Metal Bonds*; Chisholm, M. H., Ed.; ACS Symposium Series 155; American Chemical Society: Washington DC, 1981; pp 85-110.
- 28. Wrighton, M.; Bredesen, D. J. Organomet. Chem. 1973, 50, C35.
- 29. (a) Balzani, V.; Carassiti, V. Photochemistry of Coordination Compounds, Academic: New York, 1970. (b)Geoffroy, G. L.; Wrighton, M. S. Organometallic Photochemistry; Academic: New York, 1979. (c) Wrighton, M. S.; Ginley, D. S. J. Am. Chem. Soc. 1975, 95, 2065.
- 30. (a) Nieckarz, G. F.; Weakley, T. J. R.; Miller, W. K.; Miller, B. E.; Lyon, D. K.; Tyler, D. R. *Inorg. Chem.* **1996**, *35*, 1721. (b) Male, J. L.; Davis, H. B.; Pomeroy, R. K.; Tyler, D. R. *J. Am. Chem. Soc.* **1994**, *116*, 9353. (c) Avey, A.; Weakley, T. J. R.; Tyler, D. R. *J. Am. Chem. Soc.* **1993**, *115*, 7706. (d) Mao, F.; Tyler, D. R.; Bruce, M. R. M.; Bruce, A. E.; Rieger, A. L.; Rieger, P. H. *J. Am. Chem. Soc.* **1992**, *114*, 6418.
- 31. Levenson, R. A.; Gray, H. B. J. Am. Chem. Soc. 1975, 97, 6042.
- 32. (a) Steigman, A. E.; Tyler, D. R. Acc. Chem. Res. 1984, 17, 61. (b) Steigman, A. E.; Tyler, D. R. J. Am. Chem. Soc. 1982, 104, 2944.
- 33. Turro, N. J. Modern Molecular Photochemistry; University Science Books: Sausalito, California, 1991; pp 215-221.
- 34. Mulliken, R. S. Phys. Rev. 1932, 41, 75.
- 35. (a) Mulliken, R. S. Phys. Rev. 1936, 50, 1017. (b) Coulson, C. A.; Fischer, I. Philos. Mag. 1949, 40, 386.

- 36. (a) Zewail, A. H. Science 1988, 242, 1645. (b) Rosker, M. J.; Dantus, M.; Zewail, A. H. Science 1988, 241, 1200.
- 37. Cotton, F. A.; Walton, R. A. Multiple Bonds Between Metal Atoms; Clarendon: Oxford, 1993; p 632.
- 38. Hopkins, M. D.; Gray, H. B.; Miskowski, V. M. Polyhedron 1987, 6, 705.
- 39. Zietlow, T. C.; Hopkins, M. D.; Gray, H. B. J. Solid St. Chem. 1985, 59, 112.
- 40. Mulliken, R. S. J. Chem. Phys. 1939, 7, 20.
- 41. (a) Cotton, F. A.; Eglin, J. L.; Hong, B.; James, C. A. Inorg. Chem. 1993, 32,
- 2104. (b) Cotton, F. A.; Eglin, J. L.; Hong, B.; James, C. A. J. Am. Chem. Soc. 1992, 114, 4915.
- 42. Hopkins, M. D.; Zietlow, T. C.; Miskowski, V. M.; Gray, H. B. J. Am. Chem. Soc. 1985, 107, 510.
- 43. Engebretson, D. S.; Zaleski, J. M.; Leroi, G. E.; Nocera, D. G. Science 1994, 265, 759.
- 44. Partigianoni, C. M.; Turró, C.; Shin, Y.-g. K.; Motry, D. H.; Kadis, J.; Dulebohn, J. I.; Nocera, D. G. In *Mixed Valency Systems: Applications in Chemistry, Physics and Biology*; Prassides, K., Ed.; NATO ASI Series C: Mathematical & Physical Sciences; Kluwer Academic: Dordrecht, 1991; Vol. 343, pp 91-106.
- 45. Winkler, J. R.; Nocera, D. G.; Netzel, T. L. J. Am. Chem. Soc. 1986, 108, 4451.
- 46. Chang, I-J.; Nocera, D. G. Inorg. Chem. 1989, 28, 4309
- 47. Hsu, T.-L. C.; Chang, I-J.; Nocera, D. G. Inorg. Chem 1994, 33, 2932.

- 48. (a) Partigianoni, C. M.; Nocera, D. G. *Inorg. Chem.* **1990**, 29, 2033. (b) Partigianoni, C. M.; Turró, C.; Hsu, T.-L. C.; Chang, I-J.; Nocera, D. G. In *Photosensitive Metal-Organic Systems*; Kutal, C., Serpone, N., Eds.; Advances in Chemistry 238; American Chemical Society: Washington, DC, 1993; pp 147-163.
- 49. Hay, P. J. J. Am. Chem. Soc. 1982, 104, 7007.
- 50. (a) Nocera, D. G. Acc. Chem. Res. 1995, 28, 209. (b) Nocera, D. G. J. Clust. Sci. 1994, 5, 185.
- 51. Collman, J. P.; Hegedus, L. S.; Norton, J. R.; Finke, R. G. *Principles and Applications of Organotransition Metal Complexes*; University Science Books: Mill Valley, California, 1987; Ch 5.
- 52. (a) Chernick, C. L.; Pedley, J. B.; Skinner, H. A. J. Am. Chem. Soc. 1957, 79, 1851. (b) Hall, K. A.; Critchlow, S. C.; Mayer, J. M. Inorg. Chem. 1994, 33, 3593.
- 53. Streitweiser, A. Jr; Heathcock, C. H. *Introduction to Organic Chemistry*, 3rd ed.; Macmillan: New York, 1985.
- 54. Benson, S. W. Chem. Rev. 1978, 78, 23.
- 55. Holm, R. H.; Donahue, J. P. Polyhedron 1993, 12, 571.

CHAPTER 2

EXPERIMENTAL

A. General Procedures

All manipulations were carried out under an argon atmosphere of a Vacuum Atmosphere drybox or the manifold of a Schlenk line. Molybdenum (V) chloride, (Mo₂Cl₁₀, Aldrich Chemicals), tungsten (VI) chloride (WCl₆, Aldrich Chemicals), and tungsten (IV) chloride (WCl₄) were purified by sublimation. Monodentate phosphines (trimethyl phosphine (PMe₃), dimethylphenyl phosphine (PMe₂Ph), methyldiphenyl phosphine (PMePh₂), tributyl phosphine (PBu₃)), triphenyl phosphine sulfide (Ph₃PS) and antimony sulfide (Sb₂S₃) were purchased from Strem Chemicals, triphenyl phosphine (Ph₃P) was purchased from Baker, diphenyl disulfide (PhSSPh), diethyl disulfide (EtSSEt), chlorotrimethyl silane (Me₃SiCl), and bis(diphenylphosphino)methane (dppm) were purchased from Aldrich Chemicals. All chemicals were reagent grade and used as received, except PhSSPh and EtSSEt. PhSSPh was recrystallized from benzene and dried in vacuo and EtSSEt was dried over activated 4 Å sieves. Nitrous oxide (N₂O, Purity Cylinder Gases) was breathing quality and oxygen was removed by freezing the N₂O in liquid nitrogen and removing O₂ in vacuo.

Solvents used for synthesis were dried by general procedures.² Benzene (C_6H_6) , toluene and tetrahydrofuran (THF) were refluxed over Na/benzophenone

ketyl. Hexanes, dichloromethane (CH₂Cl₂) and acetonitrile (CH₃CN) were refluxed over CaH₂. PMe₃, PMe₂Ph, PMePh₂ and PBu₃ were stored in flasks with Kontes quick-release valves. Benzene, toluene, THF, 2-methyltetrahydrofuran, 2-MeTHF, and 2-methylpentane for transfer on the high vacuum manifold were stored over NaK/benzophenone ketyl in flask with Kontes quick-release valves.

B. Synthesis

1. Homonuclear Molydenum and Tungsten Complexes

a. $Mo_2Cl_4(PR_3)_4$ $(PR_3 = PMe_3, PMe_2Ph, PMePh_2)^3$

K₄Mo₂Cl₈ or (NH₄)₅Mo₂Cl₉ (0.5 g, 0.807 mmol) and four equilavents of PR₃ were refluxed in methanol for 5 hours until a blue precipitate formed. The blue crystals were filtered in the air and washed with water, methanol, and diethyl ether and dried in vacuo. Mo₂Cl₄(PR₃)₄ was then purified on a Florisil column under argon with CH₂Cl₂ as the eluent. This was characterized by UV-vis, ¹H and ³¹P{¹H} NMR.

b. $W_2Cl_4(PR_3)_4$ $(PR_3 = PR_3 = PMe_3, PMe_2Ph, PMePh_2, PBu_3)^4$

WCl₄ (2.6 g, 8 mmol) was added to 0.5% Na/Hg amalgam in THF in a dry ice/acetone bath. This was followed by 4 equivalents of PR₃. The solution was allowed to warm slowly by replacing the dry ice/acetone bath with a dry ice/acetonitrile bath, an ice bath and finally allowed to warm to room temperature. The dark blue-green solution was filtered through Celite and the THF removed. The oily residue was extracted with hexanes in the air. The solution was filtered and the volume reduced. MeOH was added and a blue-green precipitate formed.

This was dried overnight under vacuum and characterized by UV-vis, ¹H and ³¹P{¹H} NMR.

c. $W_2Cl_4(dppm)_2^5$

 $W_2Cl_4(PBu_3)_4$ (2.6 g, 2.0 mmol) and dppm (1.5 g, 4.0 mmol) were refluxed in a 40/60 mixture of hexanes/toluene for 4 hours. The solution was allowed to cool and a brown crystalline precipitate formed. This was filtered and washed with hexanes. The solid was dried overnight under a flow of argon and brought into the drybox. UV-vis (C_6H_6 , nm): $\lambda_{max} = 740$, 508, 370. ¹H NMR (C_6D_6 , ppm): 7.62 (s), 6.83 (t), 5.15 (t).

d. W₂Cl₆(dppm)₂⁶

 $W_2Cl_4(dppm)_2$ was dissolved in CH_2Cl_2 and stirred at room temperature for several days. The solvent was removed to give $W_2Cl_6(dppm)_2$. ¹H NMR (CD_2Cl_2 , ppm): δ 8.0-7.0 (m, 40H); 3.85 (t, 4H). ³¹P{¹H} NMR (CD_2Cl_2 , ppm): δ -106 (br). UV-vis (CH_2Cl_2 , nm): 822, 465, 384.

e. W₂Cl₄(dppm)₂(SPh)₂

 $W_2Cl_4(dppm)_2$ (0.1 g, 78 µmol) and PhSSPh (0.02 g, 92 µmol) were dissolved in 25 ml of toluene and gently heated for a half hour. The solution changed from brown to dark maroon. $W_2Cl_4(dppm)_2(SPh)_2$ was precipitated by the addition of hexanes and filtered. UV-vis (CH₂Cl₂, nm): 730, 504. FAB/MS (amu): 1496 ($W_2Cl_4(dppm)_2(SPh)_2$), 1387 ($W_2Cl_4(dppm)_2(SPh)_2$).

$f. W_2Cl_5(dppm)_2(SEt)$

W₂Cl₄(dppm)₂ (0.048 g, 37.6 μmol) and EtSSEt (0.011 g, 89 μmol) were dissolved in toluene and heated to produce a red-brown solution. A mixture of

 $W_2Cl_5(dppm)_2(SEt)$ and $W_2Cl_4(dppm)_2$ was isolated as above. FAB/MS (amu): 1373 ($W_2Cl_5(dppm)_2(SEt)$), 1347 ($W_2Cl_6(dppm)_2$), 1312 ($W_2Cl_5(dppm)_2$).

2. Heteronuclear Molybdenum-Tungsten Complexes

a. Mo(⁶η-PhPMePh)(PMePh₂)₃⁷

A THF/ PMePh₂ (6.7 g, 33 mmol) solution was bubbled with Ar in a three neck round bottom flask with activated Mg (3.5 g, 0.15 mol) turnings in a side arm. The Mg was activated proir to use with I₂. This was placed in an ice bath and Mo₂Cl₁₀ (2.0 g, 7.3 mmol) was added via a Shlenk flask. Mg was added over the course of an hour. The solution was allowed to warm slowly to room temperature producing an orange-red solution over the course of 2 hours. The solution was filtered through Celite and concentrated. MeOH was added and an orange solid precipitated. This was washed with MeOH to remove any excess phosphines and dried under a flow of Ar. Mo(⁶η-PhPMePh)(PMePh₂) was recrystallized by dissolving in benzene, filtering through Celite and precipitating with MeOH. This compound is extremely air and moisture sensitive and better yields can be obtained by avoiding the use of a vacuum when filtering. (Note: Ar is necessary since $Mo(^6n-PhPMePh)(PMePh_2)_3$ reacts with N_2 .) ¹H NMR (C_6D_6 , ppm): δ 7.3-7.0 (m, 30H, Ph_2MeP); 4.4 (s, 1H, $^6\eta$ -Ph-PMePh); 4.2 (s, 2H, $^6\eta$ -Ph-PMePh); 3.7 (s, 1H, $^{6}\eta$ -Ph-PMePh); 3.6 (s, 1H, $^{6}\eta$ -Ph-PMePh); 1.76 (s, 9H, Ph₂MeP); 1.2 (d, 3H, $^{6}\eta$ -Ph-PMePh); ${}^{31}P\{{}^{1}H\}$ NMR (C₆D₆, ppm): δ +36.1 (s, 3P, Ph₂MeP); -29.1 (s, 1P, ⁶η-Ph-PMePh).

b. Mo(⁶η-PhPMe₂)(PMe₂Ph)₃⁸

The experimental set up was the same as above, except that heat is required. Mo_2Cl_{10} (0.7 g, 13 mmol) was added to a THF solution of PMe_2Ph (1.8 g, 13 mmol) in an ice bath to give a green solution. The ice bath was removed and activated Mg (2.0 g, 82 mmol) added. The solution was heated at 70 °C for two hours. After 15 minutes the solution turned orange-brown. The solution was cooled, filtered through Celite and concentrated. MeOH was added and the solution stored at -20 °C for several hours to maximize precipitation. This was filtered and dried under a flow of Ar. As with the above compound, $Mo(^6\eta-PhPMe_2)(PMe_2Ph)_3$ is extremely air and moisture sensitive and it is best to avoid using the vacuum when filtering. Better yields can be obtained if glassware is flame-dried. 1H NMR (C_6D_6 , ppm): δ 7.5 (m, 6H, o- $PhMe_2P$); 7.3-7.2 (m, 9H, m,p- $PhMe_2P$); 4.0 (m, 2H, $^6\eta-PhPMe_2$); 3.4 (m, 1H, $^6\eta-PhPMe_2$); 3.2 (m, 2H, $^6\eta-PhPMe_2$); 1.5 (br, 18H, $PhMe_2P$); 1.0 (d, 6H, $^6\eta-PhPMe_2$). $^{31}P\{^1H\}$ NMR (C_6D_6 , ppm): δ + 15.8 (s, 3P, $PhMe_2P$); -46.7 (s, 1P, $^6\eta-PhPMe_2$).

c. WCl₄(PPh₃)₂⁹

The complex was prepared by the reduction of WCl₆ by amalgated mossy Zn. The Zn was prepared prior to use by reaction with HgO (0.2 g, 0.9 mmol) dissolved in hot 12M HCl (~2 ml). The Zn was filtered, washed with water and acetone and dried in the oven. Amalgated Zn (5.5 g, 84 mmol) was added to WCl₆ (6.6 g, 17 mmol) under argon. WCl₆ was dissolved in CH₂Cl₂ to produce a dark orange-red solution. Ph₃P (8.5 g, 32 mmol) was added slowly (~3 min) and the solution started to gently reflux and turn green producing an orange precipitate. The precipitate was filtered and the remaining Zn picked out under a flow of Ar.

The solid was washed with CH_2Cl_2 and dried under vacuum. ¹H NMR (C_6D_6 , ppm): 11.2 (d, 2H), 8.2 (t, 2H), 7.8 (t, 1H); ³¹P{¹H} NMR (C_6D_6 , ppm): 7.2 (s).

d. MoWCl₄(PMePh₂)₄¹⁰

A benzene solution of $Mo(^6\eta-PhPMePh)(PMePh_2)_3$ (0.1 g, 0.11 mmol) was added dropwise to a benzene solution of $WCl_4(PPh_3)_2$ (0.25 g, 0.3 mmol) in a glove bag inside of the dry box. This step is very sensitive to water and all glassware was flame-dried on a high vacuum manifold (10^{-5} torr). The benzene was predried over Na/benzophenone ketyl and stored over activated 4Å sieves. The bright green solution was filtered through Celite and the benzene removed in vacuo. This green residue was dissolved in toluene and filtered. The solution was concentrated and any additional $WCl_4(PPh_3)_2$ was removed by filtration. MeOH was added to precipitate a blue-green solid. This was filtered, washed with MeOH and dried in vacuo. UV-vis (C_6H_6 , nm): 650, 460, 320. ¹H NMR (C_6D_6 , ppm): δ 7.1-7.4 (m, 20H, Ph_2MeP); 1.79 (s, 6H, Ph_2MeP -W); 1.62 (s, 6H, Ph_2MeP -Mo). $^{31}P\{^1H\}$ NMR (C_6D_6 , ppm): δ +22.6 (t, $^{1}J_{WP}$ = 267 Hz); -12.4 (t, $^{2}J_{WP}$ = 95 Hz).

e. MoWCl₄(PMe₂Ph)₄¹¹

The procedure was the same as that for MoWCl₄(PMePh₂)₄. A benzene solution of Mo($^6\eta$ -PhPMe₂)(PMe₂Ph)₃ (120 mg, 0.185 mmol) was added dropwise to WCl₄(PPh₃)₂ (180 mg, 0.213 mmol) in benzene to yield MoWCl₄(PMe₂Ph)₄. UV-vis (C₆H₆, nm): 645 (ϵ = 1597 M⁻¹ cm⁻¹); 460 (ϵ = 205 M⁻¹ cm⁻¹); 320 (ϵ = 2663 M⁻¹ cm⁻¹). 1 H NMR (C₆D₆, ppm): δ 7.61 (m, p-*Ph*Me₂P–W); 7.16 (m, p-*Ph*Me₂P–Mo); 7.03 (s, o, m-*Ph*Me₂P–W); 6.91 (s, o, m-*Ph*Me₂P–Mo); 1.90 (t,

Ph Me_2 P-W); 1.82 (t, Ph Me_2 P-Mo). ³¹P{¹H} NMR (C₆D₆, ppm): δ +18.0 (t, ¹J_{WP} = 271 Hz); -19.4 (t, ²J_{WP} = 98 Hz).

f. MoWCl₄(PMe₃)₄¹⁰

PMe₃ (73.5 mg, 0.97 mmol) was added to a benzene solution of MoWCl₄(PMePh₂)₄ (146 mg, 0.120 mmol) on a high vacuum manifold. This was heated at 80 °C for 8 hours. PMe₂Ph, excess PMe₃ and the solvent were removed by heating at 55 °C under vacuum. The blue residue was dissolved in benzene and MeOH added. The resulting blue precipitate was filtered, washed with MeOH and dried under vacuum. UV-vis (C_6H_6 , nm): 634. ¹H NMR (C_6D_6 , ppm): δ 1.45 (q, 36H). ³¹P{¹H} NMR (C_6D_6 , ppm): δ +10.9 (t, ¹J_{WP} = 269 Hz); - 27.3 (t, ²J_{WP} = 97 Hz).

3. W(S)Cl₄(PMe₂Ph)

W(S)Cl₄(PMe₂Ph) was synthesized following a modified literature procedure. A mixture of WCl₆ (6g, 15 mmol) and Sb₂S₃ (1.7g, 5.1 mmol) was heated at 60 °C until a red molten liquid formed. This was dissolved in CS₂ (20 ml), S₈ (0.36g, 1.4 mmol) added and the mixture stirred. After about 10 minutes the red solution was filtered, washed with CS₂ and the solution concentrated in vacuo. Hexanes were added and the solution heated until most of the solids were dissolved. Any residual solids were filtered away from the solution and the solution cooled to room temperature. PMe₂Ph (3.1 ml, 22.4 mmol) was added slowly and an orange solid crashed out immediately leaving a clear solution. This was dissolved in benzene, filtered and the solvent removed. W(S)Cl₄(PMe₂Ph) was recrystallized by dissolving in benzene and inducing precipitation by the addition

of hexanes. ¹H NMR (C_6D_6 , ppm): δ 7.65 (m); 7.03 (m); 1.36 (d, ¹J_{PH} = 13 Hz); ³¹P{¹H} NMR (C_6D_6 , ppm): δ +30 (s). IR (C_6H_6 , cm⁻¹): 594 (m); 578 (m); 482 (w); 394 (w). GC (direct inlet, benzene, amu): 493. FAB/MS (C_6H_6 , amu): 751 (W(S)Cl₄(PMe₂Ph)•S₈); 494 (W(S)Cl₄(PMe₂Ph)).

4. Reactions of W₂Cl₄(dppm)₂

a. Photoreaction of W₂Cl₄(dppm)₂ with PhSSPh, EtSSEt

Toluene solutions of $W_2Cl_4(dppm)_2$ (0.035 g, 0.027 mmol) and a 20-fold excess of PhSSPh were photolyzed ($\lambda > 495$ nm, -10 °C) to completion in 45 minutes (for EtSSEt, 3 days at -20 °C), as determined by UV-vis spectroscopy. The solution was concentrated and the photoproduct precipitated by the addition of hexanes. The compound was further purified by chromatography on a Florisil packed column with CH_2Cl_2/CH_3CN as the eluent. The product was isolated in a 47% yield. In the case of PhSSPh, the FAB/MS and UV-vis were identicle to those of $W_2Cl_4(dppm)_2(SPh)_2$. TAB/MS (amu): 1496 ([M]⁺), 1419 ([M–C₆H₅]⁺), 1387 ([M–C₆H₅–S]⁺). UV-vis (toluene, nm): 730, 504. In the case of EtSSEt, the FAB/MS was identicle to that of $W_2Cl_6(dppm)_2$ and $W_2Cl_5(dppm)_2(SEt)$. FAB/MS (amu): 1378 ($W_2Cl_5(dppm)_2(SEt)$), 1348 ($W_2Cl_6(dppm)_2$), 1314 ($W_2Cl_5(dppm)_2$). No photoreaction is observed in the absence of substrate.

b. Thermal reactions of W₂Cl₄(dppm)₂ with PhSSPh, EtSSEt

 $W_2Cl_4(dppm)_2$ (0.05g, 0.04 mmol) and excess PhSSPh were dissolved in toluene, and the solution shielded from the light at -20 °C. The reaction was complete in 24 hours (for EtSSEt, 1 month), as monitored by UV-vis. The isolated product was shown to be $W_2Cl_4(dppm)_2(SPh)_2$ by FAB/MS and UV-vis. The

products for EtSSEt were shown to be W₂Cl₆(dppm)₂ and W₂Cl₅(dppm)₂(SEt) by FAB/MS.

c. Photoreaction of W₂Cl₄(dppm)₂ with N₂O

W₂Cl₄(dppm)₂ (8.7 mg, 6.8 μmol) was added to the absorption cell of the evacuable cell described in the photolysis section. THF was vacuum distilled to the bulb side on a high-vacuum manifold and O₂ rigorously removed. W₂Cl₄(dppm)₂ was dissolved in THF and isolated from the bulb by a Kontes valve. 1 atm of N₂O was transferred to the bulb on a high-vacuum manifold and O₂ removed. N₂O and the THF solution of W₂Cl₂(dppm)₂ were allowed to mix. Irradiation ($\lambda > 375$ nm, -80 °C) of this solution was complete after 1 week, as determined by UV-vis spectroscopy. The inorganic product was identified by UV-vis, ¹H and ³¹P{¹H} NMR and FAB/MS and is consistent with W₂Cl₆(dppm)₂. W₂Cl₆(dppm)₂: ¹H NMR (CD₂Cl₂, ppm): δ 8.0-7.0 (m, 40H); 3.85 (t, 4H). ³¹P{¹H} NMR (CD₂Cl₂, ppm): δ -109 (br). UV-vis (THF, nm): 822, 468, 387. FAB/MS (CH₂Cl₂, amu): 1348.

5. Reactions of MoWCl₄(PMe₂Ph)₄

a. Photoreaction of MoWCl₄(PMe₂Ph)₄ with Ph₃PS

MoWCl₄(PMe₂Ph)₄ (2.1 mg, 21 μ mol) was dissolved in benzene containing a two-fold excess of triphenyl phosphine sulfide and irradiated with $\lambda > 375$ nm (20 ± 5 °C). After 16 days the reaction is near completion, as monitored by UV-vis, producing W(S)Cl₄(PMe₂Ph); 26% yield (by NMR). NMR of photoreaction: ¹H (C₆D₆, ppm): $\delta = 7.8$ (m, Ph_3PS); 7.7 (m, W(S)Cl₄(PMe₂Ph)); 7.6 and 7.3 (m, MoWCl₄(PMe₂Ph)₄); 7.4 (m, Ph_3P); 7.0 (m, Ph_3PS , Ph_3P , MoW, W(S)Cl₄(PMe₂Ph)), 1.86 (d of t, MoWCl₄(PMe₂Ph)₄); 1.36 (d, ¹J_{PH} = 13 Hz,

W(S)Cl₄(PMe₂Ph)). 31 P(C₆D₆, ppm): $\delta = +43.1$ (s, Ph₃PS); +31.6 (s, W(S)Cl₄(PMe₂Ph)); +18.0 (t, 1 J_{wp} = 271 Hz, MoW); -4.7 (s, Ph₃P); -19.4 (t, 2 J_{wp} = 98 Hz, MoW). IR (C₆H₆, cm⁻¹): 594 (m, W(S)Cl₄(PMe₂Ph)); 570 (m, W(S)Cl₄(PMe₂Ph)); 541 (s, Ph₃P); 517 (vs, Ph₃P + Ph₃PS); 480 (m, Ph₃PS); 440 (m, Ph₃PS). GC (direct inlet, MeOH, amu): 355 (W(S)Cl₄); 294 (Ph₃PS); 262 (Ph₃P). EPR (2-methyl tetrahydofuran, -150 C): g = 1.9757; 1.9345.

b. Thermal reaction MoWCl₄(PMe₂Ph)₄ with Ph₃PS

Benzene solutions of MoWCl₄(PMe₂Ph)₄ and Ph₃PS, prepared as above, are indefinitely stable in the absence of light. This was determined by UV-vis spectroscopy.

6. Reactions of $M_2Cl_4(PMe_2Ph)_4$ with Ph_3PS (M = Mo, W)

No reactions of benzene solutions of $M_2Cl_4(PMe_2Ph)_4$ and Ph_3PS upon irradiation (M = Mo, $\lambda_{exc} > 335$ nm after 24 hrs; M = W, $\lambda_{exc} > 375$ nm after 36 hrs) or at room temperature in the dark was observed, as determined by UV-vis spectroscopy.

C. Instrumentation and Methods

1. Photolysis

Sample irradiations were performed by using a collimated beam from a Hanovia 1000W Hg/Xe high pressure lamp. Excitation wavelengths were selected with a Schott glass, high-energy cutoff filters purchased from the Oriel Corporation. Photolysis experiments were performed on solutions at constant temperatures contained in two-arm evacuable cells consisting of a solvent bulb

isolated from an absorption cell by a Kontes quick-release Teflon valve. Solution were prepared by bulb-to-bulb distillation of solvent on high vacuum manifold. For photochemical quantum yields, the excitation wavelength was isolated by using an interference filter purchased from the Oriel Corporation with a half-widtl of less than 10 nm at a given mercury line. Quantum yields for $W_2Cl_4(dppm)$ photochemistry were determined on toluene solutions containing 1 x 10^{-4} M $W_2Cl_4(dppm)_2$ and a 20-fold excess of PhSSPh. Quantum yields for MoWCl₄(PMe₂Ph)₄ photochemistry were determined on benzene solutions containing 1 x 10^{-3} M of MoWCl₄(PMe₂Ph)₄ and a 2-fold excess of Ph₃PS. Both quantum yields were determined by monitoring the disappearance of the $^1\delta^2 \rightarrow ^1\delta\delta^3$ transition ($W_2Cl_4(dppm)_2$: $\epsilon_{740} = 2585$ M⁻¹cm⁻¹, MoWCl₄(PMe₂Ph)₄: $\epsilon_{645} = 2169$ M⁻¹cm⁻¹) and were standardized by using a ferrioxalate actinometer.¹⁴

2. Absorption Spectroscopy

Absorption spectra were measured on a CARY-17D spectrometer modified by OLIS. Extinction coefficients were determined in the high vacuum cells described previously, by successive dilutions and were calculated by a Beer-Lambert plot using 7 points.

3. Solution Infrared Spectroscopy

Solution IR spectra were recorded on benzene or THF solutions on a Nicolet 750 IR spectrometer in a Perkin-Elmer KBr sealed liquid IR cell. The appropriate solvent was subtracted out as a reference.

4. Nuclear Magnetic Resonance Spectroscopy (NMR)

¹H and ³¹P{¹H} NMR spectra were obtained on Varian Inova-300 and Varian VXR-500 MHz spectrometers, with the ³¹P{¹H} experiment recorded at 121.4 MHz and referenced externally to 85% H₃PO₄. C₆D₆ (Aldrich Chemicals), THF-d₈ (Cambridge Isotope Laboratories), CD₂Cl₂ (Matheson) were used as received.

5. Electron Paramagnetic Resonance Spectroscopy (EPR)

EPR spectra were recorded on a Varian E-4 spectrometer by using a X-band TE 102 cavity with 100 KHz modulation, a 2.5 G modulation amplitude, and a microwave power of 45.7 mW at -151 °C. G-values were measured directly from the chart paper. 2-methyl tetrahydrofuran was distilled from CaH₂ and stored over NaK.

6. Electron Spin Echo Envelope Modulation (ESEEM)

ESEEM data were collected on a home built spectrometer¹⁵ using a three pulse stimulated echo (90°-τ-90°-T-90°) pulse sequence at 4K. Prior to Fourier transform, dead time was reconstructed, as described before.¹⁶ The experimental data was analyzed utilizing software written by Matlab (Mathworks, Nantick, MA).

7. Steady-State Luminescence Spectroscopy

Emission spectra were recorded on a spectrometer constructed at Michigan State University.¹⁷ The original experimental set up was modified by replacing the EG&G Princeton Appled Research Model 5209 lock-in amplifier with a Stanford Research Systems SR4000 two channel gated photon counter and using a

Hamamatsu R943 PMT. Absolute emission quantum yields on optically dilute samples (A < 0.2) were measured using $Mo_2Cl_4(PMe_3)_4$ (Φ_{em} = 0.256 at λ_{exc} = 583 nm in 2-methylpentane¹⁸) as standard for $Mo_2Cl_4(PR_3)_4$ and $Mo_2I_4(PMe_3)_4$ (Φ_{em} = 0.12 at λ_{exc} = 636 nm in 2-methylpentane¹⁸) as a standard for $W_2Cl_4(PR_3)_4$ and $MoWCl_4(PR_3)_4$. The quantum yields were calculated using the following equation¹⁹:

$$\Phi_{em} = \Phi_s \left[\frac{A_s(\lambda_s)}{A_u(\lambda_u)} \right] x \left[\frac{\eta_u^2}{\eta_s^2} \right] x \left[\frac{D_u}{D_s} \right]$$
 (2.1)

where u and s represent the unknown and the standard, respectively, η is the average refractive index of the solution, D is the integrated area under the corrected emission spectrum, and $A(\lambda)$ is the absorbance per unit length (cm) of the solution at the excitation wavelength.

8. Time-Resolved Laser Spectroscopy

a. Nanosecond Lifetimes and Transient Absorption

Nanosecond lifetimes were measured using an experimental set-up described elsewhere. The original set-up was modified by the use of the third harmonic (2.5 ns pulse width) of a Coherent Infinity Nd:Yag laser pumping a Lambda Physik scanmate OPPO using the corresponding dye to obtain the correct wavelengths to seed the optical parametric oscillator. Rhodamine 6G (Exciton) was used to obtain $\lambda = 580$ nm and sulforhodamine B (Lambda Physik) for $\lambda = 630$ nm; the corresponding Idler wavelengths were filtered out using a KG3 heat absorbing Schott filter. 355 nm light was removed with a CG-385 nm Schott highenergy glass filter. Nanosecond transient absorption measurements were made with the pulse-probe technique with instrumentation housed in the LASER

(Laser Applications in Science and Engineering Research) Laboratory at Michigan State University. The same excitation source described above was used.

b. Picosecond Transient Absorption

The transient absorption signals on the picosecond timescale were obtained using a pump-probe technique described in detail elsewhere²¹ and were measured by Dr. Turró.

9. Variable-Temperature Emission, Absorption and Nanosecond Lifetimes

Variable-temperature emission, lifetime and absorption measurements were recorded on samples cooled with an Air Products closed cycle cryogenic system by methods described elsewhere.²⁰ Samples, contained in a sealed Pyrex square emission cell, were held in contact with copper block by a copper cell holder and wrapped in indium foil. Temperatures were also measured near the sample by a K-type thermocouple using a Digi-Sense thermocouple thermometer from the Cole-Parmer Instrument Company and were found to vary by ±2K.

10. Electrochemistry

Electrochemical measurements were made with a PAR Model 173 potentiostat, 175 universal programmer, 179 digital coulometer, and a Housten Instruments Model 2000 X-Y chart recorder. Cyclic voltametry was performed at room temperature in THF by using a conventional H-cell design in an inert drybox atmosphere and a three-electrode system consisting of a Pt button electrode (A = 0.08 cm²), a Pt wire auxiliary electrode and a Ag wire provided a reference potential with ferrocene used as the internal standard. Potentials were related to SCE reference scale by using a ferrocinium-ferrocene couple of 0.307 V vs SCE.²²

11. Mass Spectrometry

a. FAB/MS

Fast atom bombardment mass spectrometry (FAB/MS) analyses were performed on a JEOL HX-110 double focusing mass spectrometer housed in the National Institute of Health/Michigan State University Mass Spectrometry facility. Samples were dissolved in 3-nitrobenzyl alcohol matrices and the instrument run in the positive ion detection mode.

b. GC/MS

Analyses by GC/MS were carried out on a JEOL JMS-AX505H double focusing MS coupled to a Hewlett Packard 5890J GC via a heated interface by direct probe injection at 30 °C for 2 minutes followed by 10 °C / minute.

D. References

- 1. Santure, D. J.; Sattelberger, A. P. *Inorg. Synth.* **1989**, 26, 221.
- 2. Gordon, A. J.; Ford, R. A. The Chemist's Companion: A Handbook of Practical Data, Techniques and References; Wiley-Interscience: New York, 1972; p 429.
- 3. SanFilippo, J. Jr. *Inorg. Chem.* **1972**, *11*, 3140.
- 4. Schrock, R. R.; Stugeoff, L. G.; Sharp, P. R. Inorg. Chem. 1983, 22, 2801.
- 5. Canich, J. M.; Cotton, F. A. *Inorg. Chim. Acta.* **1988**, *142*, 69.
- 6. Fanwick, P. E.; Harwood, W. S.; Walton, R. A. *Inorg. Chem.* **1987**, *26*, 242.
- 7. Luck, R. L.; Morris, R. H.; Sawyer, J. F. Organomet. 1984, 3, 247.
- 8. Cotton, F. A.; Luck, R. L.; Morris, R. H. Organomet. 1989, 8, 1287.

- 9. (a) Butcher, A. V.; Chatt, J.; Leigh, G. H.; Richards, R. L. J. Chem. Soc. Dalton Trans. 1972, 1064. (b) Dilworth, J. R.; Richards, R. L. Inorg. Synth. 1980, 20, 124.
- 10. (a) Luck, R. L.; Morris, R. H.; Sawyer, J. F. *Inorg. Chem.* **1987**, *26*, 2422. (b) Morris, R. H. *Polyhedron* **1987**, *76*, 793.
- 11. Cotton, F. A.; Falvello, L. R.; James, C. A.; Luck, R. L. *Inorg. Chem.* **1990**, 29, 4759.
- 12. Baratta, W.; Calderazzo, F.; Daniels, L.M. Inorg. Chem., 1994, 33, 3842.
- 13. Canich, J. M.; Cotton, F. A.; Dunbar, K. R.; Falvello, L. R. *Inorg. Chem.* **1988**, 27, 804.
- 14. Calvert, J. G.; Pitts, J. N. *Photochemistry*; Wiley-Intersceince: New York, 1966.
- 15. McCracken, J.; Shin, D.-H; Dye, J. L. Appl. Magn. Reson. 1992, 3, 30.
- 16. Mims, W. B. J. Magn. Reson. 1984, 59, 291.
- 17. Mussell, R. D.; Nocera, D. G. J. Am. Chem. Soc. 1988, 110, 2764.
- 18. Zietlow, T. C.; Hopkins, M. D.; Gray, H. B. J. Solid St. Chem. 1985, 57, 112.
- 19. Demas, N. J.; Crosby, G. A. J. Phys. Chem. 1971, 75, 991.
- 20. Newsham, M. D.; Giannelis, E. P.; Pinnavaia, T. J.; Nocera, D. G. J. Am. Chem. Soc. 1988, 110, 3885.
- 21. Turró, C. Ph.D. Michigan State University, 1992.
- 22. Gagne, R. R; Koval, C. A.; Lisensky, G. C. Inorg. Chem. 1980, 19, 2854.

CHAPTER 3

PHOTOREDUCTION OF DIARYL/DIALKYL DISULFIDES BY QUADRUPLY BONDED DITUNGSTEN COMPLEXES

A. Background

Without a flexible coordination sphere the redox reactions of M-4-M complexes often proceed no further than the one electron oxidation product. This is evident in the thermal and photochemical redox chemistry of quadruply bonded bimetallic complexes with four rigid bridging ligands, $M_2(LL)_4$ (M = Mo, W; LL = bidentate ligand).¹

A typical one electron oxidation is the reaction of $Mo_2(O_2CR)_4$ (R = C_2H_5 , CMe₃, Ph) with I_2 to give $[Mo(O_2CR)_4]I_3$. This is not sursprising since an electrochemical study of $Mo_2(O_2CC_3H_7)_4$ in acetonitrile, dichloromethane and ethanol revealed only one electron quasi-reversible oxidations at + 0.39, + 0.45, and + 0.30 V vs. SCE, respectively. Similar one electron oxidations are observed for the oxidation of $W_2(O_2CCMe_3)_4$ by I_2 to yield $[W_2(O_2CCMe_3)_4]I$. This difficulty in accessing the two electron oxidation product is preserved in the photochemisry of $Mo_2(LL)_4$ complexes.

Photolysis ($\lambda > 254$ nm) of $Mo_2(SO_4)_4^{4-}$ in 5M H_2SO_4 results in the reduction of H^+ ; for each mole of the one electron oxidized product, $Mo_2(SO_4)_4^{3-}$, a ½ mole H_2 is produced.⁵ Likewise, the product of irradiations of

Mo₂[O₂P(OPh)₂]₄ with dichlorohydrocarbons is the one electron product Mo₂[O₂P(OPh)₂]₄Cl, as discussed in Chapter 1. Replacing SO₄²⁻ or O₂P(OPh)₂⁻ with HPO₄²⁻, increases the reduction potential of the Mo₂ core by almost 1V and two electron chemistry is observed.⁶ The reason for this increase in reduction potentials is unclear. HPO₄²⁻, SO₄²⁻ and O₂P(OPh)₂⁻ are structurally and electronically similar, so it is unreasonable to account for the ~1V increase of Mo₂(HPO₄)₄²⁻ on this basis. The chemical properties of the three differ, however. It is possible to protonate the phosphate ligand, while this is unlikely with the sulfate and the diphenyl phosphate. This may be the reason for the disparities in the reduction potentials. Irradiation of 2M H₃PO₄ solutions of Mo₂(HPO₄)₄²⁻ with $\lambda > 335 \ nm$ results in the formation of 1 mol each of H_2 and the two electron oxidized product, Mo₂(HPO₄)₄²⁻. Detailed mechanistic studies revealed that the photochemistry proceeds through two consecutive one-electron reactions. Another example of a two electron oxidation, is the thermal reaction of $(Ph_4P)_2[Mo_2(O_2CPh)_4Cl_2]$ with CCl_4 in CH₂Cl₂ to give $(Ph_4P)_2[Mo_2(O_2CPh)_4Cl_4] \bullet CH_2Cl_2$, where two of the μ - η^2 benzoate ligands have rearranged to μ - η^1 ligands, Figure 3.1. The rearrangement of the benzoate ligands in the last system raises the issue of a flexible coordination sphere. If two of the bidentate ligands are replaced by ligands that are capable of rearranging, two electron oxidations of quadruply bonded bimetallic complexes are conceivable.

Such multielectron chemistry is observed in the thermal reactions of the complexes $M_2X_4L_4$ (M = Mo, W; X = anionic ligand; L = neutral ligand). The formation of edge-sharing bioctahedrals (ESBO) upon two electron oxidation is a common structural motif for these M-4-M complexes, Figure 3.2. The bridging

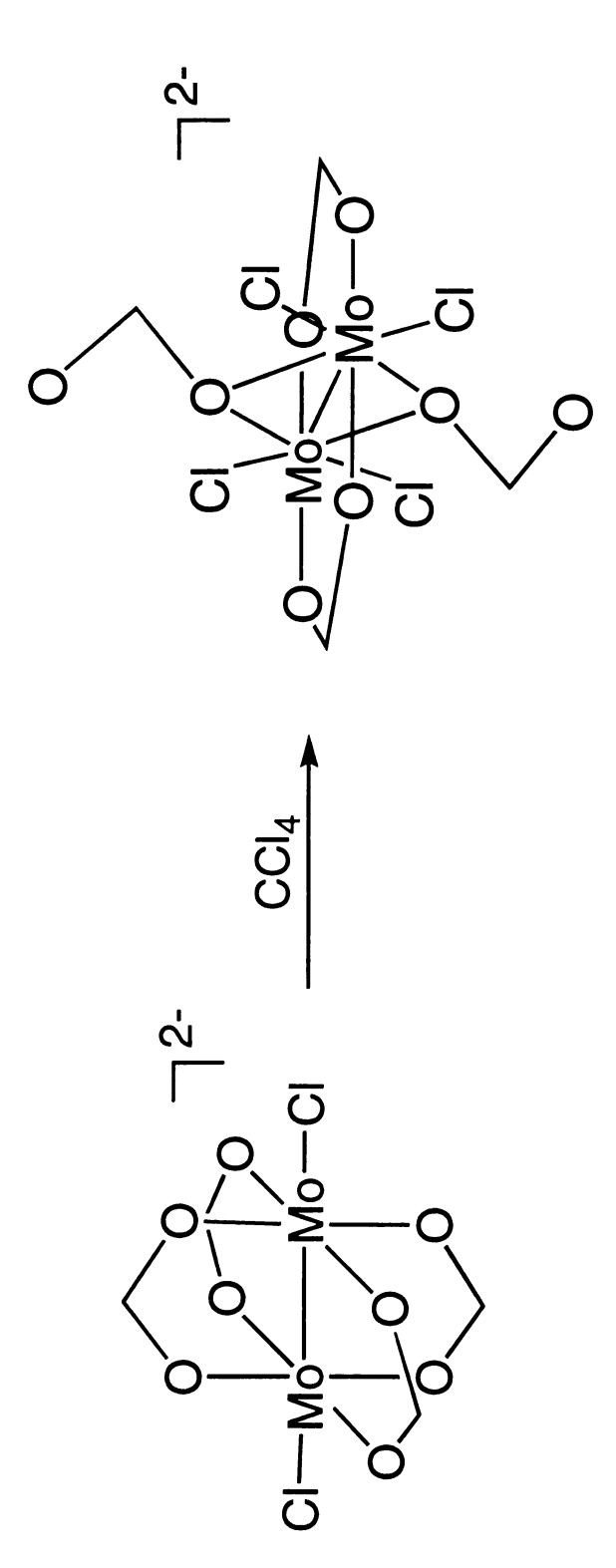
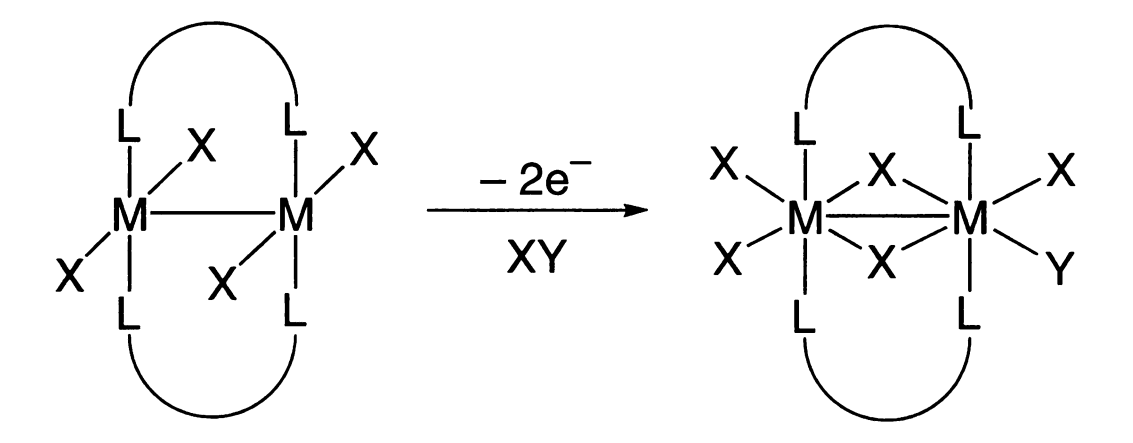


Figure 3.1 The two electron oxidation of $[Ph_4P]_2[Mo_2(O_2CPh)_4Cl_2]$ by CCl_4 . Two benzoate ligands rearrange from μ - η^2 to μ - η^1 bonding modes.



edge-sharing bioctahedron (ESBO)

Figure 3.2 The formation of an edge-sharing bioctahedron (ESBO) upon two electron oxidation of a quaduply bonded bimetallic complex.

ligands make a flexible coordination sphere crucial in forming the octahedral geometry of the ESBO; without this flexibility, one electron oxidations are often the result. These complexes undergo oxidative addition with a variety of substrates, such as X_2 , ¹⁰ disulfides, ¹¹ diselenides, ¹² and HCl; ¹³ all of which form an ESBO structure.

A similar trend is observed in the photochemistry of this structure type. Single photon concerted two electron photochemistry is observed upon replacing two of the bridging ligands with chlorides, as opposed to the two photon two electron chemistry observed with $Mo_2(HPO_4)_4^{4-}$. When CH_3I (MeI) solutions of $W_2Cl_4(dppm)_2$ are irradiated with $\lambda > 435$ nm, the observed photoproduct is consistent with the oxidative addition of MeI, ¹⁴ as shown below:

While the coordination geometry about the M-M core has not been unequivocally established, the absorption profile is similar to that of reported ESBO structures. Additionally, the Me is proposed to be in a terminal position based on 13 C NMR. This is consistent with the proposed open equatorial coordination site of the intermediate, as discussed in Chapter 1. The observed photchemistry is in contrast to the thermal chemistry of the system. The thermal reaction of $W_2Cl_4(dppm)_2$ with alkyl iodides results in $W_2Cl_5(dppm)_2I$ and $W_2Cl_4(dppm)_2I_2$, the formation of

which can be explained by invoking a radical mechanism. W^{II}₂Cl₄(dppm)₂ can react with RI to produce the mixed valence complex, W₂Cl₄(dppm)₂I. This can disproportionate by either chloride or iodide atom abstraction to yield W₂Cl₅(dppm)₂I and W₂Cl₄(dppm)₂I₂, respectively. The formation of these products is indicative of a radical mechanism. Since neither are observed in the mass analysis of the photoreaction, this indicates that the oxidative addition of MeI is concerted. This is further supported by the absence of any ethane as a product of the photoreaction. We wished to broaden the scope of this chemistry to diaryl/dialkyl disulfides.

B. Photochemistry of W₂Cl₄(dppm)₂ and PhSSPh

The spectral changes associated with the irradiation of toluene solutions of $W_2Cl_4(dppm)_2$ and PhSSPh ($\lambda > 495$ nm, -10 °C) are shown in Figure 3.3. The isosbestic point indicates the formation of only one photoproduct. The absorption maxima at 730 and 504 nm compare well with independently prepared $W_2Cl_4(dppm)_2(SPh)_2$. Additionally, the FAB/MS spectrum of the purified photoproduct shows a molecular ion peak at 1496 amu and fragments at 1419 and 1387 amu corresponding to $W_2Cl_4(dppm)_2(SPh)_2^+$ (= [M]⁺), [M-C₆H₅]⁺ and [M-C₆H₅-S]⁺, Figure 3.4. This has also been confirmed by ES/MS analysis. $W_2Cl_5(dppm)_2(SPh)$ is not seen in the FAB/MS, indicating that the reaction does not proceed through the radical mechanism shown below.

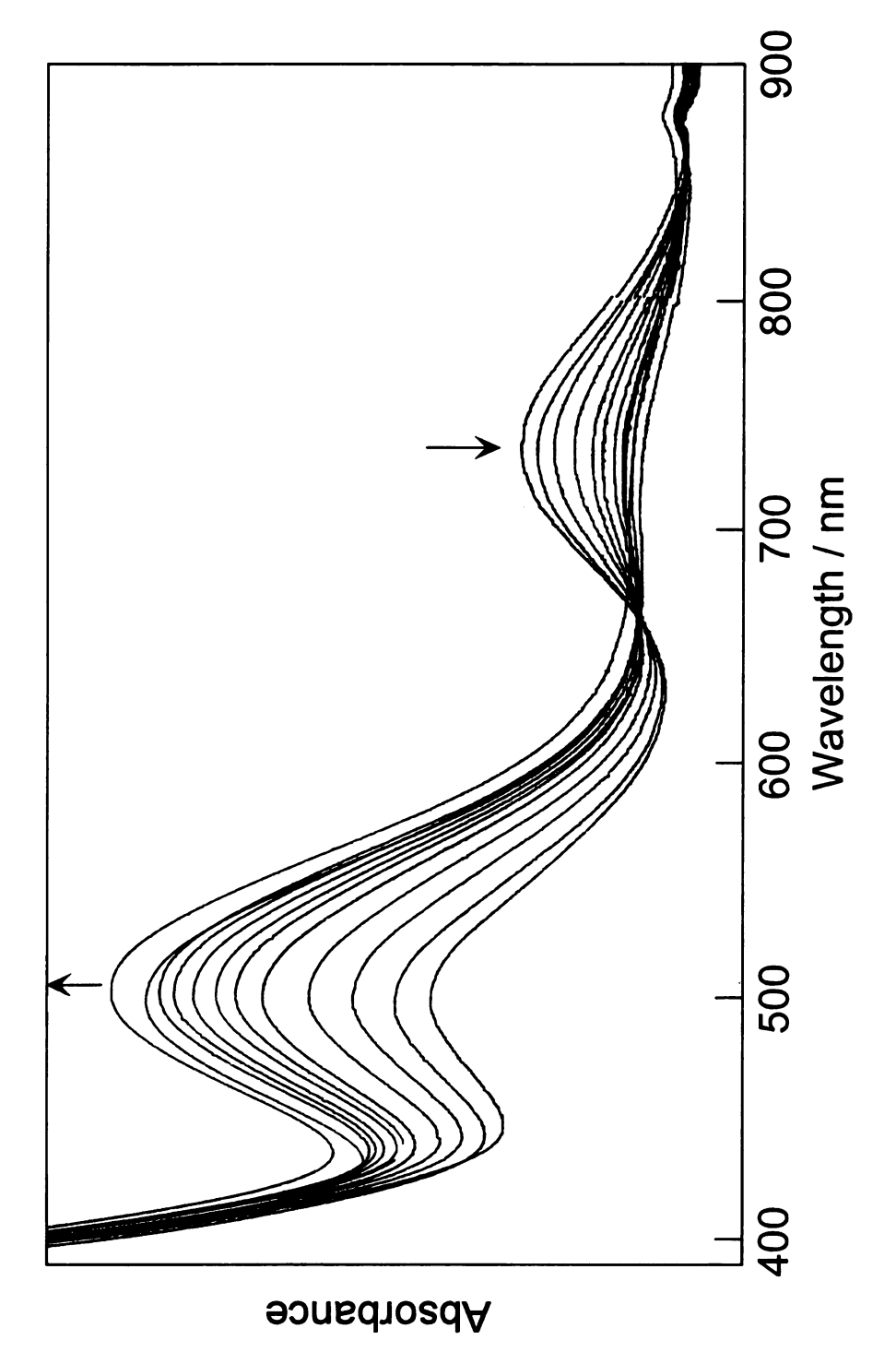


Figure 3.3 Electronic absorption spectral changes during photolysis ($\lambda > 495$ nm) of toluene solutions of W₂Cl₄(dppm)₂ with excess PhSSPh at -10 °C.

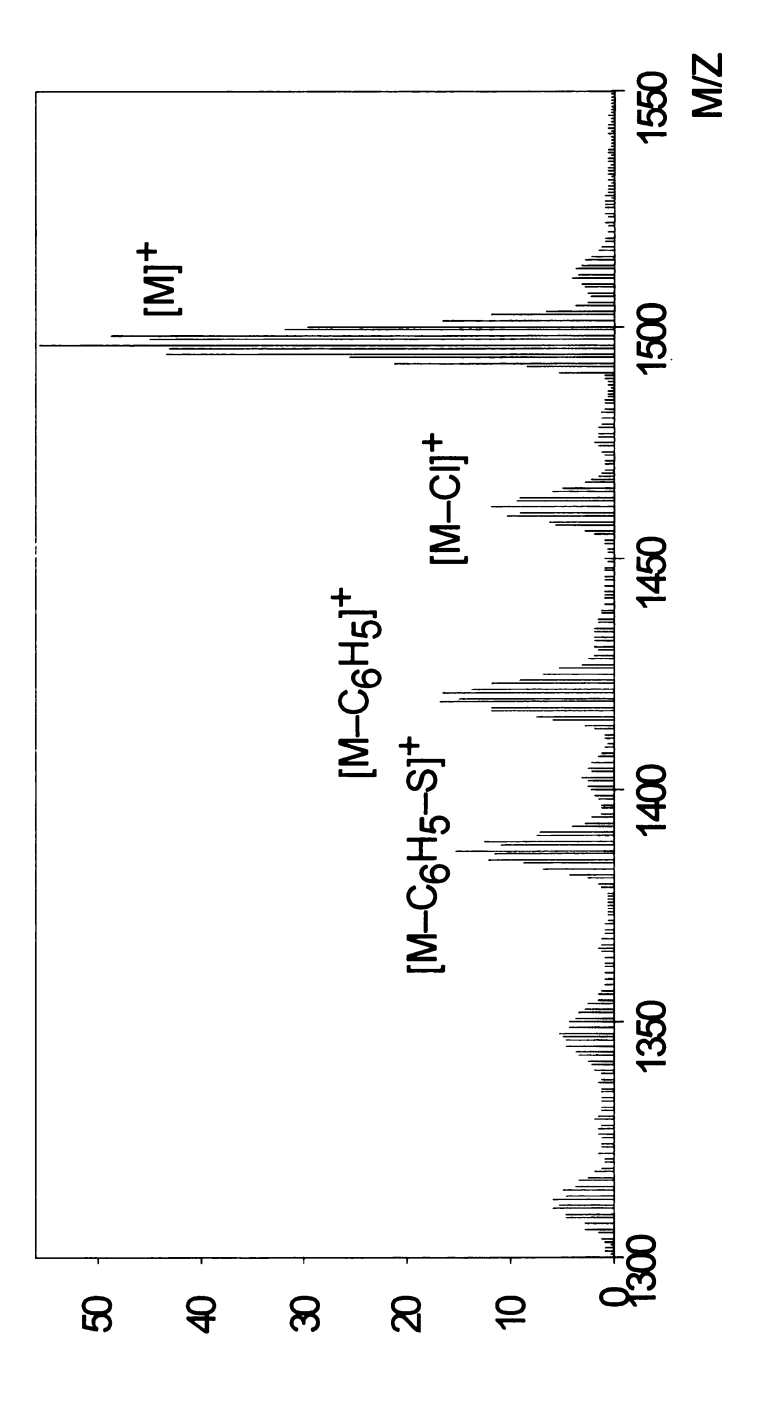


Figure 3.4 FAB/MS spectrum of the photoproducts isolated from the irradiation of toluene solutions of W₂Cl₄(dppm)₂ and excess PhSSPh.

$$W_2Cl_4(dppm)_2 \xrightarrow{hv} W_2Cl_4(dppm)_2^*$$

$$W_2Cl_4(dppm)_2^* + PhSSPh \longrightarrow W_2Cl_4(dppm)_2(SPh) + \bullet SPh$$

$$\begin{array}{c} & \text{Cl atom} \\ \text{abstraction} \end{array} \quad \text{W}_2\text{Cl}_5(\text{dppm})_2(\text{SPh}) + \text{"W}_2\text{Cl}_3(\text{dppm})_2\text{"} \\ 2 \text{ W}_2\text{Cl}_4(\text{dppm})_2(\text{SPh}) + \text{W}_2\text{Cl}_4(\text{dppm})_2 \end{array}$$

While toluene solutions of $W_2Cl_4(dppm)_2$ and PhSSPh do react in the dark at -10 °C, there is virtually no reaction on the time scale of the photoreaction. Under the above conditions the thermal reaction is complete in 24 hours as opposed to 45 minutes for the photoreaction.

1. Quantum Yields

The action spectrum of $W_2Cl_4(dppm)_2/PhSSPh$ photochemistry is consistent with the reaction originating from the metal complex. $W_2Cl_4(dppm)_2$ reacts with PhSSPh when irradiated with wavelengths as low as 546 nm with a quantum yield (Φ) of 0.025. The quantum yields increase to the blue, as shown in Table 3.1. The onset of photochemistry is coincident with the absorption band immediately to higher energy of the $\delta^2 \rightarrow {}^1\delta\delta^*$ transition ($\lambda_{max} = 710$ nm). This coincidence between the position of the absorption band immediately to higher energy of $\delta^2 \rightarrow {}^1\delta\delta^*$ and the action spectrum of $W_2Cl_4(dppm)_2$ is preserved in the analogous photoreaction of $Mo_2Cl_4(dppm)_2/PhSSPh$, 15 Table 3.1.

Table 3.1 Wavelength Dependent Quantum Yields for the Photoreaction of M₂Cl₄(dppm)₂ and PhSSPh.

λ _{exc} / nm	$\Phi_p[W_2Cl_4(dppm)_2]^a$	$\Phi_p[Mo_2Cl_4(dppm)_2]^b$
546	0.025	<10 ⁻⁵
405	0.048	0.010
435	0.075	0.11
365	0.15	0.23
313	0.39	0.27

a. T = 0 °C in toluene; b. T = 16 °C in CH_2Cl_2 .

The ~50 nm blue shift of the Mo₂Cl₄(dppm)₂ action spectrum, as compared to that of the W₂Cl₄(dppm)₂ homologue, is consistent with the ~50 nm blue shift of the absorption spectrum of the dimolybdenum complex, Figure 3.5. This wavelength dependence of the photochemistry demonstrates that the photoreaction is metal-based and excludes the possibility of the photochemistry being derived from PhSSPh, by direct homolysis of the disulfide bond to produce RS• radicals.

Comparison of the action spectrum of $W_2Cl_4(dppm)_2$ to $Mo_2Cl_4(dppm)_2$ reveals the nature of the excited state responsible for the photochemistry. For quadruply bonded bimetallic complexes, ligand-to-metal charge transfer (LMCT) transitions blue shift upon exchange of W for Mo, due to greater difficulty in reducing W^{II} . Metal localized transitions, however, red shift when the metal is changed from Mo to W, as demonstrated by the $\delta^2 \rightarrow {}^1\delta\delta^*$. Therefore, even the transitions in the higher energy range (450-300 nm) which are typically ligand-to-

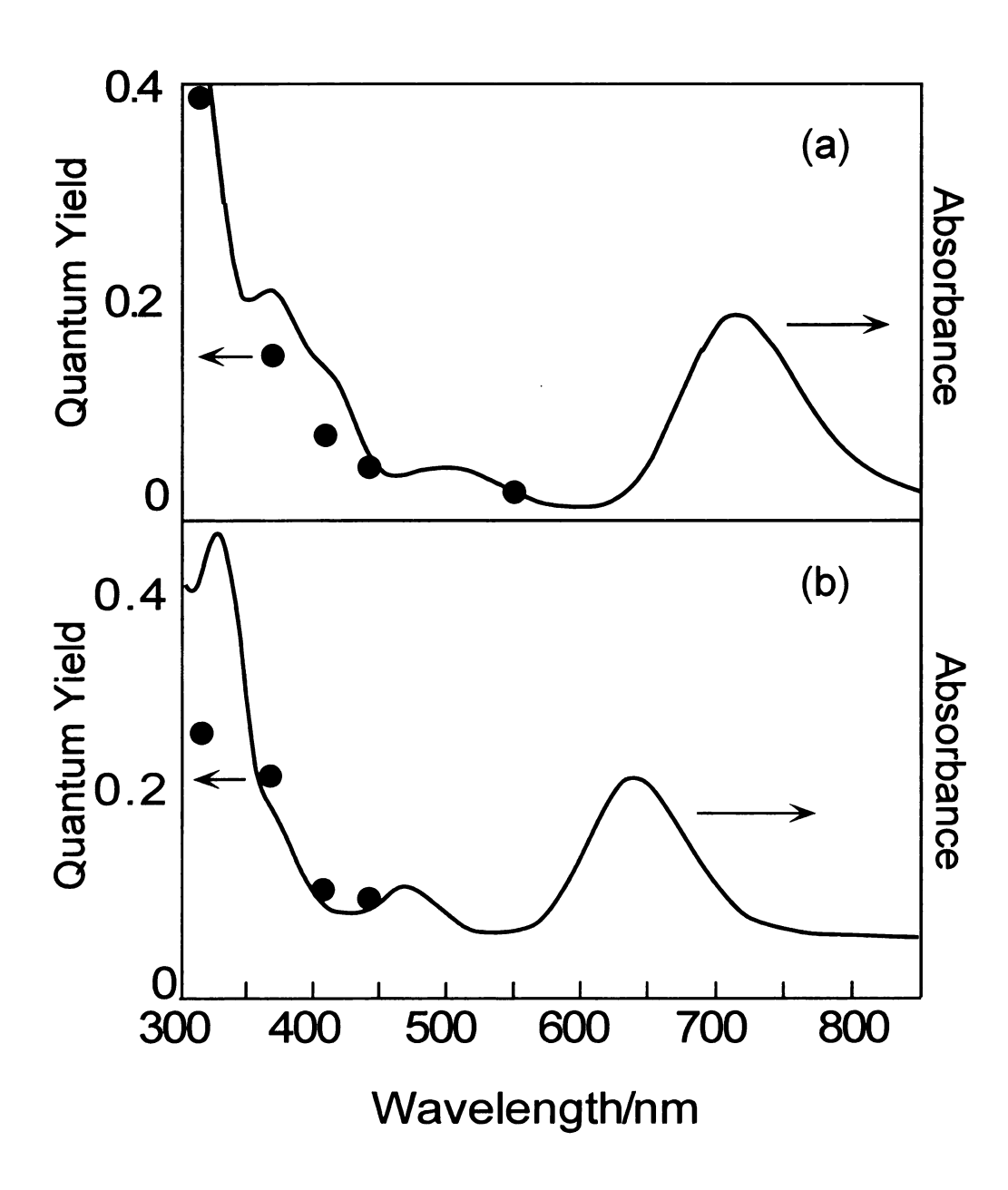


Figure 3.5 Quantum yields for the photolysis of $M_2Cl_4(dppm)_2$ and excess PhSSPh. Panel (a) is $W_2Cl_4(dppm)_2$ in toluene at 0 °C; (b) is $Mo_2Cl_4(dppm)_2$ in CH_2Cl_2 at 20 °C.

metal or metal-to-ligand charge transfer transitions, are still metal-localized transitions.¹⁶ As a result, the Mo \rightarrow W red shift of the action spectra implies the $M_2Cl_4(dppm)_2$ photochemistry is metal localized.

The red shift of the transitions upon substitution of Mo with W of the $M_2Cl_4(dppm)_2$ (D_{2h}) complexes in the near-UV is in sharp contrast to the blue shift of the near-UV transitions of the $M_2Cl_4P_4$ (D_{2d}) complexes, indicating a LMCT transition of the latter.¹⁶ As a result, the photochemisty of the D_{2d} complexes is characterized by LMCT reactivity.¹⁷ The differences in parentage of the high energy transitions of the D_{2h} complexes as compared to the D_{2d} complexes is due to the nondegeneracy of the π d_{yz} and π d_{xz} orbitals in the former,¹⁸ Figure 3.6. The presence of metal localized transitions in the near-UV is likely manifested in the photochemistry of these complexes.

C. Transient Absorption

The photochemistry was complemented by transient absorption $Mo_2Cl_4(dmpm)_2^{19}$ derivative, spectroscopy. The dmpm (dmpm bis(dimethylphosphino) methane), was used due to stimulated emission of the dppm ligand $(\tau \sim 1 \text{ ns})^{20}$ upon high energy excitation ($\lambda_{\text{exc}} = 355 \text{ nm}$). Stimulated emission over the wavelength range 450-520 nm, although weak, was problematic due to the weak changes in optical density (Δ ODs) of the transient absorption band of Mo₂Cl₄(dppm)₂ in this region. Replacement of dppm with dmpm eliminated the stimulated emission and allowed sufficient signal to noise ratio. The absorption of Mo₂Cl₄(dppm)₂ is nearly identical to that of Mo₂Cl₄(dmpm)₂ but is red shifted by about ~40 nm. Also, the irradiation of Mo₂Cl₄(dmpm)₂ and PhSSPh, under

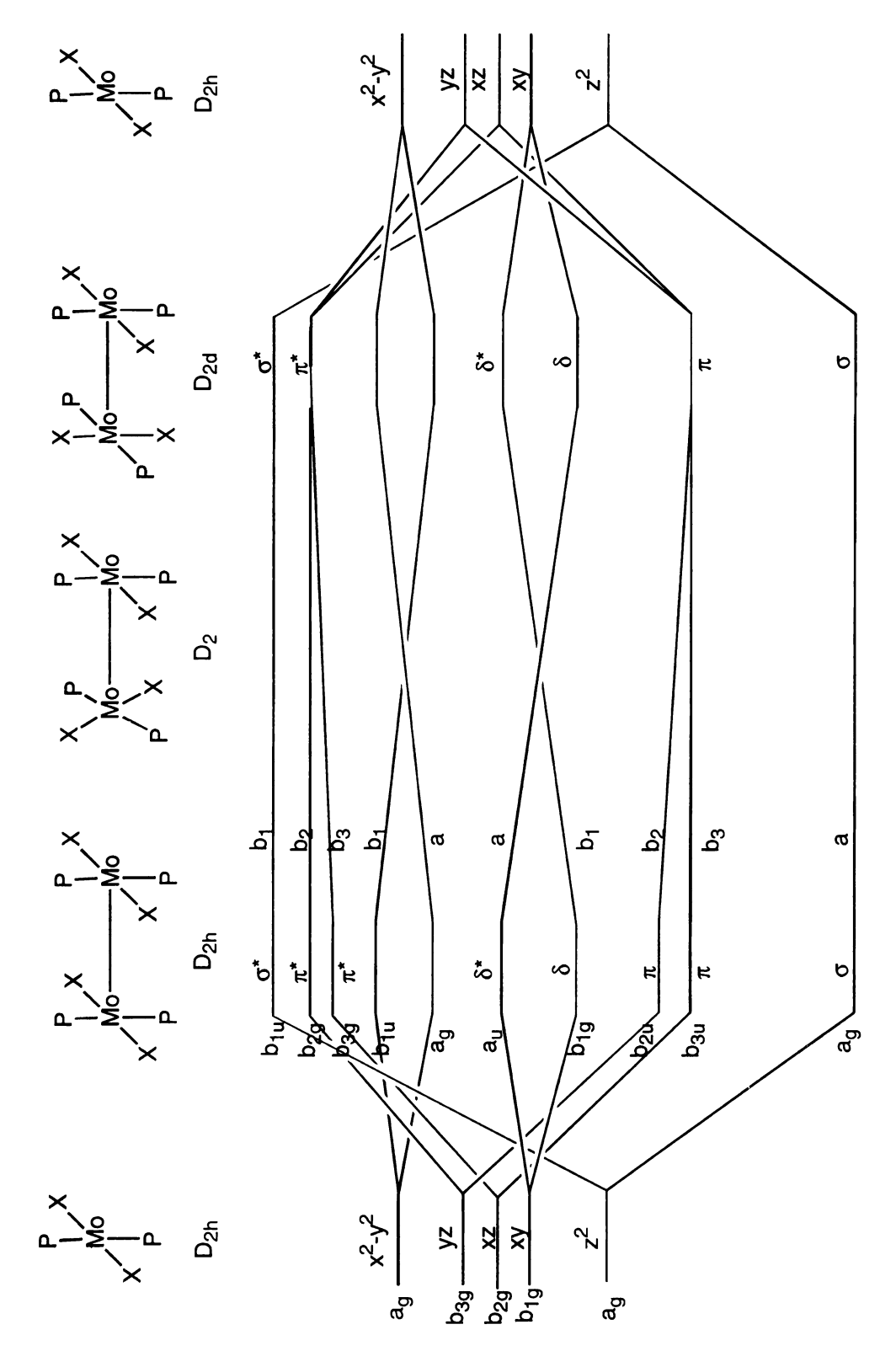


Figure 3.6 Qualitative correlation diagram for D_{2h} and D_{2d} symmetry quadruply bonded bimetallic complexes. (reference 17).

identical conditions as $Mo_2Cl_4(dppm)_2$, produces $Mo_2Cl_5(dmpm)_2(SPh)$. Based on this, the electronic structure of $Mo_2Cl_4(dmpm)_2$ is expected to be similar to that of $Mo_2Cl_4(dppm)_2$. The problem of stimulated emission in the transient absorption of $W_2Cl_4(dppm)_2$ did not arise due to the red shift of the absorption spectrum, as compared to Mo_2 , which allows the use of lower energy excitation. Picosecond transient absorption of $W_2Cl_4(dppm)_2$ and $Mo_2Cl_4(dmpm)_2$ affords a short lived intermediate with lifetimes of < 1 ns and 40 ps, respectively. The transient absorption profile of $Mo_2Cl_4(dmpm)_2$ following a 3 ps excitation pulse at 600 nm at 2, 20 and 50 ps after the pulse is shown in Figure 3.7. Concurrent with this absorption is the recovery of the bleach of the $\delta\delta^*$ transition at 630 nm on the same time scale. The short lifetimes of the $\delta\delta^*$ excited states preclude bimolecular photochemistry and explain the absence of any $M_2Cl_4(dppm)_2/PhSSPh$ photochemistry upon $\delta\delta^*$ excitation.

If the absorption profile immediately to higher energy of $\delta\delta^*$ is excited, a long-lived transient is observed. Benzene solutions of $W_2Cl_4(dppm)_2$, excited at $\lambda_{exc} = 532$ nm, display the transient absorption spectrum ($\lambda_{max} = 500$ nm, $\tau = 46$ µs) in Figure 3.8. The transient absorption profile is similar to the ground state absorption spectrum of the edge-sharing bioctahedron, $W_2Cl_6(dppm)_2$. A similar result is observed for $Mo_2Cl_4(dmpm)_2$. Dichloromethane solutions of $Mo_2Cl_4(dmpm)_2$ ($\lambda_{exc} = 355$ nm) have a transient absorption profile ($\lambda_{max} = 520$ nm) that is similar to the ground state absorption of $Mo_2Cl_6(dmpm)_2$. The correlation of the spectra of the transients and the edge-sharing bioctahedra suggest that the long-lived nonluminescent transient is derived from a chemically distorted ESBO, the formation of which is consistent with the electronic structure

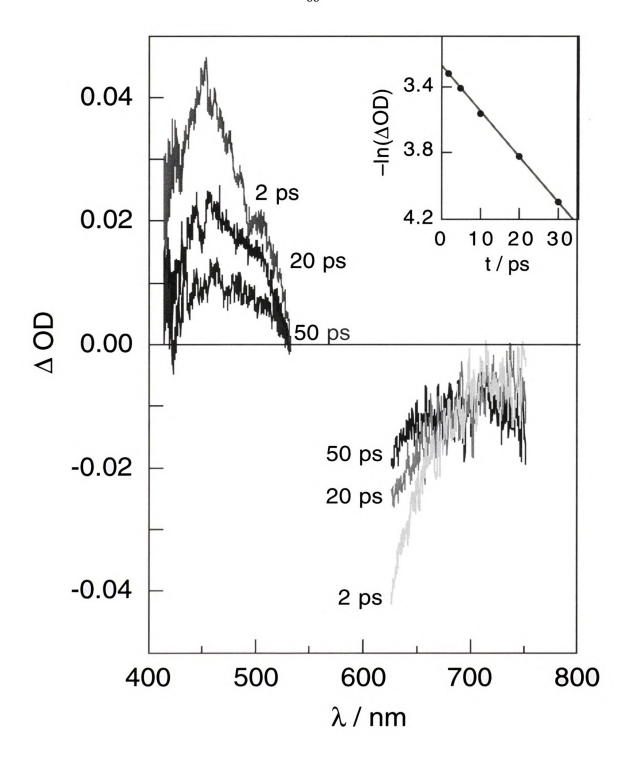


Figure 3.7 Picosecond transient absorption of $Mo_2Cl_4(dmpm)_2$ in CH_2Cl_2 following a 3 ps excitation pulse at 600 nm. Spectra were recorded at 2, 20 and 50 ps following excitation. The inset shows the ln plot of the recovery of the bleach at 630 nm.

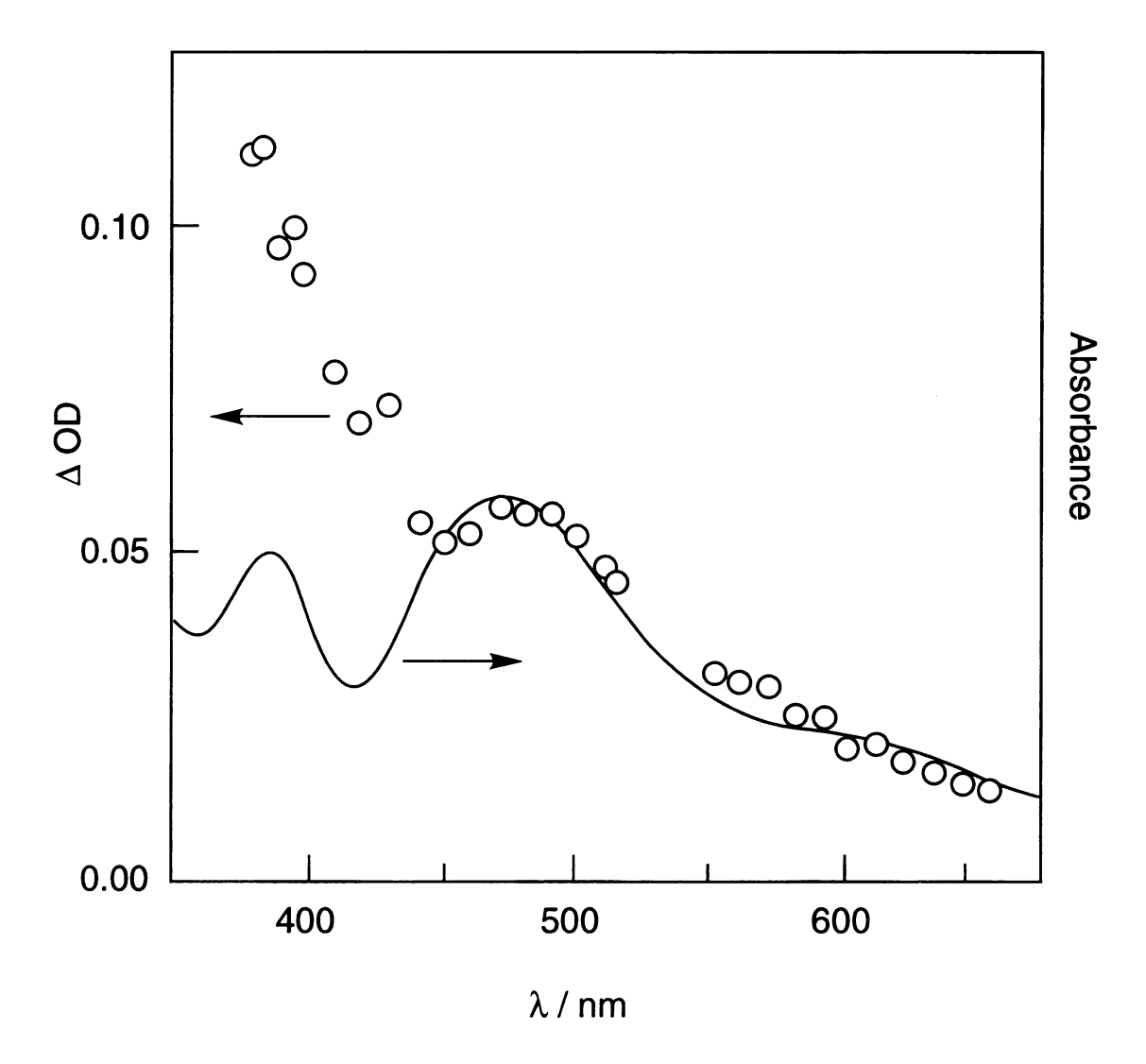


Figure 3.8 Comparison of the transient absorption, following a 532 nm excitation pulse, of $W_2Cl_4(dppm)_2$ (O) to the ground state absorption of $W_2Cl_6(dppm)_2$ (—), both are in benzene.

of quadruply bonded bimetallic complexes. Although the electron count of the chemically distorted ESBO ($M^{I}M^{III} = d^{5}-d^{3}$) differs from that of $M_{2}X_{6}(LL)_{2}$ complexes $(M_{2}^{III} = d^{3}-d^{3})$ the absorption profiles of the two species should be similar. The ordering of the molecular orbitals of the $M_2X_6(LL)_2$ complexes are σ $<<\pi<\delta^*-\delta<\pi^*<<\sigma^*$, with a small δ^*/δ splitting.²² As a result, the $\pi\to\delta^*$, $\pi\to\delta$, $\delta^* \rightarrow \pi^*$ transitions in the d^3-d^3 ESBO should be energetically similar to the $\delta \rightarrow \pi$ and $\delta^* \rightarrow \pi^*$ transitions of the d^5-d^3 chemically distorted intermediate. Additionally, if a lone pair of electrons is contained in a π orbital in the equatorial plane, the electron count of the intermediate would be $d^3-d^3(\pi_{in-plane})^2$. The metal localized transitions from this electronic configuration would even more closely resemble the metal localized transitions of the native d³-d³ ESBO complex. The metal localized excited states associated with δ and δ^* have charge transfer character, $M_2^* = M^I M^{III.23}$ The chemical distortion to the ESBO can provide cooperative stabilization with an octahedral geometry about the partially oxidized metal center and a diminished electron density about the partially reduced metal center. Furthermore, the existence of an activation barrier may prevent the formation of the ESBO upon $\delta\delta^*$ excitation. The formation of the long-lived nonluminescent intermediate is summarized in Figure 3.9. Excitation into the π manifold is predicted to be necessary in order to diminish the metal-metal π bonding relative to the ground state. This is expected to enhance the formation of the ESBO because the bridging M-L π d_{yz} or π d_{xz} bonds occur at the expense of the M–M π bonds.

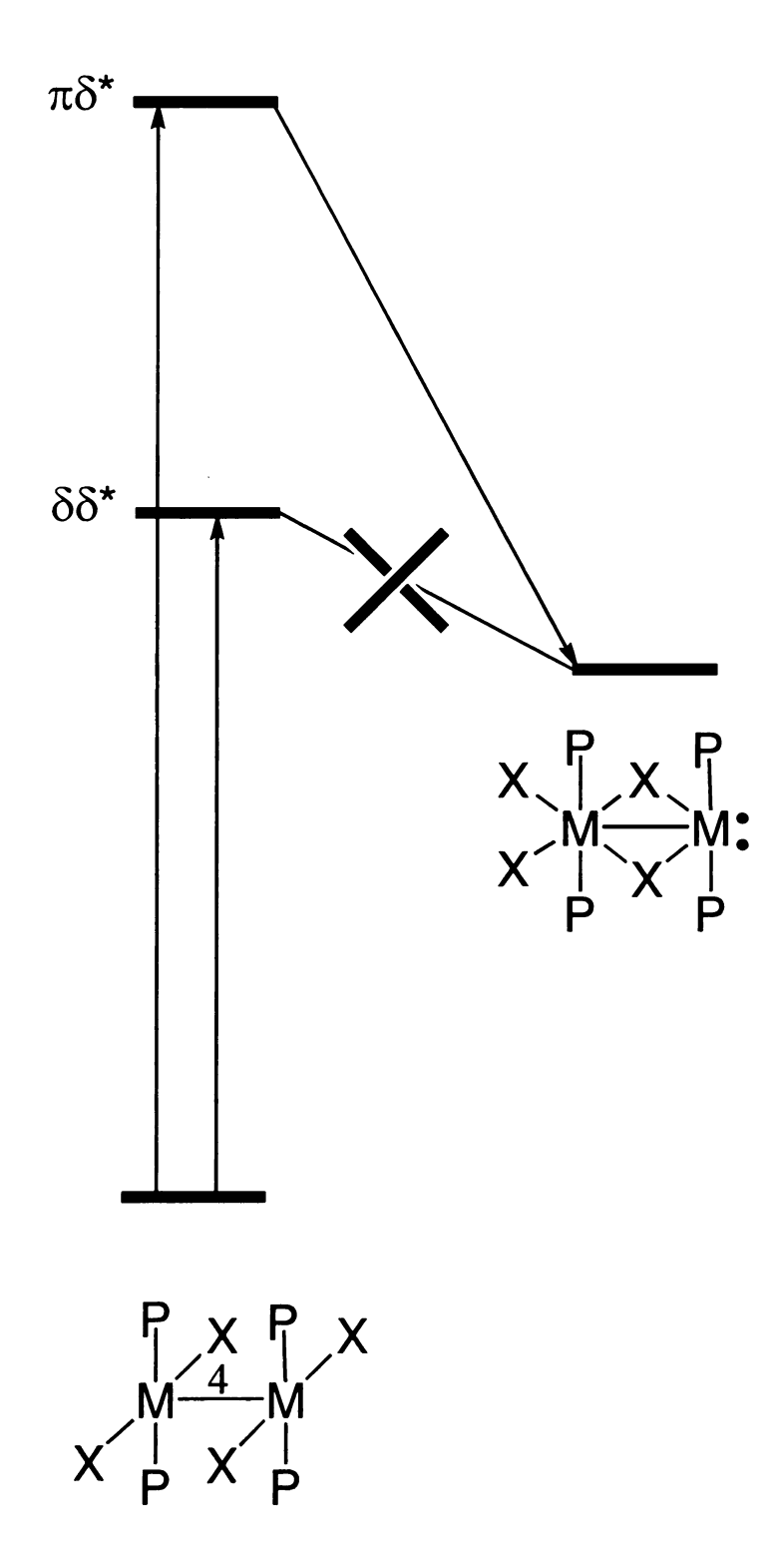


Figure 3.9 Formation of the chemically distorted ESBO upon excitation of the $\pi\delta^*$ absorption band of $M_2Cl_4(LL)_2$ complexes.

D. Photochemistry of W₂Cl₄(dppm)₂ and EtSSEt

The spectral changes associated with the irradiation ($\lambda > 495$ nm, -20 °C) of toluene solutions of W₂Cl₄(dppm)₂ and EtSSEt, over the course of three days, are shown in Figure 3.10. The lack of isosbestic point indicates the formation of more than one product. These products are consistent with the formation of W₂Cl₅(dppm)₂(SEt) and W₂Cl₆(dppm)₂, as determined by FAB/MS (1374 and 1394 amu, respectively). Some insight into the mechanism can be gained if the photoreaction is stopped prior to completion. Figure 3.11 shows the absorption spectra and FAB/MS after 1 hour and 45 minutes of irradiation. A significant amount of W₂Cl₄(dppm)₂(SEt)₂ (1400 amu) has formed along with $W_2Cl_5(dppm)_2(SEt)$ and $W_2Cl_6(dppm)_2$. The UV-vis spectrum shows an absorbance at 570 nm, which is believed to be due to W₂Cl₄(dppm)₂(SEt)₂, as well as those due to the final absorbances. The formation of W₂Cl₄(dppm)₂(SEt)₂ early in the photoreaction implies that it is the primary photoproduct but decomposes to W₂Cl₅(dppm)₂(SEt) and W₂Cl₆(dppm)₂. The isosbestic point also indicates that, at this point, the reaction is clean. A similar result was observed for Mo₂Cl₄(dppm)₂/RSSR photochemistry in toluene. ¹⁵ When the photoproducts are isolated prior to completion, Mo₂Cl₄(dppm)₂(SR)₂ is observed, which then decomposes to Mo₂Cl₅(dppm)₂(SR). No Mo₂Cl₆(dppm)₂ is observed.

While no crystal structure of $W_2Cl_5(dppm)_2(SEt)$ has been obtained, ^{13}C NMR can reveal some information about the structure. In the ^{13}C NMR of $W_2Cl_5(dppm)_2(SEt)$ resonances at δ +123.6 and +88.1 ppm can be assigned to the dppm ligands, based on the ^{13}C NMR of $W_2Cl_4(dppm)_2$, δ +123.2 and +87.6 ppm.

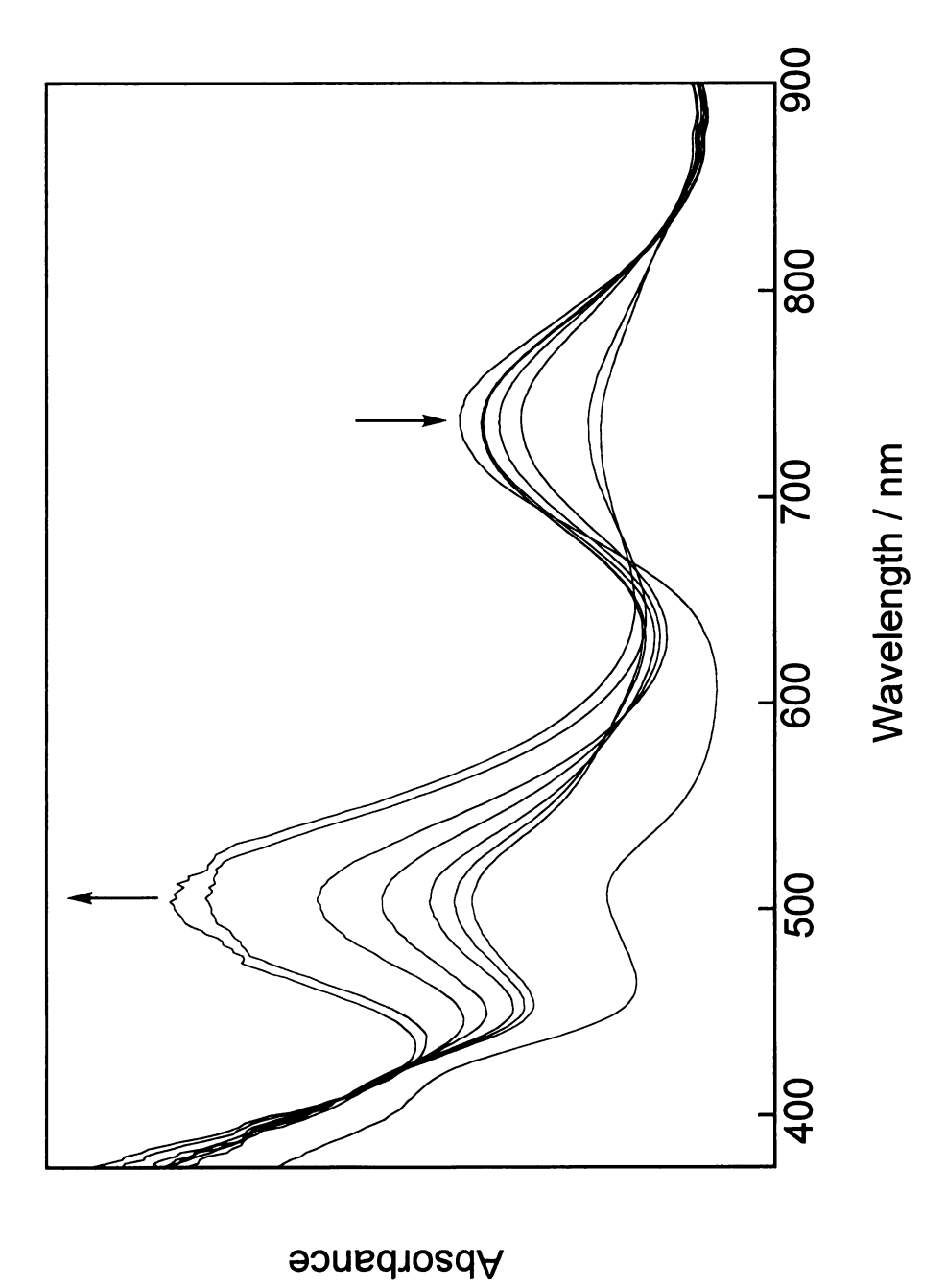


Figure 3.10 Electronic absorption spectral changes during photolysis ($\lambda > 495 \text{ nm}$) of toluene solutions of W₂Cl₄(dppm)₂ with excess EtSSEt at -20 °C.

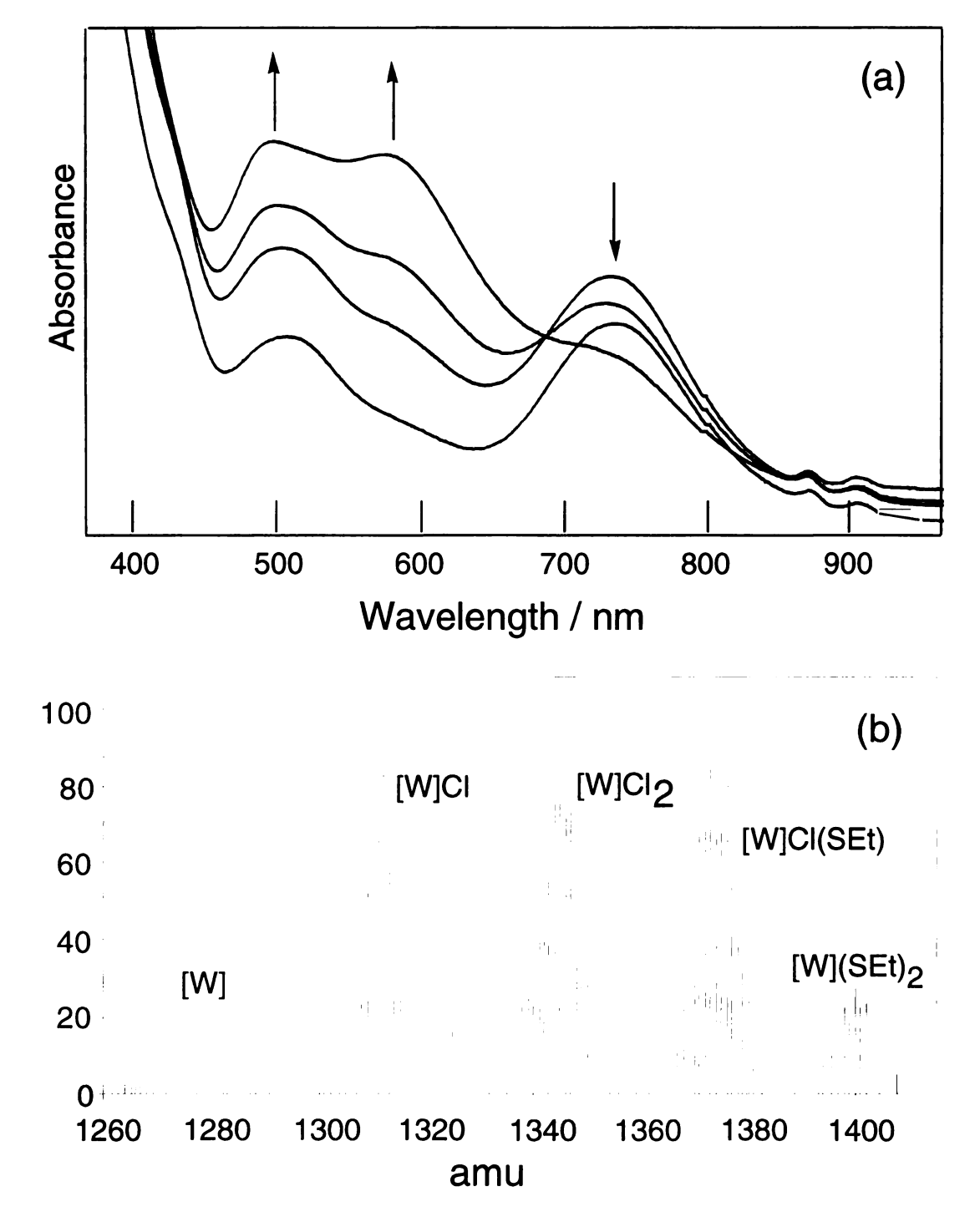


Figure 3.11 (a) Spectral absorption changes associated with the irradiation of $W_2Cl_4(dppm)_2$ and EtSSEt in toluene at -20 °C. The irradiation was stopped after 1 hour and 45 minutes. (b) FAB/MS spectrum of the photoproducts isolated from the final spectrum above.

Resonances at δ +30.1 and -50.5 ppm have been assigned to a terminal SEt group. The diamagnetic anisotropy of the multiple metal-metal bond typically induces a upfield shift in terminal ligands and an downfield shift in ligands bridging the two metals. Based on the large upfield shift of the resonance at -50.5 ppm, +14.7 ppm in uncoordinated EtSSEt, this has been assigned to the -CH₂- group of the EtS ligand. The resonance at +30.1 ppm is shifted from +33.3 ppm in uncoordinated EtSSEt. The relatively small upfield shift indicates that this is less reduced than the methylene group. The position of the SEt group, although not the primary photoproduct, is consistent with the proposed chemically distorted intermediate. Similar to the photoreaction of $W_2Cl_4(dppm)_2$ and PhSSPh, no appreciable reaction occurs at -20 °C for the duration of the photoreaction. The dark reaction is complete in a month, as opposed to 3 days for the photoreaction.

E. Conclusions

The reaction of RSSR with $W_2Cl_4(dppm)_2$ shows oxidative addition to be a general photoreaction pathway for this complex. Additionally, the transient absorption studies show that the $^1\delta\delta^*$ is not efficiently trapped upon excitation into this absorption band and therefore gives rise to no photochemistry. If higher excitation energy is used, the excited state can be adequately trapped via a chemically distorted ESBO and used for substrate reduction. That $W_2Cl_4(dppm)_2(SEt)_2$ is unstable is not easily explained. However, since it is seen in the early stages of the photoreaction, the photochemical mechanism for EtSSEt activation appears to be oxidative addition.

F. References

- 1. Cotton, F. A.; Walton, R. A. Multiple Bonds Between Metal Atoms; Clarendon: Oxford, 1993; pp 161-162, 233.
- 2. McCarley, R. E.; Templeton, J. L.; Colburn, T. J.; Kotavic, V.; Hoxmeier, R. J. Adv. Chem. Ser. 1976, 150, 318.
- 3. Cotton, F. A.; Pederson, E. Inorg. Chem. 1975, 14, 399.
- 4. Santure, D. J.; Huffman, J. C.; Sattelberger, A. P. Inorg. Chem. 1985, 24, 371.
- 5. Erwin, D. K.; Geoffroy, G. L.; Gray, H. B.; Hammond, G. S.; Solomon, E. I.; Trogler, W. C.; Zagars, A. A. J. Am. Chem. Soc. 1977, 99, 3620.
- 6. Chang, I-J.; Nocera, D. G. J. Am. Chem. Soc. 1987, 109, 4901.
- 7. Nocera, D. G. J. Cluster Sci. 1994, 5, 185.
- 8. Jansen, K.; Dehnicke, K.; Fenske, D. Z. Naturforsch 1987, 426, 1097.
- 9. (a) Cotton, F. A. Polyhedron 1987, 6, 677. (b) Cotton, F. A.; Hong, B.; Shang,
- M.; Stanley, G. G. Inorg. Chem 1993, 32, 3620. (c) Cotton, F. A.; Maloney, D. J.;
- Su, J. Inorg. Chim. Acta 1995, 236, 21. (d) Poli, R.; Torralba, R. C. Inorg. Chim. Acta. 1993, 212, 123.
- 10. (a) Cotton, F. A.; Daniels, L. M.; Dunbar, K. R.; Falvello, L. R.; O'Connor, C.
- J.; Price, A. C. Inorg. Chem. 1991, 30, 2509. (b) Canich, J. M.; Cotton, F. A.;
- Daniels, L. M.; Lewis, D. B. Inorg. Chem. 1987, 26, 4046. (c) Agaskar, P. A.;
- Cotton, F. A.; Dunbar, K. R.; Falvello, L. R.; O'Connor, C. J. *Inorg. Chem.* 1987, 26, 4051.
- 11. Cotton, F. A.; Diebold, M. P.; O'Connor, C. J.; Powell, G. L. J. Am. Chem. Soc. 1981, 107, 7438.

- 12. Canich, J. M.; Cotton, F. A.; Dunbar, K. R.; Falvello, L. R. *Inorg. Chem.* 1988, 27, 804.
- 13. (a) Cotton, F. A.; James, C. A.; Luck, R. L. *Inorg. Chem.* **1991**, *30*, 4370. (b) Fanwick, P. E.; Harwood, W. S.; Walton, R. A. *Inorg. Chem.* **1987**, *26*, 242.
- 14. (a) Partigianoni, C. M.; Nocera, D. G. *Inorg. Chem.* **1990**, *29*, 2033. (b) Partigianoni, C. M.; Turro, C.; Hsu, T.-L. C.; Chang, I-J.; Nocera, D. G. In *Photosensitive Metal-Organic Systems*; Kutal, C., Serpone, N., Eds.; Advances in Chemistry 238; American Chemical Society: Washington, DC, 1993; pp 147-163.
- 15. Hsu, T.-L. C.; Helvoigt, S. A.; Partigianoni, C. M.; Turró, C.; Nocera, D. G. *Inorg. Chem.* **1995**, *34*, 6186.
- 16. Hopkins, M. D.; Miskowski, V. M.; Gray, H. B. J. Am. Chem. Soc. 1988, 110, 1787.
- 17. Hsu, T.-L. C.; Engebretson, D. S.; Helvoigt, S. A.; Nocera, D. G. *Inorg. Chim. Acta.* **1995**, 240, 515.
- 18. Agaskar, P. A.; Cotton, F. A.; Fraser, I. F.; Manojlovic-Muir, L.; Muir, K. W.; Peacock, R. D. *Inorg. Chem.* **1986**, *25*, 2511.
- 19. Cotton, F. A.; Falvello, L. R.; Harwood, W. S.; Powell, G. L.; Walton, R. A. *Inorg. Chem.* **1986**, 25, 3949.
- 20. Fife, D. J.; Morse, K. W.; Moore, W. M. J. Photochem. 1984, 24, 249.
- 21. Cotton, F. A.; Eglin, J. L.; James, C. A. Inorg. Chem. 1992, 31, 5308.
- 22. (a) Shaik, S.; Hoffman, R.; Fisel, R.; Summerville, R. H. J. Am. Chem. Soc.
- 1980, 102, 4555. (b) Chakravarty, A. R.; Cotton, F. A.; Diebold, M. P.; Lewis, D.
- B.; Roth, W. J. J. Am. Chem. Soc. 1986, 108, 971. (c) Cotton, F. A.; Diebold, M.
- P.; O'Connor, C. J.; Powell, G. L. J. Am. Chem. Soc. 1985, 107, 7438.

- 23. (a) Engebretson, D. S.; Zaleski, J. M.; Leroi, G. E.; Nocera, D. G. Science 1994, 265, 759. (b) Hopkins, M. D.; Gray, H. B.; Miskowski, V. M. Polyhedron 1987, 6, 705.
- 24. Cotton, F. A.; Walton, R. A. Multiple Bonds Between Metal Atoms; Clarendon: Oxford, 1993; p 648.

CHAPTER 4

ATOM TRANSFER PHOTOCHEMISTRY OF W₂Cl₄(dppm)₂ AND MoWCl₄(PMe₂Ph)₄

A. Background

1. Atom Transfer

Atom transfer reactions have been the subject of research for many years owing to the importance in oxidation-reduction chemistry. ^{1,2,3,4,5} The basic reaction is ubiquitous in chemistry and biology. ⁶ Molybdenum enzymes, ⁷ for example, are known to catalyze oxygen atom transfer for a variety of substrates, such as xanthine (to uric acid), ⁸ sulfite (to sulfate), ⁹ nitrate (to nitrite), ¹⁰ dimethyl sulfoxide (to dimethyl sulfide)¹¹ and aldehydes (to carboxylic acids). ⁸ The area of atom transfer chemistry was pioneered by Henry Taube's studies of the late 1950s. With the use of isotopic labelling and product appearance studies, it was determined that some atom transfer occurs by what Taube coined an inner sphere electron transfer mechanism. ¹² This reaction type was first demonstrated with the reaction below.

$$Cr(H_2O)_6^{2+} + Co(NH_3)_5Cl^{2+} \xrightarrow{H_2O} Cr(H_2O)_5Cl^{2+} + Co(H_2O)_6^{2+}$$
 (4.1)

From the appearance of Cl⁻ in the substitutionally inert Cr^{III} product, it was reasoned that when the electron transfer occured both metal centers were bound by the Cl⁻, a tenet that was later verified by Cl isotope studies. After the electron

transfer, the substitutionally labile Co^{II} loses the CI^{-} ligand to the inert Cr^{III} complex. The simple fact that the electron transfer occurs by an inner sphere mechanism introduces an element of structural definition. The electron transfer distance is defined by the bridging ligand and the relative positions of the reducing agent and oxidizing agent are determined by the structures of the complexes. The atom transfer event can accordingly be reduced to a series of steps, which are outlined in Figure 4.1, where any of the steps can be rate limiting in the reaction. Diffusion-controlled formation of the precursor complex, equation 4.2, So formulated by Taube, the activated complex is formed with an atom bridging both the oxidizing and reducing center. The electron transfer step occurs in equation 4.4, leading to the formation of the successor complex, which subsequently dissociates to products $Cr(H_2O)_5CI^{2+}$ and $Co(NH_3)_5(H_2O)^{2+}$, equation 4.5. Due to the lability of Co^{II} , the ammonia ligands dissociate to yield $Co(H_2O)_6^{2+}$, equation 4.6, in a kinetically unimportant step.

The electron equivalents transferred in an atom transfer are typically determined by the atom that is transferred. For instance, the transfer of univalent atoms will usually mediate one electron reactions. ¹⁴ Divalent atoms, such as sulfur and oxygen, are known to mediate two electron redox reactions, ¹⁴ and as such are quintessential in the study of multielectron chemistry. For this reason, such atom transfer reactions form the foundation upon which multielectron photochemistry may be built.

A major focus of oxygen atom transfer studies has been the study of model enzymatic reactions. For example, the work of Holm has focused, in part, on

Figure 4.1 General reaction mechanism for atom transfer reactions.

synthetic analogues for molybdenum oxotransferases.¹⁵ One system that has developed from this large body of research is the oxygen transfer to/from a Mo^{IV}O/Mo^{VI}O₂ complex, as shown below, equation 4.7.¹⁶

$$Mo^{VI}O_2(^tBuL-NS)_2 + X \longrightarrow Mo^{IV}O(^tBuL-NS)_2 + NO$$
 (4.7)

Whereas the work of Holm has focused mostly on atom transfer between metal complexes and organic substrates, the research efforts of Woo¹⁷ and, separately, West, have concentrated on gaining a better understanding of intermetal atom transfer. Two examples of typical reactions studied are shown below.

$$(TTP)Ti=O + (OEP)TiCI \longrightarrow (TTP)TiCI + (OEP)Ti=O$$
 (4.8)

$$(TPP)Cr + O=Cr(TPP) \longrightarrow (TPP)Cr-O-Cr(TPP)$$
 (4.9)

The atom transfer reaction between titanium porphyrines, equation 4.8, is referred to as complete atom transfer since the transferred atom is no longer bound by the donor molecule,⁴ while equation 4.9 is an example of incomplete atom transfer since the atom maintains bonds to the donor and acceptor molecules.⁴

Oxygen and sulfur atom transfer reactions that are of relevance to this thesis occur with MCl_2P_4 (M = Mo, W; P = PMe₃, PMePh₂). PMePh₂ The reactions involve the dissociation of the PR₃ ligand from the octahedral $M^{II}Cl_2P_4$ complex and ensuing oxidation to $M^{IV}(E)Cl_2P_3$ (E = O^{2-} or S^{2-}) octahedral complexes upon atom transfer from the substrate. A typical sulfur atom transfer reaction of WCl_2P_4 is shown below.

$$P = \begin{array}{c} CI \\ P \\ P \\ CI \end{array} \qquad P + X + P$$

$$CI \\ P \\ CI \\ CI \\ EX = SPR_3, \stackrel{S}{\triangle} \qquad CI \\ P \\ CI \\ P \\$$

In these reactions, atom transfer does not control the reaction kinetics; phosphine dissociation is the rate limiting step in these reactions. Correspondingly, PMe₃ dissociates from MoCl₂(PMe₃)₄ and WCl₂(PMe₃)₄ with a half-life of 18 minutes at ambient temperature and 7 minutes at 69 °C, respectively, thereby determining the reaction rate of the system.¹⁹ Likewise, the bulky labile PMePh₂ is substituted by PMe₃ in WCl₂(PMePh₂)₄, and the substitution is complete within 24 hours.¹⁹ Despite that the atom transfer is inconsequential to the overall kinetics, the reactions are important to studies discussed herein. Dissociation of a phosphine ligand creates an intermediate where the d⁴ metal is in a square pyramidal

MCl₂P₄ Complexes

M₂Cl₄P₄ Complexes

Figure 4.2 Comparison of the coordination spheres of MCl_2P_4 and $M_2Cl_4P_4$. Dissociation of a phosphine ligand is the first step in the reactions of MCl_2P_4 complexes. As a result, atom transfer occurs at a square pyramidal coordination sphere in both complexes.

coordination sphere. This is analogous to the reactive site of M-4-M complexes, as summarized in Figure 4.2. It is, therefore, conceivable that similar products would result from sulfur atom transfer reactions with quadruply bonded bimetallic complexes. Moreover, because phosphine dissociation is not relevant to the M-4-M systems, the direct atom transfer should be kinetically resolved thus allowing us, in principle, to study the details of two electron atom transfer.

While there are many examples of thermal atom transfer reactions,²³ photoinitiated atom transfer is less well known. An atom can be transferred to a photochemically generated transition metal intermediate or through direct interaction with the transtion metal excited state. The first type of reactivity is well established. This is typified by the creation of a reactive intermediate by M–M or M–L bond homolysis in the excited state followed by atom abstraction.²⁴ For example, excitation of [CpM(CO)₃]₂ (M = Mo, W)²⁵ and MM'(CNMe)₆²⁺ (M = M' = Pd, Pt; M = Pd, M' = Pt)²⁶ results in the formation of the 17 electron species CpM(CO)₃ and the 15 electron species M(CNMe)⁺⁺, both of which are coordinatively unsaturated and very reactive. These intermediates can abstract halogen atoms from alkyl/aryl halides to yield CpM(CO)₃X and M(CNMe)X⁺, respectively. Examples of these reactions are shown in equations 4.11 and 4.12, below.

$$[CpW(CO)_3]_2 \xrightarrow{hv} 2 CpW(CO)_3$$

$$CpW(CO)_3 + Ph_3CBr \longrightarrow CpW(CO)_3Br + Ph_3C\bullet$$
(4.11)

$$[(CNMe)_{3}Pd]^{2+} \xrightarrow{h\nu} 2 (CNMe)_{3}Pd^{+}$$

$$(CNMe)_{3}Pd^{+} + CCI_{4} \longrightarrow (CNMe)_{3}PdCI^{+}$$

$$(4.12)$$

Another recent example of atom transfer via a photochemically generated intermediate involves the complex, Cp₂Ta(CH₃)(C₂H₄) (1).²⁷ The photoreactivity of this complex is summarized in Figure 4.3. The photoreaction of (1) is driven by the dissociation of ethylene from the excited state Ta complex to form of the coordinatively unsaturated intermediate, Cp₂Ta(CH₃) (2). This reacts with stoichiometric amounts of thiirane or SPMe₃ to generate Cp₂Ta(=S)(CH₃) (3). Irradiation of (1) with 0.5 equivalents of thiirane results in the formation of Cp₂(CH₃)Ta(μ-S)Ta(CH₃)Cp₂ dimer(4), which can also be prepared by irradiation of (1) in the presence of (3). Complex (3) undergoes migratory insertion of the Ta–CH₃ bond upon irradiation to form "Cp₂Ta–SCH₃", which then reacts with thiirane to yield Cp₂Ta(=S)(SCH₃) (5). This is in contrast to the thermal chemistry of (3), which reacts with thiirane to give the persulfido complex, Cp₂Ta(μ-S₂)(CH₃) (6) and can be regenerated upon reaction of (6) with PR₃. Irradiation of (6) yields the atom abstraction products (3), (5), SPR₃ and other products, in low yields.

The above systems are all examples of atom transfer to/from a reactive intermediate generated from an excited state. Examples of direct atom transfer to an excited state are not as pervasive. Certainly, the most developed chemistry in this front is that of the d^8-d^8 dimers.²⁸ The $^3A_{2u}$ ($d\sigma^*p\sigma$) excited state of $Pt_2(pop)_4^{4-}$ abstracts hydrogen atoms from (CH₃)₂CHOH, PhCH(OH)CH₃, Bu₃SnH, Et₃SiH and H₃PO₃. The triplet state of $Pt_2(pop)_4^{4-}$ can also abstract halogens from alkyl and aryl halides. Transient absorption spectroscopy shows that the initial product is a $Pt^{II}Pt^{III}$ mixed valence species, $Pt_2(pop)_4X^{4-}$, ^{29,30} which then undergoes thermal X atom transfer to give a $Pt^{III}Pt^{III}$ final product. Likewise, the d^8-d^8 system $Rh_2L_2(dppm)_2^{2+}$ (L = 2,5-di-isocyano-2,5-dimethylhexane) undergoes

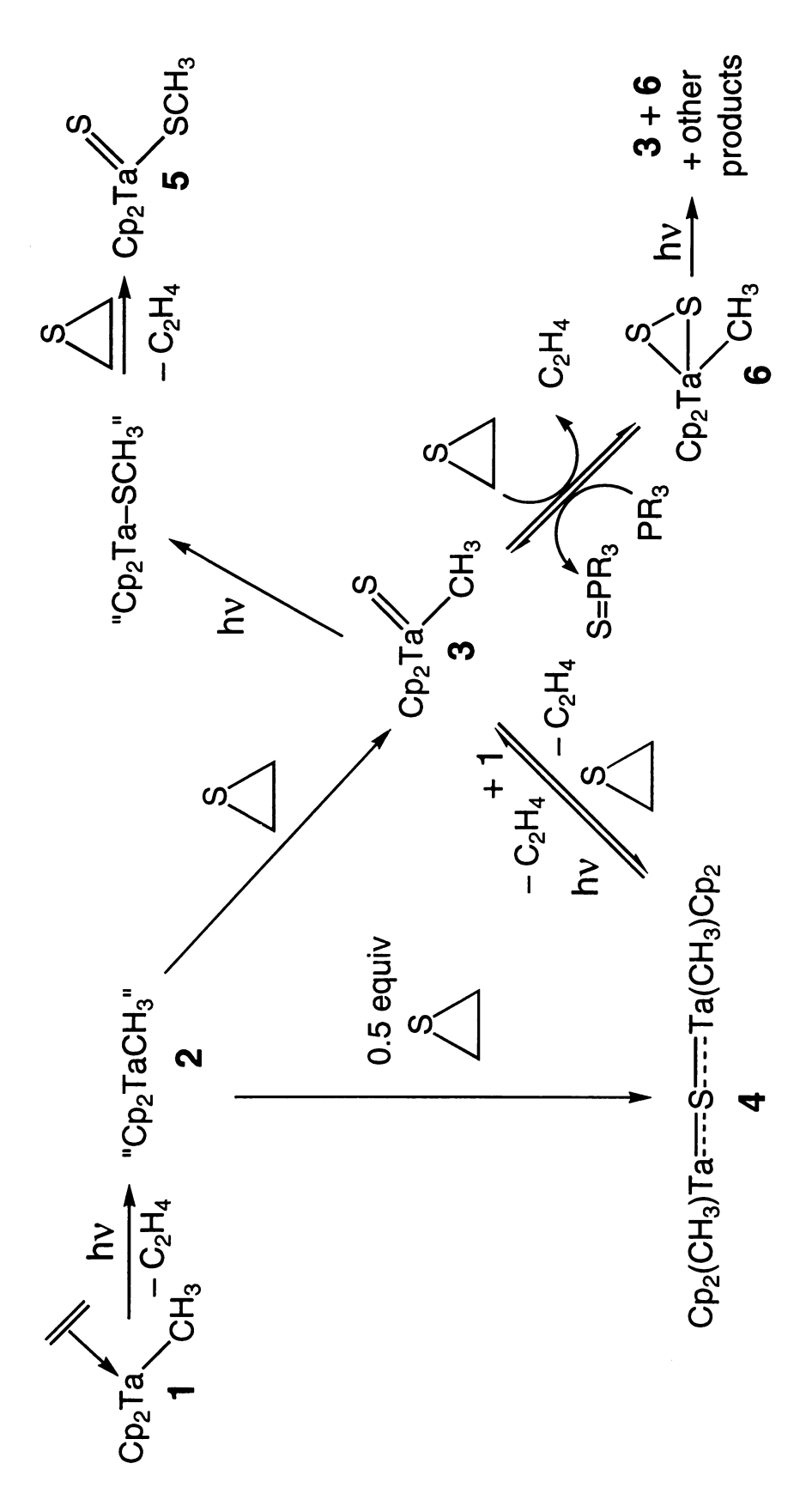


Figure 4.3 The photoreactivity of $Cp_2Ta(C_2H_4)CH_3$. The coordinatively unsaturated " Cp_2TaCH_3 " is generated upon photolysis of $Cp_2Ta(C_2H_4)CH_3$.

photoinitiated atom abstraction with alkyl and aryl halides directly from the excited state,³¹ along the same mechanistic lines described for $Pt^{II}Pt^{II}$ system. The Rh–Rh system has an advantage over the $Pt_2(pop)_4^{4-}$ system in that it can be excited in the visible region (595 nm), as opposed to excitation at 367 nm for $Pt_2(pop)_4^{4-}$. Therefore, the Rh–Rh complex has some potential for use in solar energy conversion.

Because the transferring atom is univalent, the above examples are confined to one electron redox processes. Can two electron processes be photochemically induced? The place to look is O²⁻ transfer. There are some examples in the literature, but these are all photoinitiated; atom transfer does not directly occur with the excited state species. The photochemical oxygen atom transfer from Noxides to 1-phenyl-1,2-ethanediol (PED) is catalyzed by CrTPP(Cl).³² Irradiation of (TPP)Cr^{III}Cl in the presence of the oxygen atom transfer reagent, p-cyano-N,N-dimethylaniline N-oxide (NO) forms the strong oxidant (TPP)Cr^VO and p-cyano-N,N-dimethylaniline (DMA). (TPP)Cr^{IV}O can then either disproportionate with the starting material, (TPP)Cr^{III}Cl, to form (TPP)Cr^{IV}O or transfer on oxygen to PED to form benzaldehyde, formaldehyde, water and (TPP)Cr^{III}Cl. This reaction is summarized in equations 4.13 - 4.15.

$$(TPP)Cr^{III}CI + NO \xrightarrow{h\nu} \longrightarrow (TPP)(CI)Cr^{V}O + DMA$$
 (4.13)

$$(TPP)(CI)Cr^{V}O + (TPP)Cr^{III}CI \xrightarrow{H_2O} 2(TPP)Cr^{IV}O + 2HCI$$
 (4.14)

$$(TPP)(CI)Cr^{V}O + PED \longrightarrow$$

$$(TPP)Cr^{III}CI + PhCHO + HCHO + H2O (4.15)$$

Likewise, irradiation of MnTPP(OAc) in the presence of IO₄⁻ and various hydrocarbons (R₃CH) results in the catalytic production of R₃COH.³³ Upon dissolution of MnTPP(OAc) and R₄NIO₄, the complex MnTPP(IO₄) is formed. Irradiation of MnTPP(IO₄) creates the strong oxidant O=MnTPP⁺ by oxygen atom abstraction from IO₄⁻. This oxo then oxidizes R₃CH to R₃COH, as shown below.

$$MnTPP(OAc) + IO_4^- \longrightarrow MnTPP(IO_4) + OAc^- (4.16)$$

$$MnTPP(IO_4) \xrightarrow{hv} O=MnTPP^+ + IO_3^- \qquad (4.17)$$

$$O=MnTPP^+ + R_3CH \longrightarrow MnTPP^+ + R_3COH$$
 (4.18)

B. Photoreaction of W₂Cl₄(dppm)₂ and N₂O

We have shown that quadruply bonded bimetallic complexes form a long-lived high energy intermediate with two electrons localized on one W metal center upon excitation of the $^1(\pi\delta^*)$ transition. The localization of two electrons on one metal of the bimetallic core ideally sets the stage for atom transfer reactions with two electron substrates such as oxygen or sulfur. In an effort to demonstrate the principle of a two electron reaction, the most energetically favorable structure for atom transfer was crafted. The W_2 quadruple bond systems are the most easily oxidized. Thus, $W_2Cl_4(dppm)_2$ was chosen as the M-4-M photoreagent. With regard to the atom transfer reagent, nitrous oxide (N_2O) is ideal. There is a large driving force for the loss of N_2 ($\Delta G_f^{\circ} = 25$ kcal/mol), which upon atom transfer is the only side product. Due to its high activation barrier (59 kcal/mol), it has potential as a selective reagent.

There are many examples of reactions between transition metals and N_2O that involve the formation of M-O bonds.³⁷ A characteristic reaction is the formation of metal-oxo clusters; for example the reaction of Cp_2M (M = V, Cr) with N_2O affords the cluster compounds, $(\eta^5-Cp)_5V_5(\mu^3-O)_6$ and $(\eta^5-Cp)_4Cr_4(\mu^3-O)_4$.³⁸ In contrast, a terminal M=O bond is less commonly observed owing to the propensity of the oxygen to bridge metals to form higher nuclearity products. Cluster formation has been observed to be circumvented when σ donating ligands are also present.³⁹ For example, the reaction of $*Cp_2Ti(C_2H_4)$ and N_2O in pyridine/THF solutions results in $*Cp_2Ti(=O)(py)$ ($*Cp = Me_5C_5$; py = pyridine).

Of course, oxygen atom transfer reactivity is not the only reaction available to N_2O . There is one known complex with N_2O as a ligand, $[Ru(NH_3)_5(N_2O)]^{2+.40}$ From X-ray powder and IR results, the N_2O is bound in an $^1\eta$ -N fashion, Ru-N=NO. Moreover, $(ArRN)_3Mo$ -N and $(ArRN)_3Mo$ -NO were recently formed by the cleavage of the N=N bond of nitrous oxide by $(ArRN)_3Mo$ $(Ar = 3,5-C_6H_3Me_2; R = C(CD_3)_2CH_3).^{41}$ However, examples of this type of reactivity for N_2O have rarely been observed in the literature, 42 and N_2O typically reacts to deliver an oxygen atom to a metal center. On the basis of this literature, the photochemistry of $W_2Cl_4(dppm)_2$ with N_2O was studied.

1. Characterization of Inorganic Products

Irradiated solutions of $W_2Cl_4(dppm)_2$ and THF are stable. However, irradiation ($\lambda_{exc} > 375$ nm, -80 °C) in the presence of N_2O results in the spectral changes in Figure 4.4. The reaction requires one week to reach completion and the lack of isosbestic points indicates that more than one product is formed. The final absorption spectrum is characteristic of edge-sharing bioctahedrals and indeed

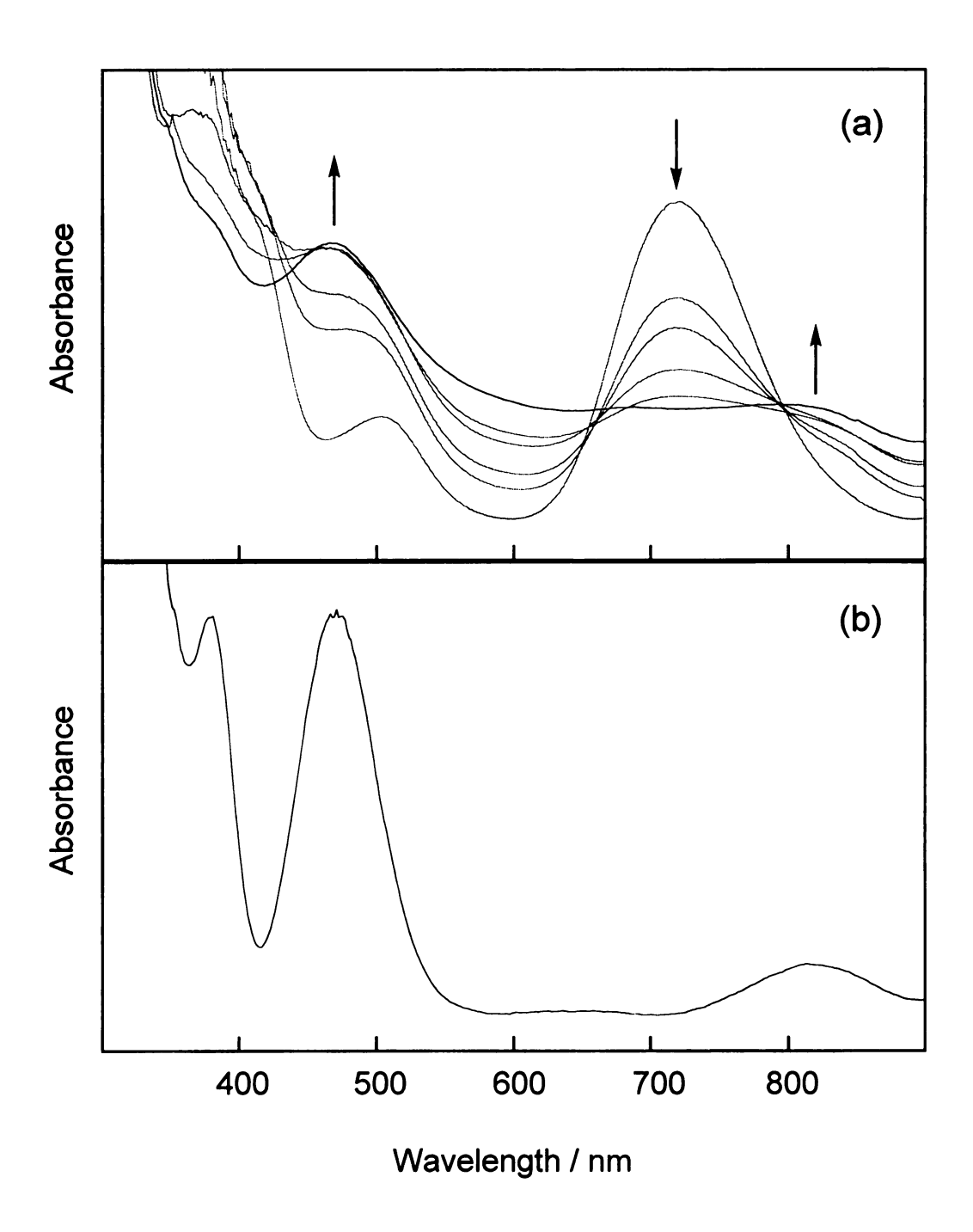


Figure 4.4 (a) Spectral changes observed upon irradiation of $W_2Cl_4(dppm)_2$ and N_2O in THF. (b) Absorption spectrum of independently synthesized $W_2Cl_6(dppm)_2$

compares well to that of independently synthesized W₂Cl₆(dppm)₂;⁴³ which is also shown in Figure 4.4. Additional evidence for the formation of W₂Cl₆(dppm)₂ is provided by NMR spectroscopy. ¹H NMR resonances due to W₂Cl₆(dppm)₂, marked with an asterisk in Figure 4.5, at δ +7.4 (m; Ph-P), 7.2 (m; Ph-P) and 3.5 (s; P-C H_2 -P) ppm correspond to the dppm ligands of $W_2Cl_6(dppm)_2$. The $^{31}P\{^1H\}$ NMR spectrum shows a broad absorption at δ -106 ppm. Both the ¹H and ³¹P values compare well to the reported literature values.⁴³ The upfield shift and broadening of the ³¹P signal as compared to that of free dppm (-22.7 ppm in CH₂Cl₂) is due to the thermal population of a low lying paramagnetic state. The nuclear relaxation effects under these conditions are expected to quench the ³¹P-¹H coupling.⁴⁴ A similar result has been observed with Re₂Cl₆(dppm)₂.⁴⁵ The NMR spectrum reveals, however, that W₂Cl₆(dppm)₂ is not the sole inorganic product. Based on integration of the ³¹P{ ¹H} NMR, the formation of W₂Cl₆(dppm)₂ accounts for only ~12% of the total inorganic product. Another ~10% accounts for free dppm and resonances at δ +26 (d; Ph₂P(O)CH₂PPh₂) and -26 (br; Ph₂P(O)CH₂PPh₂) have been assigned to dppm oxide (33 %). 46 Concordant with these observations is the formation of an insoluble blue film. The possibility that this is the slightly soluble blue W₂Cl₅(µ-H)(dppm)₂ complex has been dismissed due to the absence of the characteristic AB pattern at δ +6.14 (d) and +4.55 (d) ppm (²J_{AB} = 12 Hz; in CD₂Cl₂), of the methylene protons in the ¹H NMR.⁴³ The blue film is most likely due to the formation of tungsten oxides, which charateristically form blue, insoluble films.⁴⁷

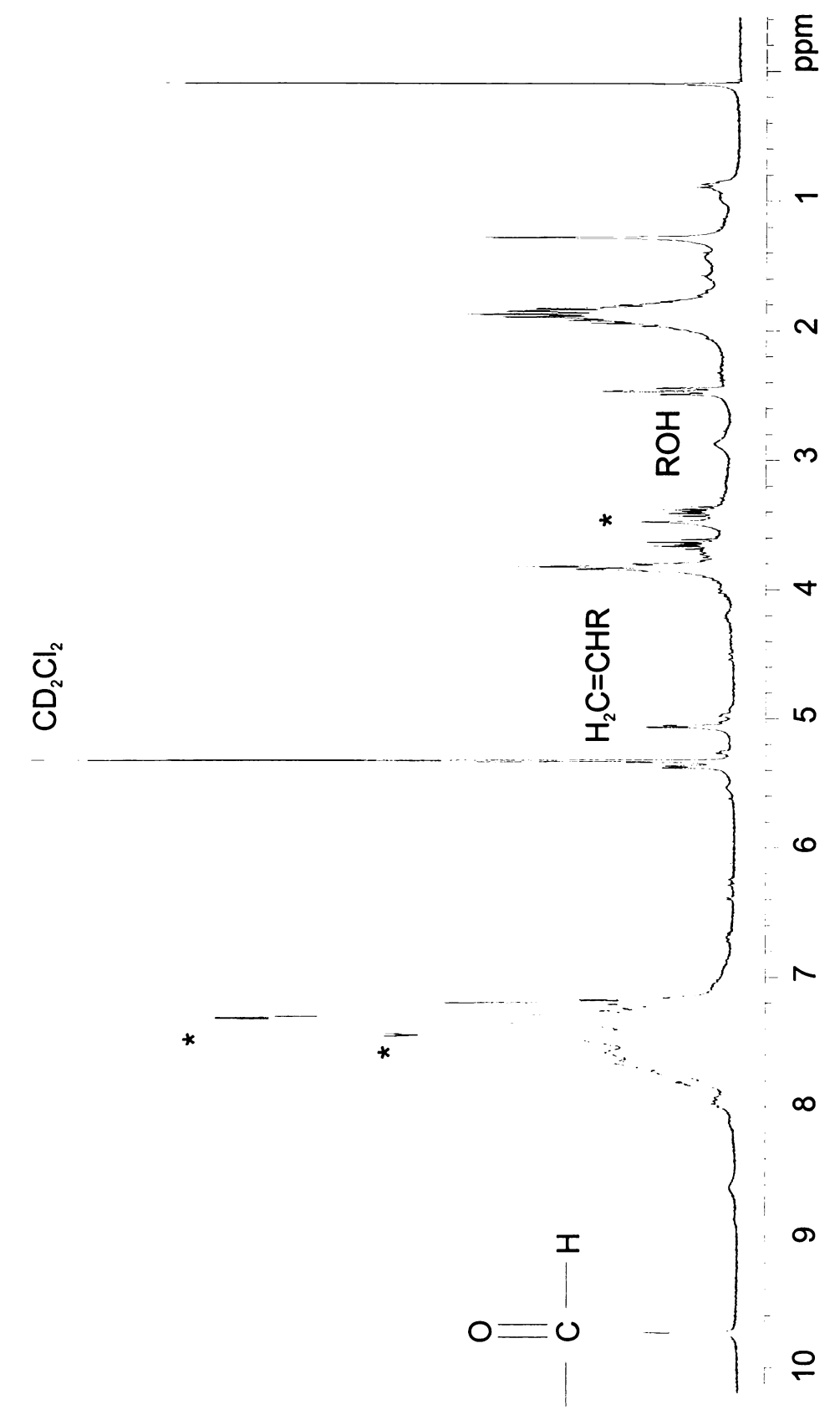


Figure 4.5 'H NMR of the photoreaction of W₂Cl₄(dppm), and N₂O. The * indicates resonances due to W₂Cl₄(dppm)₂.

2. Characterization of Organic Products

Most of the ¹H NMR resonances (Figure 4.5) of the photolyzed solution are due to organic side products from reaction of THF. While none of the organic side products have been definitively characterized, the nature of the products should be similar to those characterized previously from the direct photolysis of ethers and alcohols. 48,49 It has been shown that the photolysis ($\lambda_{exc} > 185$ nm) of THF in the liquid or gas phase results in decomposition to form the products in Figure 4.6. 48,49 For cyclic ethers, the primary reaction of the $n\sigma^*$ excited state involves C-O bond homolysis. The diradical that is produced undergoes various reactions involving fragmentation and rearrangement to aldehydes, olefins and alcohols. Resonances due to these species are observed in the ¹H NMR spectrum of the photoreacted solutions. Absorptions due to these functional groups are also observed on the IR spectrum of the organic products, as shown in Figure 4.7. In addition, an absorption at 729 cm⁻¹ in the region of C-Cl bonds (800 - 600 cm⁻¹)⁵⁰ is observed. These results suggest that the products of the photoreaction of THF are similar to those formed from the direct photolysis but also include some chlorinated products.

3. Reaction Pathway

It is clear from the above results that oxygen atom transfer from N_2O to $W_2Cl_4(dppm)_2$ is not observed. A radical mechanism is most likely responsible for the photochemistry observed with $W_2Cl_4(dppm)_2$ and N_2O , as indicated by the formation of $W_2Cl_6(dppm)_2$ (see Chapter 3). Two processes appear to be ocurring in this reaction; the coordination of THF by $W_2Cl_4(dppm)_2$ and the insertion of an

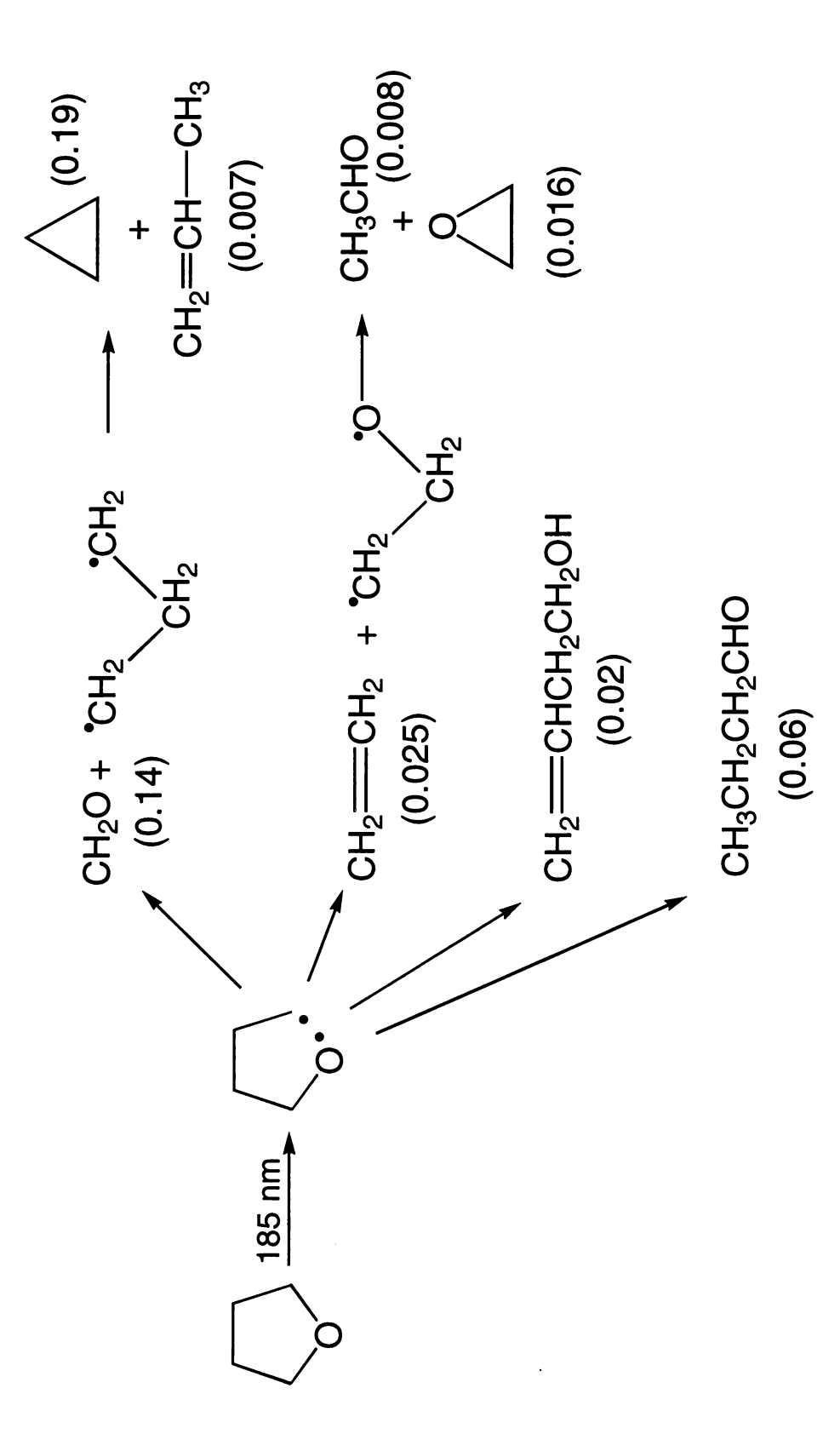


Figure 4.6 Products from the photolysis of THF ($\lambda_{\rm exc} > 185$ nm). Quantum yields are shown in parenthesis.

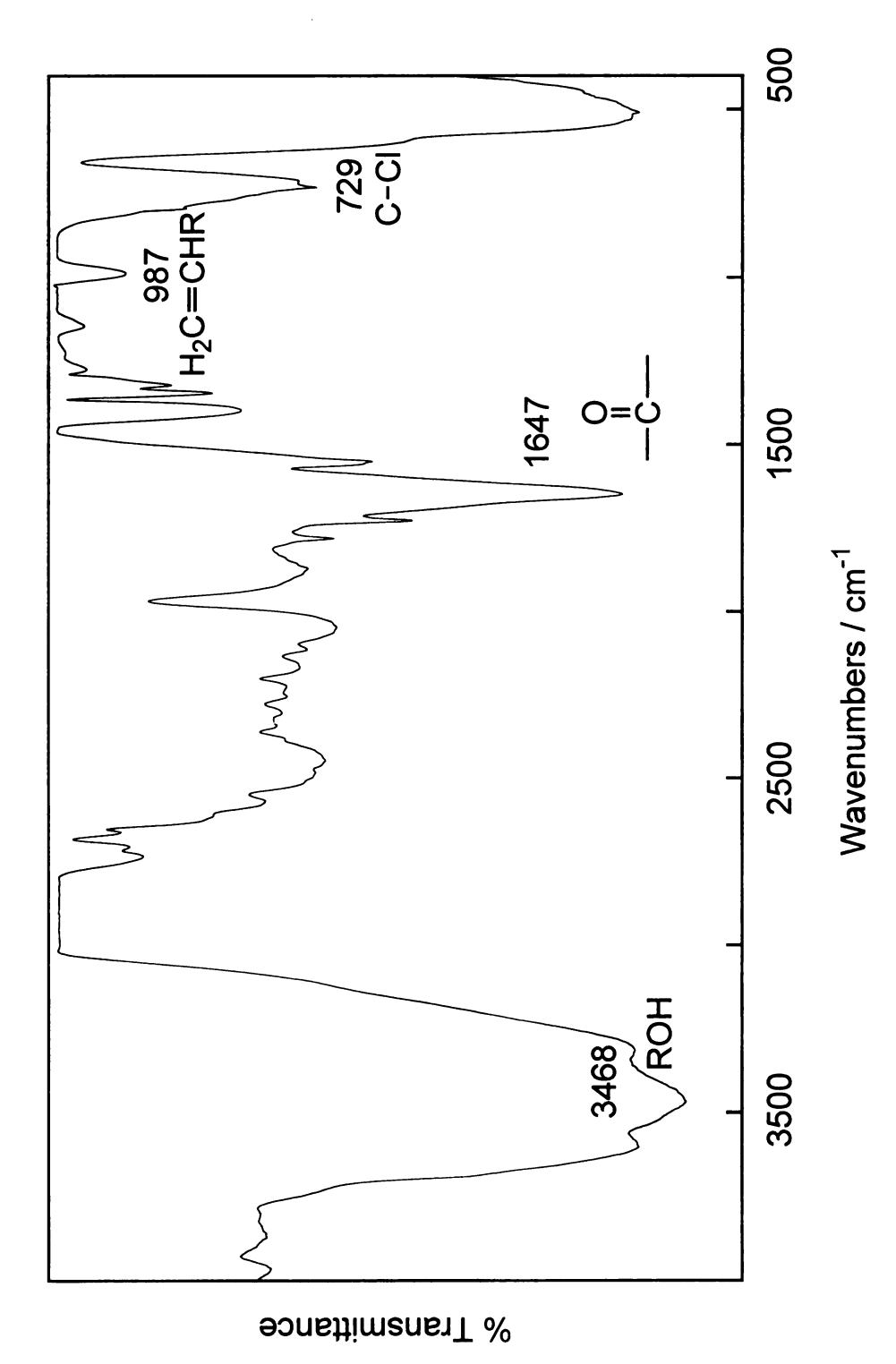


Figure 4.7 FTIR spectrum of organic side products from the photolysis of W₂Cl₄(dppm)₂ and N₂O in a THF solution.

oxygen atom into the bound THF and its ensuing cleavage. Literature precedence for both of these processes exist.

Ligation of THF in the axial position of W₂Cl₄(dppm)₂ could weaken the C–O bond, facilitating the insertion of an oxygen atom and the ring opening reaction of the newly formed metal-ester. Precedence for axial coordination of THF comes in the photochemistry of Mo₂[O₂P(OPh)₂]₄. Determination of the structure of a single crystal of Mo₂[O₂P(OPh)₂]₄ grown in THF solvent shows two molecules of THF coordinated in this position on either end of the complex.⁵¹ Consequently, the photoreaction of Mo₂[O₂P(OPh)₂]₄ with 1,2-dichloroethane is significantly hindered by coordinating solvents such as THF and CH₃CN.

Moreover, W–THF bonds are very strong. For instance, THF can cleave the W–Cl_b–W bonds of $[WCl_4(NC_6H_4Me-p)]_2$ to form $WCl_4(NC_6H_4Me-p)(THF)$. The crystal structure of the product shows that the W–O (THF) bond is elongated relative to normal W^{IV} –O oxo bonds (2.237 Å as compared to 1.7 Å for $W(O)Cl_2L_3$). Illustrating that the M-ester bond is still not as strong as the M oxo bond.

Once coordinated, the C-O bond of a THF axially ligated W₂Cl₄(dppm)₂ species is susceptible to insertion and subsequent cleavage. The ability of N₂O to insert an oxygen atom into M-L bonds is well established. Recently, it has been shown that oxygen atom transfer to organometallic complexes can introduce functionality into hydrocarbon substrates.⁵⁴ Nitrous oxide reacts with the metallocyclopentane complex, (bpy)Ni(C₄H₈), to effect oxygen atom insertion into the Ni-C bond and the elimination of N₂.⁵⁵ The product of this reaction can eliminate various hydrocarbons under different reaction conditions, as shown in



Figure 4.8. Similar reactivity has been shown to be general for the Ni^{II} alkoxides.⁵⁶ Nitrous oxide will react with both cyclic and acyclic nickel alkyls to produce a variety of nickel alkoxides, which can then be used to generate functionalized hydrocarbons.

Precedence for the cleavage of THF by transition metal complexes⁵⁷ is shown in the reaction of VCl₃(THF)₃ and the octaethylporphyrinogen macrocyclic ligand, Et₈N₄Li₄(THF)₄. This reaction results in the evolution of ethane and the formation of the vanadium ynolate, below.⁵⁸

$$\mathsf{Et_8N_4Li_4(THF)_4} + \mathsf{VCl_3(THF)_3} \longrightarrow \mathsf{R} + \mathsf{C_2H_6}$$

$$\mathsf{R} = \mathsf{CEt_2} \tag{4.19}$$

The hydrocarbon fragments are formed from the cleavage of coordinated THF, initiated by the d² V center and assisted by the Lewis acidic Li cations on the macrocycle. This occurs via the intermediate complex, (Et₈N₄)VLiCl(THF), and the cleavage of the C–O bond of THF is facilitated by Li–O coordination.

On the basis of the above results, it appears reasonable that the following process is occuring.

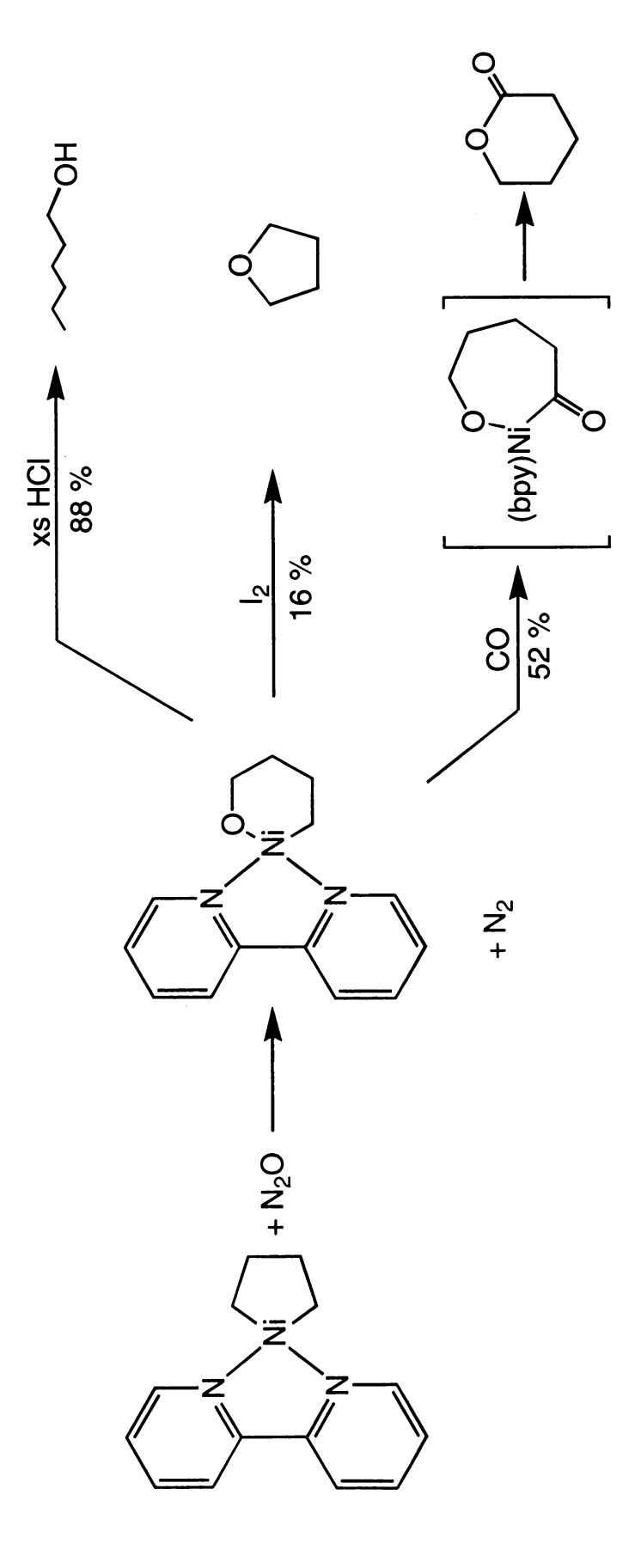


Figure 4.8 The formation of the Ni(II) alkoxide by reaction of (bpy)Ni(C₄H₈) with N₂O. A variety of functionalized hydrocarbons can be generated under different reaction conditions.

$$CI \stackrel{P}{\longrightarrow} CI \stackrel{CI}{\longrightarrow} CI \stackrel{$$

Full characterization of the liquid and gaseous organic photoproducts is neccesary to fully understand the mechanism of this photoreaction. In addition, using a noncoordinating solvent, such as toluene, could prevent the formation of organic side products and make it possible to observe oxygen atom transfer products of $W_2Cl_4(dppm)_2$.

C. Photoinitiated Sulfur Atom Transfer to MoWCl₄(PMe₂Ph)₄

The problem confronting the $W_2Cl_4(dppm)_2/N_2O$ photoreactivity appears to be of kinetic origins. In general, atom transfer involves reagents with high bond dissociation energy. Thus, even though the overall energetics of the $W_2Cl_4(dppm)_2/N_2O$ system may be favorable for atom transfer, there is still the

issue of the strong N=O bond. More generally, P-O, N-O, and S-O bonds are more stable, therefore a high activation barrier can be expected for photoinduced atom transfer reactions. Table 4.1 compares the bond energies for substrates that react by atom transfer or oxidative addition. On average, the bond strengths for atom transfer substrates are much higher than those for oxidative addition substrates. Consequently, the excited state inducing atom transfer cleavage must be energetic enough to overcome the kinetic barrier imposed by the substrate transferring the atom. The problem with quadruply bonded bimetallic complexes is that the two electron character of the homonuclear bimetallic complexes arises from an intramolecular distortion from the zwitterionic excited state. Due to this distortion, much of the energy originally put into the M₂Cl₄(PR₃)₄ excited state is lost through ligand rearrangement. As a result, their utility for multielectron photochemistry is limited to substrates with a low activation energy and therefore, oxidative addition reactions. The overall problem is schematically shown in Figure 4.9. Are there other ways to chemically trap the zwitterionic character without inducing an energy wasting intramolecular distortion? One potential solution is to build the asymmetry directly into the ground state by using a mixed-metal quadruply bonded bimetallic complex, such as MoWCl₄(PMe₂Ph)₄. This approach avoids the need for trapping the mixed valence excited state via intramolecular distortions, Figure 4.9, since the inversion center of the complex is removed. Thus electron density in these complexes may localize on a metal without distortion. In the case of Mo-W species, the electron pair is expected to reside on the Mo, since it is easier to reduce than W. Consequently, the IIIW-MoI state should have a

Table 4.1 Bond Dissociation Energies for Atom Transfer and Oxidative Addition Substrates.

Atom Transfer ^a		Oxidative Addition		
substrate	BDE ^{b,c} (kcal)	substrate	BDE ^b (kcal)	
O_3	21	I–I	36 ^d	
N_2O	34	Br–Br	46 ^d	
Cl ₂ SeO	58	PhS-SPh	55 ^e	
PhCH=N(O)Ph	63	CH ₃ –I	56 ^f	
C ₅ H ₅ NO	72	Cl–Cl	58 ^d	
$Pr^{n}N=N(O)Pr^{n}$	59	HS-SH	61 ^g	
SO_3	83	MeHg–Me	61 ^g	
Me ₂ SO	87	CH ₃ -Br	70 ^e	
$MoOCl_4$	101	H–I	71 ^e	
Ph ₃ AsO	103	PhS-H	83 ^g	
SOCl ₂	104	CH ₃ -Cl	84 ^e	
Me_2SO_2	118	H–Br	88 ^e	
Cl ₃ PO	124	R ₃ Si–H	~90 ^g	
WOCl ₄	127	Н–Н	104 ^e	
Ph ₃ PO	133			
(EtO) ₃ PO	148			

a. reference 35; b. BDE = bond dissociation energy; c. for reaction XO = X + O; d. Morrison, R. T.; Boyd, R. N. *Organic Chemistry*; Prentice Hall:Englewood Cliffs, NJ, 1992, 6th edition. e. reference 78; f. reference 77; g. *Handbook of Chemistry and Physics*, 69th ed.; CRC: Boca Raton, Florida, 1988; p F-183.

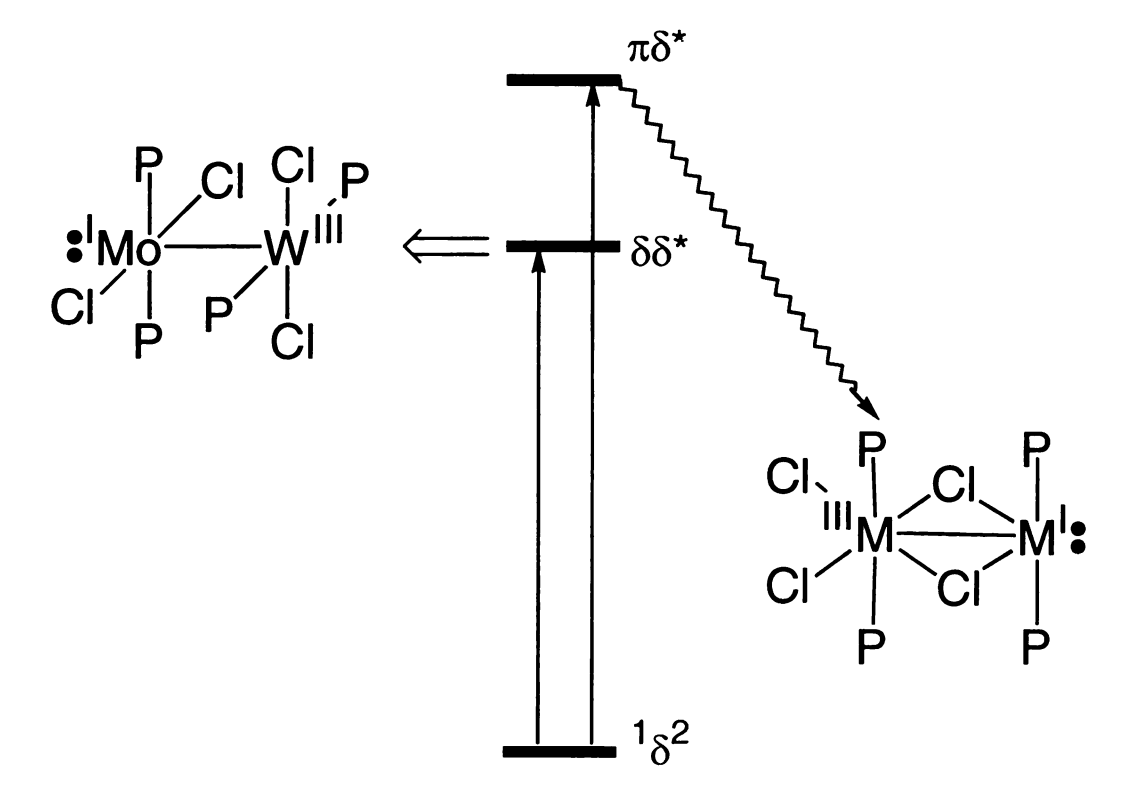


Figure 4.9 Proposed mechanism for the formation of the mixed valence excited state of heteronuclear and homonuclear quadruply bonded bimetallic complexes.

greater contribution to the linear combination of the $\delta\delta^*$ excited state, as opposed to the homonuclear complexes where each resonance form contributes equally. Along these lines, the excited state of MoWCl₄(PMe₂Ph)₄ can be expected to be more reactive than homobimetallic M-4-M complexes.

The atom transfer reactions of MCl₂(PMe₃)₄ (M = Mo, W) with a variety of substrates are well characterized and provide a good reference for developing MoWCl₄(PMe₂Ph)₄ atom transfer photochemistry. MoCl₂(PMe₃)₄ abstracts a sulfur atom from SPMe₃ to yield Mo(S)Cl₂(PMe₃)₃, which conproportionates with MoCl₂(PMe₃)₄ to form the dimer, Mo₂(μ–S)(μ–Cl)Cl₃(PMe₃)₅.²⁰ If the complexes M(S)Cl₂(PMe₃)₃ and M´Cl₂(PMe₃)₄ (M, M´ = Mo or W) are heated at 80 °C, they undergo incomplete atom transfer to form the dimer MM´(μ–S)(μ–Cl)Cl₃(PMe₃)₄,⁵⁹ as shown in Figure 4.10. These products are similar to the two-electron oxidized products of M–4–M complexes,⁶⁰ and could also reseasonably be a product of sulfur atom transfer to MoWCl₄(PMe₂Ph)₄. With this in mind, the sulfur atom transfer photochemistry of the mixed-metal quadruply bonded complex, MoWCl₄(PMe₂Ph)₄, with the sulfur atom transfer reagent, Ph₃PS, was studied.

1. Photophysics

Before the photochemistry of MoWCl₄(PMe₂Ph)₄ was undertaken, an understanding of the photophysics of the complex was desired. The visible absorption spectrum of MoWCl₄(PMe₂Ph)₄ is shown in Figure 4.11, along with those of Mo₂Cl₄(PMe₂Ph)₄ and W₂Cl₄(PMe₂Ph)₄. The assignment of the electronic transitions is consistent with the Mo₂ and W₂ homologs.⁶¹ Correspondingly, the two lowest energy transitions can be assigned to ${}^{1}(\delta \rightarrow \delta^{*})$ and ${}^{1}(\pi \rightarrow \delta^{*})$, as

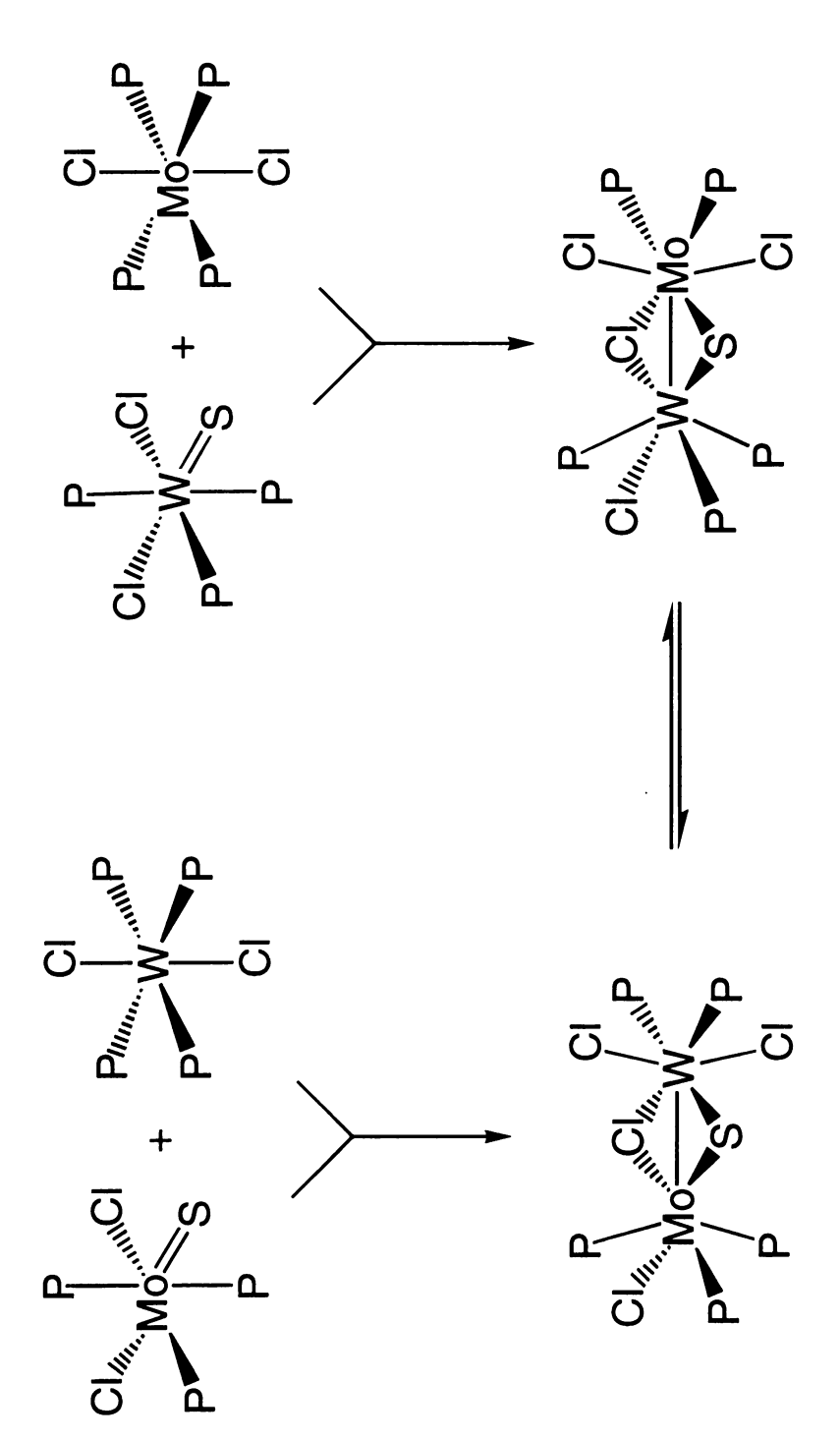


Figure 4.10 Formation of the mixed-metal dimers from MCl₂P₄ and M(S)Cl₂P₃.

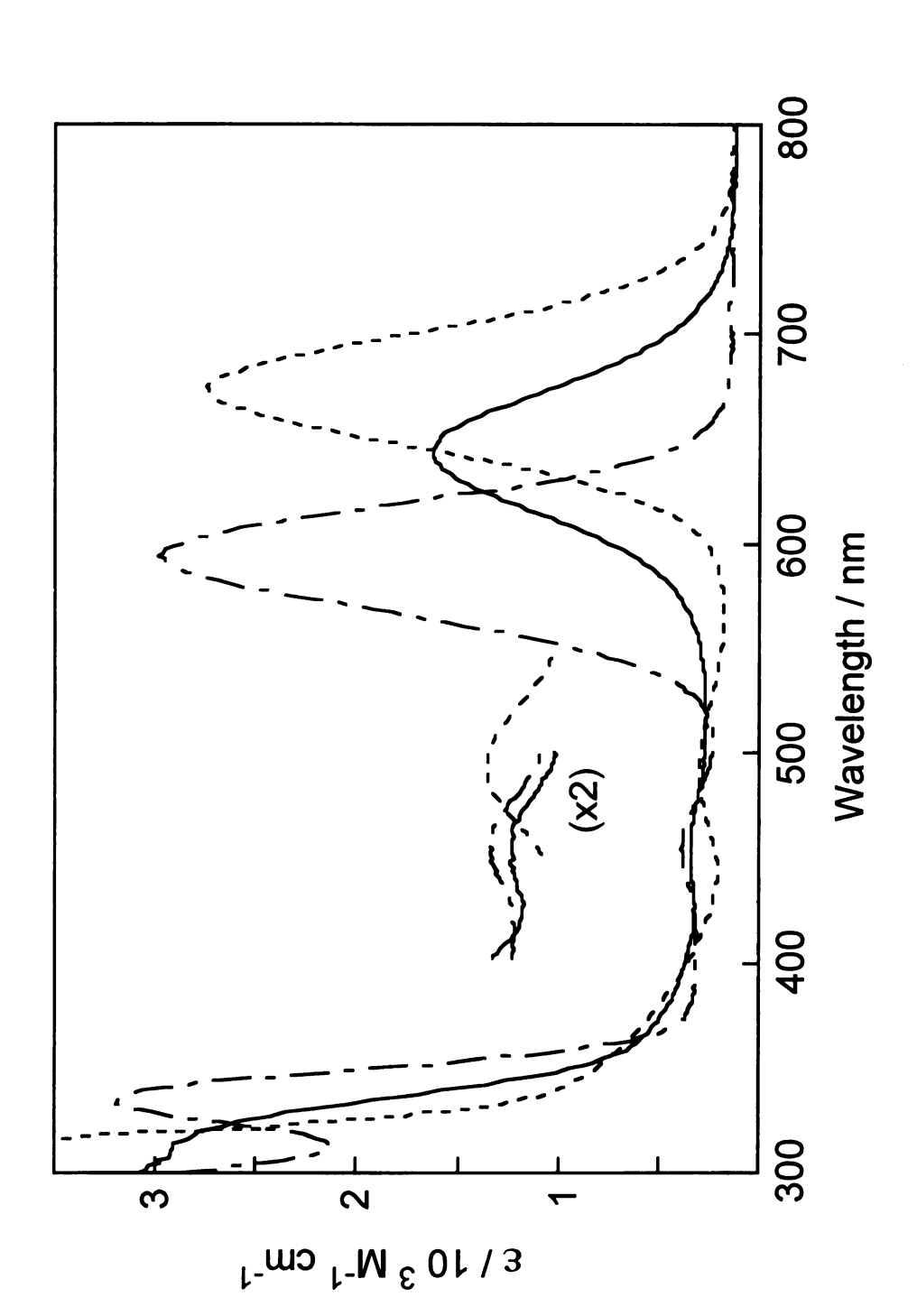


Figure 4.11 Absorbance spectra of $Mo_2Cl_4(PMe_2Ph)_4$ (— -), $MoWCl_4(PMe_2Ph)_4$ (——) and $W_2Cl_4(PMe_2Ph)_4$ (----) in benzene.



discussed in Chapter 1. These transitions for MoW fall between those for Mo_2 and W_2 . This is consistent with there MMCT character since a decrease in contributions of the two electron energy to the overall transition energy is expected on moving from Mo to W. The higher energy transitions have been assigned to LMCT in the homobimetallics. These transitions exhibit blue shifts upon substitution of W for Mo due to the larger radial extension of the W orbitals. We see that this transition for the MoW complex does indeed shift to the blue of W_2 but lies to lower energy than Mo_2 .

MoW dimer has emission and lifetime characteristics that also fall in line with its homonuclear congeners. MoWCl₄(PMe₂Ph)₄ exhibits red luminescence upon excitation of the $^1(\delta \rightarrow \delta^*)$ transition. The electronic absorption and emission spectra are essentially mirror images, Figure 4.12, indicating a small Stokes shift and an excited state with a similar geometry as the ground state. Table 4.2 lists the lifetimes, luminescent quantum yields, and the luminescence maxima for Mo₂Cl₄(PMe₂Ph)₄, MoWCl₄(PMe₂Ph)₄ and W₂Cl₄(PMe₂Ph)₄. The lifetime of MoW (44 ns) is longer than the lifetime of Mo₂ (11 ns) and very similar to W₂ (45 ns). The lifetime of MoW is long enough for a bimolecular reaction at high concentrations. The luminescent quantum yield of MoWCl₄(PMe₂Ph)₄ is 0.069 and, as expected based on the lifetimes, similar to the quantum yield for W₂Cl₄(PMe₂Ph)₄ ($\phi_e = 0.051$). The luminescent maximum of MoW ($\lambda = 810$ nm) is red shifted from both Mo₂ and W₂ ($\lambda = 690$ and 790 nm, respectively). Since the $^1\delta\delta^*$ absorption transition falls between those of Mo₂ and W₂, it is suprising that the $^1\delta\delta^*$ emission energy does not.

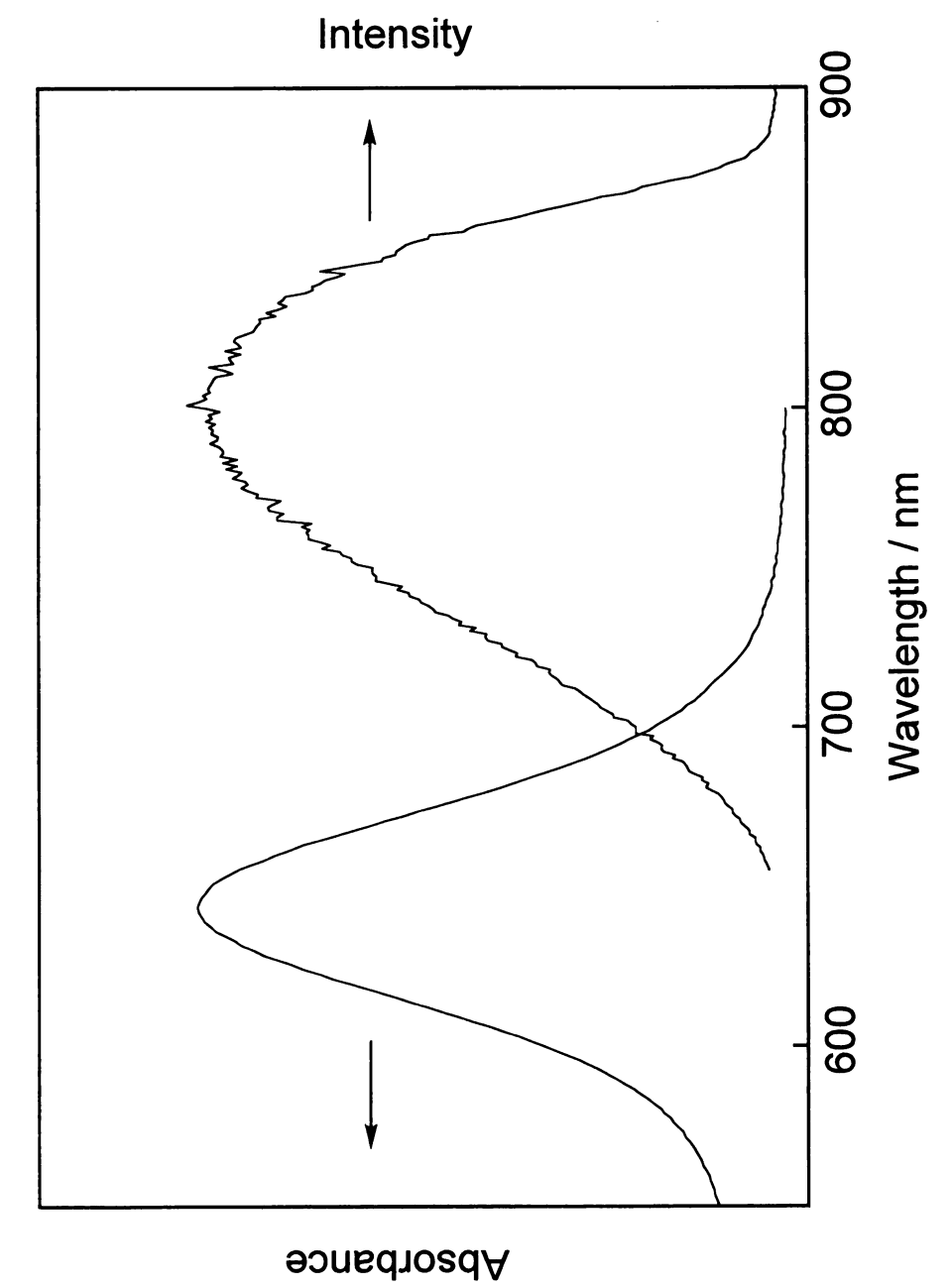


Figure 4.12 Electronic absorption and emission spectra of the $\delta\delta^*$ transition of MoWCl₄(PMe₂Ph)₄ in benzene.

Table 4.2 Physical Properties of M₂Cl₄(PMe₂Ph)₄

M_2	τ ₀ /ns	фе	$\lambda_{\text{em,max}}$ /nm	ϵ_{ox} /V	ϵ_{red} / V
Mo ₂	11 ^a	0.011 ^a	690	0.80 ^c	-1.63°
MoW	44	0.069 ^b	810	0.43 ^c	-1.73 ^c
W_2	45 ^a	0.057 ^b	790	-0.106	-2.14

a. Hsu, C. T.-L. Ph.D. Dissertation, Michigan State University, 1995.

b. Emission quantum yield was measured on dilute benzene solution of $M_2Cl_4(PMe_2Ph)_4 \ (absorbance < 0.1) \ and \ determined by using a 2-methylpentane solution of Mo_2I_4(PMe_3)_4 \ at \ \lambda_{exc} = 636 \ nm \ at \ 300K.$

c. reference 65

The zwitterionic nature of the $^1\delta\delta^*$ excited state of MoW has been confirmed by the two-photon excitation of the fluorescence of MoWCl₄(PMe₃)₄. 63 The $^1\delta^*\delta^*$ - $^1\delta\delta^*$ energy gap (ΔE) was calculated from the difference between the λ_{max} of the $^1\delta^*\delta^*$ excitation band and the absorption band of $^1\delta\delta^*$ and is equal to 6003 cm $^{-1}$. The small ΔE is consistent with the valence bond model that has been used for the M–4–M homonuclear complexes. 34,64 This establishes that the $^1\delta\delta^*$ excited state of MoWCl₄(PR₃)₄ is zwitterionic and capable of two electron chemistry.

The redox potentials for MoWCl₄(PMe₂Ph)₄⁶⁵ are listed in Table 4.2, along with those for Mo₂Cl₄(PMe₂Ph)₄ and W₂Cl₄(PMe₂Ph)₄. While, the potentials for MoW fall close to the average for Mo₂⁶⁵ and W₂, they are closer to Mo₂. This is especially apparent in the reduction potentials where the differences are $\Delta(\text{Mo}_2 - \text{MoW}) = 0.10$ and $\Delta(\text{MoW} - \text{W}_2) = 0.41$ V. Therefore, the ground state reactivity might be expected to be similar to Mo₂Cl₄(PMe₂Ph)₄.

2. Photochemistry

Whereas benzene solutions of MoWCl₄(PMe₂Ph)₄ and Ph₃PS are indefinetly stable in the absence of light at room temperature, irradiation MoWCl₄(PMe₂Ph)₄ in the presence of excess Ph₃PS produces the spectral changes in Figure 4.13. The lack of isosbestic points indicates that there is not a clean conversion from reactants to products. The ¹H and ³¹P{¹H} NMR and solution IR spectra compare well to those of independently synthesized W(S)Cl₄(PMe₂Ph). Resonances from W(S)Cl₄(PMe₂Ph) show up at δ +7.7 ppm (m), +7.03 (m), +1.36 (d, ¹J_{PH} = 13 Hz) in the ¹H NMR and at δ = +31.6 ppm (s) in the ³¹P{¹H} NMR, Figures 4.14 and 4.15. Additionally, absorbances in the IR spectrum of the

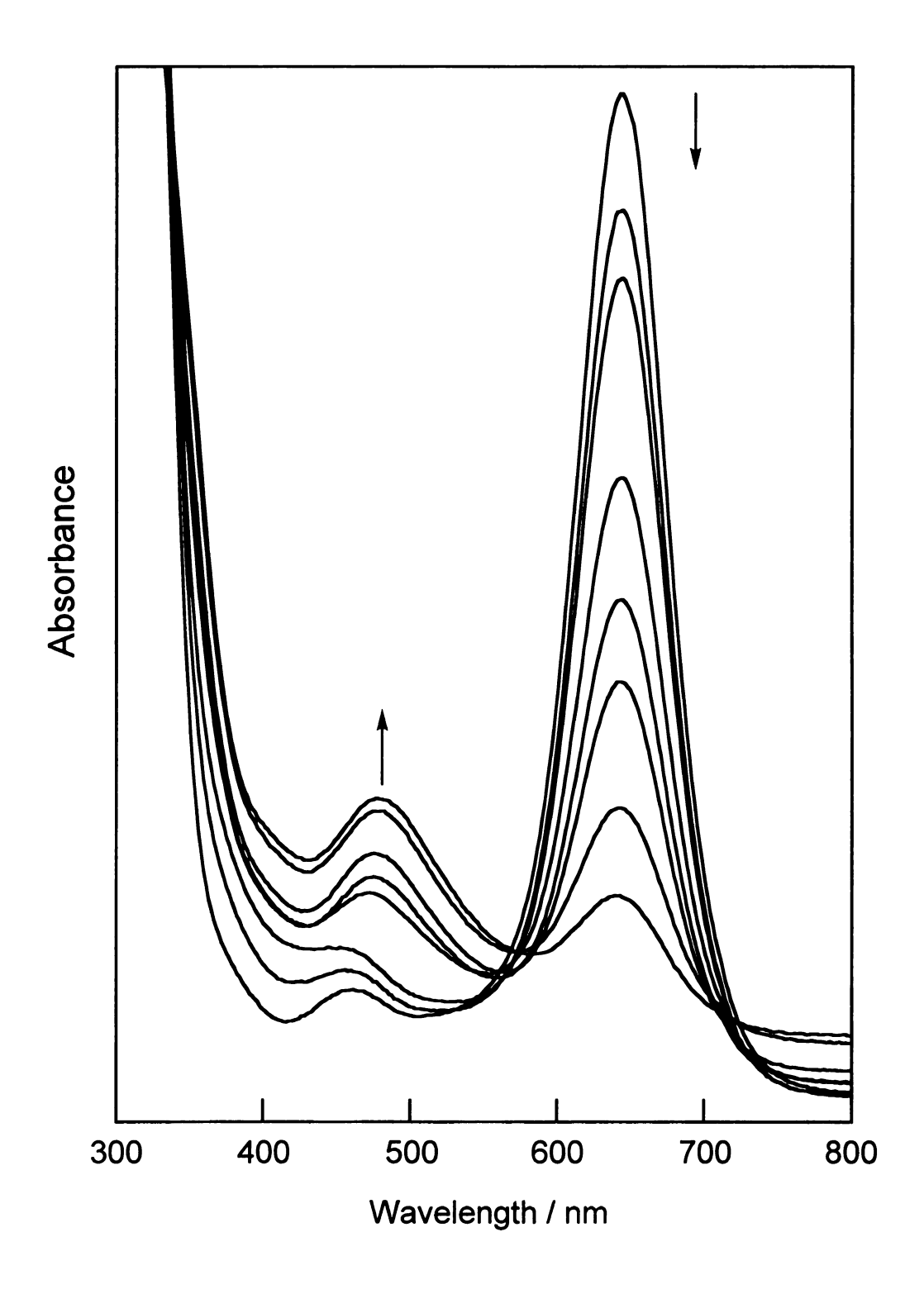


Figure 4.13 Spectral changes associated with the photolysis ($\lambda > 375$ nm) of MoWCl₄(PMe₂Ph)₄ and Ph₃PS in benzene.

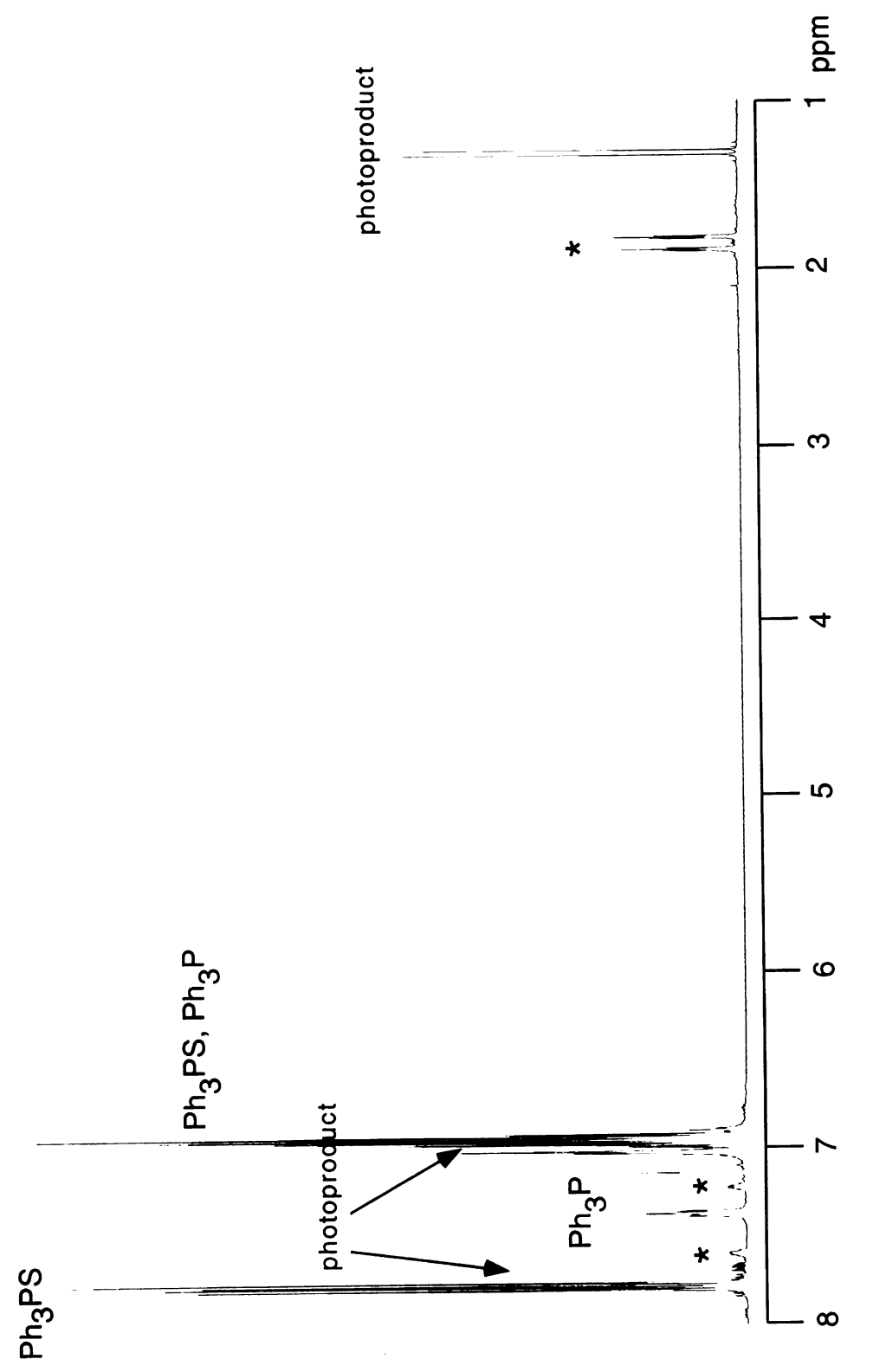
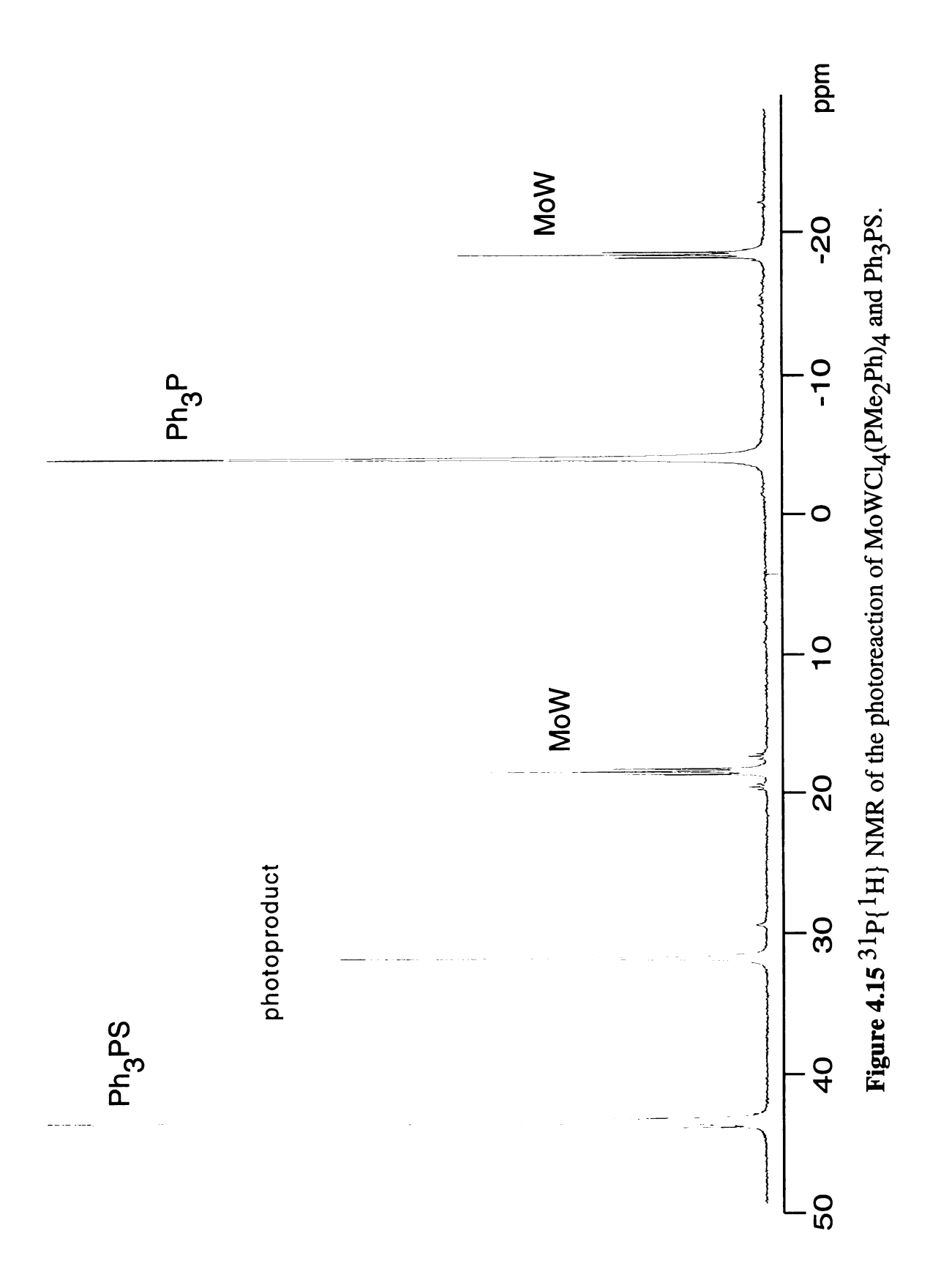


Figure 4.14 ¹H NMR of the photoreaction upon photolysis of MoWCl₄(PMe₂Ph)₄ and Ph₃PS. * denotes resonances due to MoW starting material.



photoreaction at 594 cm⁻¹ (m), 570 (m) are due to W(S)Cl₄(PMe₂Ph). Additional resonances in the ¹H and the ³¹P{¹H} NMR and absorbances in the IR spectra of the photoreaction have also been assigned (Figures 4.14 - 4.16). A molecular ion peak corresponding to W(S)Cl₄ (355 amu, MeOH) is observed in the GC/MS of the photoreaction due to the displacement of PMe₂Ph from W(S)Cl₄(PMe₂Ph) by MeOH. This is observed in the ³¹P{¹H} NMR of independently synthesized W(S)Cl₄(PMe₂Ph) in MeOH, which shows resonances due to uncoordinated PMe₂Ph. If the incomplete photoreaction is removed from the lamp and stored in the dark at about 28 °C, the reaction proceeds to completion in an additional 21 days. Attempts to isolate the photoproducts on alumina or silica columns failed due to decomposition.

The reaction of Ph₃PS and MoWCl₄(PR₃)₄ was investigated with other phosphine ligands. The photoreaction of MoWCl₄(PMe₃)₄ and Ph₃PS ($\lambda_{exc} > 375$ nm) in benzene was slower MoWCl₄(PMe₂Ph)₄ (about 5% reacted in 6 days). The reaction was not taken to completion and no products were isolated.

The atom transfer photoreaction is unique to MoWCl₄(PMe₂Ph)₄. As expected, the excited state reactivity of the heteronuclear complex is markedly different than that of the homometallic complexes. Benzene solutions of the homonuclear complexes, $M_2Cl_4(PMe_2Ph)_4$ (M = Mo, W), do not react with Ph₃PS upon irradiation (M = Mo, λ_{exc} > 335 nm after 48 hrs; M = W, λ_{exc} > 375 nm after 36 hrs) or at room temperature in the dark.

Changing the R groups on the phosphine ligand has a large effect on the reactivity of both the homonuclear and heteronuclear complexes. For example, no thermal reaction of W₂Cl₄(PMe₃)₄ or MoWCl₄(PMe₃)₄ with Ph₃PS is observed and

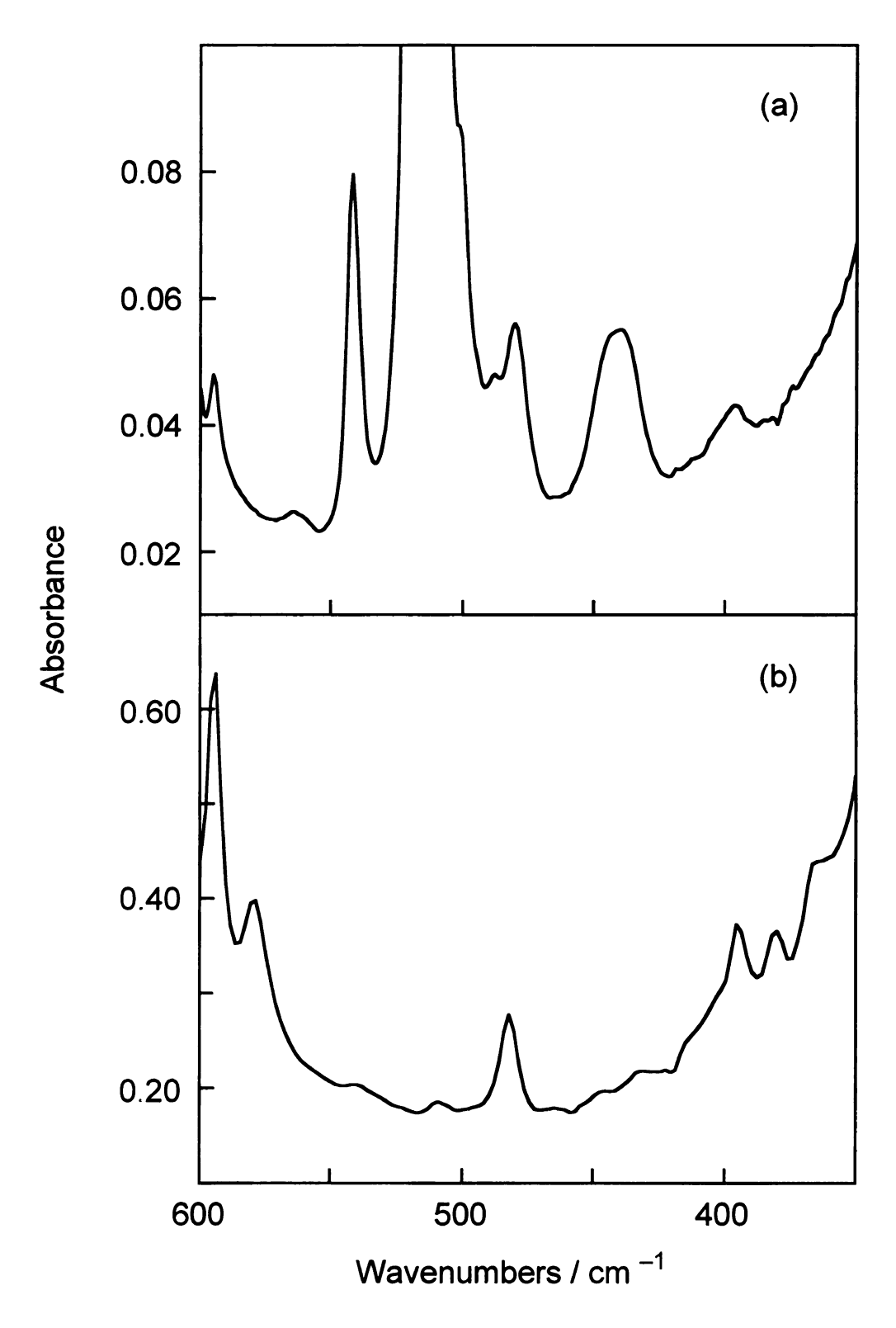


Figure 4.16 FTIR spectra of benzene solutions of (a) the neat photoreaction and (b) $W(S)Cl_4(PMe_2Ph)$. The absorbances between 550 and 400 cm⁻¹ in (a) are due to Ph_3PS and Ph_3P .

 $W_2Cl_4(PMe_3)_4/Ph_3PS$ solutions exhibit no photochemistry. However, $W_2Cl_4(PMePh_2)_4$ and $MoWCl_4(PMePh_2)_4$, both react thermally with Ph_3PS to yield Ph_2MePS , which was identified by 1H and $^{31}P\{^1H\}$ NMR. Consistent with the formation of Ph_2MePS , the 1H and $^{31}P\{^1H\}$ NMR of both reaction mixtures have doublet at δ +1.93 ppm 66 and a singlet at + 36 ppm, respectively. The reaction is probably metal mediated and not due to dissociation of Ph_2MeP , since the equilibrium constant for sulfur exchange between Ph_3PS and Ph_2MeP is only Ph_2MeP is only Ph_2MeP at 130 Ph_2MeP is only Ph_2MeP at 130 Ph_2MeP is only Ph_2MeP and Ph_2MeP is only Ph_2MeP at 130 Ph_2MeP is only Ph_2MeP and Ph_2MeP is only Ph_2MeP at 130 Ph_2MeP is only Ph_2MeP and Ph_2MeP is only Ph_2MeP at 130 Ph_2MeP is only Ph_2MeP at 130 Ph_2MeP is only Ph_2MeP and Ph_2MeP is only Ph_2MeP at 130 Ph_2MeP and Ph_2MeP is only Ph_2MeP at 130 Ph_2MeP and Ph_2MeP is only Ph_2MeP at 130 Ph_2MeP and Ph_2MeP is only Ph_2MeP and Ph_2MeP at 130 Ph_2MeP and Ph_2MeP is only Ph_2MeP at 130 Ph_2MeP and Ph_2MeP is only Ph_2MeP at 130 Ph_2MeP and Ph_2MeP is only Ph_2MeP and Ph_2MeP and Ph_2MeP is only Ph_2MeP and Ph_2MeP and Ph_2MeP is only Ph_2MeP and Ph_2MeP is only

4. Quantum Yields

wavelength dependence Table 4.3 summarizes the of th MoWCl₄(PMe₂Ph)₄/Ph₃PS photoreaction quantum yields in benzene, ϕ_p . There i considerable reaction in the visible spectral region ($\phi_{546} = 5.0 \times 10^{-4}$), with the quantum yields rising to the UV spectral region ($\phi_{365} = 1.8 \times 10^{-3}$). The fact that neither Mo₂Cl₄(PMe₂Ph)₄ nor W₂Cl₄(PMe₂Ph)₄ react with Ph₃PS when irradiated with excitation wavlengths up to 335 nm, excludes the possibility of the reaction being derived from R₃P-S bond homolysis. The photochemistry does not aris from the ${}^{1}(\delta\delta^{*})$ state, as indicated by the absence of quenching of the ${}^{1}(\delta\delta^{*})$ fluorescence until benzene solutions of MoWCl₄(PMe₂Ph)₄ are saturated wit Ph₃PS. Furthermore, no reaction is observed for $\lambda_{\rm exc} = 577$ nm, which is in th high energy tail of the $(\delta\delta^*)$ transition. The quantum yields track well with th $^{1}(\pi\delta^{*})$ transition, which lies just to higher energy of $^{1}(\delta\delta^{*})$, and suggest that th photochemistry is derived from this state. This may also imply that there is still

 $\begin{tabular}{lll} \textbf{Table 4.3} & Wavelength & Dependence of & Quantum & Yields & for Photoreaction of \\ MoWCl_4(PMe_2Ph)_4 & with Ph_3PS \\ \end{tabular}$

$\lambda_{\rm exc}$ / nm	φ _p [MoWCl ₄ (PMe ₂ Ph) ₄]
577	N.R.
546	5.0×10^{-4}
436	1.2×10^{-3}
365	1.8×10^{-3}

need for a slight intramolecular distortion in order to trap the excited state and therefore slightly higher excitation energies are necessary.

5. Electron Paramagnetic Resonance Spectroscopy

While the W photoproduct is partially characterized, the Mo species is not characterized. Thus EPR studies were undertaken to determine if there were any paramagnetic products. And as shown by the 77K EPR spectrum of the photoreaction mixture in a 2-MeTHF glass, in Figure 4.17, there are. The EPR spectrum exhibits a strong central line and surrounding hyperfine lines characteristic of Mo^V (95 Mo: 15.72 %, I = 5/2). 67 Table 4.4 lists some representative g-values for Mo^V nuclei with a variety of ligands. 68,69,70,71 The g-values of the paramagnetic photoproduct ($g_1 = 1.960$; $g_2 = 1.948$) compare well to the range reported. The only example of a monomeric complex containing a [Mo=S]³⁺ center, [HB(Me₂pz)₃]Mo^VSCl₂, has trigonal symmetry with $g_{yy} = 1.941$, $g_{zz} = 1.971$, $g_{xx} = 1.934$. 69 It is difficult to draw conclusions about the coordination sphere from this result, only that it is a Mo^V nucleus.

6. Electron Spin Echo Envelope Modulation⁷²

In an effort to acquire more information as to the nature of the paramagnetic photoproduct pulsed EPR, Electron Spin Echo Envelope Modulation (ESEEM) studies were undertaken. The description of a spin echo experiment is based on the presence of inhomogeneously broadened EPR absorption, which obscures useful information regarding the hyperfine coupling of the nuclei to the paramagnet. This inhomogeously broadened line is composed of populations of spins, or "spin packets", whose magnetic moments have the same precessional frequency but

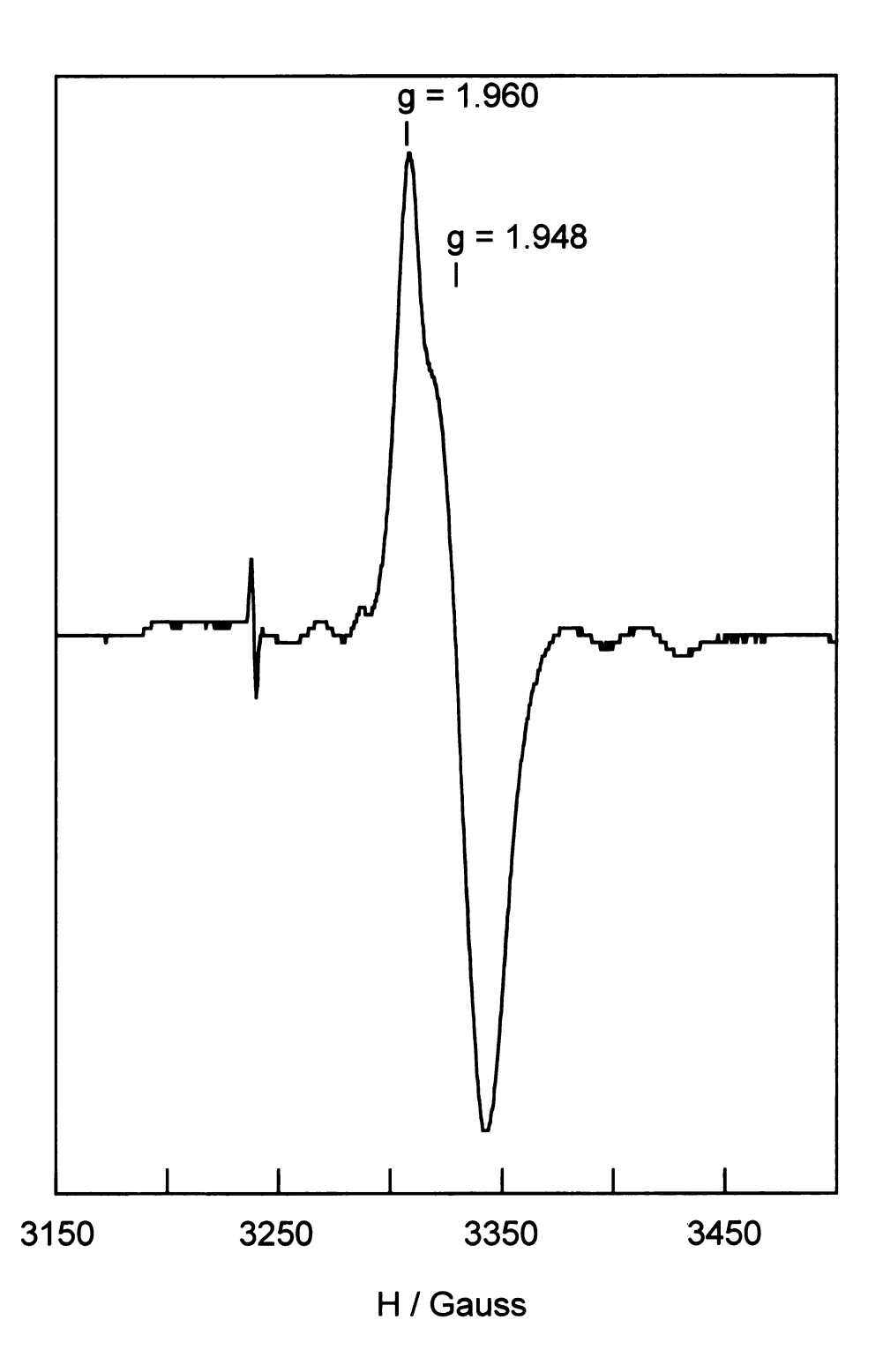


Figure 4.17 The X-band EPR spectrum of the photoreaction in a 2-MeTHF glass.

Table 4.4 Representative g-values of Mo^V Octahedral Complexes

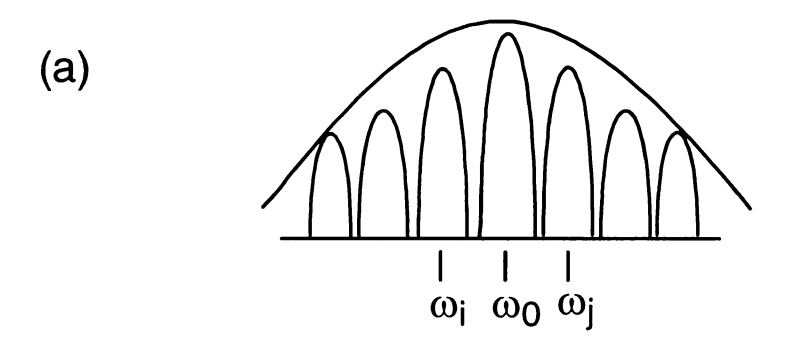
complex	g_{xx}	g_{yy}	g_{zz}	references
LMo(S)Cl ₂ ^a	1.921	1.941	1.919	68
LMo(O)Cl ₂ ^a	1.941	1.971	1.934	68
LMo(O)(OMe) ₂ ^a	1.960	1.942	1.904	69
LMo(O)(OSet) ₂ ^a	2.011	1.952	1.931	69
LMo(O)(OH)Cl ^a	1.966	1.946	1.914	70
LMo(O)(OH)NCS ^a	1.966	1.944	1.922	70
[Ph ₄ As][MoOCl ₄]	1.952	_	_	71
[Et ₄ N][MoOCl ₄ (OPPh ₃)]	1.943	_	-	71

a. L = hydrotris(3,5-dimethyl-1-pyrazloyl)borate

different phases (Figure 4.18a). Application of an external magnetic field, H₀, results in net magnetization, M_0 , both of which are parallel to Z. This magnetization has a characteristic precessional frequency, ω, that is known as the Larmor frequency and is equal to $\omega_i = \gamma H_0$; where γ is the gyromagnetic ratio. To understand the build up and decay of spin echoes, a rotating coordinate system (Figure 4.18b), with rotational frequency ω_0 and axes X', Y' and Z' is used. Following the first $\pi/2$ pulse applied along X', the magnetization will flip into the XY plane, Figure 4.19a. Since the spin packets have frequencies different from ω_0 $(\omega_i$ and ω_i in Figure 4.18a) they quickly begin to dephase, Figure 4.19b. After a time τ , a second microwave pulse that is sufficient to rotate the spin packets by 180° is applied, Figure 4.19c. The precessional frequency and the phasing are unaltered by the pulse and after a time τ , the spins packets realign along -Y'. This creates a build up of magnetization that is known as a spin echo, Figure 4.19d. The amplitude of the spin echo as a function of interpulse time τ is measured in the experiment. A three-pulse stimulated echo experiment is similar to the two-pulse experiment except the π -pulse has been broken into two $\pi/2$ pulses and the amplitude of the stimulated echo is measured as a function of $\tau+T$, where τ is the delay between the first two $\pi/2$ pulses and T is the delay between the second and the third pulses.

a. Nuclear Modulation Effect⁷²

The decay of the spin echo amplitude is not monotonic but is modulated by anisotropic hyperfine and nuclear quadrupole interactions of surrounding magnetic nuclei. These modulations are the direct result of the fact that microwaves can induce transitions that start at one pair of levels and end at another pair of levels



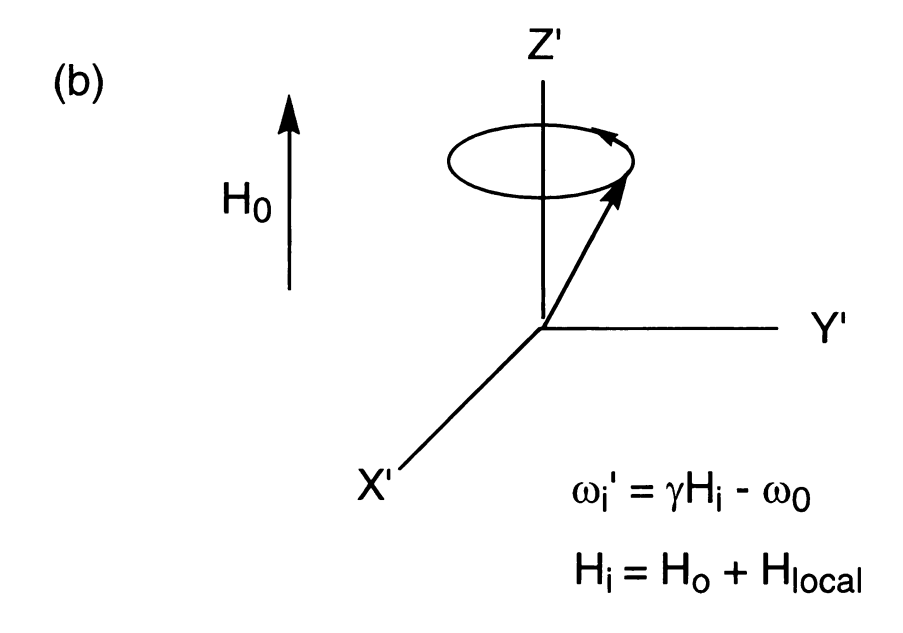


Figure 4.18 (a) The inhomogeneously broadened EPR line of a paramagnetic center. (b) Each spin packet can be considered independently from each other, each having its own Larmor frequency.

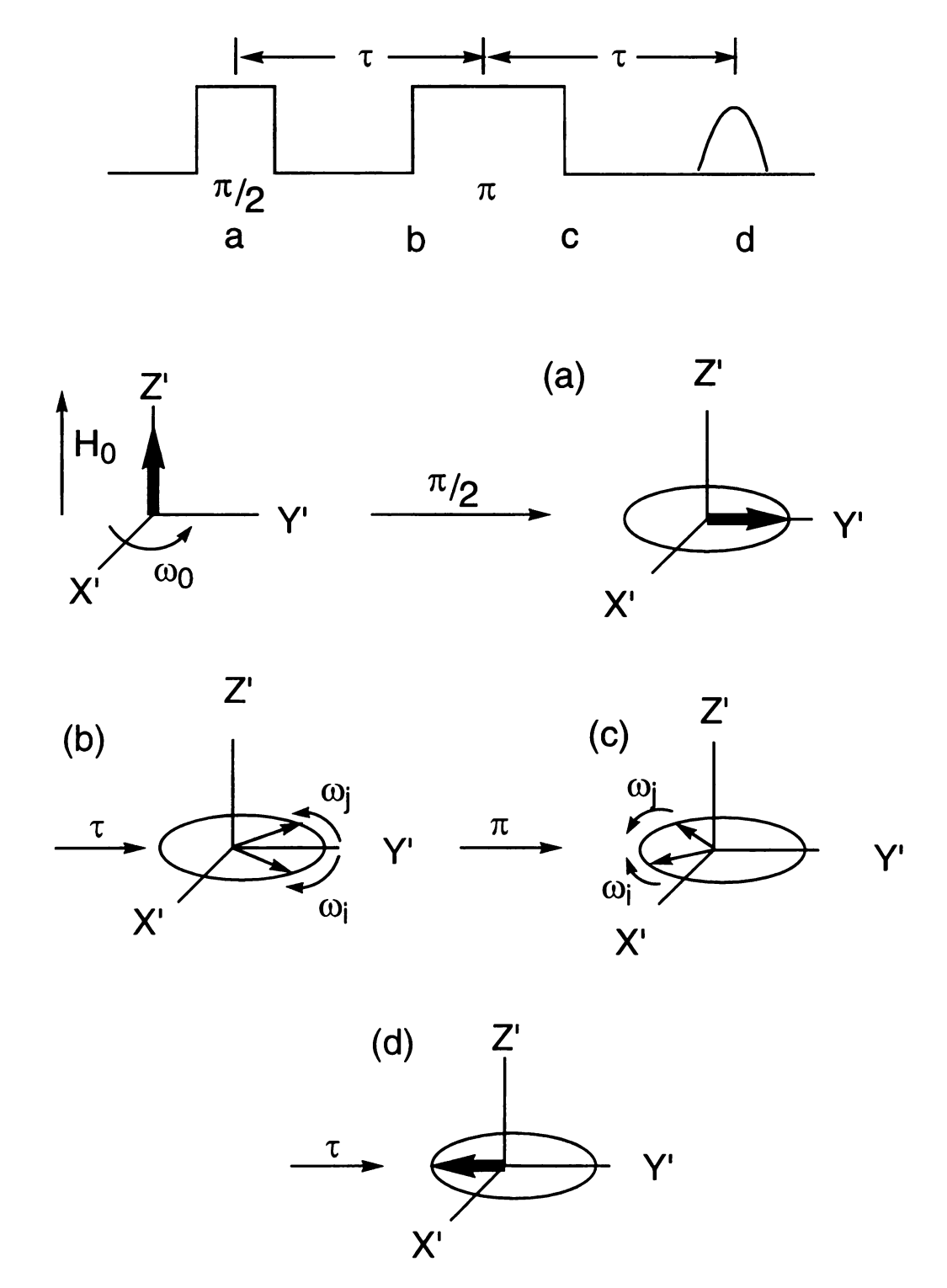
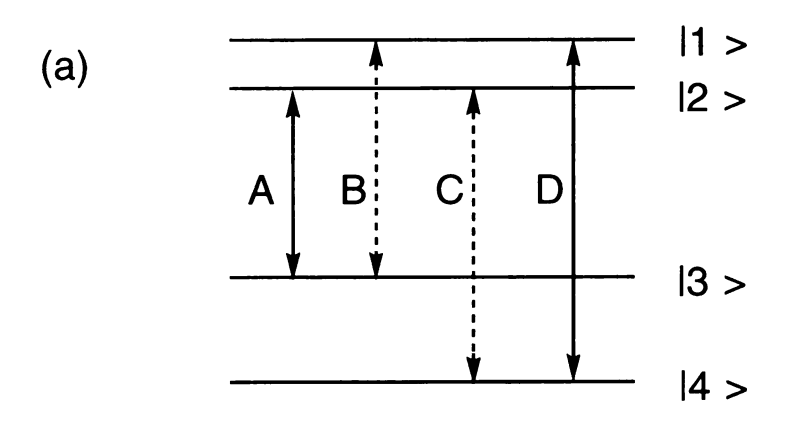


Figure 4.19 Magnetization of spin packets i and j during a two pulse experiment. (a) during a $\pi/2$ pulse; (b) after time τ ; (c) after the π pulse; (d) time τ after the π pulse.

upon the application of a second pulse. This is called branching of transitions and as a consequence, the probability for each transition is non-zero. To illustrate the effect of nuclear modulation, it is useful to follow the "allowed" spin packet "A" and the "forbidden" spin packet "B" during the pulse sequence, Figures 4.20b-d. If spin packet "A" is excited with a $\pi/2$ pulse, "A" is rotated into the XY plane and starts to dephase immediately, Figure 4.20b. Due to transition branching, transition "B" is excited along with the transition "A" during the π pulse, although the transition probabilities for "A" and "B" are not equal (Figure 4.20c). The echo amplitude at time τ is the projection of the spin packet "vectors" onto -Y'. At time τ after the π pulse, "A" is aligned along -Y' and contributes fully to the spin echo. Spin packet "B" does not fully align along -Y' because its precessional frequency is different than the rotating frame and may add or subtract to the spin echo amplitude, depending on the projection of "B". The observed experimental echo amplitude is a sum of the spin packets that are excited in the inhomogeneously broadened EPR line and the sum is the source of the modulation pattern observed in the spin echo experiment. The frequencies of the modulation yield the hyperfine couplings. Fourier transformations of the time domain data make the frequencies easier to observe and hyperfine peaks can be found centered around the Larmor frequency, v_n , for that nuclei and split by A_{iso} , the hyperfine coupling, or centered around A/2 and split by v_n .

Figure 4.21 shows the Fourier transforms of the photoproduct electron spinecho envelopes obtained at 3260 and 4375 G with a τ of 300 and 250 ns, respectively. In Figure 4.21a, a peak at 13.8 MHz corresponds closely to the



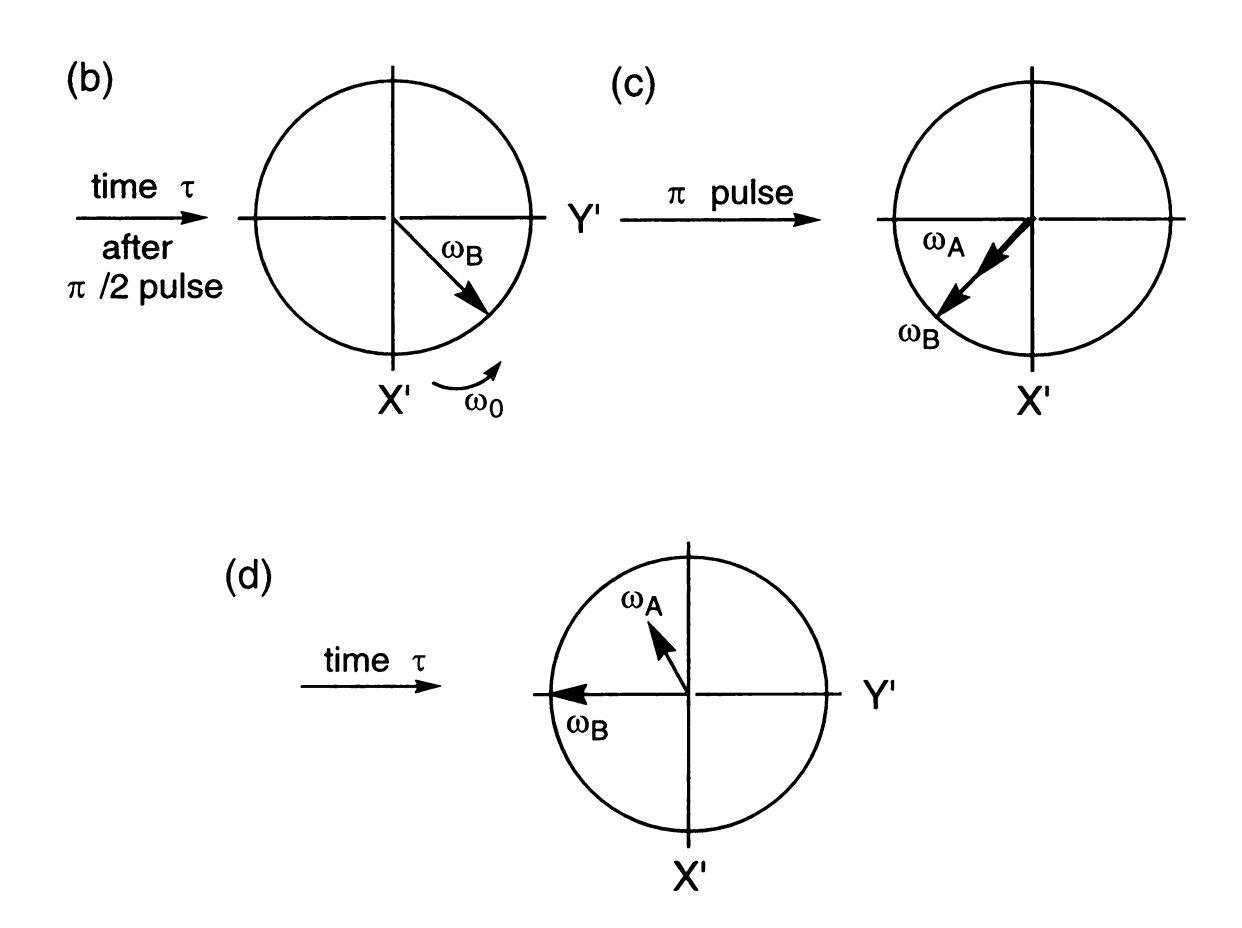


Figure 4.20 (a) Energy level diagram for a S=1/2 and I=1/2 system. Time behavior for the magnetization of "forbidden" spin packet A and "allowed" spin packet B. (b) at time τ after the π /2 pulse; (c) after the π pulse; (d) at the time of the echo.

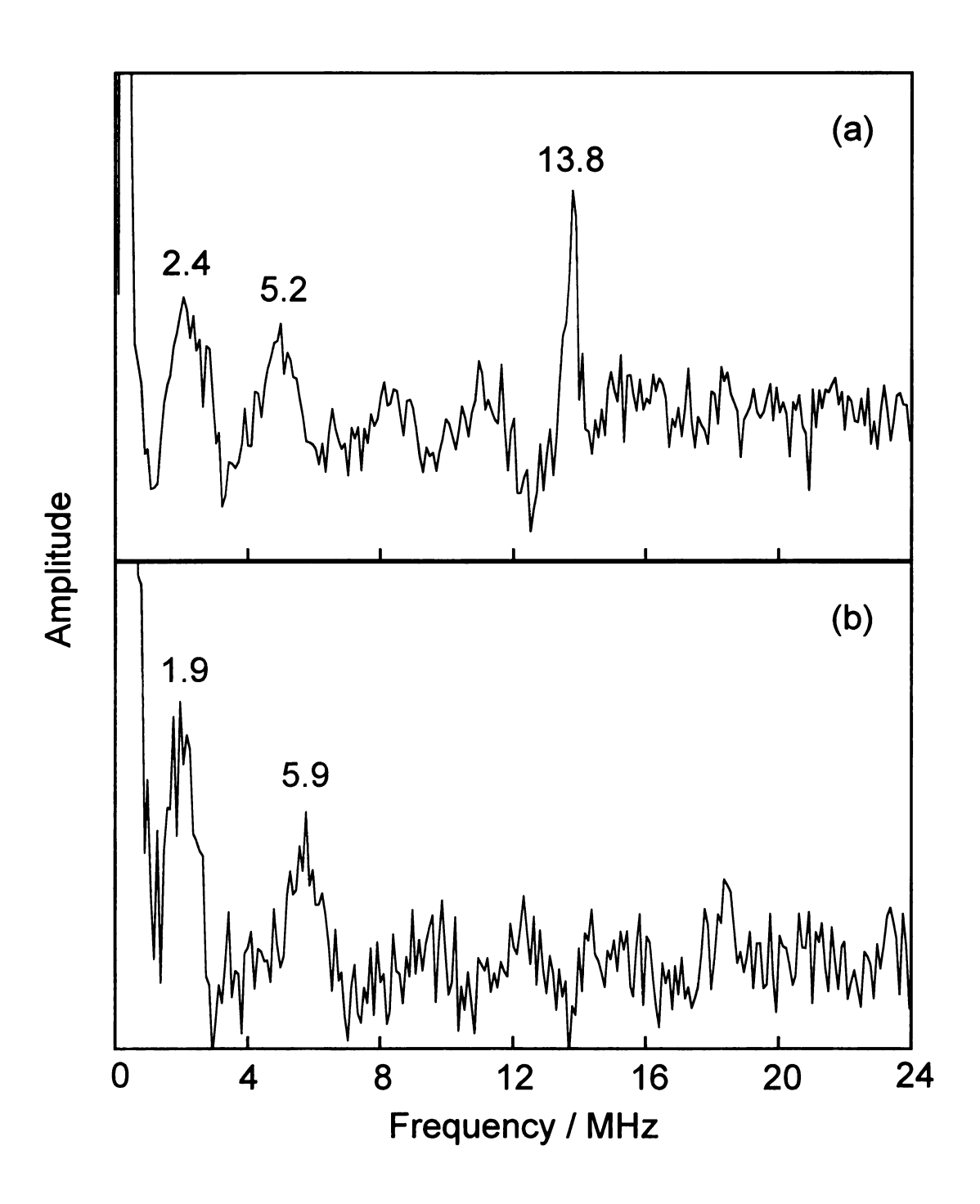


Figure 4.21 Fourier transforms of the photoproduct spin-echo envelope. (a) was measured at 3260 G and $\tau = 300$ ns and (b) was measured at 4375 G and $\tau = 250$ ns. Both were measured at 4K.

Larmor frequency of ${}^{1}H$ ($\gamma_n = 4.26$)⁷³ at 3260 G and is due to protons in the solvent. The Larmor frequency at a given field is calculated from equation 4.19^{74}

$$h\nu_n = g_n \beta_n H \tag{4.19}$$

At lower frequency, in Figure 4.21a, two peaks at 2.4 and 5.2 MHz are centered at A/2 (3.8 MHz) and split by twice the Larmor frequency for 35 Cl at 3260 G ($v_n(3260) = 1.4$ MHz). At higher field, the hyperfine coupling should remain the same, while the peaks will move further apart depending on the Larmor frequency. At 4375 G, Figure 4.21b, the peaks shift to about 1.9 and 5.9 MHz, which corresponds nicely to the expected shift of 0.4 MHz for a 35 Cl nucleus. γ_n for 35 Cl and 37 Cl are similar and v_n will differ by only about 1 MHz. Additionally, the natural abundancies of the 35 Cl and 37 Cl isotopes are 75 and 24%, respectively. Therefore, the lines due to chlorine can be expected to be broad.

Nuclei with a nuclear spin quantum number I > 1/2 have a quadrupole moment that results from the nonspherical distribution of the positive charge in the nucleus.⁷⁵ Fluctuating electric fields coming from the interaction of dipolar solvent and solute molecules can efficiently relax quadrupolar nuclei.⁷⁶ The mechanism of relaxation depends on the interaction of the quadrupole with the electric field gradient of the nucleus. The gradient arises when a quadrupolar nucleus is in a molecule in which it is surrounded by a nonspherical distribution of electrons, such as a terminal chloride ligand. This rapid relaxation can broaden the lines due to the quadrupolar nucleus. This effect can be observed in Figure 4.21a upon comparing

the width of the peaks due to ¹H and those assigned to ³⁵Cl. Based on the magnetic resonance studies, the molybdenum photoproduct is a Mo^V nucleus with Cl⁻ ligated in a terminal position.

D. Summary

The observation of atom transfer products for the photoreaction of MoWCl₄(PMe₂Ph)₄ and Ph₃PS represents a rare example of photoiniated sulfur atom transfer to a transition metal complex. The atom transfer product, W(S)Cl₄(PMe₂Ph) is formed in approximately 25% yield, with Ph₃P formed in greater than 50% yield. The Mo product has not been fully characterized, except that it is paramagnetic. The photoreaction is summarized below.

$$MoWCl_4(PMe_2Ph)_4 + Ph_3PS \xrightarrow{hv} W(S)Cl_4(PMe_2Ph) + Mo^V$$

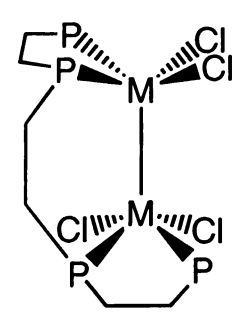
The photoreaction is unique to the heterobimetallic complex, as Mo₂Cl₄(PMe₂Ph)₄ and W₂Cl₄(PMe₂Ph)₄ do not react photochemically with Ph₃PS. The reactivity of the MoW complex with Ph₃PS illustrates that the atom transfer reaction is thermodynamically inaccessible to these complexes.

The photoreaction of the mixed-metal complex MoWCl₄(PMe₂Ph)₄ with Ph₃PS is unparalleled in the reactivity of the homonuclear quadruply bonded bimetallic complexes with Ph₃PS. Since a large intramolecular distortion is neccesary, in the case with the homometallic complexes, the excited state is deactivated and is confined to low energy substrates, such as Me–I (57 kcal⁷⁷) and PhS–SPh (55 kcal⁷⁸). The asymmetry of the MoW complex leads to a less distorted excited state and therefore more energetic. Now we are able to utilize substrates

that typically react by atom transfer and have a higher activation energy; i. e. Ph₃P-S: 92 kcal.⁷⁹ Moreover, neither the homonuclear complexes nor the MoW complexes react thermally with Ph₃PS.

E. Future Directions

It might be of interest to develop photocatalytic systems that could react with environmentally interesting molecules, such as CO₂ or SO₂. Several problems exist that must be overcome inorder to do so. First, MoWCl₄(PMe₂Ph)₄ decomposes to two monomeric complexes, which is detrimental to the development of a catalytic system and, second, the bond dissociation energies of CO₂ and SO₂ are quite high (127⁸⁰ and 132⁸⁰ kcal, respectively). The complex MoWCl₄(tetraphos),⁸¹ where tetraphos is a tetradentate phosphine, could potentially solve both problems. A tetradentate ligand would be less likely to dissociate from the metal than a mono or bidentate ligand and would keep the basic framework of the M–4–M complex intact. Also, tetraphos binds asymmetrically to the quadruple bond core, as shown below.



This, combined with the asymmetry of the Mo-4-W core, may introduce enough asymmetry to preclude any need for ligand distortion giving an excited state that is even more energetic that MoWCl₄(PMe₂Ph)₄.

F. References

- 1. Taube, H. Angew. Chem. Int. Ed. Engl. 1984, 23, 329.
- 2. Nugent, W. A.; Mayer, J. M. Metal-Ligand Multiple Bonds; John Wiley & Sons: New York, 1988.
- 3. Holm. R. H. Chem. Rev. 1987, 87, 1401.
- 4. Woo, L. K. Chem. Rev. 1993, 93, 1125.
- 5. Schwarz, C. L.; Bullock, R. M.; Creutz, C. J. Am. Chem. Soc. 1991, 113, 1225.
- 6. Steifel, E. I. Prog. Inorg. Chem. 1977, 22, 1.
- 7. Holm, R. H. Coord. Chem. Rev. 1990, 100, 183.
- 8. Couglan, M. P. In *Molybdenum and Molybdenum Containing Enzymes*; Coughlan, M. P., Ed.; Pergamon: New York, 1980; pp 119-185.
- 9 Rajagopalan, K. V. In *Molybdenum and Molybdenum Containing Enzymes*; Coughlan, M. P., Ed.; Pergamon: New York, 1980; pp 241-272.
- 10. Adams, M. W.; Mortenson, L. E. In *Molybdenum Enzymes*; Spiro, T. G., Ed.; John Wiley & Sons: New York, 1985; p 519.
- 11. Satoh, K.; Kurihara, F. N. J. Biochem Tokyo 1987, 102, 191.
- 12. (a) Taube, H.; Myers, H.; Rich, R. L. J. Am. Chem. Soc. 1953, 75, 4118. (b) Taube, H.; Myers, H. J. Am. Chem. Soc. 1954, 76, 2103.
- 13. Meyer, T. J.; Taube, H. In *Comperhensive Coordination Chemistry*, Wilkinson, G., Ed.; Pergamon Press: Oxford; vol 1, pp 331-384.
- 14. Taube, H. In *Mechanistic Aspects of Inorganic Reactions*; Rorabacher, D. B.; Endicott, J. F., Eds.; ACS Symposium Series 198; American Chemical Society: Washington, DC, 1982; p 151.

- (a) Schultz, B. E.; Holm, R. H. *Inorg. Chem.* 1993, 32, 4244. (b) Harlan, E.
 W.; Berg, J. M.; Holm, R. H. *J. Am. Chem. Soc.* 1986, 108, 6992.
- 16. Gheller, S. F.; Schultz, B. E.; Scott, M. J.; Holm, R. H. J. Am. Chem. Soc. 1992, 114, 6934.
- 17. Woo, L. K.; Hays, J. A.; Goll, J. G. Inorg. Chem. 1990, 29, 3916.
- 18. Liston, D. J.; West, B. W. Inorg. Chem. 1985, 24, 1568.
- 19. Hall, K. A.; Mayer, J. M. J. Am. Chem. Soc. 1992, 114, 10402.
- 20. Hall, K. A.; Critchlow, S. C.; Mayer, J. M. Inorg. Chem. 1991, 30, 3593.
- 21. Jang, S.; Atagi, L. M.; Mayer, J. M. J. Am. Chem. Soc. 1990, 112, 6413.
- 22. Su, F.-M.; Bryan, J. C.; Jang, S.; Mayer, J. M. Polyhedron 1989, 8, 1261.
- 23. see for example: (a) Zhang, Y.; Holm, R. H. *Inorg. Chem.* **1990**, 29, 911. (b)
- Oku, H.; Ueyama, N.; Kondo, M.; Nakamura, A. *Inorg. Chem.* **1994**, 33, 209. (c)
- Arzoumanian, H.; Lopez, R.; Agrifoglio, G. Inorg. Chem. 1994, 33, 3177. (d)
- Templeton, J. L.; Ward, B. C.; Chen, G. J.-J.; McDonald, J. W.; Newton, W. E.
- Inorg. Chem. 1981, 20, 1248. (e) Bhattacharjee, S.; Bhattacharyya, R. J. Chem.
- Soc. Dalton Trans. 1993, 1151.

Organomet. 1983, 2, 767.

- 24. (a) Roundhill, D. M. Photochemistry and Photophysics of Metal Complexes; Plenum: New York, 1994. (b) Suslick, K. S.; Watson, R. A. New J. Chem 1992, 16, 633.
- 25. Scott, S. L.; Espenson, J. H.; Zhu, Z. J. Am. Chem. Soc. 1993, 115, 1789.
- 26. (a) Lemke, F.; Kubiak, C. P. J. Organomet. Chem. 1989, 373, 391. (b) Reinking, M. K.; Kullberg, M. L.; Cutler, A. R.; Kubiak, C. P. J. Am. Chem. Soc.
- 1985, 107, 3517. (c) Miller, T. D.; St. Clair, M. A.; Reinking, M. K.; Kubiak, C. P.

- 27. Proulx, G.; Bergman, R. G. J. Am. Chem. Soc. 1994, 116, 7953.
- 28. Roundhill, D. M.; Gray, H. B.; Che, C.-M. Acc. Chem. Res. 1989, 22, 55.
- 29. (a) Roundhill, D. M.; Atherton, S. J. *Inorg. Chem.* **1986**, 25, 4071. (b) Roundhill, D. M.; Shen, Z.-P.; King, L.; Atherton, S. J. *J. Phys. Chem.* **1988**, 92, 4088.
- 30. (a) Roundhill, D. M.; Atherton, S. J. J. Am. Chem. Soc. 1986, 108, 6829. (b) Che, C.-M.; Gray, H. B.; Atherton, S. J.; Lee, W.-M. J. Phys. Chem. 1986, 90, 6747. (c) Cho, K. C.; Che, C.-M. Chem. Phys. Lett. 1986, 124, 313.
- 31. Che, C.-M.; Lee, W.-M.; Kwong, H.-L.; Yam, V. W.-W.; Cho, K.-C. . J. Chem. Soc. Dalton Trans. 1990, 1717.
- 32. Yuan, L.-C.; Calderwood, T. S.; Bruice, T. C. J. Am. Chem. Soc. 1985, 107, 8273.
- 33. Suslick, K. S.; Acholla, F. V.; Cook, B. R. J. Am. Chem. Soc. 1987, 109, 2128.
- 34. Engebretson, D. S.; Zaleski, J. M.; Leroi, G. E.; Nocera, D. G. Science 1994, 265, 759.
- 35. Holm, R. H.; Donahue, J. P. Polyhedron 1993, 12, 571.
- 36. Cotton, F. A.; Wilkinson, G. Advanced Inorganic Chemistry, 5th ed.; John Wiley & Sons: New York, 1988; p 808.
- 37. (a) Berg, D. J.; Burns, C. J.; Andersen, R. A.; Zalkin, A. *Organomet.* **1989**, 8, 1865. (b) Bottomley, F.; Egharevba, G. O.; Lin, I. J. B.; White, P. S. *Organomet.* **1985**, 4, 550. (c) Liu, H.-F.; Liu, R.-S.; Liew, K. Y.; Johnson, R. E.; Lunsford, J. H. *J. Am. Chem. Soc.* **1984**, 106, 4117.
- 38. Bottomley, F.; Paez, D. E.; White, P. S. J. Am. Chem. Soc. 1982, 104, 5651.

- 39. Smith III, M. R.; Matsunaga, P. T.; Andersen, R. A. J. Am. Chem. Soc. 1993, 115, 7049.
- 40. Bottomley, F.; Brooks, W. V. F. Inorg. Chem. 1977, 16, 501.
- 41. LaPlaza, C. E.; Odom, A. L.; Davis, W. M.; Cummins, C. C.; Protasiewicz, J.
- D. J. Am. Chem. Soc. 1995, 117, 4999.
- 42. Hintz, P. A.; Sowa, M. B.; Ruatta, S. A.; Anderson, S. L. J. Chem. Phys. 1991, 94, 6446.
- 43. Fanwick, P. E.; Harwood, W. S.; Walton, R. A. Inorg. Chem. 1987, 26, 242.
- 44. LaMar, G. N.; Horrocks, W. D., Jr.; Holm, R. H., Eds. *NMR of Paramagnetic Molecules*; Academic: New York, 1973; p 566.
- 45. Barder, T. J.; Cotton, F. A.; Lewis, D.; Schwotzer, W.; Tetrick, S. M.; Walton, R. A. J. Am. Chem. Soc. 1984, 106, 2882.
- 46. Grim, S. O.; Walton, E. D. Inorg. Chem. 1980, 19, 1982.
- 47. Greenwood, N. N.; Earnshaw, A. Chemistry of the Elements; Pergamon: New York, 1984; p 1175.
- 48. Gilbert, A.; Baggott, J. Essentials of Molecular Photochemistry; CRC: Boston, 1991; pp 468-475.
- 49. (a) von Sonntag, C.; Schuchmann, H.-P. In Advances in Photochemistry; Pitts,
- Jr., J. N.; Hammond, G. S; Gollnick, K., Eds., John Wiley & Sons: New York,
- 1977; , vol. 10, pp 59-145. (b) Roquitte, B. C. J. Am. Chem. Soc. 1969, 91, 7664.
- (c) Fleming, G.; Anderson, M. M.; Harrison, A. J.; Pickett, L. W. J. Chem. Phys. 1959, 30, 351.
- 50. Williams, D. H.; Fleming, I. Spectroscopic Methods in Organic Chemistry, 4th ed.; McGraw-Hill: New York, 1987.

- 51. Hsu, T.-L. C.; Chang, I-J.; Ward, D. L.; Nocera, D. G. *Inorg. Chem.* **1994**, *33*, 2932.
- 52. (a) Baratta, W.; Calderazzo, F.; Daniels, L. M. Inorg. Chem. 1994, 33, 3842.
- (b) Bradley, D. C.; Errington, R. J.; Hursthouse, M. B.; Short, R. L.; Ashcroft, B.
- R.; Clark, G. R.; Nielson, A. J.; Rickard, C. E. F. J. Chem. Soc. Dalton Trans. 1987, 2067.
- 53. (a) Bryan, J. C.; Mayer, J. M. J. Am. Chem. Soc. 1990, 112, 2298. (b) Su, F.-
- M.; Bryan, J. C.; Jang, S.; Mayer, J. M. *Polyhedron* **1989**, *8*, 1261. (c) Bates, J. R.; Taylor, H. S. *J. Am. Chem. Soc.* **1927**, *49*, 2438.
- 54. (a) Vaughan, G. A.; Hillhouse, G. L.; Rheingold, A. L. J. Am. Chem. Soc.
- 1990, 112, 7994. (b) Vaughan, G. A.; Sofield, C. D.; Hillhouse, G. L.; Rheingold,
- A. L. J. Am. Chem. Soc. 1989, 111, 5491. (c) Vaughan, G. A.; Rupert, P. B.; Hillhouse, G. L. J. Am. Chem. Soc. 1987, 109, 5538.
- 55. Matsunaga, P. T.; Hillhouse, G. L. J. Am. Chem. Soc. 1993, 115, 2075.
- 56. Matsunaga, P. T.; Mavropoulos, J. C.; Hillhouse, G. L. Polyhedron 1995, 14, 175.
- 57. (a) Jubb, J.; Gambarotta, S. *Inorg. Chem.* **1994**, *33*, 2503. (b) Gambarotta, S.; Edema, J. J. H.; Minhas, R. K. *J. Chem. Soc. Chem. Commun.* **1993**, 1503.
- 58. Jubb, J.; Gambarotta, S. J. Am. Chem. Soc. 1993, 115, 10410.
- 59. (a) Hall, K. A.; Mayer, J. M. *Inorg. Chem.* **1995**, *34*, 1145. (b) Hall, K. A.; Mayer, J. M. *Inorg. Chem.* **1994**, *33*, 3289.
- 60. (a) Cotton, F. A. Polyhedron 1987, 6, 677. (b) Cotton, F. A.; Hong, B.; Shang,
- M.; Stanley, G. G. Inorg. Chem 1993, 32, 3620. (c) Cotton, F. A.; Maloney, D. J.;

- Su, J. Inorg. Chim. Acta 1995, 236, 21. (d) Poli, R.; Torralba, R. C. Inorg. Chim. Acta. 1993, 212, 123.
- 61. Miskowski, V. M.; Gray, H. B.; Hopkins, M. D. Inorg. Chem. 1992, 32, 2085.
- 62. Turro, N. J. *Modern Molecular Photochemistry*; University Science Books: Sausalito, CA, 1991; pp 316-317.
- 63. Engebretson, D. S. Ph.D. Dissertation, Michigan State University; 1997.
- 64. Hopkins, M. D.; Gray, H. B.; Miskowski, V. M. Polyhedron 1987, 6, 705.
- 65. Luck, R. L.; Morris, R. H.; Sawyer, J. F. Inorg. Chem. 1987, 26, 2422.
- 66. Baechler, R. D.; Stack, M.; Stevenson, K.; Vanvalkenburgh, V. *Phosphorus*, Sulfur, and Silicon 1990, 48, 49.
- 67. Chang, C.-S. J.; Pecci, T. J.; Carducci, M. D.; Enemark, J. H. *Inorg. Chem.* 1993, 32, 4106.
- 68. Young, C. G.; Enemark, J. H.; Collison, D.; Mabbs, F. E. *Inorg. Chem.* 1987, 26, 2927.
- 69. (a) Cleland, W. E., Jr.; Barnhart, K. M.; Yamanouchi, K.; Collison, D.; Mabbs,
- F. E.; Ortega, R. B.; Enemark, J. H. Inorg. Chem. 1987, 26, 1017. (b) Enemark, J.
- H.; Cleland, W. E., Jr.; Collison, D.; Mabbs, F. E. In *Frontiers in Bioinorganic Chemistry*; Xavier, A. V., Ed.; VCH Verlagsgesellschaft:Weinhem, FRG, 1986; p 47.
- 70. Xiao, Z.; Bruck, M. A.; Doyle, C.; Enemark, J. H.; Grittini, C.; Gable, R. W.; Wedd, A. G.; Young, C. G. *Inorg. Chem.* **1995**, *34*, 5950.
- 71. Boorman, P. M.; Garner, C. D.; Mabbs, F. E. J. Chem. Soc. Dalton Trans. 1975, 1299.

- 72. Keijers, C. P.; Reijers, E. J.; Schmidt, J. *Pulsed EPR: A new field of applications*; Koninkijke Nederlandse Akademie van Wetenschappen: New York, 1989; pp 11-27.
- 73. Handbook of Chemistry and Physics, 69th ed.; CRC: Boca Raton, Florida, 1988; p E-80.
- 74. Wertz, J. E.; Bolton, J. R. *Electron Spin Resonance*; McGraw-Hill: New York, 1972.
- 75. West, A. R. Solid State Chemistry and Its Applications; John Wiley & Sons: New York, 1984; p 98.
- 76. Drago, R. S. *Physical Methods for Chemists*, 2nd Ed.; Saunders College Publishing: New York, 1992; pp. 269-270.
- 77. Streitweiser, A. Jr.; Heathcock, C. H. *Introduction to Organic Chemistry*, 3rd Ed.; Macmillan Publishing: New York, 1985.
- 78. Benson, S. W. Chem. Rev. 1978, 78, 23.
- 79. Chernick, C. L.; Pedley, J. B.; Skinner, H. A. J. Chem. Soc. 1957, 1851.
- 80. Handbook of Chemistry and Physics, 69th ed.; CRC: Boca Raton, Florida, 1988; p F-183.
- 81. (a) Cotton, F. A.; Eglin, J. L.; James, C. A. *Inorg. Chem.* **1993**, *32*, 687. (b) Chen, J.-D.; Cotton, F. A.; Hong, B. *Inorg. Chem.* **1993**, *32*, 2343. (c) James, C. A. Ph.D. Dissertation, Texas A & M University, 1992.

CHAPTER 5

A STUDY OF THE NONRADIATIVE DECAY OF M2Cl4(PR3)4

A. Background

Since the discovery¹ of the quadruple bond in 1964 and its recognition², computations³ and experiments⁴ have provided a comprehensive and coherent description of the electronic structure of this class of compounds. Figure 5.1 shows the absorption spectra of $Mo_2Cl_4(PMe_3)_4$ and $W_2Cl_4(PMe_3)_4$ with the electronic transitions as they have been assigned. The lowest energy $^1(\delta \rightarrow \delta^*)$ transition is flanked by $^1(\pi \rightarrow \delta^*)$ and to higher energy lies $^1(M(Cl) \rightarrow d^*)$ LMCT transitions. 4b,5,6 The D_{2d} $M_2Cl_4(PR_3)_4$ complexes $(M_2 = Mo_2, MoW, W_2; PR_3 = PMe_3, PMe_2Ph, PMePh_2)$ luminesce from the $^1\delta\delta^*$ excited state with quantum efficiencies of about 0.01 to 0.3⁷ and emission lifetimes between 15-50 ns in nonpolar solvents; 8 $Mo_2Cl_4(PMe_3)_4$ is an exception with lifetimes of 135 ns in 2–methylpentane. Notwithstanding, not much is known about the excited state decay processes of M–4–M complexes to date. The goal of this study was to better understand the nonradiative decay of the $^1\delta\delta^*$ excited state and to quantify the electronic coupling between the two metal centers.

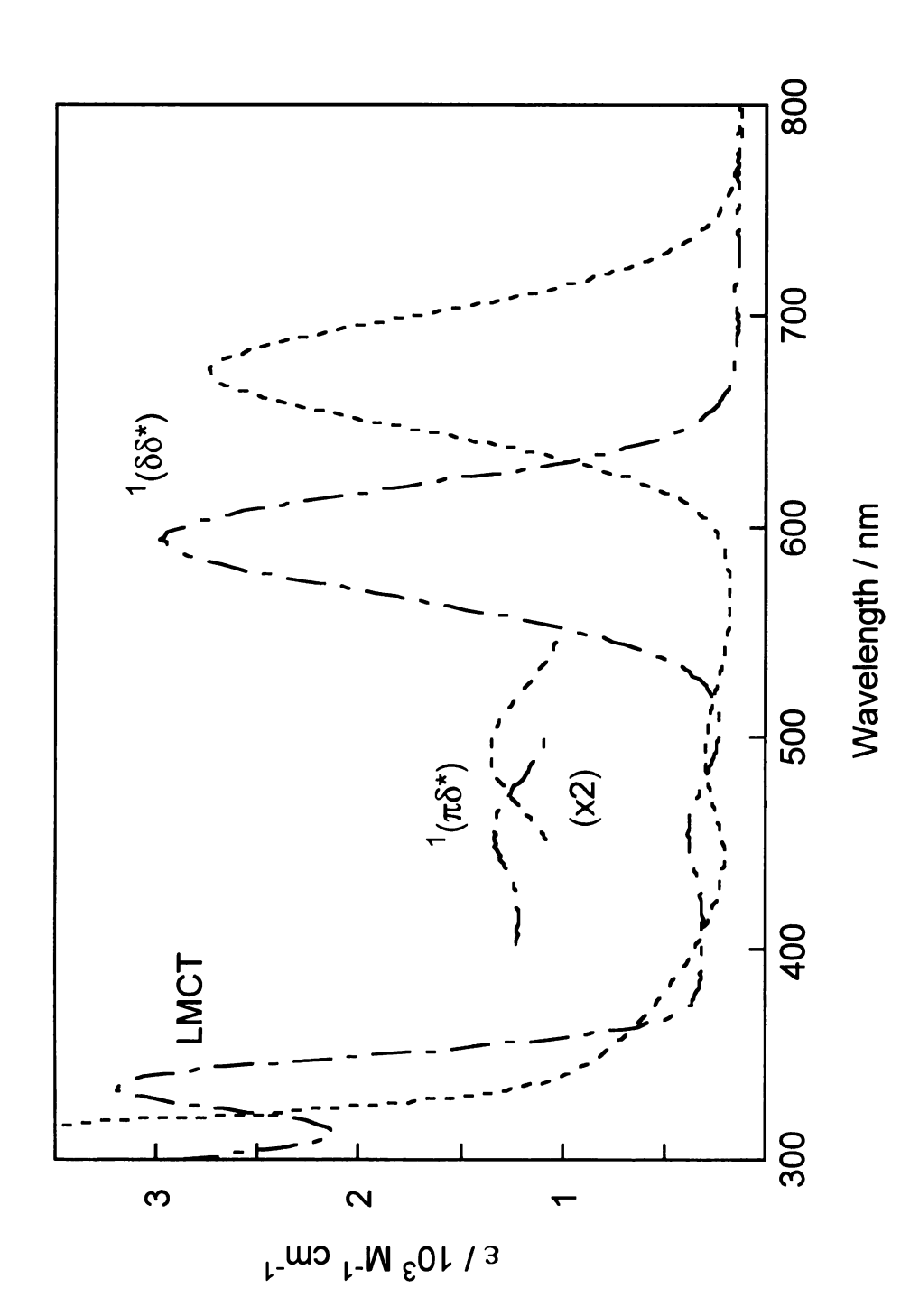


Figure 5.1 Electronic absorption spectra of Mo₂Cl₄(PMe₂Ph)₄ (— -) and W₂Cl₄(PMe₂Ph)₄ (- - - -) in benzene.

B. Temperature Dependence of Emissive Lifetimes

The intramolecular decay processes of an electronic excited state are defined by a radiative, k_r , and nonradiative, k_{nr} , rate constants. These two kinetic rate constants describe the fundamental properties of an electronic excited state, namely the lifetime, τ_0 , and emission quantum yields, ϕ_e . At a given temperature, these quantities are defined by equations 5.1 and 5.2, respectively.⁹

$$\frac{1}{\tau_0} = k_1 = k_r + k_{nr} \tag{5.1}$$

$$\phi_e = \tau_0 k_r \tag{5.2}$$

The nonradiative rate constant, k_{nr} , can therefore be calculated from a measurement of the lifetime and emission quantum yield. The temperature dependence of the emission quantum yield at temperatures other than 298 K, can be estimated by equation 5.3^{10}

$$\phi_{LT} = \phi_{298} \left(\frac{I_{LT}}{I_{298}} \right) \tag{5.3}$$

where I_{LT} and I_{298} are the integrated emission intensity at low temperature and 298 K, respectively. The temperature dependence of emission lifetimes varies according to Equation 5.4, an expression based on the excited state decay constant for a two-state Boltzmann distribution, 10

$$k_{obs} = \frac{k_1 + k_2 \exp\left(\frac{-\Delta E'}{k_B T}\right)}{1 + \exp\left(\frac{-\Delta E'}{k_B T}\right)}$$
(5.4)

where k_1 and k_2 are the decay constants for two nondegenerate states in thermal equilibrium separated by an energy gap, $\Delta E'$. The denominator is necessary when $\Delta E' \leq 3k_BT$.¹⁰ The fraction of decay that occurs through the upper excited state at a given temperature is given by equation 5.5.¹⁰

$$\eta_{1} = \frac{k_{2}\tau \exp(-\Delta E'/k_{B}T)}{k_{1} + k_{2} \exp(-\Delta E'/k_{B}T)}$$
 (5.5)

The overall form of equation 5.4 yields plots with a temperature independent region, the plateau region, followed by a temperature dependent region. An ill-defined plateau region is a major source of error in fits of equation 5.4 to experimental lifetime data and must be experimentally well-defined in order to determine a reasonable value for k_1 .¹⁰

C. Nonradiative Decay Theory¹¹

The overall treatment of k_r and k_{nr} in section B is largely phenomenological. The radiative rate constant is quantitatively defined by the transition moment integral, as formulated by the Einstein equation for spontaneous emission, equation 5.6.¹²

$$k_r = \frac{4E_{em}^3}{3\hbar^4 c^3} \left| \left\langle \Psi_{gs} | \hat{\mu} | \Psi_{es} \right\rangle \right|^2 \tag{5.6}$$

 Ψ_{gs} and Ψ_{es} are the ground and excited state electronic wavefunctions, respectively, and μ is the transition dipole moment operator. For a series of compounds with a common chromophore, the transition dipole and the emission energy do not change significantly, especially with regard to temperature. Consequently the dominating parameter with regard to the basic photophysical properties of lifetime and intensity is the nonradiative decay constant.

Nonradiative decay occurs via an isoenergetic electronic transition from a thermally equilibrated vibronic excited state, $v_{es}^{\ 0}$, to a vibronically excited ground state, $v_{gs}^{\ n}$. This is followed by vibrational relaxation to the molecule's ground state configuration, $v_{gs}^{\ 0}$. The overall process is schematically represented in Figure 5.2. The efficiency of the nonradiative decay is directly related to the vibrational overlap of $v_{es}^{\ 0}$ and $v_{gs}^{\ n}$. An estimate of the wavefunction overlap is given by equation 5.7,

$$G \approx \frac{E_m}{\hbar \omega_m} \coth \left[\frac{\beta \hbar \omega_m}{2} \right]$$
 (5.7)

G is the coupling strength, E_m is related to the Stokes shift, $\hbar\omega_m$ is the mean vibrational frequency of the accepting mode and $\beta=1/k_BT$; k_B is the Boltzmann constant. The extent of the vibrational overlap is greatly dependent on the magnitude of the vibrational wavefunction, which is greatest at the edges of the potential energy well. As the vibrational quantum number, n, increases the magnitude of the wavefunction at the classical turning point also increases. The vibrational overlap, and therefore k_{nr} , can be increased by large distortions between the ground and excited states, ΔQ_j^0 , high frequency ground state accepting vibrations, ω_m , or a small energy gap, ΔE .

The nuclear distortion (equation 5.8) between the equilibrium configurations of the excited, $Q_j^{0(e)}$, and ground states, $Q_j^{0(g)}$, defines two coupling limits, strong and weak, shown schematically in Figure 5.3.

$$\Delta Q_i^0 = Q_i^{0(e)} - Q_i^{0(g)} \tag{5.8}$$

The weak coupling limit occurs when the displacement between the energy wells is small. Because vibrational overlap is poor, Figure 5.3a, coupling is weak, as

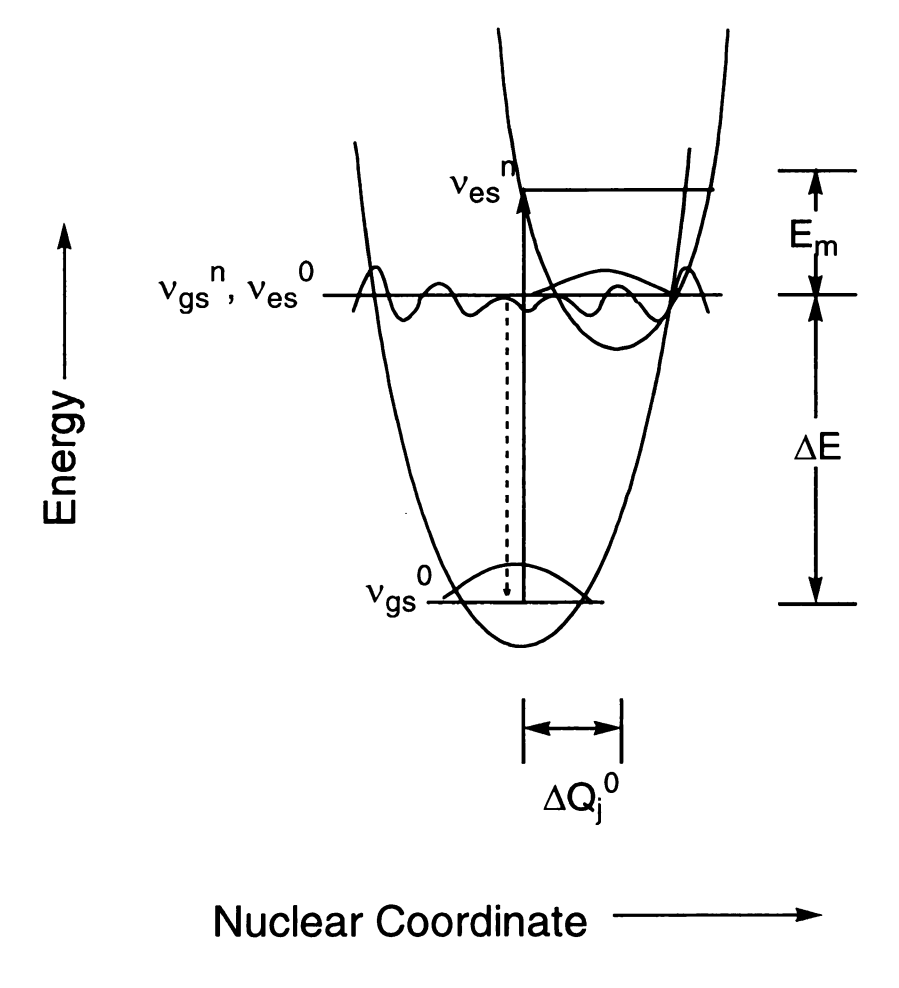


Figure 5.2 Potential energy diagram for nonradiative excited state decay.

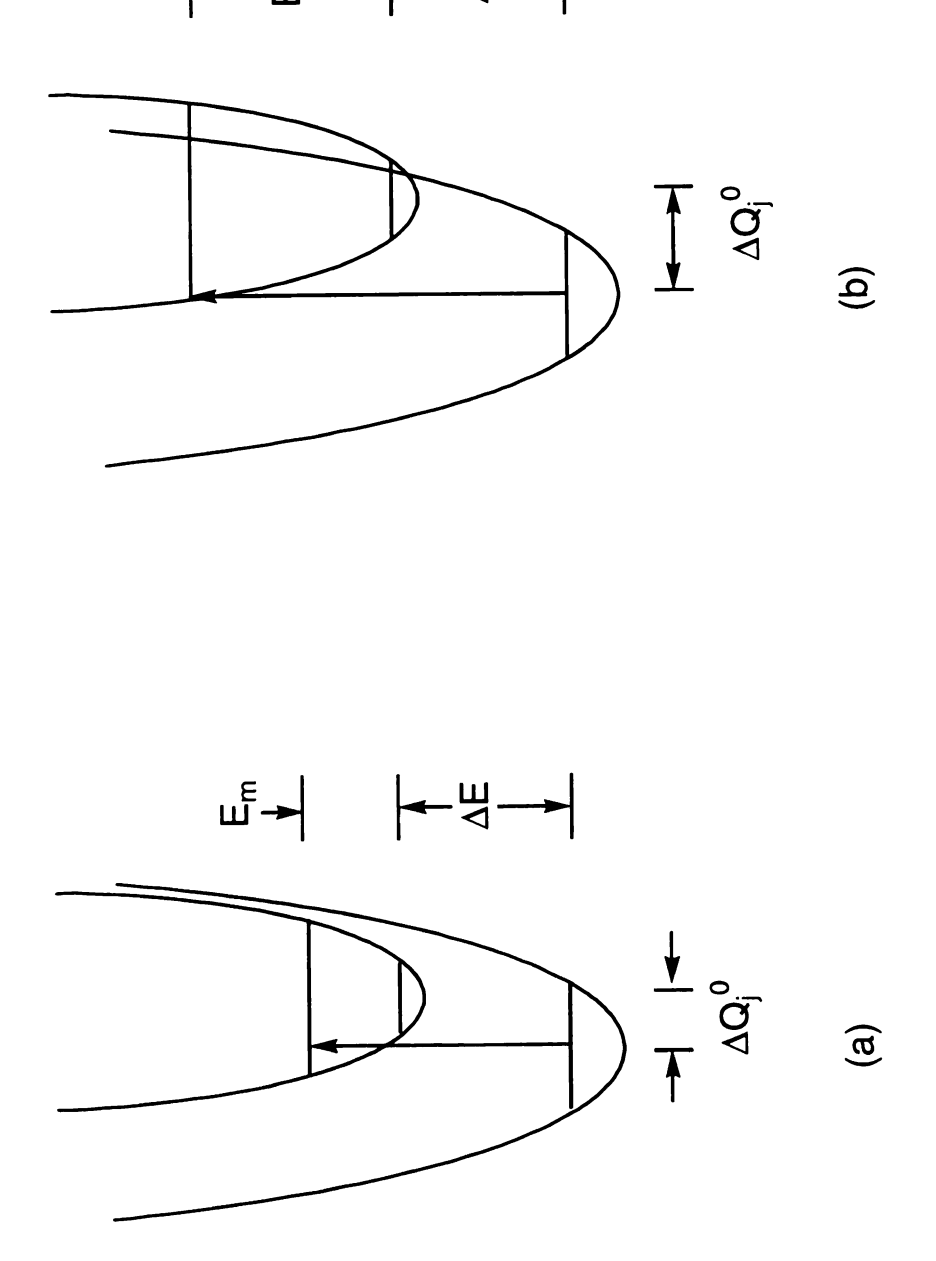


Figure 5.3 Potential energy wells in the weak coupling limit (a) and the strong coupling limit (b) of nonradiative decay.

compared to the strong coupling limit, which is defined by the interaction of the wells.

1. Calculation of the Huang-Rhys Factor

The important quantity, ΔQ_j^0 can be approximated by a Franck-Condon analysis. Experimentally, this distortion is provided by the Huang-Rhys factor, S_m^{-13}

$$S_m = \frac{1}{2} \sum \Delta Q_j^{0^2} \tag{5.9}$$

which is related directly to the Franck-Condon factor. S_m can be approximated from equation 5.10^{14}

$$S_m = \left(\frac{2\pi^2 M_m \nu_m}{h}\right) R^2 \tag{5.10}$$

where M_m is the reduced mass, $v_m (=\hbar\omega_m)$ is the accepting frequency and R is the difference between the equilibrium bond distances in the ground and excited states

For the case of M-4-M species, the major accepting mode may logically be assumed to be the M-M bond stretch. Detailed Raman studies of $Mo_2X_8^4$ ions (X = Cl, Br) demonstrates that these complexes exhibit a strong resonance enhancement of the totally symmetric $A_1(Mo_2)$ vibration along with excitation of $\delta\delta^*$. Therefore, the majority of the distortion in the excited state will be along this axis. The extent of nuclear distortion along the metal-metal axis will largely determine whether these systems are in the weak or strong coupling limits.

The change in M-M bond lengths in the excited state of various quadruple bonds are listed in Table 5.1. These are calculated either by a Franck-Condon

Table 5.1 Vibrational Frequencies of the Excited and Ground State for several M–4–M Complexes and Their Corresponding Change in the M–M Bond Length in the Excited State.

complex	v / cm^{-1}	v*/cm ⁻¹	R/Å
$Mo_2Cl_8^{4-a}$	346	336	0.03^{g}
$Mo_2Cl_4(6-mhp)_2(PEt_3)_2^b$	389	370	0.048 ^g
Mo ₂ Cl ₄ (PEt ₃) ₄ c	342	320	0.07^{g}
$\mathrm{Re_2Cl_8}^{2-\mathrm{d}}$	272	248	0.079^{g}
$Mo_2[(CH_2)_2P(CH_3)_2]_4$ e	388	345	0.092 ^h
$Mo_2[O_2CCH_3]_4$ f	406		0.11 ^h

- a. Clark, R. J. H.; Franks, M. L. J. Am. Chem. Soc. 1975, 97, 2691. Fanwick, P. E.; Martin, D. S.; Cotton, F. A.; Webb, T. R. Inorg. Chem. 1977, 16, 2103.
- b. Macintosh, A. M.; Nocera, D. G. Inorg. Chem. 1996, 35, 7134.
- c. Filippo, J. S.; Sniadoch, H. J. *Inorg. Chem.* **1974**, *12*, 2326. Filippo, J. S.; Sniadoch, H. J.; Grayson, R. L. *Inorg. Chem.* **1974**, *13*, 2121.
- d. Cowman, C. D.; Gray, H. B. J. Am. Chem. Soc. 1973, 95, 8177. Clark, R. J. H.; Franks, M. L. J. Am. Chem. Soc. 1976, 98, 2763. Bratton, W. K.; Cotton, F. A.; Debeau, M.; Walton, R. A. J. Coord. Chem. 1971, 1, 121.
- e. reference 14b. Martin, D. S.; Newman, R. A.; Fanwick, P. E. *Inorg. Chem.* 1979, 18, 2511.
- f. Cotton, F. A.; Fanwick, P. E. J. Am. Chem. Soc. 1979, 101, 5252.
- g. Calculated using the method in reference 25.
- h. Calculated by a Franck-Condon analysis of the low temperature absorption.

analysis of the low temperature absorption spectrum or from the M-M vibrational frequencies of the excited and ground states, as discussed above. In general the increase in the M-M bond length in the excited state is < 0.11 Å. From the small nuclear displacement in the excited state, it can be concluded that M-4-M complexes are in the weak coupling limit of nonradiative decay theory. Therefore, only the weak coupling limit will be discussed.

2. Weak Coupling Limit¹¹

Within the weak coupling limit of nonradiative decay, there are two limits; these are called the low-temperature and temperature-dependent limits. In the low-temperature limit the quantum spacings for the acceptor modes are large compared to k_BT , $\hbar\omega_m >> k_BT$ and the nonradiative decay takes place from the lowest vibrational component of the higher electronic state. The expression for nonradiative decay in this limit has been developed by Meyer for the d^6 monomers, the M(bpy)₃ complexes and their derivatives (M = Ru, Os, Re), d^6 and is applicable to other transition metal systems. In the temperature-dependent limit the quantum spacings for the acceptor modes are small compared to d^6 to in this case.

a. Low-Temperature Limit of Weak Coupling

The nonradiative decay constant in the low temperature, weak coupling limit is given by equation 5.11.

$$k_{nr} = \frac{C^2}{\hbar} \left[\frac{2\pi}{\hbar \omega_m \Delta E} \right]^{\frac{1}{2}} \exp(-S_m) \exp\left[\frac{-\gamma \Delta E}{\hbar \omega_m} \right]$$
 (5.11)

where, C is the electronic coupling matrix element, ΔE is the energy gap between the excited state and the ground state. γ is defined below by equation 5.12.

$$\gamma = \ln \left[\frac{2\Delta E}{\sum \hbar \omega_m \Delta Q_j^{0^2}} \right] - 1$$
 (5.12a)

$$\gamma \approx \ln \left[\frac{\Delta E}{S_m \hbar \omega_m} \right] - 1 \tag{5.12b}$$

If there is one primary deactivating accepting mode then equation 5.12a can be reduced to equation 5.12b and Equation 5.11 reduces to

$$\ln k_{nr} = \left(\ln \alpha - S_m\right) - \frac{\gamma \Delta E}{\hbar \omega_m} \tag{5.13}$$

$$\alpha = \frac{C^2}{\hbar} \left[\frac{2\pi}{\hbar \omega_m \Delta E} \right]^{\frac{1}{2}} \tag{5.14}$$

For a series of compounds, changes in C and S_m are expected to be small and γ and $\ln \alpha$ should be invariant with ΔE . Therefore, if γ and $\ln \alpha$ are considered constants, a linear relationship between $\ln k_{nr}$ and ΔE can be expected, with the rate of excited state deactivation inceasing as the energy gap decreases.

b. Temperature-Dependent Limit of Weak Coupling

As developed previously, a reasonable acceptor mode for M-4-M complexes is the M-M bond stretching mode, which is $\sim 260-350$ cm⁻¹.¹⁷ Because the frequency of the primary accepting mode, ω_m , small with respect to k_BT , the temperature dependent limit of the weak coupling must be used at high temperatures. This can be described by equation 5.15.¹¹

$$k_{nr} = \frac{C^2}{\hbar} \left[\frac{2\pi}{\hbar \omega_m \Delta E} \right]^{\frac{1}{2}} \exp\left(-S_m \left(2n_m + 1\right)\right) \exp\left[\frac{-\gamma' \Delta E}{\hbar \omega_m}\right]$$
 (5.15)

$$\gamma' = \ln \left[\frac{2\Delta E}{\sum \hbar \omega_j \Delta Q_j^{0^2} (n_m + 1)} \right] - 1$$
 (5.16)

$$n_m + 1 = \frac{1}{1 - \exp(-\beta \hbar \omega_m)} \tag{5.17}$$

Equation 5.17 is the thermally averaged population number for mode m and incorporates the temperature dependence of the coupling parameter G. Equation 5.15 can be treated in a similar manner as equation 5.11, to give equation 5.18. Based on this equation, a linear dependence of $\ln k_{nr}$ and ΔE is also predicted in the temperature dependent limit of weak coupling.

$$\ln k_{nr} = \left[\ln \alpha - S_m \left(2n_m + 1\right)\right] + \frac{\gamma' \Delta E}{\hbar \omega_m}$$
 (5.18)

3. Intervalence Charge Transfer

Typically, MMCT absorption bands of mixed-valence ground state complexes are observed at low energy in the absorption spectra. This type of transition has been termed intervalence charge transfer (IT) by Hush. The band shape, absorption energy, extinction coefficient and the electron transfer distance can used to determine the electronic coupling between the electron donor and acceptor. This can be derived from the following relationships. Equation 5.19 gives the expression for the oscillator strength, f, of an electronic transition. In

$$f = (1.085x10^{11})G\overline{\nu}_{\text{max}}M^2 \tag{5.19}$$

where G is the degeneracies of the states concerned, $\bar{\nu}_{max}$ is the transition energy in cm⁻¹ and M is the transition dipole moment. The oscillator strength can be calculated from the following experimental properties.¹⁹

$$f = 4.61x10^{-9} \varepsilon_{\text{max}} \overline{\nu}_{1/2} \tag{5.20}$$

where ε_{max} is the extinction coefficient and $\Delta \overline{\nu}_{1/2}$ the bandwidth at half-height. For weakly coupled systems, the transition dipole moment can be approximated by the following expression.¹⁹

$$M \approx e \alpha R$$
 (5.21)

where e is the electronic charge, α is the mixing coefficient of the donor and acceptor wavefunctions and R is the transition dipole length. The mixing coefficient, α , is given by equation 5.22.²⁰

$$\alpha = \frac{H_{AB}}{\overline{V}_{\text{max}}} \tag{5.22}$$

H_{AB} is the electronic coupling. From these relations, it can be seen that the electronic coupling can be defined by equation 5.23. This approximation is only valid at room temperature.

$$H_{AB} \cong \frac{2.05 \times 10^{-2}}{R} \left(\varepsilon_{\text{max}} \overline{\nu}_{\text{max}} \Delta \overline{\nu}_{1/2} \right)^{\frac{1}{2}}$$
 (5.23)

Mixed-valence complexes have been grouped in three classes.²¹ In class I, the interaction between the two metal centers is very weak and the properties of the complex are essentially those of the individual components of the complex. In class II, there is a greater interaction between the metals and the properties of the complex may or may not be those of the constituent parts. In class III, the interaction between the two metal centers is large and the properties of the complex are unique from those of the fragments. The two metals are connected by a bridge, which may range from a long organic molecule to a single atom or to nothing (M–M bond). The nature of the bridge and distance between the electron donor and acceptor greatly affects the extent of the electronic coupling between the

metal centers.²¹ The effect of the distance between the electron donor and acceptors can be seen with the electronic coupling of complexes (1) and (2), below.²²

$$6.8 \text{ Å}$$

$$(NH_3)_5 \text{Ru}^{II} - N N - \text{Ru}^{III} (NH_3)_5]^{5+} \qquad H_{AB} \sim 3300 \text{ cm}^{-1} \quad (1)$$

$$[(NH_3)_5Ru^{II}-N]^{5+}$$
 $H_{AB} \sim 400 \text{ cm}^{-1}$ (2

The distance between Ru^{II}/Ru^{III} is 6.8 Å and 11.3 Å in complexes (1) and (2), respectively. This has a dramatic effect on H_{AB} , which drops by an order of magnitude for complex (2), as compared to complex (1).

D. Results and Discussion

In order to understand the nonradiative decay of the $^1\delta\delta^*$ excited state of M-4-M complexes fully, a study of the temperature dependence of the emission lifetimes of Mo₂Cl₄(PR₃)₄, MoWCl₄(PR₃)₄ and W₂Cl₄(PR₃)₄, where PR₃ = PMe₃, PMe₂Ph, PMePh₂, was initiated.

1. $Mo_2Cl_4(PR_3)_4$

Absorption and emission spectra of glasses of 2-MeTHF solutions of Mo₂Cl₄(PR₃)₄ exhibit vibrational fine structure at 40 K. The half-width of the

emission band is temperature dependent, increasing by about 300 cm⁻¹ between 40 and 290 K.

Figures 5.4 - 5.6 display the temperature dependence of the excited state decay constants of $Mo_2Cl_4(PR_3)_4$, the experimental fits to equation 5.4 are shown as solid lines in each Figure. The lifetimes could be fit to a monoexponential decay expression for all three complexes at all temperatures. Table 5.2 tabulates the rate constants, k_1 and k_2 , and energy gaps for $Mo_2Cl_4(PR_3)_4$ as calculated from equation 5.4. k_1 is ~5 x 10^6 and k_2 is about 2 x 10^{11} ; with the exception of $Mo_2Cl_4(PMePh_2)_4$ for which k_2 is an order of magnitude faster. The energy gap between $^1\delta\delta^*$ and the higher energy state is about 1750 cm $^{-1}$ for $Mo_2Cl_4(PR_3)_4$.

Figure 5.5 displays a sharp discontinuity between the temperatures 130 and 180 K. The expression for k_{nr} , equations 5.14 and 5.20, contain the Franck-Condon factor in the term $\exp(-S_m(2n_{m+1}))\exp[-\gamma'\Delta E/\hbar\omega_m]$, which accounts for both intramolecular and solvent vibrational modes. This discontinuity is consistent with solvent modes coupled to the intramolecular vibrations. In a rigid glass, the solvent dipoles are immobile in the time scale of the excited state lifetime and do not have time to reorient themseleves to the electronic structure of the excited state. As the glass begins to soften, the reorientation time becomes comparable to the lifetimes and ΔE decreases due to an enhanced stabilization of the excited state by partial dipole reorientation. At higher temperatures, as the glass becomes fully fluid, the solvent reorientation time is fast compared to the time scale for the excited state decay and the solvent has time to fully reorient itself in response to the change in electronic structure. This has been observed in the temperature dependence of the lifetimes of $[Os(bpy)_3]^{2+}$, which shows a relatively sharp discontinuity between the

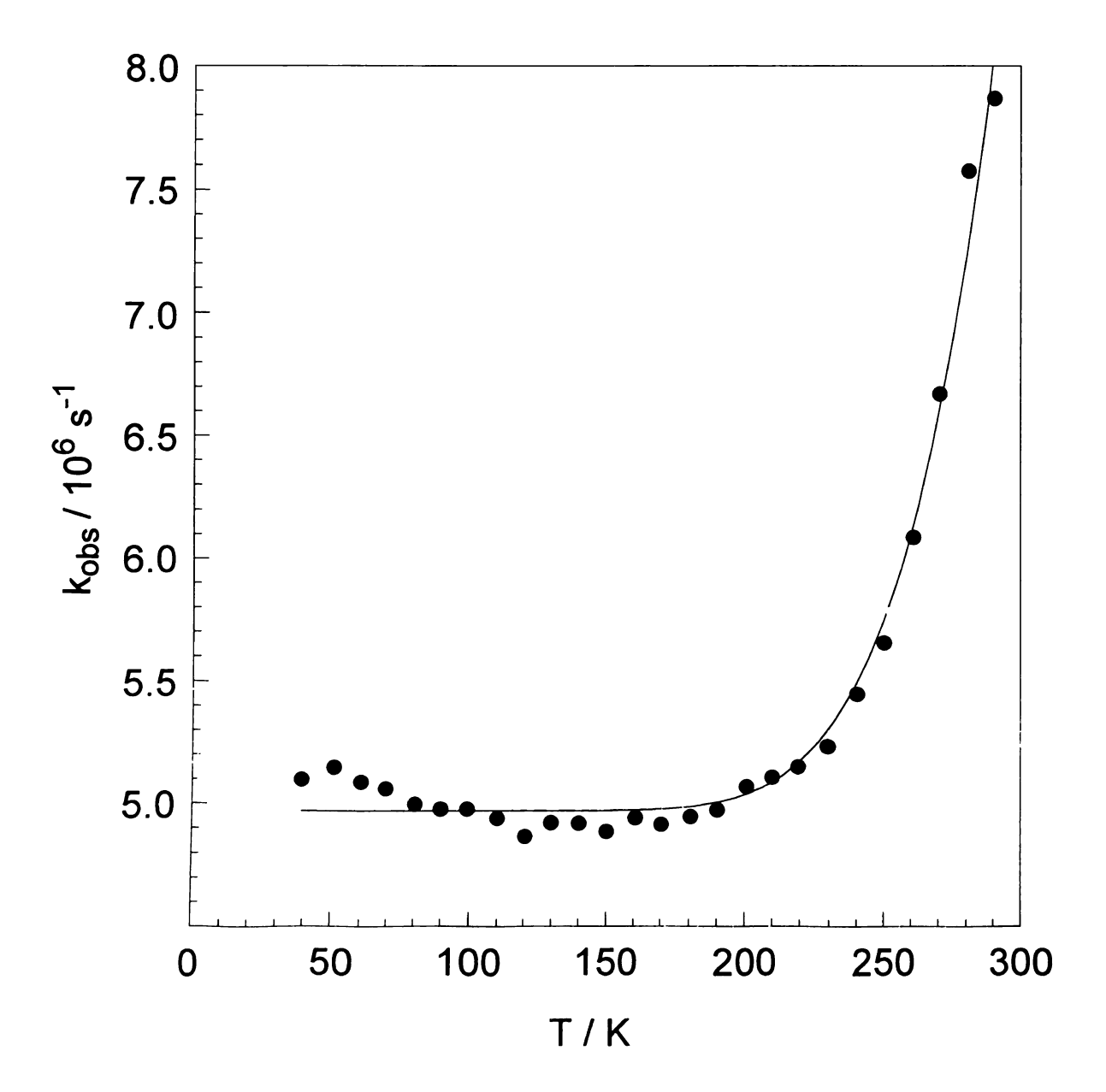


Figure 5.4 Fit of the variation of the observed emission decay constant of Mo₂Cl₄(PMe₃)₄ to equation 5.4 in the 40-290 K temperature range.

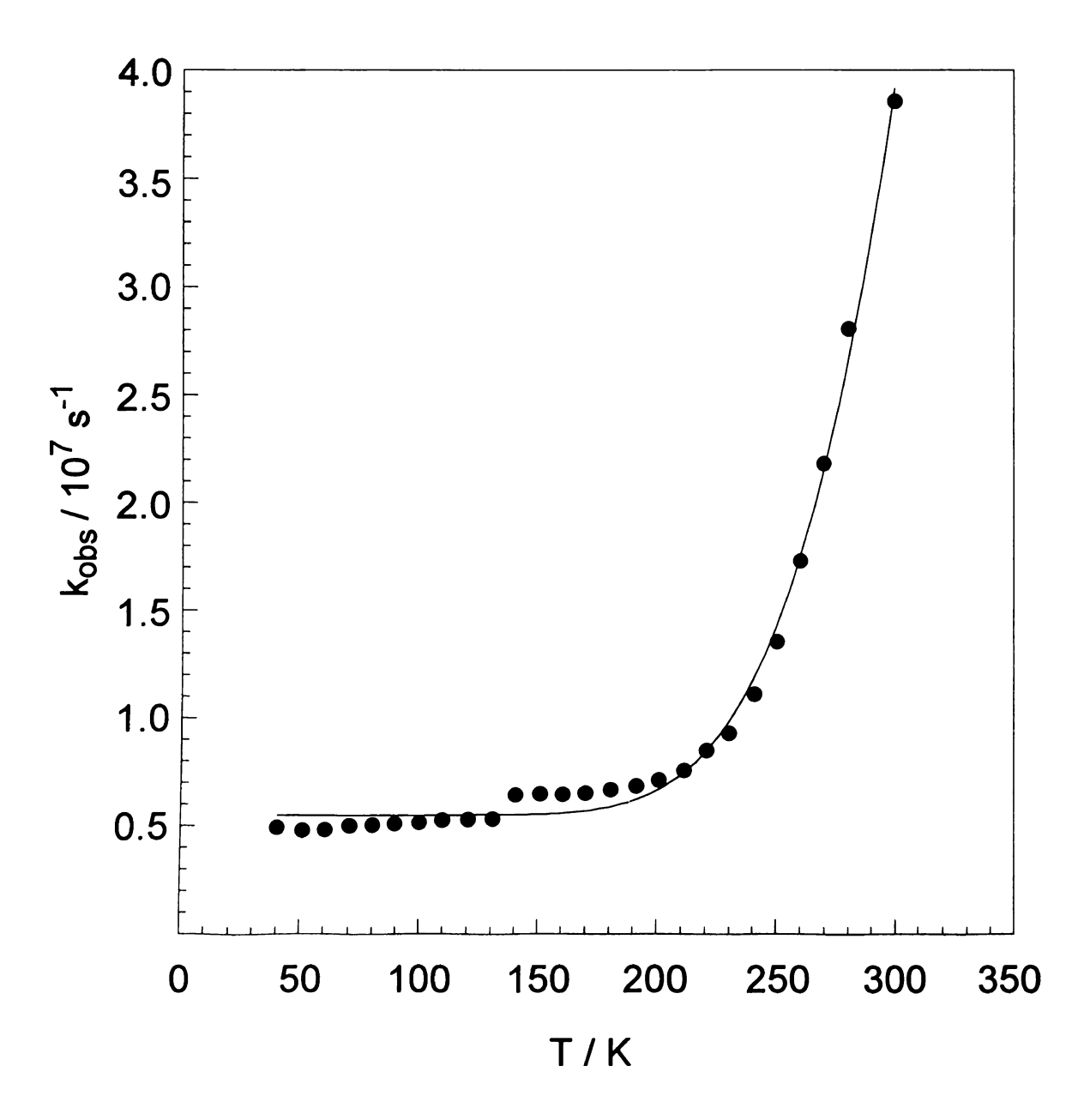


Figure 5.5. Fit of the variation of the observed emission decay constant of Mo₂Cl₄(PMe₂Ph)₄ to equation 5.4 in the 40-290 K temperature range.

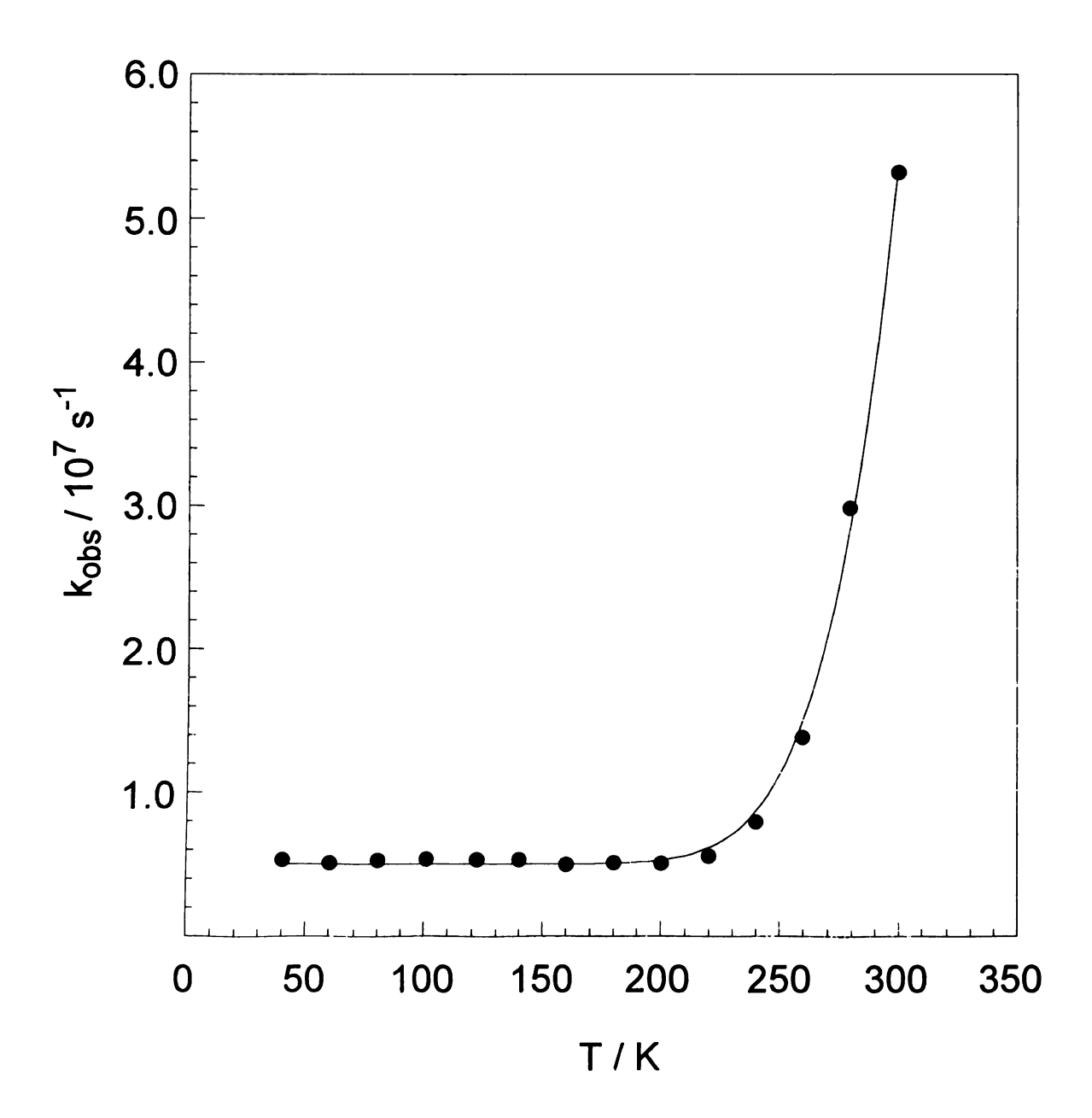


Figure 5.6 Fit of the variation of the observed emission decay constant of Mo₂Cl₄(PMePh₂)₄ to equation 5.4 in the 40-290 K temperature range.

Table 5.2 Temperature Dependence of ΔE , k_1 and k_2 of $M_2Cl_4(PR_3)_4$

	-		
	Mo ₂ Cl ₄	$(PR_3)_4$	
PR ₃	Δ E/ cm ⁻¹	$k_1/10^6$	k ₂ / 10 ¹¹
PMe ₃	1400	5.0	0.16
PMe ₂ Ph	1730	5.5	0.28
PMePh ₂	2155	5.0	15
	MoWCl	4(PR ₃) ₄	
PR ₃	$\Delta E/ cm^{-1}$	$k_1/10^6$	k ₂ / 10 ¹⁰
PMe ₃	291	8.9	0.0027
PMe ₂ Ph	1980	15	8.9
PMePh ₂	1480	5.4	3.7
	W ₂ Cl ₄ ((PR ₃) ₄	
PR ₃	$\Delta E/ cm^{-1}$	$k_1/10^6$	$k_2/10^6$
PMe ₃	625	1.8	8.2
PMe ₂ Ph	496	1.9	11
PMePh ₂	679	0.93	6.5

temperatures 100 to 150 K.²³ The change in dipole in the excited state for $[Os(bpy)_3]^{2+}$, ~13 D, is significant in terms of solvent interactions, therefore producing a large effect at the glass-to-fluid transition temperature when the solvent dipoles are able to reorient themselves again. As a consequence of the polar nature of the M-4-M excited state, 4 D,²⁴ this phenomenon at the glass-to-fluid temperature is also observed for these complexes.

Tables 5. 3 - 5.5 list ϕ_e , τ , k_r and k_{nr} for $Mo_2Cl_4(PR_3)_4$ over the temperature range of 40 - 290 K. In order to correct for the change in the absorption with temperature, the absorption spectrum of $W_2Cl_4(PMe_3)_4$ was measured as a function of temperature. A correction file was generated from this and used to correct the $\phi_e(T)$ for all complexes. The rates measured, Table 5.3, at 290 K for $Mo_2Cl_4(PMe_3)_4$ are in good agreement with those previously reported ($k_r = 1.96 \text{ x} \cdot 10^6 \text{ s}^{-1}$; $k_{nr} = 5.5 \text{ x} \cdot 10^6 \text{ s}^{-1})^8$. The nonradiative decay constants for $Mo_2Cl_4(PR_3)_4$ are about 3 x 10^7 s^{-1} , with the exception of $Mo_2Cl_4(PMe_3)_4$, which is an order of magnitude slower at 6 x 10^6 s^{-1} . The smaller rate for $Mo_2Cl_4(PMe_3)_4$ is consistent with its much longer lifetime, 127 ns at 290 K, as compared to 26 and 34 ns for $Mo_2Cl_4(PMe_2Ph)_4$ and $Mo_2Cl_4(PMePh_2)_4$, respectively. Clearly, there is a thermal decay pathway for the other complexes that is not available to $Mo_2Cl_4(PMe_3)_4$.

The fraction of decay that occurs through the upper excited state can be calculated from equation 5.5. This has been calculated for 290 and 40 K, Table 5.6. At 290 K there is significant deactivation of the $^1\delta\delta^*$ excited state through this higher energy excited state, while at 40 K there is considerably less. The fraction of decay, η_1 , and k_{nr} are consistent with an activationless decay at low temperature, indicative of direct internal conversion to the ground state, while at high

Table 5.3 Temperature Dependence of $\phi_e,\,\tau,\,k_r$ and k_{nr} of $Mo_2Cl_4(PMe_3)_4$

T/K	φ _e / 10 ⁻²	τ/ns	k _r / 10 ⁶	k _{nr} / 10 ⁶
39	66	196	3.3	1.8
51	67	194	3.5	1.7
61	68	197	3.5	1.6
70	68	198	3.4	1.6
80	67	200	3.4	1.6
90	65	201	3.3	1.7
99	64	201	3.2	1.8
110	65	202	3.2	1.8
121	67	205	3.3	1.6
130	67	203	3.3	1.6
141	66	203	3.3	1.7
150	66	205	3.2	1.7
161	64	203	3.2	1.8
170	63	204	3.1	1.8
181	62	202	3.1	1.9
190	61	201	3.0	1.9
201	59	197	3.0	2.0
210	57	196	2.9	2.1
220	56	194	2.9	2.3
230	53	191	2.8	2.5
241	51	184	2.8	2.7
250	47	177	2.7	3.0
261	43	164	2.6	3.4
270	38	150	2.5	4.1
281	33	132	2.5	5.0
290	29	127	2.3	5.6

Table 5.4 Temperature Dependence of $\varphi_e,\,\tau,\,k_r$ and k_{nr} of $Mo_2Cl_4(PMe_2Ph)_4$

T/K	$\phi_{\rm e} / 10^{-2}$	τ/ns	$k_{\rm r} / 10^6$	k _{nr} / 10 ⁶
40	39	202	2.0	3.0
51	40	208	1.9	2.9
60	39	206	1.9	2.9
71	36	199	1.8	3.2
80	36	198	1.8	3.2
90	39	196	2.0	3.1
100	43	194	2.2	2.9
110	44	190	2.3	3.0
121	44	189	2.3	3.0
131	44	187	2.3	3.0
141	43	155	2.8	3.7
151	42	154	2.7	3.8
161	40	154	2.6	3.9
170	39	153	2.5	4.0
181	36	149	2.4	4.3
191	34	146	2.3	4.5
202	31	140	2.2	4.9
211	28	132	2.1	5.5
221	24	118	2.1	6.4
230	20	108	1.9	7.4
241	16	89.9	1.8	9.3
250	14	73.7	1.9	12
260	11	57.8	1.9	15
270	7.9	45.9	1.7	20
281	5.8	35.6	1.6	26
300	3.5	25.9	1.3	37

Table 5.5 Temperature Dependence of $\varphi_e,\,\tau,\,k_r$ and k_{nr} of $Mo_2Cl_4(PMePh_2)_4$

T/K	$\phi_{\rm e} / 10^{-2}$	τ/ns	$k_{\rm r} / 10^5$	$k_{nr}/10^6$
40	8.5	187	4.6	4.9
60	9.0	195	4.6	4.7
80	8.7	189	4.6	4.8
100	8.2	186	4.4	4.9
120	7.4	187	3.9	4.9
140	6.8	187	3.6	5.0
161	6.2	199	3.1	4.7
181	5.8	196	3.0	4.8
201	4.8	193	2.5	4.9
221	4.2	179	2.4	5.4
241	3.0	126	2.3	7.7
261	1.9	72	2.7	14
280	1.2	34	3.6	29

Table 5.6 Fractional of Decay Through the Upper Excited State at 290K and 40K

complex	η ₁ (290 K)	$\eta_1 (40 \text{ K})^a$
Mo ₂ Cl ₄ (PMe ₃) ₄	0.75	4.3 x 10 ⁻²⁴
$Mo_2Cl_4(PMe_2Ph)_4$	0.49	4.8×10^{-24}
Mo ₂ Cl ₄ (PMePh ₂) ₄	0.87	6.5×10^{-29}
MoWCl ₄ (PMe ₂ Ph) ₄	0.24	$6.9x\ 10^{-28}$
MoWCl ₄ (PMePh ₂) ₄	0.81	5.2x 10 ⁻²⁰
$W_2Cl_4(PMe_3)_4$	0.67	7.8x 10 ⁻⁹
$Wo_2Cl_4(PMe_2Ph)_4$	0.83	7.5 x 10 ⁷
Mo ₂ Cl ₄ (PMePh ₂) ₄	0.71	1.1 x 10 ⁻⁹

a. MoWCl₄(PR₃)₄ are calculated at 60 K.

temperature they are consistent with thermally activated decay through a potential surface crossing between ${}^{1}\delta\delta^{*}$ and some higher energy excited state.

Table 5.7 lists k_r and k_{nr} for a series of $Mo_2X_4(PR_3)_4$ complexes. k_r and k_{nr} are very similar, with the exception of PMe₃ for which the nonradiative decay is almost an order of magnitude smaller. This indicates that the nature of the phosphine ligand does not have a large effect on the nonradiative decay. When the halide is changed to Br and I, the nonradiative decay increases from 5.5 x 10^6 s⁻¹ for Cl to 9.2 x 10^6 and 3.0 x 10^7 s⁻¹, respectively. This indicates that the mixing of the halide^{4b,7,15} with the $^1\delta\delta^*$ excited state contributes significantly to the nonradiative decay.

As discussed previously, the change in the equilibrium M–M bond distance upon excitation can describe the amount of distortion in the excited state. This change in bond lengths is defined by equation 5.24, where r_e and r_e^* are the equilibrium bond distances in the ground state and the excited state, b corresponds to the total number of bonds that are changing.

$$R = \left[\sum_{j=1}^{b} \left(r_e^* - r_e\right)^2\right]^{\frac{1}{2}}$$
 (5.24)

The bond distances in the ground and excited states can be estimated from Woodruff's modification of Badger's rule.²⁵ The equilibrium bond distances for elements Rb - Xe and for elements Cs - Rn are given by equations 5.25 and 5.26, respectively.

$$r = 1.83 + 1.51 \exp\left(\frac{-k}{2.48}\right) \tag{5.25}$$

Table 5.7 k_r and k_{nr} for a Series of $Mo_2X_4(PR_3)_4$ Complexes.

complex	k _r / 10 ⁶	$k_{nr} / 10^7$
$Mo_2Cl_4(PMe_3)_4$	1.92	0.55
$Mo_2Cl_4(PMe_2Ph)_4$	1.3	3.7
Mo ₂ Cl ₄ (PMePh ₂) ₄	0.36	2.9
$Mo_2Cl_4(PEt_3)_4$	0.929	7.1
$Mo_2Cl_4(PPr^n_3)_4$	0.762	4.7
$Mo_2Cl_4(PBu^n_3)_4$	0.929	7.1
$Mo_2Br_4(PMe_3)_4$	1.92	0.92
$Mo_2I_4(PMe_3)_4$	4.24	3.0

$$r = 2.01 + 1.31 \exp\left(\frac{-k}{2.36}\right) \tag{5.26}$$

k is the force constant and can be calculated from equation 5.27.²⁵

$$k = 3.55x10^{17} M_m v_m^2 ag{5.27}.$$

The ground state and excited state stretching frequencies for the complex $Mo_2Cl_4(PMe_3)_4$ are $354^{5,26}$ and 335^7 cm⁻¹, respectively. r_e was calculated from equation 5.13 and corresponds well with the experimentally determined bond distance, ²⁷ Table 5.8. Therefore, this equation should afford a good approximation of the excited state equilibrium bond distance, r_e^* , Table 5.8. From the change in bond distance in the excited state, R = 0.08 Å, S_m was determined (equation 5.10) to be 1.5, thereby confirming that the Mo_2 complexes are in the weak coupling limit of nonradiative decay. Plots of $ln k_{nr}$ vs the emission energy, ΔE , for T = 40 and 290 K for $Mo_2Cl_4(PR_3)_4$, Figure 5.7. The largest error in the calculation of k_{nr} is due to ϕ_e and is estimated at 20%. The linear correlation indicates that this series of complexes follows energy gap theory. The nature of the chromophore for Mo_2 , MoW and W_2 changes with the metal and therefore the three series of complexes should not be expected to fall on the same line, with respect to the energy gap law.

2. W₂Cl₄(PR₃)₄

Vibrational fine structure is observed at 40K in the absorption and emission spectra of 2-MeTHF solutions of W₂Cl₄(PR₃)₄. The band width of the emission exhibits a temperature dependence, increasing by about 700 cm⁻¹ between 40 and 290 K.

Table 5.8 Calculated Excited and Ground state M-M Bond Lengths, Experimental M-M Bond Lengths and the Calculated Huang-Rhys Factor.

M_2	r _e (calc) /Å	r(exptl) /Å	r _e *(calc)/Å	Δr	S_m^{a}
$Mo_2Cl_4(PMe_3)_4$	2.17	2.13^{25}	2.25	0.08	1.51
MoWCl ₄ (PMe ₃) ₄	2.21	2.209^{27}	2.25	0.04	0.50
$W_2Cl_4(PBu_3)_4$	2.29	2.267 ²⁶	2.35	0.06	1.21

a. calculated from equation 5.10.

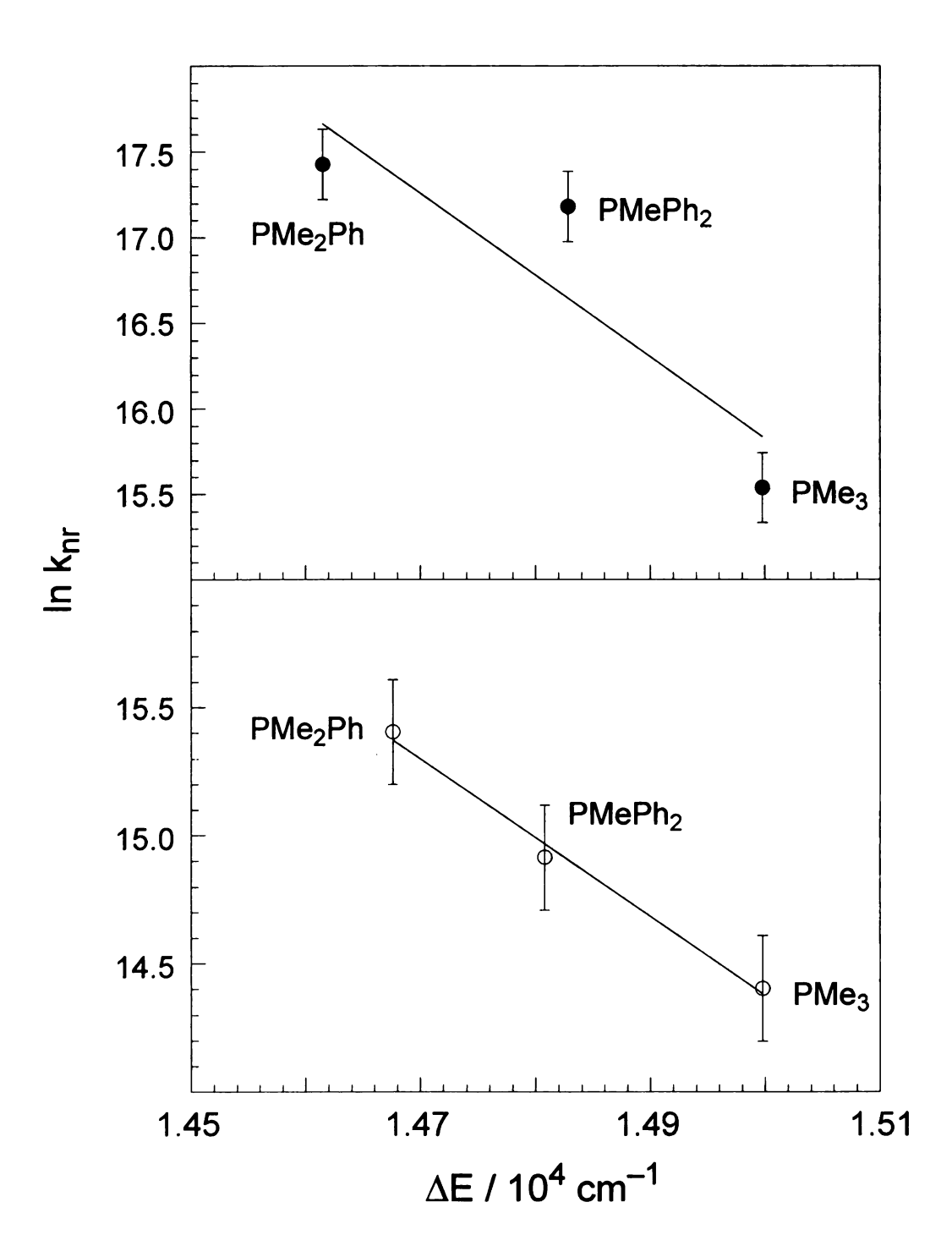


Figure 5.7 Energy gap plots for $Mo_2Cl_4(PR_3)_4$ at 290 K (\bullet) and 40 K (o).

The experimental fits to the temperature dependent lifetimes are shown as a solid line in Figures 5.8 - 5.10. The lifetimes of all complexes could be fit to a monoexponential decay expression at all temperatures. k_{obs} below 130 K for $W_2Cl_4(PMe_2Ph)_4$, Figure 5.9, could not be fit along with the high temperature data. This is possibly due the phase transition from a glass to solution at this temperature, as discussed above.

The rate constants, k_1 and k_2 , and energy gaps for $W_2Cl_4(PR_3)_4$ as calculated from equation 5.4 are listed in Table 5.2. k_1 for all three complexes is ~2 x 10^6 and k_2 is about 7 x 10^6 ; with the exception of $W_2Cl_4(PMe_2Ph)_4$, which has rate constant k_2 of 11 x 10^6 . In general, the decay rate constants for the upper excited state, k_2 , are 4 to 5 orders of magnitude slower than the $Mo_2Cl_4(PR_3)_4$ and $MoWCl_4(PR_3)$ (see below). ΔE , the energy gap between $^1\delta\delta^*$ and the higher energy excited state is calculated to be about 600 cm^{-1} .

The luminescent quantum yields, ϕ_e , and lifetimes, τ , and the radiative, k_r , and nonradiative, k_{nr} , decay constants for $W_2Cl_4(PMe_3)_4$, $W_2Cl_4(PMe_2Ph)_4$ and $W_2Cl_4(PMePh_2)_4$, respectively, are listed in Tables 5.9 - 5.11. k_r and k_{nr} are similar for all three complexes, 1.3 x 10^6 s⁻¹ and 1.8 x 10^7 s⁻¹. The lifetimes start to converge to 100 ns at 40 K.

The fraction of decay through the upper excited state at 290 and 40 K are listed in Table 5.6. The amount of deactivation of $^1\delta\delta^*$ through the upper excited state at 290 K is substantial. Due the small energy gap, the amount of deactivation at 40 K is still quite significant. This is consistent with deactivation through thermal population of some higher energy excited state and due to the small energy gap, there is still considerable deactivation at 290 K. This can be observed in the

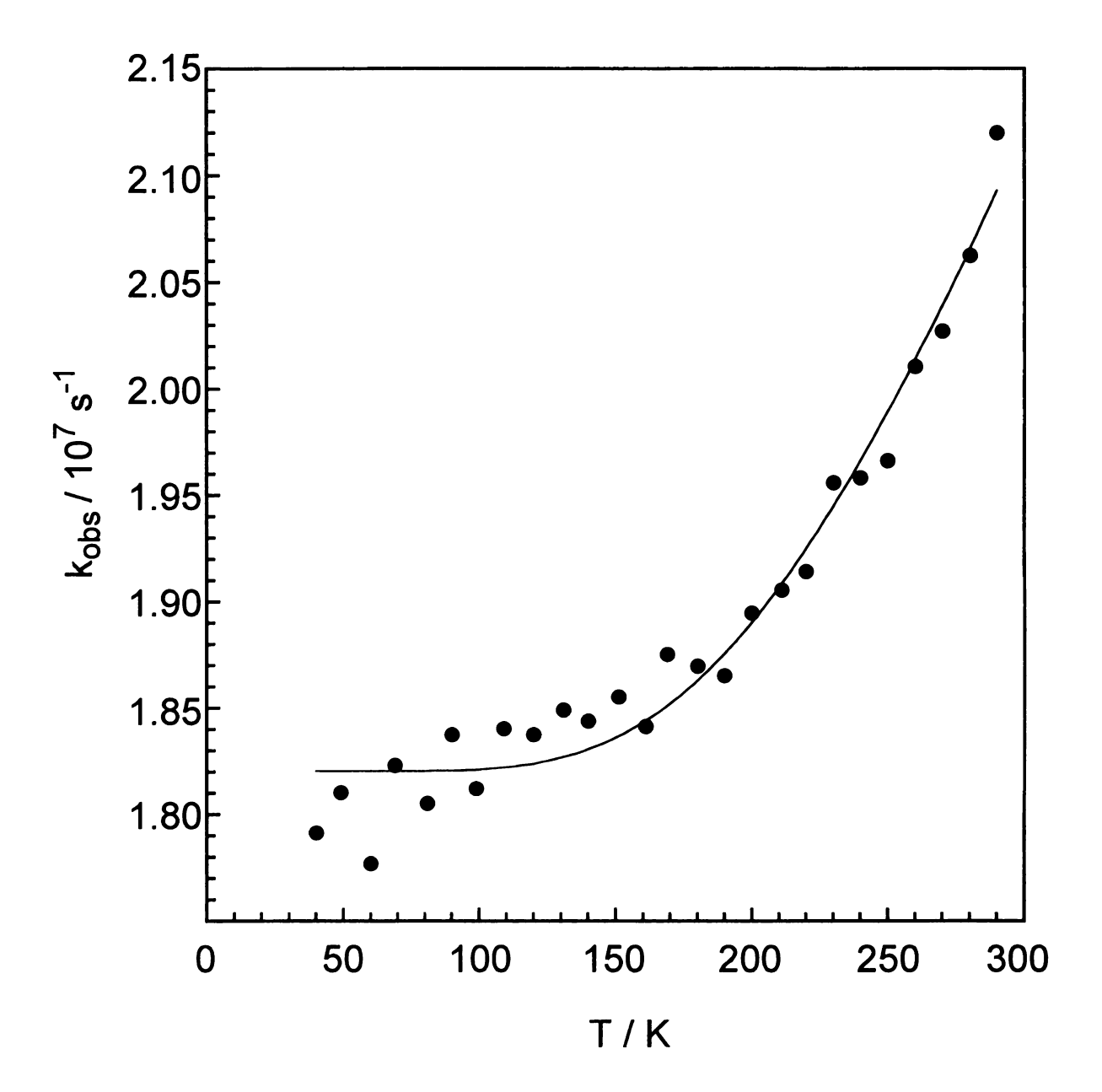


Figure 5.8 Fit of the variation of the observed emission decay constant of $W_2Cl_4(PMe_3)_4$ to equation 5.4 in the 40-290 K temperature range.

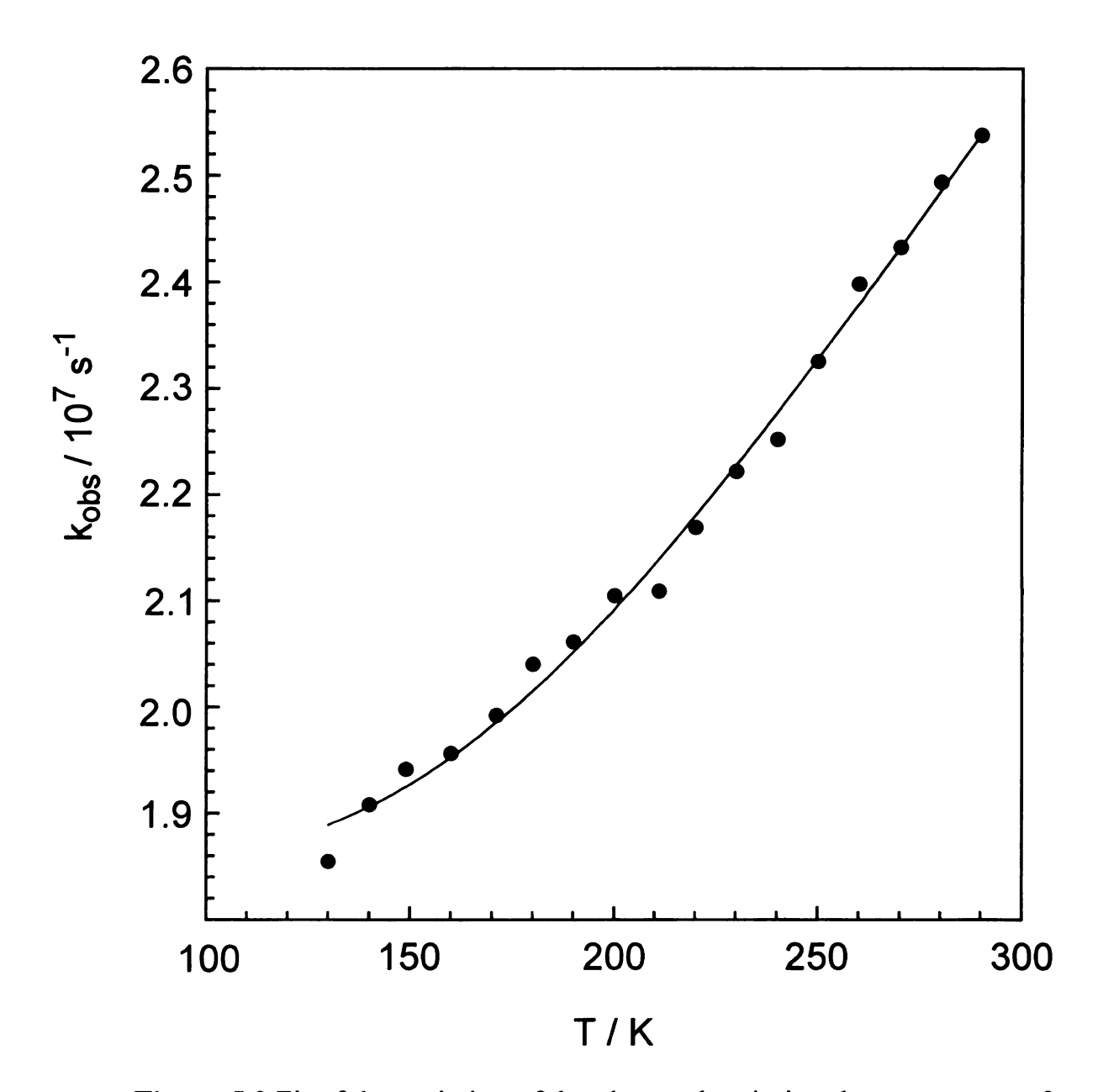


Figure 5.9 Fit of the variation of the observed emission decay constant of $W_2Cl_4(PMe_2Ph)_4$ to equation 5.4 in the 130-290 K temperature range.

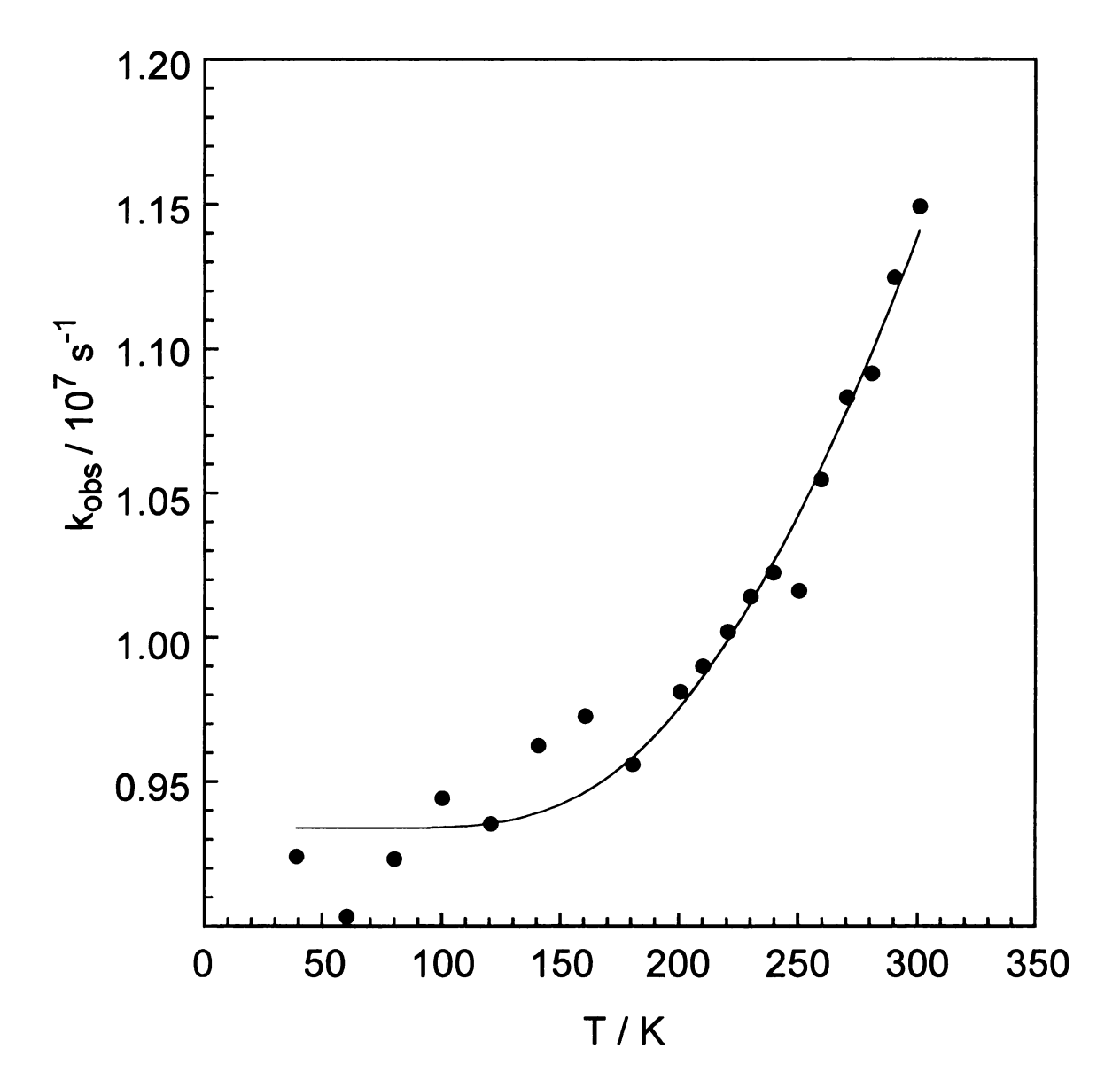


Figure 5.10 Fit of the variation of the observed emission decay constant of $W_2Cl_4(PMePh_2)_4$ to equation 5.4 in the 40-300 K temperature range.

Table 5.9 Temperature Dependence of $\varphi_e,\,\tau,\,k_r$ and k_{nr} of $W_2Cl_4(PMe_3)_4$

T/K	$\phi_{\rm e} / 10^{-2}$	τ/ns	k _r / 10 ⁶	k _{nr} / 10 ⁷
40	14	56	2.6	1.5
49	14	55	2.6	1.5
60	15	56	2.6	1.5
69	15	55	2.7	1.6
81	15	55	2.7	1.5
90	15	54	2.7	1.6
99	14	55	2.6	1.6
109	14	54	2.5	1.6
120	14	54	2.5	1.6
131	13	54	2.4	1.6
140	13	54	2.3	1.6
151	12	54	2.3	1.6
161	12	54	2.2	1.6
169	12	53	2.2	1.7
180	11	53	2.1	1.7
190	11	54	2.1	1.7
200	11	53	2.0	1.7
211	10	52	2.0	1.7
220	10	52	1.9	1.7
230	9.7	51	1.9	1.8
240	9.4	51	1.8	1.8
250	9.0	51	1.8	1.8
260	8.6	50	1.7	1.8
270	8.3	49	1.7	1.9
280	8.0	48	1.6	1.9
290	7.8	47	1.7	2.0

Table 5.10 Temperature Dependence of $\varphi_e,\,\tau,\,k_r$ and k_{nr} of $W_2Cl_4(PMe_2Ph)_4$

T/K	$\phi_e / 10^{-2}$	τ/ns	$k_{\rm r} / 10^6$	$k_{nr}/10^6$
40	17	111	1.6	7.4
49	26	111	2.3	6.7
59	24	104	2.3	7.3
70	21	96	2.2	8.2
80	15	68	2.2	12
90	12	55	2.6	16
100	14	55	2.2	16
109	12	56	2.2	16
121	12	55	2.2	16
131	12	54	2.2	17
140	11	52	2.2	17
149	11	52	2.1	17
160	11	51	2.1	17
171	10	50	2.0	18
180	9.7	49	2.0	18
190	9.3	49	1.9	19
200	8.9	48	1.9	19
211	8.5	47	1.8	19
220	8.1	46	1.8	20
230	7.6	45	1.7	20
240	7.3	44	1.7	20
250	7.1	43	1.7	22
260	6.9	42	1.6	22
270	6.6	41	1.6	23
280	6.0	40	1.5	23
290	5.5	39	1.4	24

Table 5.11 Temperature dependence of $\varphi_e,\,\tau,\,k_r$ and k_{nr} of $W_2Cl_4(PMePh_2)_4$

T/K	ф _е / 10 ⁻²	τ/ns	$k_{\rm r} / 10^6$	k _{nr} / 10 ⁶
39	20	108	19	7.4
60	10	111	9.4	8.1
80	10	108	9.6	8.3
100	10	106	9.5	8.5
121	9.9	107	9.3	8.4
140	9.6	104	9.3	8.6
160	9.4	103	9.1	8.7
181	9.1	105	8.7	8.6
201	8.7	102	8.6	8.8
210	8.4	101	8.3	8.9
221	8.2	100	8.2	9.1
230	8.0	99	8.1	9.2
240	7.8	98	7.9	9.3
250	7.5	98	7.7	9.2
260	7.1	95	7.4	9.6
270	6.9	92	7.4	9.9
281	6.5	92	7.1	10
290	6.2	89	7.0	10

lifetimes at 40 K, which start to converge to 100 ns, but are not quite as long as expected relative to the Mo₂ homologs.

The ground state stretching frequencies for W₂Cl₄(PBu₃)₄ is 260 cm⁻¹ and was measured by Raman spectroscopy.²⁸ The excited state M-M stretching frequency for Mo₂Cl₄(PMe₃)₄ changes by ~5.6% relative to the ground state. This was used to estimate the excited state M-M stretching vibration for W₂ to be 246 cm⁻¹. Using these values and equation 5.26, r_e and r_e* were calculated to be 2.29 and 2.39 Å, respectively. The experimentally determined M-M bond distance is 2.267 Å^{27} , showing that the assumptions made are valid. The change in the M-M bond length, calculated from equation 5.24, is 0.06Å. There S_m is calculated to be 1.21, establishing that the W₂ complexes are in the weak coupling limit of k_{nr}. A plot of $\ln k_{nr}$ vs the emission energy, ΔE , is shown in Figure 5.11. The error in k_{nr} of W₂Cl₄(PMe₂Ph)₄ is about 30%, while the error in the others is about 20%. There is no clear linear correlation, which is expected based on equation 5.18. This is probably due to the limited range that is spanned by the data set, which is only 15 -17 for ln k_{nr} and 1.29 - 1.35 x 10^4 cm⁻¹ for ΔE . A larger data set, i.e. more complexes, are required to clearly establish that the W-4-W complexes follow the energy gap law.

3. $MoWCl_4(PR_3)_4$

In contrast to the homobimetallic complexes, vibrational structure is absent for the heterobimetalle MoWCl₄(PR₃)₄ in 2-methylpentane down to 60 K. An explanation for this difference may lie in the greater dipole moment of the heteronuclear complex resulting in a greater coupling of the dipole with the solvent. This may lead to greater inhomogeneous line broadening. 2-

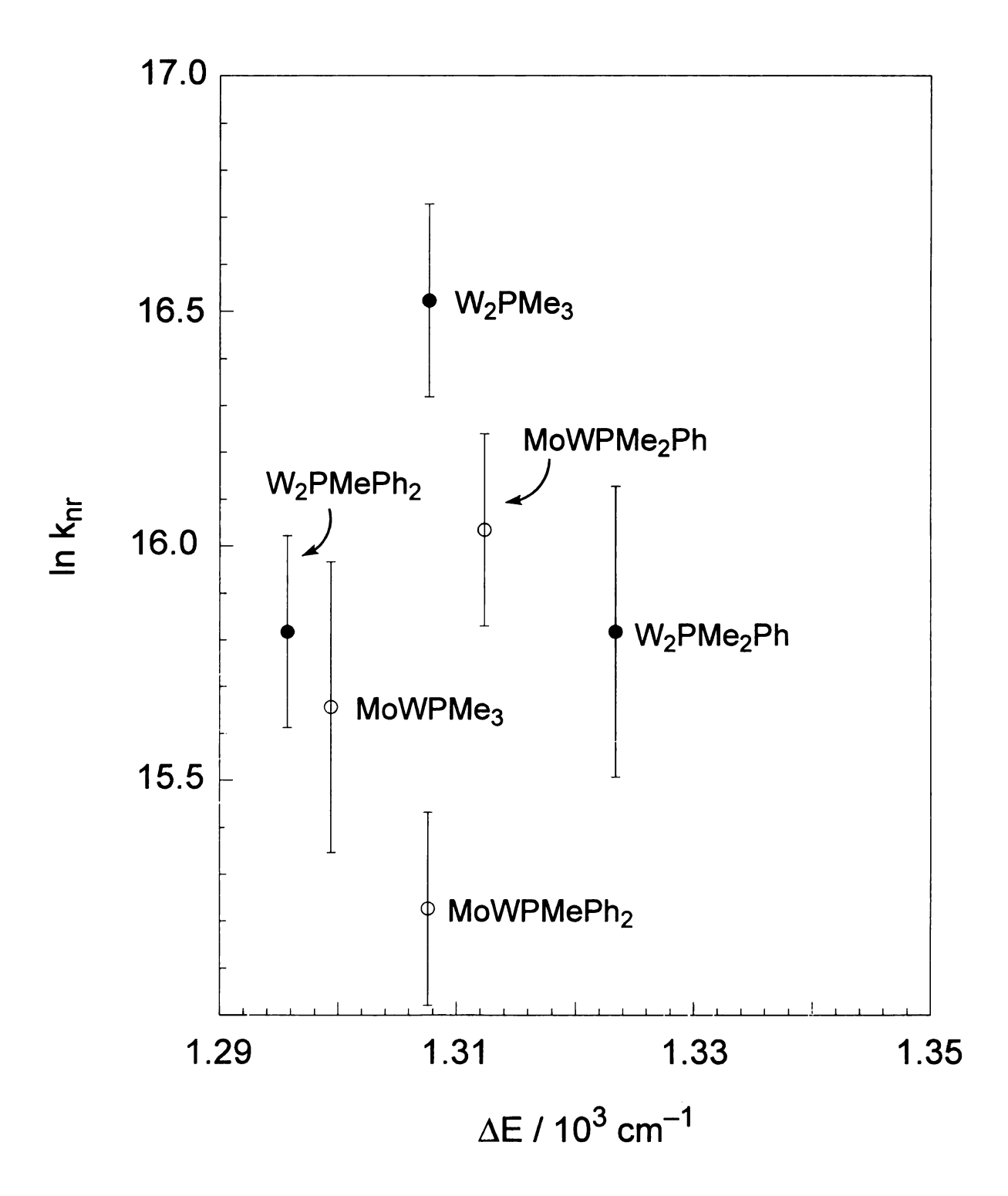


Figure 5.11 Energy gap plots for MoWCl₄(PR₃)₄ (o) and W₂Cl₄(PR₃)₄ (\bullet) at 60 and 40K, respectively.

methylpentane was used instead of 2–MeTHF for MoWCl₄(PR₃)₄ complexes due to decomposition of MoWCl₄(PR₃)₄ in the latter solvent. The formation of fissures in the optical glass below 60 K for 2–methylpentane precluded measurements below this temperature, which may be necessary in order to observe the vibrational fine structure of these complexes. In addition, the emission band width exhibits a temperature dependence and increases by 400 cm⁻¹ from 60 to 290 K.

The temperature dependence of the luminescence lifetimes of each complex is shown in Figures 5.12 - 5.14. The solid line in each Figure is the fit of equation 5.4 to the experimental data. A monoexponential decay expression could be used to fit the luminescent lifetimes of all three MoW complexes at all temperatures studied. The fit to the experimental rates of MoWCl₄(PMe₃)₄, Figure 5.12, is very poor due to the scatter in the data.

Table 5.2 lists the calculated rate constants, k_1 and k_2 , and the energy gap. $\Delta E'$. The decay rate constants, k_1 , for MoWCl₄(PMe₃)₄ and MoWCl₄(PMePh₂)₄ are the same order of magnitude, ~6-8 x 10⁶, while k_1 for MoWCl₄(PMe₂Ph)₄ is an order of magnitude faster (15 x 10⁶). The decay rate constants, k_2 , for MoWCl₄(PMe₂Ph)₄ and MoWCl₄(PMePh₂)₄ are both 10¹⁰, while MoWCl₄(PMe₃)₄ is three orders of magnitude slower (2.7 x 10⁷). This large discrepency for the latter complex is due to the poor data. Due to the large error in the data for this complex the calculated energy gap for MoWCl₄(PMe₃)₄ (291 cm⁻¹) is much lower than either MoWCl₄(PMe₂Ph)₄ or MoWCl₄(PMePh₂)₄, which is about 1730 cm⁻¹. Therefore, the energy gap for MoWCl₄(PMe₃)₄ must be discounted.

Tables 5.12 - 5.14 list the luminescent quantum yields, ϕ_e , lifetimes, τ , and the radiative, k_r , and nonradiative, k_{nr} , decay constants for MoWCl₄(PMe₃)₄,

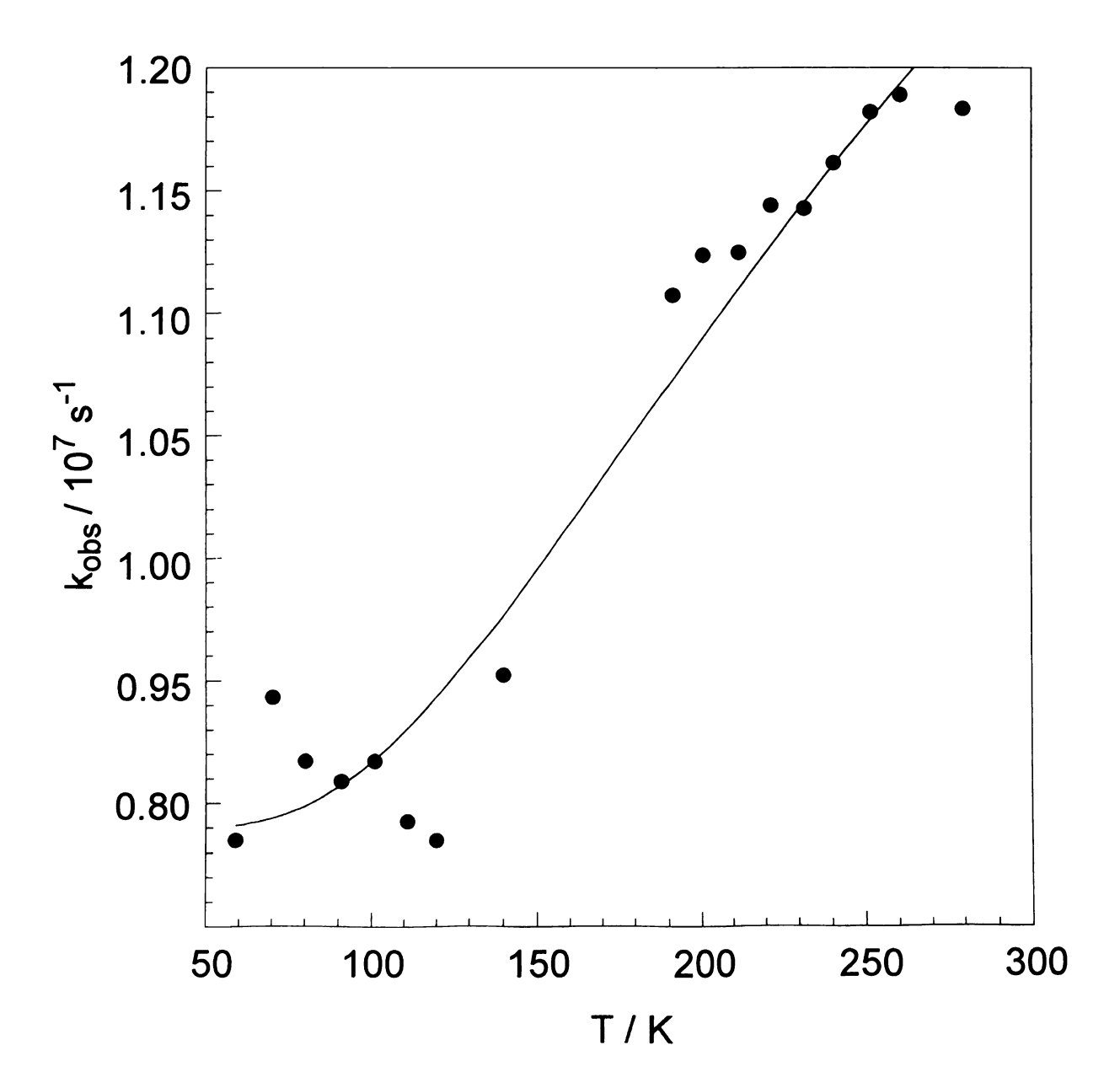
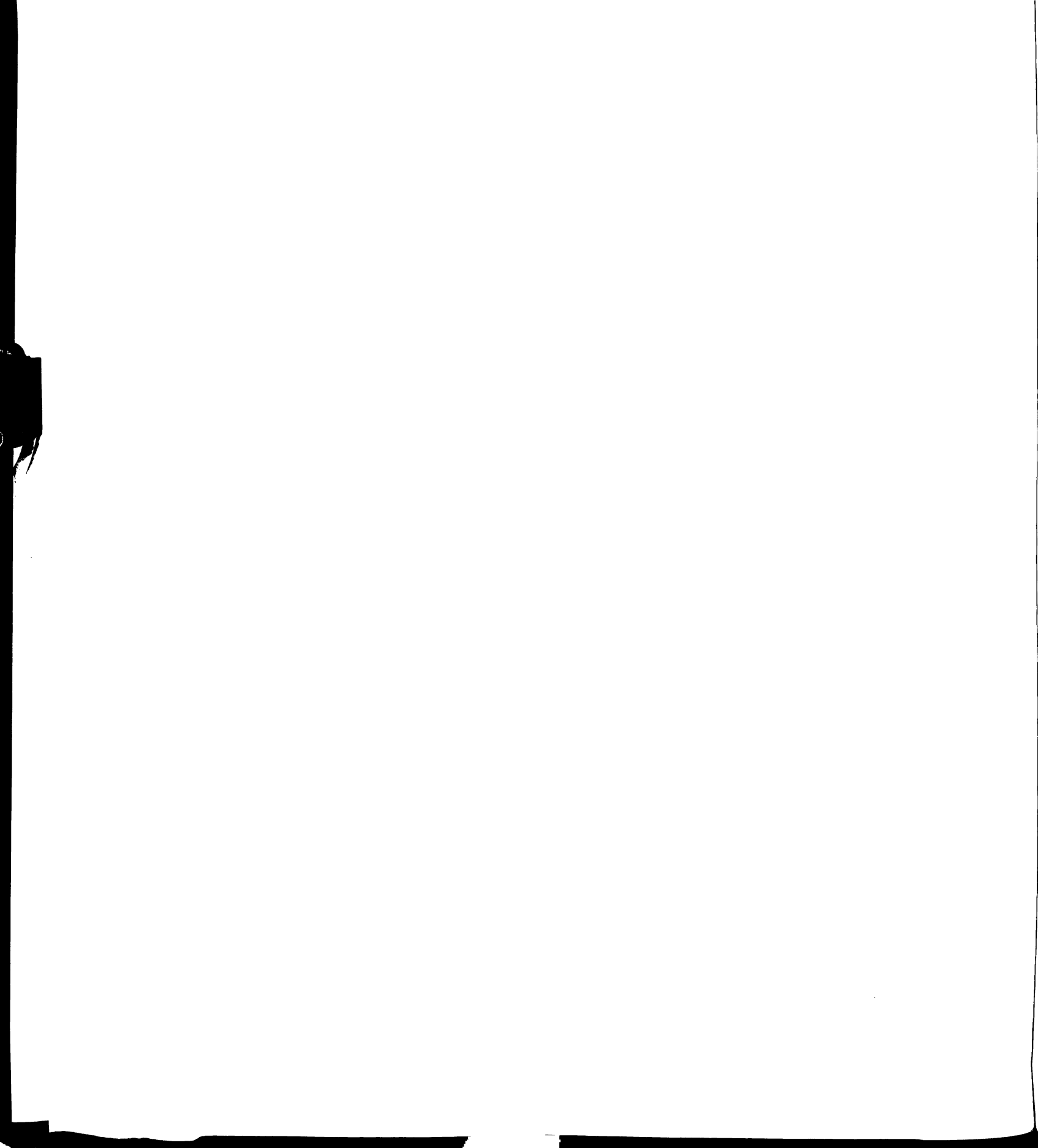


Figure 5.12 Fit of the variation of the observed emission decay constant of MoWCl₄(PMe₃)₄ to equation 5.4 in the 60-280 K temperature range.



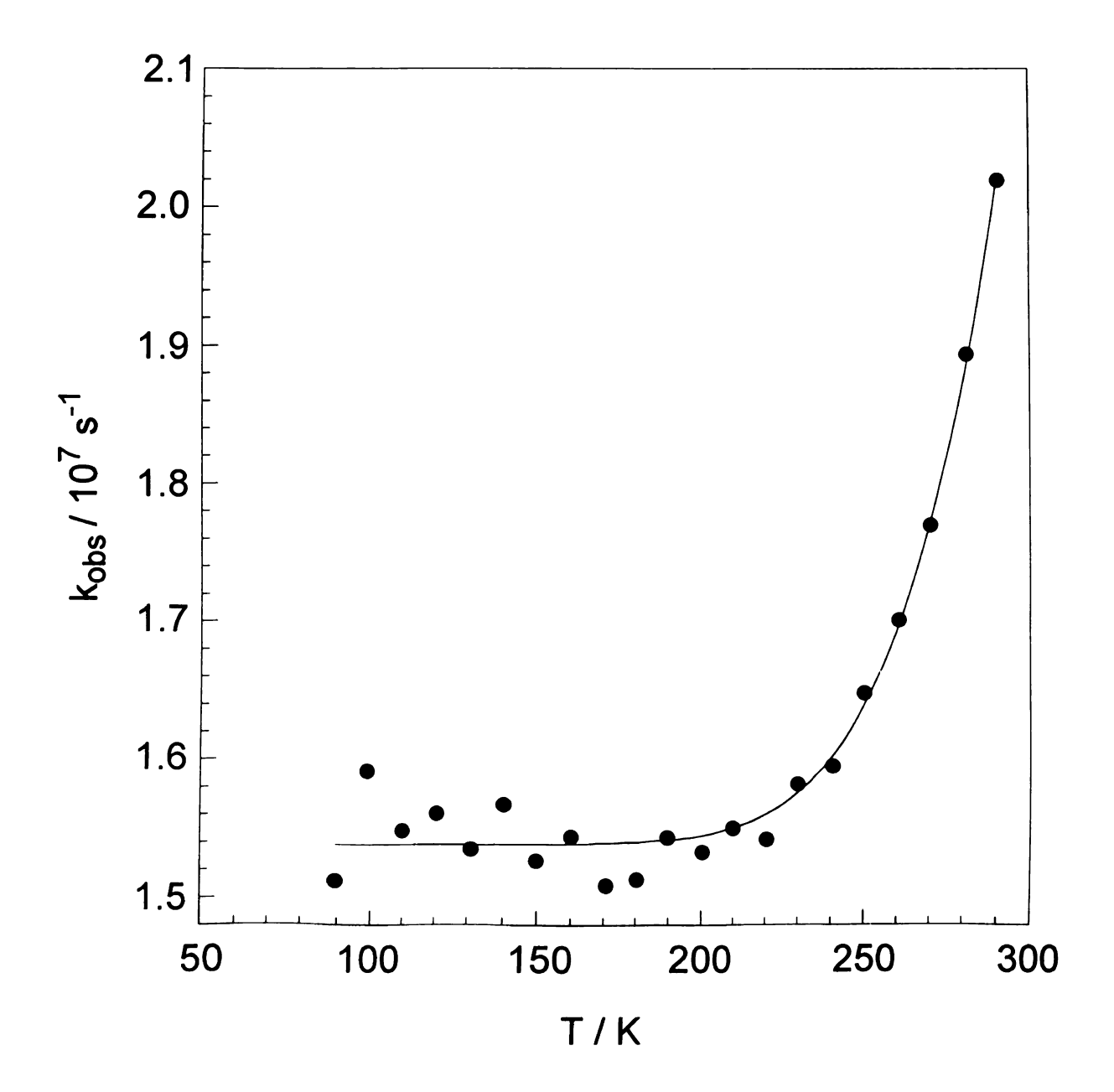


Figure 5.13 Fit of the variation of the observed emission decay constant of MoWCl₄(PMe₂Ph)₄ to equation 5.4 in the 60-290 K temperature range.

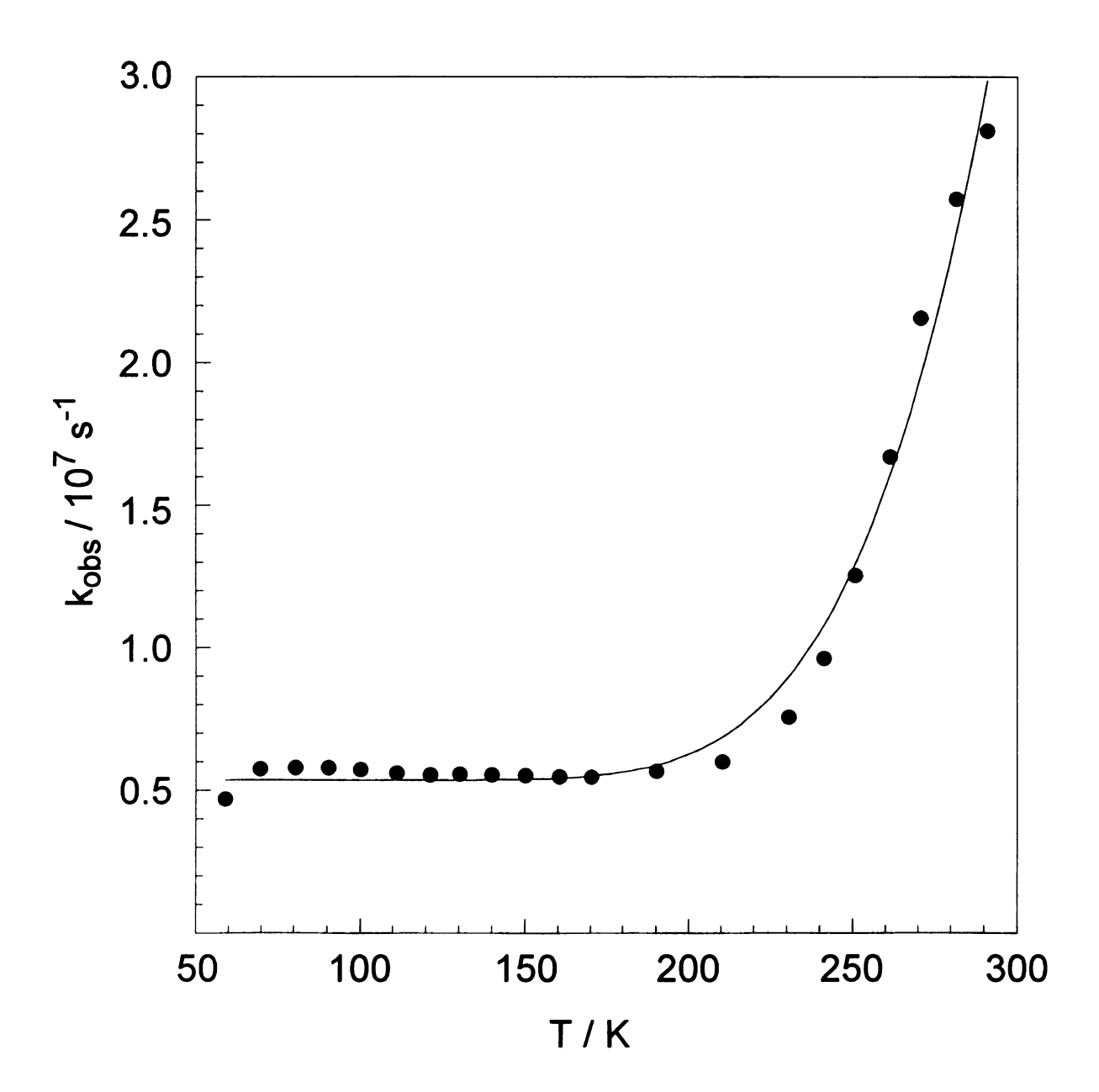


Figure 5.14 Fit of the variation of the observed emission decay constant of MoWCl₄(PMePh₂)₄ to equation 5.4 in the 60-290 K temperature range.

Table 5.12 Temperature Dependence of $\varphi_e,\,\tau,\,k_r$ and k_{nr} of MoWCl4(PMe3)4

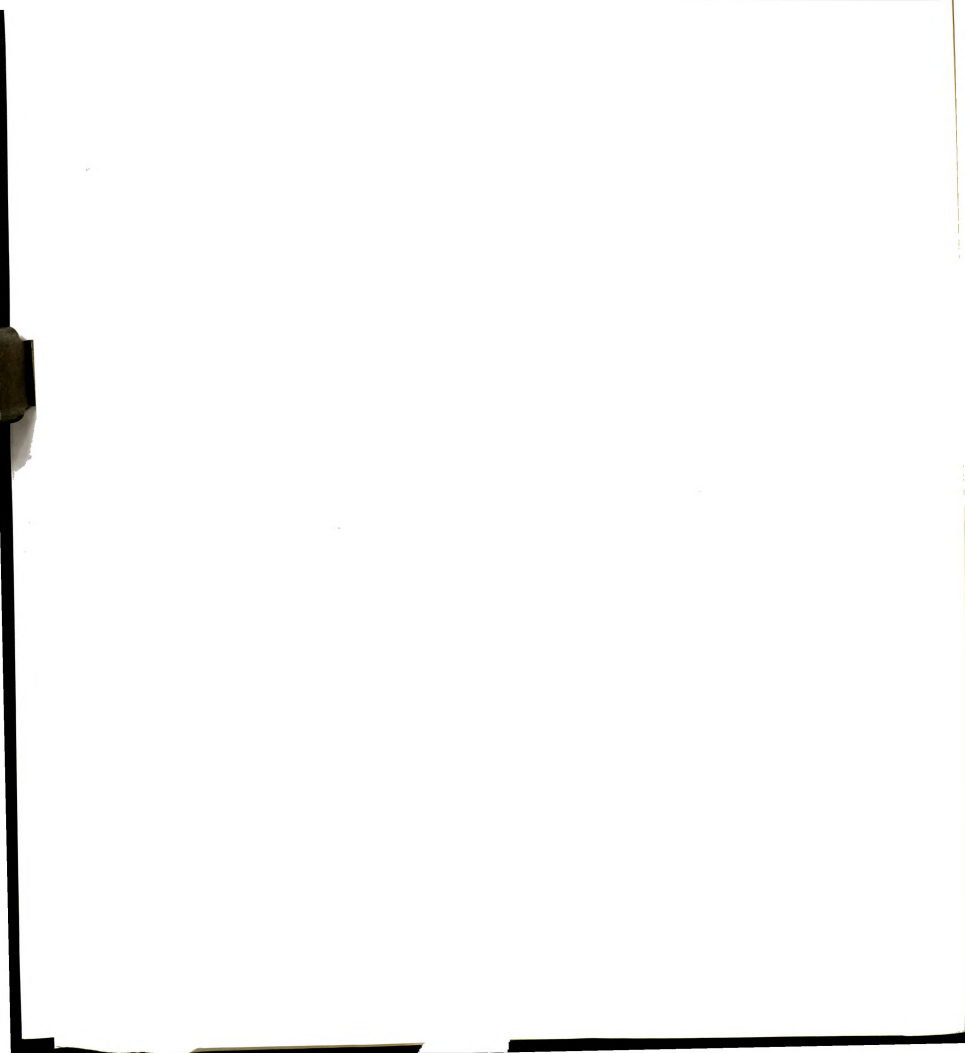
T/K	$\phi_{\rm e} / 10^{-2}$	τ/ns	k _r / 10 ⁶	k _{nr} / 10 ⁶
60	29	113	2.6	6.3
70	29	106	2.7	6.7
81	29	109	2.6	6.6
91	28	110	2.6	6.5
101	28	109	2.5	6.6
110	27	112	2.5	6.5
121	25	113	2.3	6.6
129	26	113	2.3	6.6
139	27	105	2.6	7.0
151	27	85	3.2	8.5
160	27	87	3.1	8.4
170	26	89	3.0	8.3
180	25	88	2.9	8.5
190	24	90	2.7	8.4
200	22	89	2.5	8.7
210	21	89	2.4	8.8
220	19	87	2.2	9.3
230	18	88	2.1	9.3
240	17	86	2.0	9.6
250	16	85	1.9	9.9
260	15	84	1.8	10
271	14	85	1.7	10
280	14	87	1.6	9.9
291	13	88	1.5	9.9

Table 5.13 Temperature Dependence of $\varphi_e,\,\tau,\,k_r$ and k_{nr} of MoWCl₄(PMe₂Ph)₄

T/K	$\phi_{\rm e} / 10^{-2}$	τ/ns	k _r / 10 ⁶	k _{nr} / 10 ⁶
60	22	77	3.8	9.2
70	19	75	3.9	9.4
79	19	73	3.9	9.8
90	18	66	4.2	11
99	18	63	4.4	11
110	18	65	4.3	11
121	18	64	4.0	12
131	17	65	4.0	11
141	17	64	4.2	11
150	17	66	4.2	11
161	16	65	4.1	11
171	16	66	4.0	11
181	15	66	3.8	11
190	15	65	3.7	12
201	15	65	3.4	12
210	14	65	3.3	12
221	13	65	2.9	12
230	13	63	2.9	13
241	12	63	2.8	13
250	11	62	2.7	14
261	10	59	2.6	14
270	9.3	57	2.5	15
281	8.3	53	2.6	16
290	7.6	50	2.6	18

Table 5.14 Temperature Dependence of $\phi_e,\,\tau,\,k_r$ and k_{nr} of MoWCl₄(PMePh₂)₄

T/K	$\phi_{\rm e} / 10^{-2}$	τ/ns	$k_{\rm r} / 10^5$	k _{nr} / 10 ⁶
59	13	214	6.3	4.1
70	12	174	7.1	5.0
80	12	172	7.0	5.1
90	11	172	6.5	5.1
100	11	175	6.4	5.1
111	11	178	6.3	5.0
121	11	180	6.0	4.9
130	10	180	5.8	5.0
140	9.0	181	5.0	5.0
150	9.2	181	5.1	5.0
161	8.7	182	4.8	5.0
171	7.8	183	4.3	5.0
190	8.2	176	4.6	5.2
210	8.1	167	4.9	5.5
230	7.7	132	5.8	7.0
241	7.4	104	7.1	8.9
251	7.0	80	8.8	12
261	6.9	60	12	16
270	6.4	46	14	20
281	6.7	39	16	24
291	6.0	36	17	26



MoWCl₄(PMe₂Ph)₄ and MoWCl₄(PMePh₂)₄, respectively. k_{nr} , at 290 K, increases from 9.9 x 10^6 s⁻¹, 18 x 10^6 s⁻¹ and 26 x 10^6 s⁻¹ on going from MoWCl₄(PMe₃)₄, MoWCl₄(PMe₂Ph)₄ to MoWCl₄(PMePh₂)₄, displaying a similar trend that is observed for the Mo₂Cl₄(PR₃)₄ complexes. Interestingly, this trend is not observed for W₂Cl₄(PR₃)₄.

The amount of decay, as calculated from equation 5.5, through the upper excited state at 290 K is remarkable. The convergence of the lifetimes to 200 ns is consistent with a much smaller fraction of decay through this higher energy excited state at 60 K, indicating a small contribution from this state at this temperature.

The ground and excited state M-M stretching frequencies are 322^{26} and 305 cm⁻¹, respectively, for MoWCl₄(PMe₃)₄. The ground state vibration was measured by Raman spectroscopy, while the excited state vibration was estimated in a similar manner as that for W₂. The ground state equilibruim bond length was calculated by averaging the results from equations 5.25 and 5.26, which gives a value that compares well to the experimentally determined length, 2.21 Å (calculated) and 2.209 Å (experimental).²⁹ The excited state equilibrium bond distance that was calculated for MoW is the same as that calculated for Mo₂, Table 5.8. This indicates a slightly less distorted excited state for MoW, relative to Mo₂ and W₂, and is reflected in S_m (0.5) and R (0.04 Å). This also defines a weak coupling limit of k_{nr} for the MoW series. Figure 5.11 shows the energy gap plots for MoWCl₄(PR₃)₄ at 60 K. The error in MoWCl₄(PMe₃)₄ was estimated at 30%, while the error of the other two complexes is estimated at 20%. As discussed in the case of W₂Cl₄(PR₃)₄, a greater number of complexes need to be studied to definitively determine if Mo–4–W complexes follow the energy gap law.

4. Electronic Coupling

The calculated electronic couplings for $M_2Cl_4(PR_3)_4$ ($M_2 = Mo_2$, MoW, W_2) are listed in Table 5.15, along with $\Delta \overline{\nu}_{l/2}$, ε_{max} , $\overline{\nu}_{max}$. H_{AB} for all nine complexes is about 2300 cm⁻¹. While this number seems large for valence electrons localized in parallel d_{xy} orbitals, considering the short distance for charge transfer (2.13-2.26 Å), it is entirely reasonable. When this number is compared to a coupling of 3300 cm⁻¹ for $[(NH_3)_5Ru^{II}]_2pyz^{5+}$, which is over a distance of 6.8 Å, 22 it is relatively small. If all the numbers remain the same, except to increase the M–M bond distance to 6.8Å, H_{AB} drops by an order of magnitude.

Based on this the electronic coupling between the metal centers can be considered small and the electrons localized on separate metal centers. For comparison, $L(NH_3)_4Ru(NC)Fe(CN)_5^-$ ($L=NH_3$, 4-Mepy, 3-Clpy) was calculated to have an electronic coupling of ~3200 cm⁻¹ over an electron transfer distance of 3.5 Å and is considered to be localized.³⁰ It is possible to calculate the electronic coupling from the rate expression for k_{nr} . However, the electronic coupling, as calculated from Hush theory, while not considered to be in the strong coupling limit of nonradiative decay theory, is too strongly coupled to use equation 5.11 or 5.20. The electronic coupling usually observed is ~600 cm⁻¹.³¹

In summary, the excited state dynamics of $M_2Cl_4(PR_3)_4$ clearly show the existence of efficient deactivation pathways of $^1(\delta\delta^*)$. A proposed energy diagram for $Mo_2Cl_4(PMe_2Ph)_4$ is shown in Figure 5.15. This excited state is in thermal equilibrium with a higher energy excited state, S_2 , that is ~2000 cm $^{-1}$ away for Mo_2 and MoW and ~600 cm $^{-1}$ away for W_2 . Photochemistry is observed with quadruply bonded bimetallic complexes with $\lambda_{exc} \geq ^1(\pi\delta^*)$. This absortion band

Table 5.15 $\epsilon_{max},\,\nu_{max},\,\Delta\overline{\nu}_{_{1/2}}\,$ and Calculated H_{AB} for $M_2Cl_4(PR_3)_4.$

complex	ε_{max} / M^{-1} cm ⁻¹	v_{max} / cm ⁻¹	$\Delta \overline{\nu}_{1/2}$ / cm ⁻¹	H_{AB} / cm ⁻¹
$Mo_2Cl_4(PMe_3)_4$	3110 ^a	17229	1408	2644
Mo ₂ Cl ₄ (PMe ₂ Ph) ₄	2943	16909	1307	2455
Mo ₂ Cl ₄ (PMePh ₂) ₄	2810	16782	1535	2589
			-	
MoWCl ₄ (PMe ₃) ₄	~2200 ^b	16045	1723	2290
MoWCl ₄ (PMe ₂ Ph) ₄	2169	15590	1475	2074
MoWCl ₄ (PMePh ₂) ₄	2609	15590	1478	2276
W ₂ Cl ₄ (PMe ₃) ₄	4170 ^a	15234	1154	2454
$W_2Cl_4(PMe_2Ph)_4$	3750	14902	1201	2348
W ₂ Cl ₄ (PMePh ₂) ₄	4012	15228	1437	2685

a. from reference 7; in 2-methylpentane; b. approximated

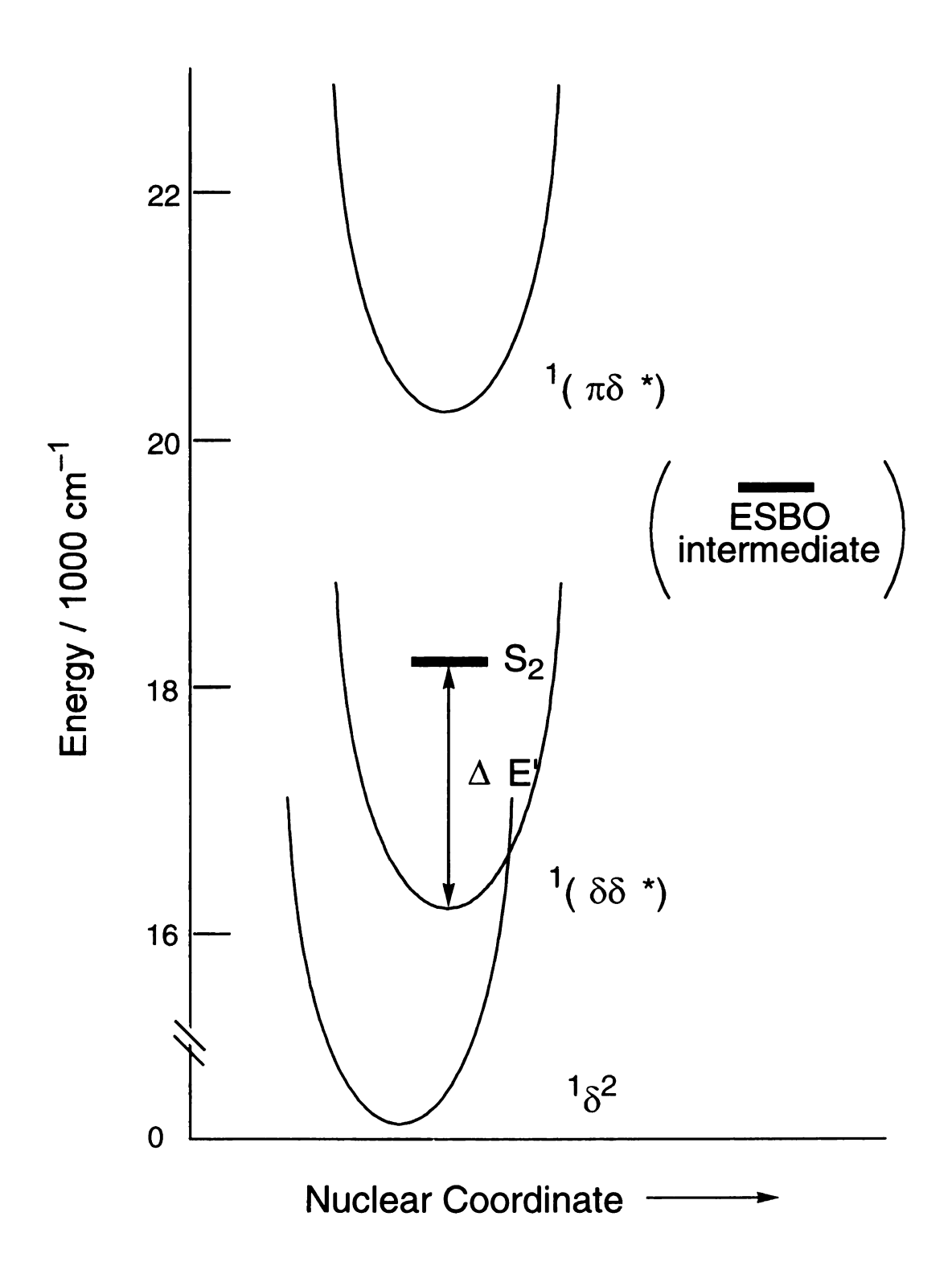


Figure 5.15 Proposed energy diagram for Mo₂Cl₄(PMe₂Ph)₄.

maximum is typically 5400 - 6300 cm⁻¹ away from the absorption maximum of $^{1}(\delta\delta^{*})$ in $M_{2}Cl_{4}(PR_{3})_{4}$ complexes. The fact that photochemistry has not been observed upon excitation of $^{1}(\delta\delta^{*})$, indicates that there is an activation barrier to reaching the high energy intermediate believed to be necessary to trap the zwitterion, as described before. It appears that the asymmetry of MoW is not enough to circumvent the need for the intramolecular rearrangement, since photochemistry is still not observed with wavelengths coincident with $^{1}(\delta\delta^{*})$, as discussed in Chapter 4. Additionally, the deactivation of S_{2} cannot occur through this distorted intermediate. As calculated from equation 5.5, the population of this state at room temperature is significant. If this state, S_{2} , underwent molecular rearrangement to the distorted ESBO, we would expect to observe photochemistry upon the population of $^{1}(\delta\delta^{*})$.

E. References

- (a) Cotton, F. A.; Harris, C. B. *Inorg. Chem.* 1965, 4, 330. (b) Cotton, F. A.;
 Curtis, N. F.; Harris, C. B.; Johnson, B. F. G.; Lippard, S. J.; Mague, J. H.;
 Robinson, W. R.; Wood, J. S. *Science* 1964, 145, 1305.
- 2. Cowman, C. D.; Gray, H. B. J. Am. Chem. Soc. 1973, 95, 8177.
- 3. Hay, J. P. J. Am. Chem. Soc. 1982, 104, 7007.
- 4. (a) Trogler, W. C.; Cowman, C. D.; Gray, H. B.; Cotton, F. A. *J. Am. Chem. Soc.* 1977, 99, 2993. (b) Hopkins, M. D.; Schaefer, W. P.; Bronikowski, M. J.; Woodruff, W. H.; Miskowski, V. M.; Dallinger, R. F.; Gray, H. B. *J. Am. Chem. Soc.* 1987, 109, 408.

- 5. Hopkins, M. D.; Miskowski, V. M.; Gray, H. B. J. Am. Chem. Soc. 1988, 110, 1787.
- 6. Miskowski, V. M.; Gray, H. B.; Hopkins, M. D. Inorg. Chem. 1992, 31, 2085.
- 7. Hopkins, M. D.; Gray, H. B. J. Am. Chem. Soc. 1984, 106, 2468.
- 8. Zietlow, T. C.; Hopkins, M. D.; Gray, H. B. J. Solid St. Chem. 1985, 57, 112.
- 9. Turro, N. J. Modern Molecular Photochemistry; University Science Books: Sausalito, CA, 1991; pp 176-180.
- (a) Lumpkin, R. S.; Kober, E. M.; Worl, L. A.; Murtaza, Z.; Meyer, T. J. J. Phys. Chem. 1990, 94, 239.
 (b) Van Houten, J.; Watts, R. J. J. Am. Chem. Soc. 1976, 98, 4853.
 (c) Durham, B.; Caspar, J. V.; Nagle, J. K.; Meyer, T. J. J. Am. Chem. Soc. 1982, 104, 4803.
- 11. Engleman, R.; Jortner, J. Mol. Physics 1970, 18, 145.
- 12. (a) Ballhausen, C. J. Molecular Electronic Structures of Transition Metal Complexes; McGraw-Hill: New York, 1978; Ch 4. (b) Hertzger, G. Molecular Spectra and Molecular Structure; Van Norstrand: New York, 1950; Vol. 1, Ch 4.
- 13. Barbara, P. F.; Meyer, T. J.; Ratner, M. A. J. Phys. Chem. 1996, 100, 13148.
- 14. (a) Caspar, J. V.; Westmoreland, T. D.; Allen, G. H.; Bradley, P. G.; Meyer, T.
- J.; Woodruff, W. H. J. Am. Chem. Soc. 1984, 106, 3492. (b) Trogler, W. C.; Solomon, E. I.; Trajberg, IB.; Ballhausen, C. J.; Gray, H. B. Inorg. Chem. 1977, 16, 828.
- 15. Hopkins, M. D.; Gray, H. B.; Miskowski, V. M. Polyhedron 1987, 6, 705.
- 16. See for example: (a) Kober, E. M.; Casper, J. V.; Lumpkin, R. S.; Meyer, T. J.
- J. Phys. Chem. 1986, 90 3722. (b) Coe, B. J.; Thompson, D. W.; Culbertson, C. T.;
- Schoonover, J. R.; Meyer, T. J. Inorg. Chem. 1995, 34, 3385. (c) Claude, J. P.;

- Meyer, T. J. J. Phys. Chem. 1995, 99, 51. (d) Strouse, G. F.; Schoonover, R.; Duesing, R.; Boyde, S.; Jones Jr., W. E.; Meyer, T. J. Inorg. Chem. 1995, 34, 473.
- 17. Trogler, W. C.; Gray, H. B. Acc. Chem. Res. 1978, 11, 232.
- 18. (a) Allen, G. C.; Hush, N. S. *Prog. Inorg. Chem.* **1967**, *8*, 357. (b) Hush, N. S. *Prog. Inorg. Chem.* **1967**, *8*, 391.
- 19. Rezvani, A. R.; Evans, C. E. B.; Crutchley, R. J. Inorg. Chem. 1995, 34, 4600.
- 20. Meyer, T. J.; Taube, H. In Comprehensive Coordination Chemistry, Wilkinson,
- G. Ed.; Pergamon Press: Oxford, 1987; Vol 1, p. 361.
- 21. Creutz, C. Prog. Inorg. Chem. 1983, 30, 1.
- 22. (a) Beattie, J. K.; Hush, N. S.; Taylor, P. R. *Inorg. Chem.* **1976**, *15*, 992. (b) Creutz, C. *Inorg. Chem.* **1978**, *17*, 3723.
- 23. Lumpkin, R. S.; Meyer, T. J. J. Phys. Chem. 1986, 90, 5307.
- 24. Zhang, X.; Kozik, M.; Sutin, N.; Winkler, J. R. In Electron Transfer in Inorganic, Organic, and Biological Systems, Bolton, J. R.; Mataga, N.; McLendon,
- G., Eds.; Advances in Chemistry No. 228, American Chemical Society: Washington, DC, 1991; p 247.
- 25. (a) Tait, C. D.; Garner, J. M.; Collman, J. P.; Sattelberger, A. P.; Woodruff, W.
- H. J. Am. Chem. Soc. 1989, 111, 9072. (b) Miskowski, V. M.; Dallinger, R. F.; Christoph, G. G.; Morris, D. E.; Spies, G. H.; Woodruff, W. H. Inorg. Chem. 1987, 26, 2127.
- 26. Carlin, R. T.; McCarley, R. E. Inorg. Chem. 1989, 28, 280.
- 27. Cotton, F. A.; Extine, M. W.; Felthouse, T. R.; Kolthammer, B. W. S.; Lay, D. G. J. Am. Chem. Soc. 1981, 103, 4040.
- 28. Sharp, P.; Schrock, R. R. J. Am. Chem. Soc. 1980, 102, 1430.



- 29. Luck, R. L.; Morris, R. H.; Sawyer, J. F. Inorg. Chem. 1987, 26, 2422.
- 30. Dong, Y.; Hupp, J. T. Inorg. Chem. 1992, 31, 3170.
- 31. Worl, L. A.; Duesing, R.; Chen, P.; Ciana, L. D.; Meyer, T. J. J. Chem. Soc. Dalt. Trans. 1991, 849.





